# Physiological processes and molecular determinants of root senescence in barley

Dissertation

zur Erlangung des

Doktorgrades der Naturwissenschaften (Dr. rer. nat.)


der


Naturwissenschaftlichen Fakultät I

– Biowissenschaften –

der Martin-Luther-Universität Halle-Wittenberg


vorgelegt von

Frau Tunc, Cevza Esin


verteidigt am 10.12.2024


Gutachter:

1. Prof. Dr. Nicolaus von Wirén
2. Prof. Dr. Klaus Humbeck
3. Prof. Dr. Thomas Schmülling

**Table of Contents**

## 1. Introduction

Developmental processes that shape morphological and physiological root traits, such as root angle, root length or metabolic activity, are important determinants for anchoring plants in their substrate and providing water and nutrients to shoots. Most of these processes undergo age-dependent progression, increasing during early vegetative growth but declining with plant age (Siqueira et al., 2022). Even when assimilate provision to the roots ceases during reproductive growth, physiological and cell biological processes in roots continue and alter root properties in order to sustain water as well as nutrient acquisition and delivery to the shoot (Schneider et al., 2017). Despite the relevance of root age-related processes for shoot development, their characterization has received little attention. Major reasons for disregarding root age-related processes so far lie in the difficulty to sample and analyze aged and often fragile root tissues, but also in the use of an inconsistent terminology. The latter results from the wide range of perspectives, under which root age-dependent processes have been investigated. Therefore, the present introduction attempts first to discern root age-related terms in their eco-/physiological context, before focusing on root senescence as a developmental process with a description of its trait changes, their regulation and their importance for overall plant performance.

### 1.1 Root aging-dependent processes in their eco-physiological context

Morphological and physiological changes taking place in aging plant roots have been characterized from various perspectives and in diverse biological context, which has led to different concepts. Aging per se refers to the chronological process of growing old from the birth to the death of an organ or organism (Thomas, 2013). Albeit associated inevitably with degenerative processes and declining viability of plant cells or tissues, aging does not lead immediately to death, e.g. when considering the vegetative growth phase of an annual species. The sequential morphological and physiological alterations accumulating during aging are regarded as a passive process that is independent of endogenous cues (Munné-Bosch, 2007).

As an episode of aging, senescence defines the terminal developmental phase of a plant following the completion of growth (Thomas, 2013). Senescence strictly depends on cell viability and describes the onset and gradual degradation of – mostly source –

tissue, which serves the purpose of carbon and nutrient remobilization to sink tissues and is a hallmark of leaf senescence in plants (Buchanan-Wollaston et al., 2003; Gregersen et al., 2008; Woo et al., 2019). Senescence is governed by an active, genetically determined program, which can be accelerated, delayed or even reversed by internal or external factors and thus shows a high degree of temporal plasticity. Nonetheless, senescence remains firmly associated with the progressing age of a given cell, tissue, organ or organism.

Depending on the lifestyle and overall life span of a plant species, senescence-related processes can become completely uncoupled at the organismal and organ level. Annual and biennial plants are monocarpic plants that complete their life cycle in one or two years, respectively. Here, whole-plant senescence is a unique developmental event strictly following flowering and fruit set (Munné-Bosch, 2008). Nonetheless, at the organ level individual leaves start senescing even before reproductive organs are formed, and even within an individual leaf, senescence follows an age gradient from the tip towards the base (Bresson et al., 2018). In monocarpic plants, leaf senescence is coordinated with whole-plant senescence and specified by the term 'monocarpic senescence' (Zentgraf et al., 2021). Polycarpic species share a perennial lifestyle with the ability to set fruits several times over a life span of many years. As an extreme, bristlecone pine can live up to 4900 years and is able to reproduce thousands of times during its life span (Gilbert, 2000). While polycarpic senescence is not a widely used term, the main determinant of whole-plant senescence in perennials is sustained meristem activity, i.e. the ability of the shoot apical meristem to divide and proliferate (Munné-Bosch, 2007). This view underlies the concept of mitotic senescence, which describes the cease of the ability of a tissue or a cell to mitotically divide (Gan, 2018), and can thus be applied also to unicellular species like algae. Along these lines, root senescence can be defined strictly as a developmental phase, in which the quiescent center (QC) cells, a group of slowly dividing cells at the center of the stem-cell niche in the root apical meristem, loses its identity (Siquiera et al., 2022). This loss is marked by a decreased size of QC cells and decreased expression of QC cell-specific markers, like *WOX5* (Timilsina et al., 2019). In consequence, QC cells undergo a transition from a mitotically quiescent state to a frequently dividing state, which is linked with a histological and molecular reorganization of the stem cell niche, already when the plant passes from the juvenile to the adult stage (Wein et al., 2020).

Following the concept of mitotic senescence, the root system should not be regarded as a single organ but consisting of multiple organs, as each root type with an apical meristem can undergo senescence independently, irrespective of whether its origin is embryonic or postembryonic. Since postembryonic roots, like adventitious or lateral roots, can proliferate continuously over a growth season, or in perennials even over more than decades, most attention has been paid to the juvenile root fraction. In trees, shrubs or grassland species, this corresponds to the fine or higher-order root fraction. Here, root senescence results from the balance of continuous growth and dieback of roots, which is better described by **root turnover** and refers to the overall living or detectable biomass of roots at the scale of a plant or plant community (Gill and Jackson, 2000; McCormack et al., 2013). In general, turnover describes a flux through a pool, and in natural settings root turnover plays a critical role in the storage and cycling of carbon (C) in soils, since the majority of the C pool that is incorporated into soil organic matter derives from belowground rather than aboveground biomass (Jackson et al., 2017). In an ecological and agricultural context, root turnover is also of major relevance for nutrient cycling in crop rotations (Freschet et al., 2013; Heuermann et al., 2022). So far, no correlation was found between leaf and root turnover timing in biennial or perennial species (Heilmeier et al., 1986; Withington et al., 2006), suggesting that there root senescence is regulated independently of shoot or leaf senescence.

Agronomic and ecological studies frequently refer to root dynamics, particularly when dealing with perennial species, trees or forests. Root dynamics refer to phenology by the timing of root birth, death and the resulting lifespan of individual roots or turnover of root populations (Freschet et al., 2021). In perennial species, it has been estimated that about 22% of the global net photosynthetic production is allocated belowground for the purpose in fine root production and functioning (McCormack et al., 2015). Respecting the difficulties in examining belowground traits of perennial plants (Lauenroth and Gill, 2003), modelling approaches based on C or nitrogen (N) isotope measurements have been employed to estimate root turnover rates of individual species in terrestrial ecosystems (Matamala et al., 2003). Relative to root dynamics, root turnover sets focus on the substantial left-over of dying roots.

As another aging-related term, root activity comprises the metabolic activity and transport processes that ultimately depend on the energy status of the root. Root

activity can be expressed by the rates of oxygen consumption (Volder et al., 2005), ATP synthesis (Gniazdowska et al., 1998) or nutrient uptake (Liu et al., 2019), representing under optimal growth conditions the physiological state of a root under consideration of its age. Sustained root activity results in expanded root longevity, which reflects the overall or potential lifespan of an individual root or a root system, whereas root lifespan is the time between the birth and the death of a root (Freschet et al., 2021). Root longevity is of particular importance during the reproductive growth phase when nutrients need to be allocated to seeds, often under conditions of nutrient or water scarcity (Fisher et al., 2002). Then, adverse growth conditions can induce premature root senescence, rendering the associated decline in metabolic activity a limiting factor for root longevity and ultimately for plant survival or crop productivity (Ramireddy et al., 2018; Siqueira et al., 2022). Hence, endogenous determinants governing root longevity rely on those regulating root senescence.

## 1.2. Senescence progression in different root types

With respect to their development higher plants form two different types of roots: Embryonic roots derive from the radicle formed in the embryo, whereas post-embryonic roots are formed later and originate either from existing roots or non-root tissues (Wahbi and Gregory, 1995; Atkinson et al., 2014). In dicotyledonous plants, the embryonic primary root with its post-embryonic lateral roots is active throughout the whole life cycle and constitutes the main root stock of the plant (Hochholdinger et al., 2004a). At the cellular level, aging-related processes in roots set in immediately with early cell differentiation in the meristematic root zone. As part of root cap differentiation, temporally coordinated programmed cell death (PCD) removes lateral root cap cells before they enter the root elongation zone (Fendrych et al., 2014). Thereby, cell death controls root cap organ size. In the root differentiation zone, caspase inhibitor-sensitive nuclear DNA fragmentation and protoplast retraction indicate that apoptosis-like PCD terminates the lifespan of root hairs, which can range between a few and > 30 days in dependence of plant species and growth conditions (Rongsawat et al., 2021; Zhu et al., 2021). During secondary, radial growth in the basal root zone, endodermal cells undergo PCD, giving rise to periderm formation and detachment of epidermal and cortical cells (Serra et al., 2022). This periderm re-seals the outer surface to protect the vascular system. In contrast to the death of lateral root cap and root hairs cells, the aging-dependent loss of epidermal and cortical cell files

4

represents senescence of a whole tissue, forming a gradient in shoot-ward direction. Since PCD occurs in individual cells at different positions along the whole root axis and is part of tissue differentiation in early organ development (van Hautegem et al., 2014), PCD markers are not suitable to display reliably senescence progression of the whole root organ. This is opposite to leaves, where developmental transitions from the tip towards the base reflect tissue age and the progression of senescence (Rankenberg et al., 2021). Moreover, primary and lower-order root axes form lateral roots with meristematic tissue (Motte et al., 2019), which makes root tissue sampling along a pure developmental or aging-related gradient practically impossible and impedes senescence studies. This is one of the major reasons why the characterization of root senescence is lagging far behind that of leaf senescence.

Monocotyledons form a fibrous root system, which is composed of embryonic, seminal roots emerging together with the radicle from the scutellar node. In species like maize or rice, the primary root formed by the radicle remains dominant among the seminal roots, while it loses dominance in barley or wheat and becomes hardly recognizable with ongoing development (Osmont et al., 2007). Later, nodal roots develop from the coleoptile or basal leaf nodes to build the allorhizic root system (Hochholdinger et al., 2018; Rich et al., 2020). Collectively, all these root types can develop lateral roots and undergo higher-order lateral branching (Osmont et al., 2007). Seminal and nodal roots differ in their anatomy, with nodal roots being thicker in diameter and having larger metaxylem volumes (Krassovsky, 1926; Hoppe et al., 1986). These nodal root-specific anatomical traits translate into higher hydraulic conductivity promoting water and nutrient uptake as well as their translocation (Ahmed et al., 2018; Liu et al., 2020), thereby contributing more effectively to water use efficiency and plant biomass production (Strock et al., 2021). On top, nodal or brace roots in maize can respond more strongly than seminal roots to locally supplied nitrate (Yu et al., 2016). As even higher-order tillers form nodal roots, the root system of cereals comprises of sequentially developing axial (seminal and nodal) roots of different age. With progressing vegetative development, nodal roots outperform seminal roots and become dominant when the plant's demand for water and nutrients is increasing (Schneider et al., 2020). These differences in developmental and physiological properties between seminal and nodal roots come along with a differential behavior in senescence. Seminal roots of hydroponically-grown barley arrested elongation and

biomass gain when nodal root growth began to increase exponentially, suggesting that endogenous, plant age-dependent signals terminate the growth of seminal roots (Liu et al., 2019).

Perennial woody plants accumulate more above-ground biomass than herbaceous species and require a root structure that provides deeper anchorage and meets an ongoing demand for water and nutrients on the same spot. While coarse or woody roots confer anchorage, active acquisition of water and nutrients from the soil is mediated by fine absorptive roots and their (mostly ecto-) mycorrhizal associates (Danjon et al., 2013). Fine roots are defined conventionally as roots with a diameter of 2 mm or less (Last et al., 1983), while more recent considerations in the scientific community suggest replacing diameter thresholds by an order-based classification (McCormack et al., 2015). In general, fine roots have higher turnover rates, making them key players in belowground cycling of water and nutrients or in carbon sequestration in the soil (Brunner and Godbold, 2007; Danjon et al., 2013). As observed in rhizotron studies, fine root life span increased with increasing root diameter, root branching order, and rooting depth, but was shorter for more distal than proximal roots while the effect of mycorrhizal symbiosis was weak or variable (Chen and Brassard, 2013). In particular when evergreen, trees had the longest fine root life spans, followed by grasses, shrubs and forbs. In a meta-analysis across many species, fine root life span increased with increasing temperature, especially in colder climates (Wang et al., 2021) but decreased with decreasing soil water availability, while adequate N availability in natural soils was mostly positive (Chen and Brassard, 2013). Fine roots dominate nutrient and water acquisition also in grasslands, where root mortality decreased with increasing species diversity (Mommer et al., 2015). Overall, these studies emphasize the strong impact of environmental conditions on the lifespan of fine roots.

## 1.3. Root senescence-related traits
### 1.3.1. Root browning or discoloration
Discoloration of senescing tissues is common to leaves, fruits and petals (Arora, 2008; Woo et al., 2019). A first visible symptom of leaf senescence is the yellowing tissue due to chloroplast dismantling and chlorophyll degradation, during which chlorophyll is converted to colorless phyllobilin, thereby allowing the yellow carotenoids to become

unmasked (Kuai et al., 2018). In flowers, discoloration of senescing petals was found to be attributed to the increased biosynthesis and accumulation of anthocyanins and flavonoids (Teppabut et al., 2018). In case of roots, the transition from white to brown color, termed root browning, has been adopted as physiological indication of tissue age and used to discriminate younger from older roots (Pregitzer et al., 1995; Steele et al., 1997; Liu et al., 2019). Beyond the visible spectrum, root senescence may be recognized also by hyperspectral imaging, which in wheat detected decreasing reflectance at higher wavelengths in response to root decay after shoot clipping (Bodner et al., 2018). A study with conifer and hardwood species associated root lifespan with the extent of root pigmentation and suggested that roots carry lower risk of mortality as long as they remain whiter (Withington et al., 2006). Also in perennial species, progressing tissue age caused older roots to become brown or darker in color, irrespective of the type of the roots (Wojciechowska et al., 2018). While in grape root pigmentation has been associated with tannin accumulation (Comas et al., 2000), the exact cause of root browning in particular for annual species remains to be elucidated. Nonetheless, discoloration or browning of the root tissue is firmly established as a typical visible symptom of root senescence and appears being under genetic control (Kosslak et al., 1997).



**Figure 1. Structure of a barley root system.** Change of color from white-to-brown reflects the differences of tissue age. The photo was taken from 54 days-old plants from the present study.

### 1.3.2. Root cortical senescence

When monitored non-invasively by magnetic resonance imaging (MRI), signal intensities of soil-grown seminal and nodal barley roots continuously decreased during aging as well as with distance from root apex, because outer degraded cortical cell files were no longer detectable and the root diameter was decreased (Schneider et al., 2020). Disintegration of outer cortical cell files with subsequent inward progression towards the endodermis is a phenomenon being observed particularly in graminaceous species and described as root cortical senescence (RCS; Henry and Deacon, 1981; Liljeroth, 1995). RCS typically develops along aging-related gradients that either display from the tip to the base of an individual root axis or appears first in the same developmental zone of an older root compared to a younger root (Schneider et al., 2017; Liu et al., 2019), indicating that not only tissue age but also plant age regulate RCS. In barley or maize, this loss of tissue integrity in basal root zones coincided with the termination of root elongation and biomass increase (Chen et al., 2015; Liu et al., 2019). While RCS is typically related to a certain root age it can be triggered also by nutrient limitations, such as N, P or K deficiency (Schneider et al., 2017). The development of RCS is comparable to cortical aerenchyma formation, since both processes are initiated by programmed cell death (PCD) and promoted by ethylene (Schneider et al., 2018). As marked by the disappearance of stainable nuclei and DNA fragmentation in cereal roots, RCS increased progressively from the tip to the base (Henry and Deacon, 1982; Liljeroth and Bryngelsson 2001). Thereby, DNA and nucleosomal fragmentation started already in two days-old root segments and proceeded at a faster rate in wheat than in barley. In senescing leaves, DNA degradation has been associated with elevated expression of the exonuclease DPD1 (Defective in Pollen organelle Degradation; Matsushima et al., 2011; Sakamoto and Takami, 2014), and since DPD1 is expressed also in senescing roots (Tang and Sakamoto, 2011) DPD1-mediated DNA decay may underlie RCS.

### 1.3.3. Root activity

Disintegration of the plasma membrane is a typical symptom of senescing leaf cells (Lim et al., 2007) and was also recorded in senescing roots when stained by Evan's blue (Liu et al., 2019). The physiological consequence of membrane disintegration is ion leakage and loss of cellular metabolic activity. Indeed, the increasing loss of cell layers during RCS has been linked directly with decreased respiration and lower

hydraulic conductivity (Schneider et al., 2017). Due to the strong dependence of nutrient uptake on respiratory activity (Bouma et al., 2001; Volder et al., 2005; Baldi et al., 2010), barley roots with maximal RCS exhibited 84-92% less radial water, nitrate and phosphorus transport (Schneider et al., 2017). Likewise, seminal roots of barley revealed a sharp drop in uptake and root-to-shoot translocation of $^{15}$N-labeled nitrate as soon as RCS set in (Liu et al., 2019). A consistent age-dependent decline in respiration is also common in fine roots of trees (Ceccon et al., 2016; Wang et al., 2022), and the corresponding loss of cell viability goes along with root browning (Bagniewska-Zadworna et al., 2014). Taken together, root browning, RCS and loss of root activity represent recordable read-outs of root senescence. In consideration of growth conditions, plant species and root type, these traits allow monitoring the progression of senescence-related changes in a plant and tissue age-dependent manner.

### 1.3.4. Metabolism and nutrient remobilization in senescing roots

The physiological benefit of programmed leaf senescence is the re-allocation of energy-rich macromolecules and essential mineral elements to the sink organs. In this process, declining protein and macronutrient contents but accumulating sugar levels are reliable read-outs (Avila-Ospina et al., 2014; Havé et al., 2017; Wingler and Henriques, 2022). Soluble carbohydrates constitute the primary source for ATP production and sustained physiological activity also in roots. During seasonal senescence in poplar roots, soluble carbohydrates and starch accumulated as well, whereas root N levels dropped and were accompanied by enhanced gene and protein expression of glutamine synthetase, suggesting enhanced resorption of recycled N (Wojciechowska et al., 2020b). Similarly, cysteine protease expression increased with age in barley roots, however, without concomitantly altered protein levels (Liu et al., 2019). Here, sustained N supply to aging roots may have prevented a net loss of protein while directing N metabolism towards the synthesis of aromatic amino acids, in particular of tryptophan and its downstream products tryptamine and serotonin. Serotonin is accumulating typically in reproductive organs (Hano et al., 2017; Commisso et al., 2019) or during leaf senescence in consequence of tryptophan decarboxylase induction that determines the rate-limiting step in serotonin biosynthesis (Kang et al., 2009). As revealed by overexpression of tryptophan decarboxylase in rice, elevated serotonin levels can attenuate leaf senescence (Kang

et al., 2009). Whether this relates to the ROS-scavenging activity of serotonin or its interference with auxin signaling remains to be elucidated (Negri et al., 2021). So far, tryptamine and serotonin are among the most promising metabolic markers for root senescence.

Besides enzymatic protein hydrolysis, bulk protein degradation is also mediated by autophagy especially in the later phase of leaf senescence (Avila-Ospina et al., 2014; Wang and Schippers, 2019). Progressing senescence in fine roots of poplar increased gene and protein expression of the autophagy marker ATG8 (Wojciechowska et al., 2018), a ubiquitin-like conjugate required for formation of autophagosomes that deliver cellular constituents to lysosomes or the vacuole for degradation (Soto-Burgos et al., 2018). Ultrastructural analyses indicated the onset of autophagy in senescing poplar roots, when autophagosome-like vesicular structures accumulated in the vacuoles of cortical parenchyma cells (Wojciechowska et al., 2018). In Arabidopsis, 21 days-old autophagy-defective *atg4a4b-1* mutants showed inhibited root elongation after transfer to nitrogen-depleted conditions (Yoshimoto et al., 2004). This may point to a role of autophagy in nutrient recycling in roots even before whole-plant senescence sets in.

With respect to the recycling of cytosolic constituents autophagy can either precede or follow programmed cell death (PCD) that marks the initiation of cellular self-destruction in consequence of developmental signals or adverse growth conditions (Üstün et al., 2017). In fibrous poplar roots, vacuole rupture, which is also indicative for PCD, has been defined as terminal process in root senescence, rendering it difficult to distinguish sharply between PCD and developmentally-induced autophagy as cytological triggers for root senescence (Bagniewska-Zadworna et al. 2014). Based on the observation that transcriptional signatures of developmentally-controlled cell death are distinct from those associated with environmentally-induced cell death, specific promoter-reporter lines have been established that indicate developmental PCD in Arabidopsis (Olvera-Carrillo et al., 2015). Respecting that roots show a high degree of cell-type specificity in autophagy functions (Feng et al., 2022), employing these reporters for in-vivo monitoring of PCD processes bears great potential to elucidate the role of PCD in tissue-specific progression of developmental senescence in roots.

### 1.3.5. Altered phytohormone homeostasis

Phytohormones are endogenous mediators of senescence in various plant organs. In leaves, cytokinins (CKs) and auxin are known to delay the senescence, while jasmonic acid (JA), abscisic acid (ABA), salicylic acid (SA), ethylene and even gibberellins (GA) promote or initiate developmental senescence (Woo et al., 2019). Also enhanced strigolactone production under N or P deficiency has been proposed to accelerate leaf senescence (Yamada and Umehara, 2015). Changes in phytohormone concentrations and transcript levels of the respective phytohormone biosynthesis-related genes have also been reported with progressing root age. In poplar, ABA and jasmonic acid (JA) levels gradually increased during root senescence, while this increase was attributed to their role in secondary processes that may take place during senescence rather than in the onset of this process (Wojciechowska et al., 2020a). Strikingly, in two independent studies involving Poales, root ABA levels marked specifically one time point preceding the onset of senescence symptoms. In *Hordeum vulgare* and *Sparganium emersum,* ABA was the only phytohormone showing a sharp peak that could be associated with the onset or early phase of root or leaf senescence (Liu et al., 2019; Ryser et al., 2020). Together with the observation that cortical senescence was accelerated upon exposure to exogenous ethylene in barley roots (Schneider et al., 2018), ethylene and ABA act prominently as hormonal triggers promoting senescence-related processes in roots.

### 1.3.6. Transcriptional regulation of root senescence

Leaf senescence is regulated at multiple levels, including epigenetic, transcriptional, posttranslational and metabolic control. In this regulatory network, transcriptional activation and repression by transcription factors (TFs) takes in a key role, as TFs take control of senescence-associated genes (SAGs; Woo et al., 2019). The latter comprise of genes predominantly involved in chlorophyll catabolism, hormone response pathways, protein degradation, and lipid or carbohydrate metabolism (Li et al., 2012). Among the major transcriptional regulators are members of the NAC-, WRKY-, C2H2-type zinc finger-, AP2/EREBP- and MYB-type protein families, which can act either as activators or suppressors on SAGs (Buchanan-Wollaston et al., 2005; Shippers, 2015; Woo et al., 2019). Since these TFs are only in part hierarchically organized and by themselves subject to mutual induction or repression, they form a dynamic gene regulatory network (GRN) that effectively integrates multiple

developmental and environmental signals into the developmental program of leaf senescence. Among the NAC-type TFs in Arabidopsis, ORESARA1 (ORE1) and NAC-LIKE ACTIVATED BY AP3/PI (NAP) directly activate several chlorophyll catabolic genes and other SAGs (Qiu et al., 2015). Since ORE1 and NAP are downstream targets of the TF ETHYLENE-INSENSITIVE-3 (EIN3), they compose together an EIN3-ORE1-NAP regulatory module that integrates ethylene into the senescence program in response to developmental or environmental cues (Woo et al., 2019). Also, ABA can be included in this module, e.g. when leaf exposure to dark activates ABSCISIC ALDEHYDE OXIDASE3 (AAO3) via its upstream regulator AtNAP to trigger ABA synthesis and further downstream ORE1 induction. Despite the wealth of data on NAC gene regulation in senescing leaves, NAC gene regulation in roots has been investigated so far almost exclusively under biotic or abiotic stress (Hao et al., 2011; Huang et al., 2015; Chen et al., 2018). Based on transcriptome and qRT-PCR analyses in barley roots, the NAC-type genes *HvNAC3*, *HvNAC5*, *HvNAM1* and *HvNAM2* were all upregulated during senescence (Liu et al., 2019), suggesting that they may exert a regulatory role belowground, similarly as they do in leaves (Distelfeld et al., 2014; Christansen et al., 2016). In this scenario, increasing transcript levels of *HvNACs* upon root aging may activate the ABA biosynthesis genes *HvNCED1* and *HvNCED2* and lead to the observed ABA peak in roots that preceded the expression of morphological and metabolic senescence markers (Liu et al., 2019).

One of the best characterized senescence-regulated TF is WRKY53 in Arabidopsis leaves. In a multilayered regulation that involves histone modification at the chromatin level, transcriptional regulation by several other TFs as well as protein phosphorylation to improve its DNA-binding activity, WRKY53 acts as central hub in the overall senescence regulatory network (Zentgraf and Doll, 2019). Downstream targets of WRKY53 include TFs, also of the WRKY family, stress- or defence-related genes and other SAGs (Miao et al., 2004). Interestingly, Zhao et al. (2020) have shown that in wheat WRKY40-D is upregulated during leaf senescence and acts as a positive regulator in age- or dark-induced senescence. Overexpression of WRKY40-D upregulated the expression of ABA and JA biosynthesis and signaling genes, raising evidence for a WRKY40-D-NCED2-ABA signaling cascade. According to a comparable temporal activation pattern of *WRKYs*, *NCEDs* and ABA, a highly similar signaling cascade may also exist in senescing barley roots (Liu et al., 2019).

In two independent transcriptome studies with barley and poplar roots, gene ontology analysis of deregulated genes revealed ''oxidative stress'' and ''S-adenosylmethionine biosynthetic process'' among the most significant terms arising with root age (Liu et al., 2019; Wojciechowska et al., 2020a). These terms included genes associated with ABA and JA or with the detoxification of reactive oxygen species (ROS), such as catalases or peroxidases. In particular several catalases exhibited a pronounced and continuous upregulation with root age in barley (Liu et al., 2019). In senescing Arabidopsis leaves, WRKY53 and ORS1, an ORE1 paralog that shares many target genes with ORE1, are both involved in ROS signaling during leaf senescence. Both TFs are induced by $H_2O_2$ and accelerate senescence further in presence of $H_2O_2$ (Miao et al., 2004; Balazadeh et al., 2011). Taken together, these pieces of evidence point to a gene regulatory network and downstream signaling cascade in senescing roots that connects WRKY-type TFs with ABA and ROS signaling and is reminiscent of that in senescing leaves.

### 1.4. Aims of this thesis

So far, it has been shown that barley roots undergo senescence like other plant organs. The onset, progression and the completion of root senescence is associated with changes in morphological, physiological, and molecular traits (Liu et al., 2019). However, it remains unclear whether and to what extent the senescence of roots is regulated independently from the shoot or whole plant. Collectively, the present thesis aimed at identifying endogenous regulators of seminal root senescence in barley mainly through genetic and physical manipulation of aging processes in seminal roots. In this sense, the experimental chapters dealt with the following points:

- In grasses, seminal roots are important for early seedling vigor and growth, whereas nodal roots become dominant and responsible for the water and nutrient uptake at later developmental stages. To investigate whether the signal for the onset of seminal root senescence comes from nodal roots, in a hydroponic culture, nodal roots from hydroponically-grown barley were cut off daily and plants were allowed to grow only in the presence of seminal roots. Over a 53-day period senescence-related processes were monitored.

- A sharp accumulation of ABA during the onset of root senescence has been proposed to trigger senescence-associated events in roots (Liu et al., 2019). Since this peak went along with a sharp drop in cytokinins, the hypothesis was raised that root senescence can be accelerated when degrading cytokinins. To understand the role of cytokinins as a physiological signal during the onset of root senescence, transgenic barley lines with root-specific overexpression of Arabidopsis *CYTOKININ OXIDASE/DEHYDROGENASE 2* were grown hydroponically and were monitored for the onset and progression of root senescence.

- Two so far uncharacterized TFs (*HvWRKY53* and *HvMYB15*) have been shown to be strongly upregulated just before the onset of root senescence in barley (Liu et al., 2019). As the expression of these two TFs were found to be highly root-specific, it has been postulated that *HvWRKY53* and *HvMYB15* regulate root senescence. To characterize these TFs and verify their regulatory function, root-specific overexpression and knock-out lines were generated. Transgenic lines were assessed for the dynamics of root growth in a fully-automated high-throughput phenotyping system. Moreover, transgenic lines were grown in soil-filled pots until maturity to evaluate the impact of modulated *HvWRKY53* or *HvMYB15* expression on overall plant performance.

## 2. Materials and Methods

### 2.1. Plant material

In this study, all experiments were performed with spring barley (*Hordeum vulgare* cv. Golden Promise) plants. All transgenic lines were generated in the background of this cultivar. Transgenic lines used in this study include the three independent root-specific overexpression lines of *HvWRKY53* (BG805-derivatives) and *HvMYB15* (BG804-derivatives), three independent CRISPR/Cas9-lines of *HvWRKY53* (BE301-derivatives) and *HvMYB15* (BE204-derivatives) and two independent root-specific overexpression lines of Arabidopsis *CYTOKININ OXIDASE/DEHYDROGENASE 2 (AtCKX2)*.

### 2.2. Selection of candidate genes and generation of transgenic lines

Based on the transcriptome study in Liu et al. (2019), TFs that are upregulated in both apical and basal root zones just before the onset of root senescence were evaluated. In particular, one WRKY-type (HORVU3Hr1G080860, *HvWRKY53*) and one MYB-type TF (*HORVU6Hr1G058580, HvMYB15*) were upregulated one week before the onset of root senescence. Moreover, database search revealed that the expression of both genes is highly root-specific (IPK Barley Blast Server; https://apex.ipk-gatersleben.de/apex/f?p=284:57::::::). Thus, these two TFs were selected as candidate genes involved in the regulation of root senescence in barley.

#### 2.2.1. Generation of vectors for overexpression

To generate overexpression lines of the candidate genes (i.e., HORVU3Hr1G080860, *HvWRKY53; HORVU6Hr1G058580, HvMYB15*), coding sequences of both transcription factors were amplified by polymerase chain reaction (PCR) using a high-fidelity Phusion® polymerase (NEB, USA) (Table 2.1).

The PCR product was then run on a 1 % agarose gel at 120 V for 30 min in 0.5 % TBE (Tris-Borate-EDTA) buffer. Fragments with the expected size were excised from the agarose gel using NucleoSpin™ Gel and PCR Clean-up Kit (Macherey-Nagel) by following the manufacturer's protocol. Extracted fragments were cloned into the pENTR™ /D-TOPO™ vector (Thermo Fisher Scientific, USA). Positive clones were selected by restriction digestion and further confirmed by Sanger sequencing carried

out by an external company (Eurofins, Germany) before generating the overexpression cassette.

**Table 1. Sequences of the primers and conditions used to amplify the coding sequences of the candidate genes *HvWRKY53* and *HvMYB15*.** Each forward primer was designed to bear overhangs at the 3'-end (lowercase) for cloning purposes. F, forward primer; R, reverse primer; bp, base pair.

| Target gene ID | Target gene | Primers | Fragment Size (bp) | Annealing Temperature (°C) |
|---|---|---|---|---|
| HORVU3Hr1G080860 | HvWRKY53 | F: caccATGAGGGGGAGCAGCAT<br>R: CTATTCTACGAACCAACCCAAATCCAA | 771 | 65 |
| HORVU6Hr1G058580 | HvMYB15 | F: caccATGGGGAGGTCTCCTTG<br>R: CTAAATGTGAGACAAACTCTGCACCT | 732 | 63 |

Establishment of the binary overexpression vectors was carried out by Gateway cloning (Reece-Hoyes and Walhout, 2018). The destination vector (pIPKb001_ExpressedProteinPromoter), carrying a root-specific promoter from rice (*Expressed protein; EPP; LOC_Os04g11040*; Ramireddy et al., 2018), was kindly provided by Prof. Dr. Thomas Schmülling (Freie Universität Berlin). Confirmed positive clones were further cloned into the destination vector by LR Clonase II (Invitrogen, USA). Finally, positive binary vectors carrying the gene of interest were selected by restriction digestion and used for the transformation of *Agrobacterium.*

### 2.2.2. Generation of CRISPR/Cas9 vectors

### 2.2.2.1. gRNA design

Guide RNAs (gRNAs) were designed and analyzed using the free-online tool DESKGEN (Doench et al., 2014; 2016; https://www.deskgen.com/). The secondary structure of the selected gRNAs was analyzed using RNAfold (Gruber et al., 2008; Lorenz et al., 2011; http://rna.tbi.univie.ac.at/cgi- bin/RNAWebSuite/RNAfold.cgi). Finally, selected gRNAs were obtained as oligo primers from an external company (Metabion, Germany).

### 2.2.2.2. Vector assembly

Firstly, forward and reverse oligos (100 μM) of each gRNA were annealed at 95 °C for 5 min. To generate a CRISPR/Cas9 vector carrying a single gRNA, annealed oligos were ligated to pSH91 vector, carrying both the rice *OsU3*-promoter and the maize *POLYUBIQUITIN 1* (*ZmUbi1*) promoter to drive the gRNA and *Cas9* expression,

respectively. Positive clones were selected by colony PCR and further confirmed by Sanger sequencing carried out by the company LGC Genomics (Germany). Intermediate vectors carrying the desired gRNAs were further ligated into a binary vector (p6i_d35S_TE9), which was then used for the transformation of *Agrobacterium*.

In parallel, vectors carrying two gRNAs to target a single gene were also generated. Firstly, annealed oligos of each gRNA were cloned into two different vectors (i.e., pIK5 and pIK6). pIK5 and pIK6 carry the *TaU6*-promoter which drives the gRNA expression. Positive clones were then selected by colony PCR followed by Sanger sequencing carried out by the company LGC Genomics (Germany). Both plasmids carrying desired gRNAs were then assembled into a single gRNA module harbored in pIK60. This single module carrying double gRNAs was further assembled with pIK84 carrying xCas9 (Kim et al., 2020) and pIK22 (final assembly vector). Generated vectors were further ligated with the binary vector (p6i_d35S_TE9) to be used for the transformation of *Agrobacterium*.

All vectors and plasmids were kindly provided by Dr. Götz Hensel and Dr. Jochen Kumlehn (IPK Gatersleben).

### 2.2.3. Transformation of *Agrobacterium* by electroporation

Prior to transformation, all binary vectors generated above (Table 2.2) were diluted 1:10. 1 $\mu$l of the desired plasmid was mixed briefly with 50 $\mu$l electro-competent *Agrobacterium tumefaciens* strain AGL-1 cells. This mixture was then transferred to electroporation cuvettes (Bio-rad, USA) and electroporated at 2.5 kV for 2 sec using a Bio-rad Electroporator (Bio-rad, USA). 950 $\mu$l of SOC-medium was immediately added to the mixture, transferred to a reaction tube and incubated at 28 °C for 3 h. Cell cultures were then spread onto selective MG-L plates containing carbenicillin, rifampicin and spectinomycin, and incubated at 28 °C for 2 days. 3-5 colonies were selected to start an overnight liquid culture in 3 ml MG-L medium. On the next day, plasmids were extracted using the GeneJet Plasmid Mini-Prep Kit (Thermo Fischer Scientific, USA) following the manufacturer's protocol. Plasmids were subjected to restriction digestion analysis to confirm the positive cultures.

**Table 2. Summary of binary vectors generated in this study for the transformation of barley.** pEPP, expressed protein promoter; CDS, coding sequence; GE, genome editing.

| Construct ID | Description | Key components | Binary backbone |
|---|---|---|---|
| BG 804 | Overexpression of HvMYB15 | pEPP; HvMYB15-CDS | pIPKb001 |
| BG 805 | Overexpression of HvWRKY53 | pEPP; HvWRKY53-CDS | pIPKb001 |
| BE 201 | CRISPR/Cas9-mediated GE HvWRKY53 | OsU3:gRNA1; ZmUbi-1:cas9 | p6i_d35S_TE9 |
| BE 202 | CRISPR/Cas9-mediated GE HvWRKY53 | OsU3:gRNA4; ZmUbi-1:cas9 | p6i_d35S_TE9 |
| BE 203 | CRISPR/Cas9-mediated GE HvMYB15 | OsU3:gRNA6; ZmUbi-1:cas9 | p6i_d35S_TE9 |
| BE 204 | CRISPR/Cas9-mediated GE HvMYB15 | OsU3:gRNA7; ZmUbi-1:cas9 | p6i_d35S_TE9 |
| BE 301 | CRISPR/Cas9-mediated GE HvWRKY53 | TaU6:gRNA1:gRNA4; ZmUbi-1:xcas9 | p6i_d35S_TE9 |
| BE 302 | CRISPR/Cas9-mediated GE HvMYB15 | TaU6:gRNA6:gRNA7; ZmUbi-1:xcas9 | p6i_d35S_TE9 |

## 2.2.4. Generation of *Agrobacterium* glycerol stocks

Upon confirmation, overnight cell cultures were used to generate the glycerol stocks. 200 $\mu$l of the overnight cell culture ($OD_{600}$=2) was mixed with 20 $\mu$l of 15 % glycerol. The glycerol-cell culture mixture was incubated at room temperature for 3-4 hours and stored at -80°C to be used later for the transformation of barley.

## 2.2.5. Agrobacterium-mediated transformation of immature barley embryos

*Agrobacterium*-mediated transformation of immature barley embryos was performed as described in Hensel et al. (2009).

## 2.2.6. Genetic analysis of primary transformants (T$_0$-plants)

All primary transformants resulting from the transformation events described above were subjected to genetic analysis. To determine the putative overexpression lines and the CRISPR/Cas9 mutants, genomic DNA of each transformant was investigated for transgene insertion by PCR (Table 2.3). Putative overexpression lines then grown in the greenhouse and brought to the next generation after selfing.

Putative CRISPR/Cas9 mutants that were positive for the transgene, *Cas9*, were further analyzed for their genomic sequence of the target gene. The target sequence of each positive transformant was amplified using the high-fidelity Phusion polymerase (NEB, USA) and sequenced by an external company (LGC Genomics, Germany). Obtained sequences and chromatograms were visualized and evaluated using

SnapGene (Dotmatics, USA). A noisy chromatogram of the target region was accepted as an indicator for a heterozygous or chimeric mutation and thus, these plants were brought to the next generation by selfing.

**Table 3. Summary of the investigated genes for the identification of transgenic lines generated in this study.** hpt, hygromycin phosphotransferase; Cas9, CRISPR-associated 9; F, forward primer; R, reverse primer; bp, base pair.

| Target gene | Primers | Description | Fragment Size (bp) | Annealing Temperature (°C) |
|---|---|---|---|---|
| hpt | F: TTTAGCCCTGCCTTCATACG<br>R: GATTCCTTGCGGTCCGAATG | Molecular marker for T-DNA insertion | 1000 | 55 |
| cas9 | F: TTTAGCCCTGCCTTCATACG<br>R: TTAATCATGTGGGCCAGACC | Molecular marker for T-DNA insertion | 734 | 55 |
| HvWRKY53 | F: ACGAGCCAAAGGATCGATCA<br>R: CCGACACGTGCCTTCCTATT | Cas9-target sequence of HvWRKY53 | 462 | 65 |
| HvMYB15 | F: GTCAACACACTGAGCAATCC<br>R: TGGCGGCAATGGTGGACCAT | Cas9-target sequence of HvMYB15 | 374 | 63 |

## 2.2.7. Genetic analysis of T$_1$ generation

Roughly 30 progenies from each primary transformant (T$_0$) were grown in the greenhouse and used for genomic DNA isolation. Firstly, plants were investigated for the transgene, *Cas9*, by PCR. Those plants that had lost the transgene were further analyzed for the target sequence by sequencing. Chromatograms were firstly evaluated to identify homozygous mutations. Modified sequences of the target gene were aligned against the wild-type sequence using the online multiple sequence alignment tool Clustal Omega (EMBL-EBI; https://www.ebi.ac.uk/Tools/msa/clustalo/). Then, nucleotide sequences were translated into protein sequences using the freeware Expasy (SIB Swiss Institute of Bioinformatics; https://web.expasy.org/translate/) and were aligned against wild-type protein of interest. CRISPR/Cas9 mutants carrying the desired modifications that resulted in the synthesis of truncated or non-functional proteins in the target gene were selected to be used further for physiological analyses and brought to the next generation by selfing.

Around 15 progenies of each individual primary transformant ($T_0$), were grown in the greenhouse and used for genomic DNA extraction. Since overexpression lines were expected to be in a heterozygous state, progenies were again confirmed for the presence of the transgene *Hpt* and were brought to the next generation by selfing.

### 2.2.8. Genetic analysis of $T_2$ and $T_3$ generation

Throughout this study, seeds from the $T_2$ generation of the CRISPR/Cas9 mutants were used for physiological analyses. Although homozygous lines were already identified during the $T_1$ generation, target genes from all $T_2$ plants used for physiological analyses were again sequenced for confirmation.

Plants from the $T_2$ generation of overexpression lines were grown in the greenhouse and were used for genomic DNA isolation. These plants were investigated for the segregation pattern of the transgene *Hpt*. Only those plants that showed a 3:1 segregation pattern were selected to be grown further until maturity. To confirm homozygosity, 30 progenies of the $T_2$ plants were again grown and analyzed for the presence of the transgene *Hpt*. $T_3$ plants (100 % presence of *Hpt*) were used for physiological analyses throughout this study. In each experiment, genomic DNA was used to confirm the transgene integration. Additionally, gene expression levels of the target genes *HvWRKY53* or *HvMYB15* were assessed by quantitative real-time PCR (qPCR).

### 2.3. Experimental design and plant culture

### 2.3.1. Hydroponic experiments

### 2.3.1.1. Seminal root growth and development in the absence of nodal roots

Barley (*Hordeum vulgare* cv. Golden Promise) seeds were surface sterilized in 40 % sodium hypochlorite solution for 15 min and then washed with distilled water twice. Sterilized seeds were stratified on a wet tissue paper at 4°C for 5 days. Then, germinated seedlings were transferred to vermiculite and cultured for 6 days in the climate chamber under following conditions:

Temperature: 20°C/16°C - day/night
Photoperiod: 16h/8h - light/dark

Humidity: 70%

Light intensity: 250 $\mu$mol m$^{-2}$ s$^{-1}$

Young seedlings were then transferred to 5 L pots containing 2 mM $Ca(NO_3)_2$, 1 mM $K_2SO_4$, 0.5 mM $MgSO_4$, 0.1 mM $KH_2PO_4$, 0.1 mM KCl, 1 µM $H_3BO_3$, 0.5 µM $MnSO_4$, 0.5 µM $ZnSO_4$, 0.2 µM $CuSO_4$, 0.01 µM $(NH_4)_6Mo_7O_{24}$ and 0.1 mM Fe-EDTA. The nutrient solution was constantly aerated and renewed every 3 to 4 days.

To monitor the developmental changes in aging roots, starting from 18 DAS (days after sowing), plants were harvested once every week until 53 DAS. Starting from ~ 21 DAS, newly emerging nodal roots were cut off daily to investigate the aging-related processes in seminal roots in the absence of nodal roots. Plants were subjected to $^{15}$N-labelled nitrogen influx assays as described below during each harvesting. Different tissues (i.e., shoots, 4$^{th}$ leaf, seminal roots and nodal roots) were harvested separately for further analysis.

### 2.3.1.2. Aging-related processes in transgenic barley lines with root-specific overexpression of cytokinin oxidase/dehydrogenase

To investigate the phytohormonal regulation of aging-related processes in roots, transgenic barley (*Hordeum vulgare* cv. Golden Promise) lines were used with root-specific overexpression of cytokinin oxidase/dehydrogenase (*pEPP:AtCKX2*) (Ramireddy et al., 2019). T$_3$-seeds were kindly provided by Prof. Dr. Thomas Schmülling (Freie Universität Berlin) and were used for further seed amplification and subsequent analysis. Transgenic barley lines were monitored and assessed using the same experimental conditions as described in 2.3.1.1..

### 2.3.2. Soil/pot experiments

Transgenic lines generated throughout this study (i.e. overexpression lines and CRISPR/Cas9 mutants of *HvWRKY53*) were pre-cultured in a peat-based, moderately-fertilized substrate (Substrate 1, Klasmann-Deilmann GmbH, Geeste, Germany) in the climate chamber under a 14°C/12°C - day/night, and 14h/10h - light/dark regime for two weeks. Young seedlings were then transferred to 2.5 L pots containing standard cereal soil mix, consisting of a peat-based, moderately-fertilized soil (Substrate 2, Klasmann-Deilmann GmbH, Geeste, Germany) compost and sand

at a ratio of 2:2:1, fertilized with Plantacote Depot 4M (Manna, Germany) and grown in the greenhouse under a 18°C /16°C - day/night and 16h/8h - light/dark regime until maturity. At different developmental stages, plants were assessed for growth parameters (i.e., plant height, tiller number, heading, flowering). Around heading (BBCH 55), the 4th leaf from the top of each plant was collected. To allow the spikes to dry completely, later stages of maturation (BBCH 97-99) took place under a 21°C /19°C - day/night and 16h/8h - light/dark regime. Different tissues (spikes, flag leaf, rest of the shoot) of fully matured barley plants were harvested separately for further analysis.

### 2.3.3. Mini-rhizotron experiment

Different transgenic lines (i.e., overexpression lines and CRISPR/Cas9 mutants of *HvWRKY53*) along with the wild-type barley (*Hordeum vulgare* cv. Golden Promise) were germinated on a wet tissue paper at room temperature overnight. On the next day, germinated seedlings with visible radicle and hypocotyl were placed into mini rhizoboxes (W x L x D: 26cm x 40cm x 1.5cm) filled with approx. 0.850 kg of Substrate 1 (Klasmann-Deilmann GmbH, Geeste, Germany). Rhizoboxes were placed in a greenhouse and plants were grown under a 18°C /16°C - day/night and 16h/8h - light/dark regime. Through slanted positioning of the rhizoboxes, the roots were forced to grow along the transparent front glass (Figure 2).
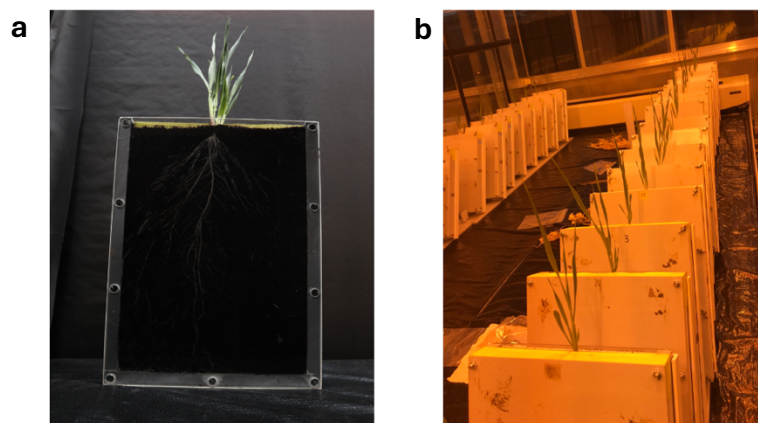


**Figure 2. Rhizobox system used to monitor root growth and development in real-time. (a)** Soil-filled rhizoboxes consisting of an acrylic front glass used to monitor the root growth and development. **(b)** Slanted positioning of the rhizoboxes to force root growth along the transparent front glass.

Root growth was monitored manually by tracing and measuring every newly formed and grown root proportion daily. Rhizoboxes were scanned using a scanner (Epson Expression 10000XL, EPSON, Japan) at 23 DAS, when the root tips have started to touch the bottom of the rhizobox before starting to overgrow. Following scanning, seminal root tips were collected separately, immediately frozen and stored at -80° for RNA extraction and gene expression analysis. Rest of the roots were collected, washed off and allowed to dry at 65°C for a week. Whole shoots were collected for mineral element analysis.

### 2.3.4. Rhizotron experiment

Different transgenic lines (i.e., overexpression lines and knock-out mutants of *HvWRKY53* and *HvMYB15*) along with the wild-type barley (*Hordeum vulgare* cv. Golden Promise) were germinated on wet tissue paper at room temperature overnight. On the next day, germinated seedlings with visible radicle and hypocotyl were placed into rhizotrons (W x L x D: 60cm x 90cm x 5cm) filled with 10 kg Potgrond® (Klasmann-Deilmann GmbH, Geeste, Germany) substrate in the PhenoSphere, IPK Gatersleben (20°C/14°C - day/night). Through both slanted positioning of the rhizotrons and the narrow body (depth: 5 cm), roots were forced to grow along the transparent front disc, allowing monitoring of root growth in real-time. Daily imaging of the rhizotrons and the irrigation were carried out by two identical imaging towers in a fully automated manner. At 55 DAS, rhizotrons were opened to collect fresh seminal and nodal root tips for RNA extraction and subsequent gene expression analysis. Rest of the roots were dug out from the soil and washed off. Shoots and washed roots were dried at 65°C for a week and dry weights were recorded. Shoots were further analyzed for mineral elements.

### 2.3.5. $^{15}$N-labelled nitrogen influx assay

To monitor the root activity with progressing tissue age, hydroponically grown barley lines were subjected to $^{15}$N-labelled nitrogen influx assays once every week over approx. 53 days. First, roots were rinsed in 1 mM $CaSO_4$ solution for 1 min. Then, roots were placed in nutrient solution containing 1 mM $K^{15}NO_3$, 0.5 mM $K_2SO_4$, 0.5 mM $MgSO_4$, 0.1 mM $KH_2PO_4$, 0.1 m M KCl, 1 μM $H_3BO_3$, 0.5 μM $MnSO_4$, 0.5 μM $ZnSO_4$, 0.2 μM $CuSO_4$, 0.01 μM $(NH_4)_6Mo_7O_{24}$ and 0.1 mM Fe-EDTA for 10 min followed by washing of the roots again in 1 mM $CaSO_4$ solution 1 min. Subsequently,

the 4th leaf, rest of the shoots, seminal roots and nodal roots were harvested separately in liquid nitrogen and stored at –80°C until further analysis.

## 2.3.6. Gene expression experiments

To validate root-specific expression of *HvWRKY53* and *HvMYB15*, WT barley plants were grown in soil-filled pots in greenhouse under a 18°C /16°C - day/night and 16h/8h - light/dark regime. Different tissues including whole roots, old leaf blade, old leaf sheath, flag leaf blade, flag leaf sheath, 1st node, 3rd node, 5th node, grains, rachis and caryopses were collected and used to determine *HvWRKY53* and *HvMYB15* expression in different tissues with different developmental tissue age. In parallel, WT plants were grown in a hydroponic solution for 15 days as described in 2.3.1.1. To check whether *HvWRKY53* and *HvMYB15* expression is induced by different phytohormones or abiotic stress factors, plants were treated with ABA, PEG, NaCl for 48 hours. Moreover, N and P deficiency was induced by removing N or P sources from the nutrient solution. Root samples were collected after 0, 3, 24 and 48 hours after treatment for the determination of gene expression levels.

## 2.4. Analysis

## 2.4.1. Isolation of genomic DNA

### 2.4.1.1. Waite method

To extract genomic DNA, around 8-10 cm of leaf blades from 10-15 days-old barley plants were cut into small pieces, placed in a 2 ml reaction tube and immediately frozen in liquid nitrogen. Frozen material was homogenized into fine powder using a Retsch mill (MM400, Retsch, Germany). Leaf powder was then suspended in 800 $\mu$l extraction buffer. Then, 800 $\mu$l phenol:chloroform:isoamyl alcohol (25:24:1) was added. The mixture was centrifuged at 5000 rpm for 3 min. The upper phase was transferred into a new reaction tube and mixed with 80 $\mu$l 3 M sodium acetate (pH 5.2). After the addition of 800 $\mu$l isopropanol, the tubes were gently inverted and centrifuged at 13000 rpm, 4°C for 10 min. The pellet was then resuspended in 800 $\mu$l 70 % ethanol and again centrifuged at 13000 rpm, 4°C for 1 min. Finally, the pellet was allowed to dry at room temperature for 30 min and then resuspended in 100 $\mu$l R40.

### 2.4.1.2. 96-well method

To isolate gDNA from larger number of plants, another extraction method in a 96-well plate was adopted as described in Stein et al. (2001).

### 2.4.2. Gene expression analysis

### 2.4.2.1. RNA extraction

Around 30 mg of homogenized fresh root material was used to isolate RNA using NucleoSpin RNA Plant (Macherey-Nagel, Germany) following the manufacturer's protocol. Subsequently, RNA concentration and quality was measured and evaluated using NanoDrop 2000c spectrophotometry (Thermo Fischer Scientific, USA).

### 2.4.2.2. cDNA synthesis

1 $\mu$g of total RNA was used to synthesize cDNA using GoScript Reverse Transcriptase (Promega, USA) according to manufacturer's instructions.

### 2.4.2.3. qPCR assay

cDNA samples were subjected to quantitative real-time PCR (qPCR) to monitor the changes in gene expression levels. In a 384-well plate system, 2 $\mu$l of 1:20 diluted cDNA was mixed with 5 $\mu$l 2x iQ SYBR Green Mastermix (Bio-rad, USA), 0.9 $\mu$l gene-specific forward primer (10 mM), 0.9 $\mu$l gene-specific reverse primer (10 mM) and 1.2 $\mu$l distilled water. The PCR reaction was then run using a CFX384 Touch Real-Time PCR System (Bio-rad, USA) under following conditions: 3 min at 95 °C (1x), 15 sec at 95 °C followed by 30 sec 58 °C (40x), and a melting curve cycle from 65 to 95 °C in 5 sec (0.5 °C increment).

Resulting $C_t$ values were evaluated by calculating the PCR amplification efficiency and normalization factors using *ADP* and *UBQ* as reference genes. Normalization factors were obtained by geNORM (Vandesompele et al., 2002). Relative changes in the gene expression were then calculated as described in Pfaffl (2001).

### 2.4.4. Measurement of soluble sugars

Concentrations of soluble sugars were determined as described in Ahkami et al. (2009). 50 mg of homogenized fresh root material was suspended in 0.75 ml 80% (v/v) ethanol and incubated at 80 °C for 60 min followed by the centrifugation at 14000 rpm

for 5 min at 4 °C. The supernatant was concentrated using a speed vacuum concentrator at 45 °C for 3 hours. The pellet was resuspended in 0.3 ml HPLC-grade water and shaken for 15 min at 4 °C. Then, 10-20 $\mu$l was mixed with 280-290 $\mu$l buffer (100 mM imidazole-HCl, pH 6.9, 5 mM $MgCl_2$, 2 mM NAD and 1 mM ATP). Finally, 1 $\mu$l glucose 6-phosohate dehydrogenase was added to each sample. Using a microplate reader, the baseline was recorded for 15 min, and then 1 $\mu$l hexokinase was added to measure glucose. To determine fructose, 1 $\mu$l phosphoglucoisomerase was added, when the maximum OD was reached. Finally, sucrose was measured after the addition of 2 $\mu$l invertase.

### 2.4.5. Measurement of phytohormones

Phytohormones were extracted as described in Šimura et al. (2018). Frozen seminal roots were homogenized into fine powder. Around 30 mg of homogenized fresh root material was weighed into a 2 ml reaction tube along with two 3 mm zirconium oxide beads and resuspended in 1 ml 50% acetonitrile containing the internal standards. Then, samples were sonicated at 4°C for 3 min using a Sonorex ultrasonic bath (BANDELIN Electronic GmbH, Germany). Samples were shaken at room temperature for 30 min using a Reax 32 overhead shaker (Heidolph Instruments GmbH, Germany). Finally, samples were centrifuged at 14000 rpm, 4°C for 10 min. The supernatant was then transferred to a new reaction tube. The purification of the samples was performed by using solid-phase extraction columns, which were firstly rinsed with 1 ml 100 % methanol, then with 1 ml of de-ionized water and finally equilibrated with 50 % acetonitrile. Samples were loaded onto columns and the flow-through was collected. Then, columns were rinsed again with 1 ml 30 % acetonitrile and the flow-through was collected in the same tube. Collected flow-through was then allowed to evaporate until dry in reaction tubes. Dried pellets were dissolved in 40 $\mu$l 30 % acetonitrile and used to measure phytohormone levels using an ACQUITY Ultra-Performance LC system coupled with a Xevo TQ mass spectrometer (Waters, USA) as described in Eggert and von Wirén (2017).

### 2.4.6. Light microscopy

To examine seminal root anatomy during growth and development, 0.5-1 cm long root segments were cut 20 cm under the hypocotyl and stored in 70 % ethanol. Segments were then embedded in 3 % agar and sliced horizontally into 100-150 $\mu$m thin pieces

using a vibratome (Carl Zeiss, Germany). Root cross-sections were visualized under a light microscope (Axio Imager 2, Carl Zeiss, Germany).

### 2.4.6. Mineral element analysis

For the mineral element analysis, tissues to be analyzed (i.e., flag leaves, shoots) were allowed to completely dry off at 65°C for a week following harvest. Dried material was then homogenized and ground into fine powder using a mixer mill (MM400, Retsch, Germany). 15 mg of each sample (or 50 mg of unprocessed seeds) w then weighed into PTFE digestion tubes, digested in 2 ml 65 % nitric acid ($HNO_3$) using a high-performance microwave reactor (Ultraclave 4, MLS GmbH, Germany) and then brought to a final volume of 15 ml by adding de-ionized water. Nutrient concentrations were determined by inductively coupled plasma optical emission spectrometry (iCAP 6500 dual OES spectrometer, Thermo Fisher Scientific Inc., USA).

### 2.4.7. Determination of $^{15}N$

Freeze-dried samples were homogenized into fine powder using a mixer mill (MM400, Retch GmbH). 1.5 mg of homogenized plant material were weighed into tin foils and used to determine $^{15}N$ concentration by isotope ratio mass spectrometry (Horizon, NU Instruments).

### 2.4.8. Root image analysis

### 2.4.8.1. Semi-automated root image analysis

Root scans of the mini-rhizotron experiment described above were analyzed by the semi-automated root image analysis (saRIA) software (Narisetti et al., 2019). Due to low contrast imaging, generated scans were converted into enhanced segmented images by the Image Analysis Group, IPK Gatersleben.

### 2.4.8.2. Fully automated root image analysis

Images of the rhizotron experiment described above were analyzed by Image Analysis Group, IPK Gatersleben using fully automated root image analysis (faRIA) software (Narisetti et al., 2021).

### 2.4.9. Analysis of seed parameters

Grains obtained from the pot experiment described above were used to analyze the seed properties of the transgenic lines. Approximately 100-150 seeds were randomly

selected and analyzed using the MARVIN ProLine I Seed Analyzer (Marvitech GmbH, Germany).

### 2.4.10. Phylogenetic Analysis

Protein sequences from the barley reference genome (Morex_V2) were downloaded from the Ensembl database (https://plants.ensembl.org/Hordeum_vulgare/Info/Index). The 'blastp' command from the command-line tool BLAST+ was then used to identify all coding regions containing the conserved domain sequence of the protein family of interest (i.e., WRKY or MYB). Resulting proteins were further filtered to remove duplicates. Obtained unique protein sequences were then used for sequence alignment and construction of a phylogenetic tree. A phylogenetic tree was generated using the neighbor joining method via the online tool Clustal Omega (https://www.ebi.ac.uk/Tools/msa/clustalo/). The resulting output file was then used to create the cladogram using the ITOL website (https://itol.embl.de/).

To identify orthologues of *HvWRKY53* and *HvMYB15* in other species (*Arabidopsis thaliana* and *Oryza sativa*), protein sequences of the reference genomes from *Arabidopsis thaliana* (https://www.arabidopsis.org/download/index-auto.jsp?dir=%2Fdownload_files%2FSequences) and *Oryza sativa* (http://rice.uga.edu) were investigated for conserved domain sequences of the protein family of interest (i.e., WRKY or MYB). Identified protein sequences of each gene family from Arabidopsis, rice and barley were then used to construct a phylogenetic tree using Clustal Omega.

### 2.4.11. Promoter Analysis

To identify *cis*-acting elements that might be important for gene regulation, promoter sequences of *HvWRKY53* and *HvMYB15* were extracted from Ensembl Plants (https://plants.ensembl.org/index.html) and analyzed for important motifs using the online databases PLACE (Higo et al., 1999; http://www.dna.affrc.go.jp/htdocs/PLACE/) and PlantCARE (Lescot et al., 2002; https://bioinformatics.psb.ugent.be/webtools/plantcare/html/)

### 2.4.12. Statistical Analysis

To compare significant differences among multiple means, results were evaluated for normal distribution and then by either one- or two-way analysis of variance (ANOVA)

and a subsequent Tukey's post-hoc test at p<0.05. The statistical significance between two groups was determined by two-tailed Student's $t$ test. Nonparametric pairwise comparison by the Wilcoxon method was applied to all data, which did not show a normal distribution. All statistical analyses were performed on a statistics software JMP Pro 17 (JMP Statistical Discovery LLC, USA).

## 3. Results

### 3.1. Manipulation of senescence-associated processes in seminal roots

### 3.1.1. Seminal root senescence as affected by the removal of nodal roots

To investigate the relationship between nodal root growth and development and aging-related processes of seminal roots, barley plants were grown hydroponically for 53 days, and the nodal roots were removed daily by cutting them off early from their emergence on, i.e. from 21 DAG (days after germination) onwards. Seminal roots, nodal roots and shoots were separated and harvested weekly.
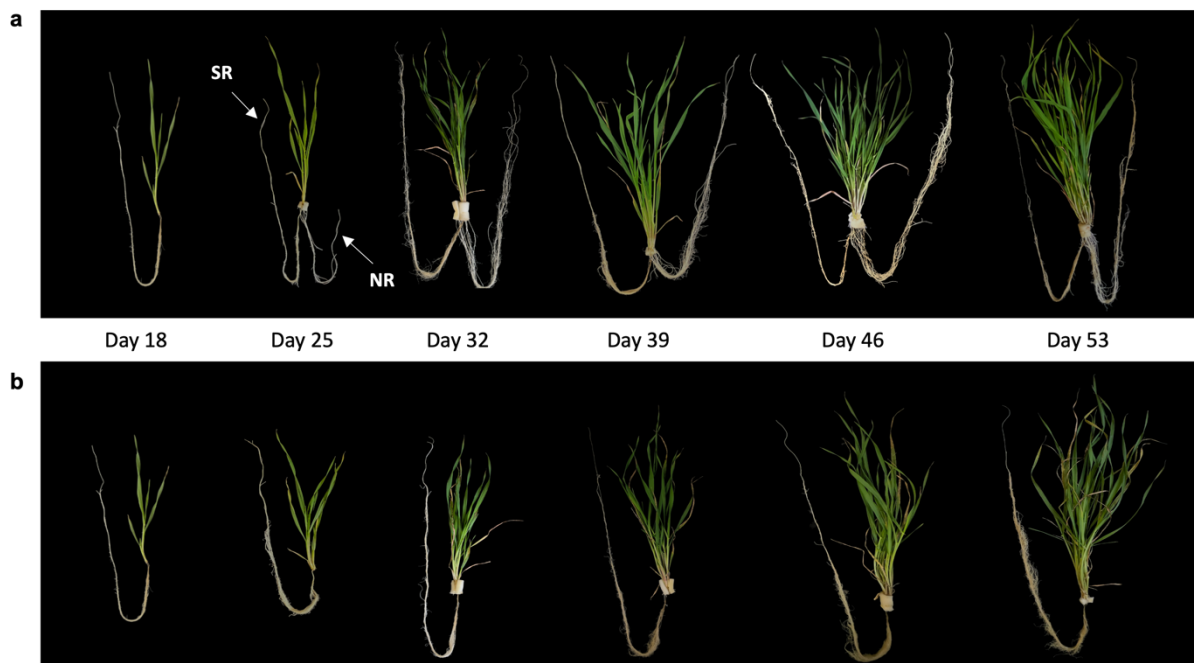


**Figure 3. Root and shoot phenotypes as affected by removal of nodal roots. (a, b)** Visual appearance of barley (cv. *Golden Promise*) plants grown hydroponically under control conditions over 53 days. In **(b)**, plants were allowed to grow only in the presence of seminal roots (SR) through daily removal of nodal roots (NR) from their emergence onwards (i.e., 21 days after germination). SR are placed on the left and NR on the right side.

The first nodal root emerged on 21 DAG (Figure 4.a) and starting from 32 DAG, an exponential increase in nodal root biomass began to appear (Figure 4.b). Removal of nodal roots did not have a significant impact on aboveground plant growth, and shoot biomass remained highly similar (Figure 4.c). Tillering started at around 25 DAG and the removal of nodal roots did neither affect the onset of tillering nor the number of tillers produced (Figure 4.d).
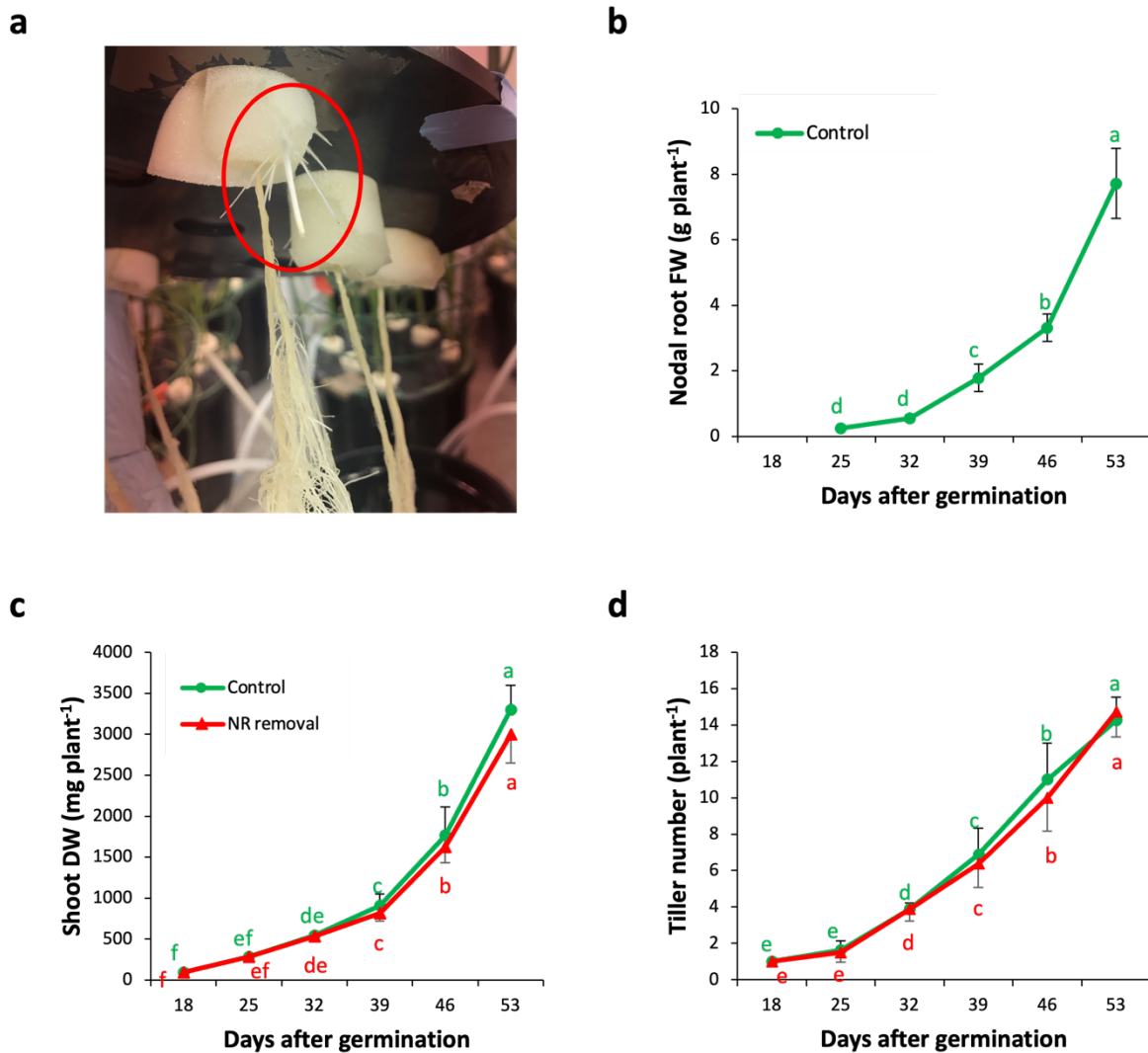
**Figure 4. Plant development after removal of nodal roots. (a)** Newly emerging nodal roots (marked by red circle) were removed daily (NR removal) starting from their emergence on (i.e., 21 days after germination). **(b)** Nodal root fresh weight (FW) of barley plants from control treatments with progressing tissue age. **(c-d)** Shoot dry weight (DW) **(c)** and tiller number **(d)** without (green) or with removal (red) of nodal roots. Symbols show means ± SD (n=7-11 biological replicates). Different letters indicate significant differences between means according to one- **(b)** or two-way ANOVA **(c-d)** followed by Tukey's test at $p<0.05$.

In control plants, the increase in seminal root biomass and elongation leveled off starting from 39 DAG on (Figure 5.a, b), coinciding with the rapid proliferation of the nodal roots (Fig 4.b). Interestingly, removing nodal roots increased seminal root biomass beyond the level of control plants and led to almost 2-fold higher biomass at 53 DAG (Figure 5.a). Moreover, seminal roots continued to elongate significantly in the absence of nodal roots even after 39 DAG (Figure 5.b). A closer look at the seminal root tips revealed that the root tips started degrading from 39 DAG (Figure 5.c). At 53 DAG, the proportion of degraded seminal root tips reached to 51%. Remarkably, removing nodal roots decreased the proportion of degraded seminal root tips by up to 28% at 53 DAG (Figure 5.c), which suggests a prolonged activity of the seminal root meristem. Taken together, continued biomass increase and the higher proportion of the intact root apices in the absence of nodal roots imply extended developmental life span of seminal roots.

To investigate the impact of removing nodal roots on seminal root architecture, seminal roots were collected, combed, and scanned individually after 10 days of consecutive removal of nodal roots, i.e. at 31 DAG. Due to the low contrast of the root scans, original scans were converted into enhanced black/white images (Figure 6.a, b) enabling the root skeleton to be detected by the image analysis software. Indeed, removal of nodal roots increased total root length, root area and total root volume by 1.5-fold when expressed in pixel numbers (px) (Figure 6.c, d, e). A closer glimpse at the root images revealed that the removal of nodal roots increased the number of 1st-order lateral roots significantly by 36 % (Figure 6.f). More importantly, the number of 2nd-order lateral roots increased by 180% (Figure 6.g) and 3rd-order lateral roots started to emerge (Figure 6.h). Taken together, removal of nodal roots enhanced lateral root branching in seminal roots, and this was reflected in higher total root length, area, volume, and biomass (Figure 5.a, 6.c, d, e).
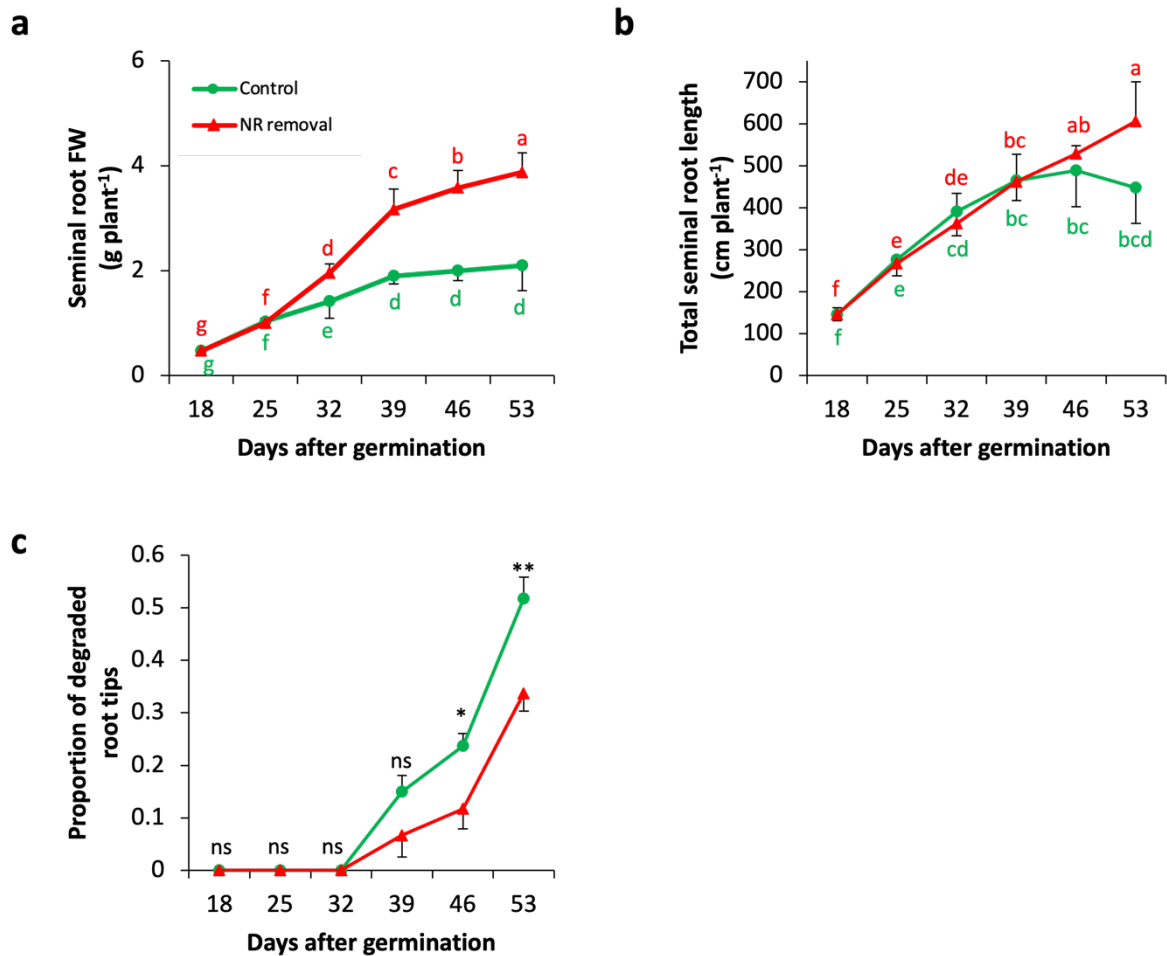
**Figure 5. Seminal root growth as affected by the removal of nodal roots. (a-b)** Total seminal root fresh weight (FW) **(a)** and total seminal root length **(b)** with progressing plant age. **(c)** Proportion of degraded tips of seminal roots, which refers to the ratio of the number of degraded seminal root tips to the total number of seminal root tips. Barley plants were grown hydroponically, and the nodal roots were removed daily from their emergence on (i.e. 21 days after germination) (NR removal, red). Symbols show means ± SD (n=8). Different letters indicate significant differences between means according to two-way ANOVA followed by Tukey's post-hoc test at p<0.05. In **(c)**, asterisks denote significant differences between control and treatment at ∗ P < 0.05 or ∗∗ P < 0.01 by two-tailed Student's *t* test. ns, not significant.

**Figure 6. Impact of continuous removal of nodal roots on architectural traits of barley seminal roots. (a-b)** Representative images of individual seminal roots from control **(a)** and treatment **(b)** groups. Treatment refers to the daily removal of nodal roots (NR removal) for 10 consecutive days from their emergence on (i.e., 21 days after germination). **(c-e)** Root traits collected at 31 days after germination. Total length **(c)**, root area **(d)** and total volume **(e)** measured by saRIA software (Narisetti et al., 2019) in pixels using the enhanced segmentation images from **(a)**. **(f)** Number of first-order lateral roots. **(g)** Number of second-order lateral roots. **(h)** Number of third-order lateral roots. Hydroponically grown plants were harvested, seminal roots were combed, scanned individually and subjected to morphological analysis. Bars show means ± SD (n = 5). Asterisks denote significant differences between control and treatment at ∗ P < 0.05, ∗∗ P < 0.01 or ∗∗∗ P < 0.001 by two-tailed Student's *t* test.

Figure is shown on the next page.
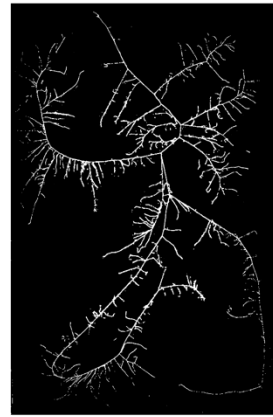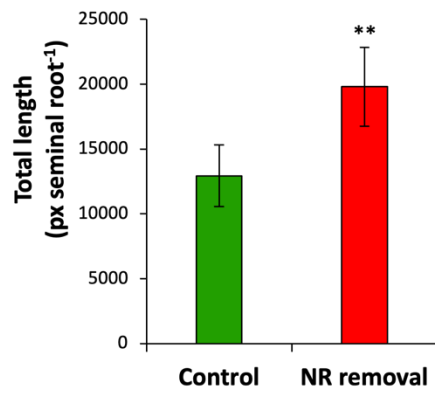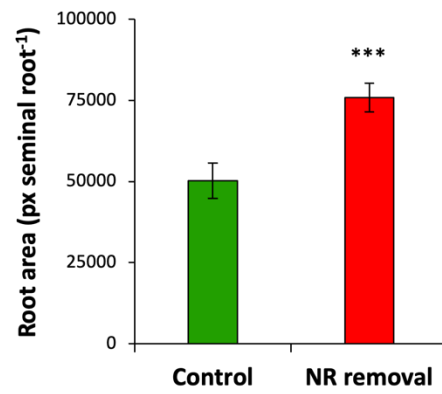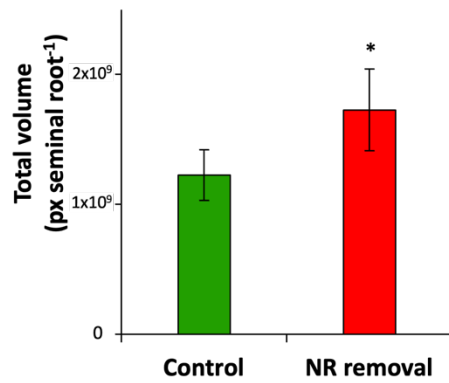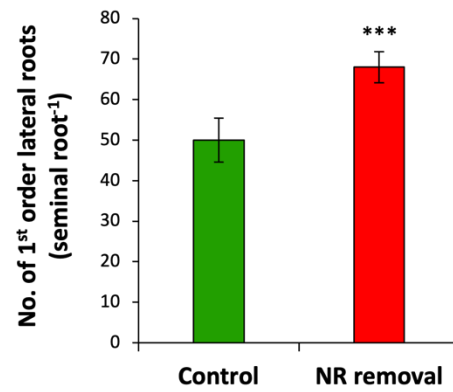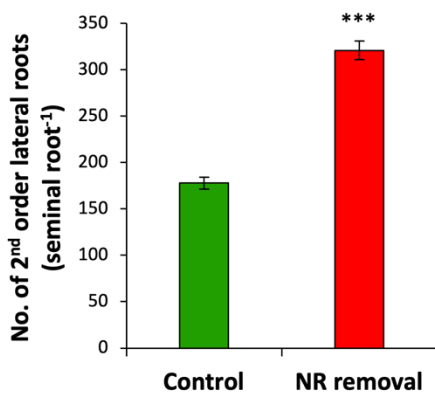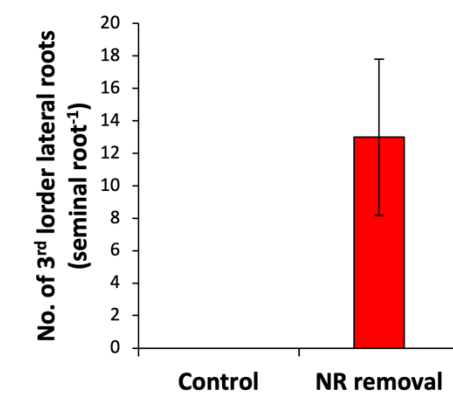
To monitor changes in seminal root activity in the absence of nodal roots, barley plants were subjected to a short-term influx assay using $^{15}$N-labelled $NO_3^-$ once every week, as an adequate nutrient acquisition from the rhizosphere highly depends on the physiological status of the roots. Under control conditions, seminal root N uptake capacity remained constant until 39 DAG but showed a steady decline afterwards (Figure 7). In contrast, in the absence of nodal roots, seminal root N uptake capacity remained constant over time with a slight increase at 53 DAG. This nodal root removal-induced increase in the nutrient uptake capacity suggests that in the absence of nodal roots, seminal root physiological activity can be sustained for a longer period of time.
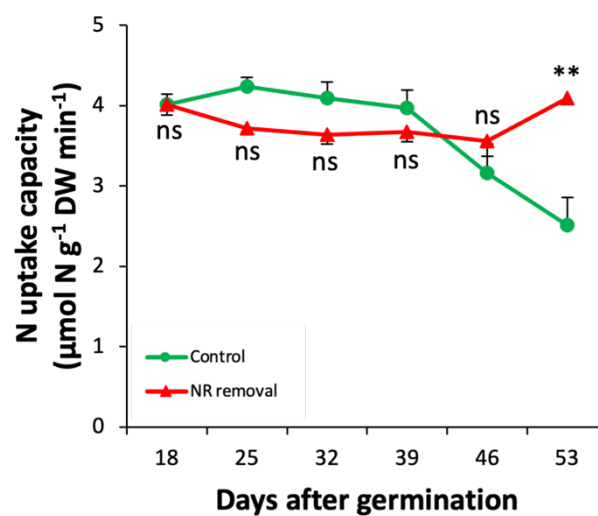


**Figure 7. Nutrient uptake capacity of seminal roots as affected by the removal of nodal roots.** Temporal changes in the nitrogen uptake capacity of seminal roots from control (green) and treatment (red) groups. Here, treatment refers to the daily removal of nodal roots from their emergence on (i.e., 21 days after germination). Barley plants were subjected to an $^{15}$N-labeled nitrate-influx assay once every week to monitor the changes in the root activity over time. Roots were exposed to 1 mM $^{15}$N-labeled $KNO_3^-$ for 10 min. Symbols show means ± SE (n=5). Asterisks denote significant differences between control and treatment at ∗∗ P < 0.01 by two-tailed Student's $t$ test. ns, not significant.

To address the question whether a lower root energy status was a cause for the changes in the root activity, soluble sugar concentrations in the seminal roots were determined, as sugars are required for ATP production and sustained root activity. Under control conditions, glucose concentrations gradually declined over time (Figure 8.a). Moreover, fructose and sucrose concentrations dropped sharply at 25 DAG (Figure 8.b, c), but remained at similar levels thereafter. Interestingly, removal of nodal roots had almost no effect on the soluble carbohydrate levels in the seminal roots (Figure 8).

To assess the phytohormonal homeostasis and to what extent it is influenced by the removal of nodal roots, an attempt was made to profile hormones in the seminal roots. Unexpectedly, most of the hormones and their conjugates fell below the quantification limit. Among the quantifiable phytohormones, isopentenyl adenine-riboside (iPR) and cis-zeatin riboside (cZR) concentrations decreased in control plants (Figure 9.a, b). Removal of nodal roots led to higher iPR concentrations especially at earlier time points, while the temporal profile over time was similar to that of control plants. *cis-zeatin-riboside* (cZR) concentrations, on the other hand, were maintained at relatively higher levels after 39 DAG in the absence of nodal roots (Figure 9.b), which might result from the prolonged activity in the root meristem. Overall, auxin (IAA) levels gradually declined over time under control conditions and remained unaffected by the removal of nodal roots (Figure 9.c). Salicylic acid (SA), a positive regulator of leaf senescence in Arabidopsis (Guo et al., 2021), accumulated gradually up to 2.5-fold until 53 DAG under control conditions (Figure 9.d). Interestingly, in the absence of nodal roots, SA concentrations remained constant over time, suggesting that this may be a consequence of delayed progression of root senescence.

Abscisic acid (ABA) was of particular interest since a sharp peak in ABA levels was observed coinciding with the onset of root senescence in barley, which was postulated to act as a physiological signal driving senescence-related processes (Liu et al., 2019). Supposing that the lifespan of seminal roots will increase in the absence of nodal roots, it was expected that the accumulation of ABA may be delayed. As ABA and its derivatives including the degradation forms phaseic acid (PA) and diphaseic acid (DPA) could not be detected, the transcript levels of genes involved in ABA biosynthesis and catabolism were assessed. In control plants, transcript levels of *HvNCED1* and *HvNCED2* peaked on day 32, and while *HvNCED1* mRNA levels dropped thereafter, those of *HvNCED2* remained at an elevated level (Figure 10.a, b). By contrast, after nodal root removal transcript levels of *HvNCED1* and *HvNCED2* were toned down and peaked one week later. Likewise, transcript levels of *ABSCISIC ACID 8'-HYDROXYLASE-1* (*HvABA8'OH-1*) and *HvABA8'OH-3* were also slightly lower after nodal root removal whereby the time-dependent trend remained similar (Figure 10.c). These results indicated that the removal of nodal roots suppressed both, timely ABA biosynthesis and its degradation.
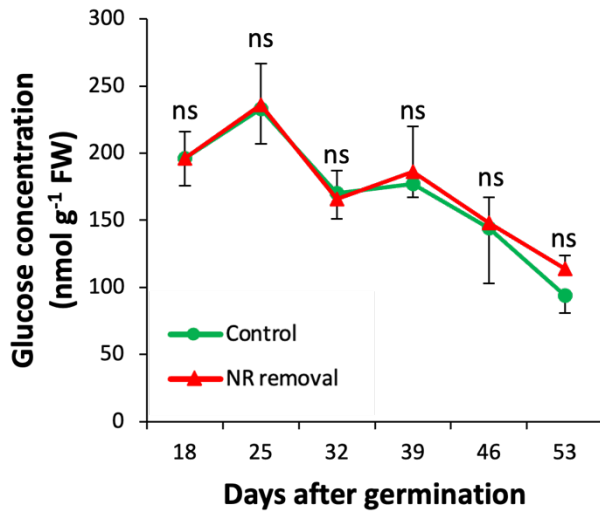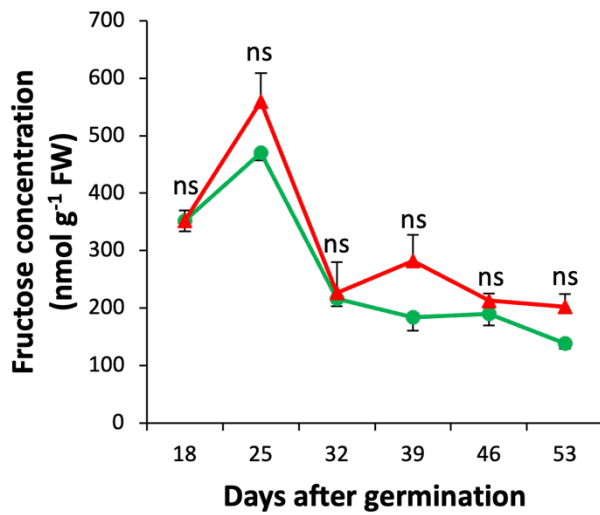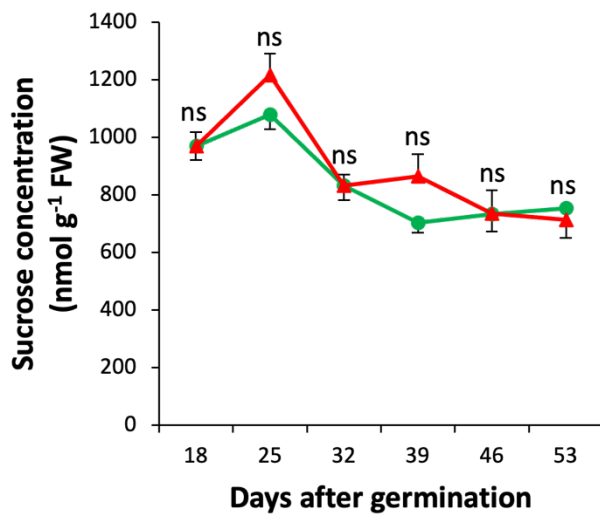
**Figure 8. Impact of removing nodal roots on soluble sugar concentrations in the seminal roots. (a-c)** Concentrations of glucose **(a)**, fructose **(b)** and sucrose **(c)** in seminal roots of control (green) and treatment (red) groups. Here, treatment refers to the continuous removal of nodal roots from their emergence onwards (i.e. 21 days after germination). Symbols show means $\pm$ SE (n=5). Significance of differences between means was evaluated by two-tailed Student's *t* test. ns, not significant.
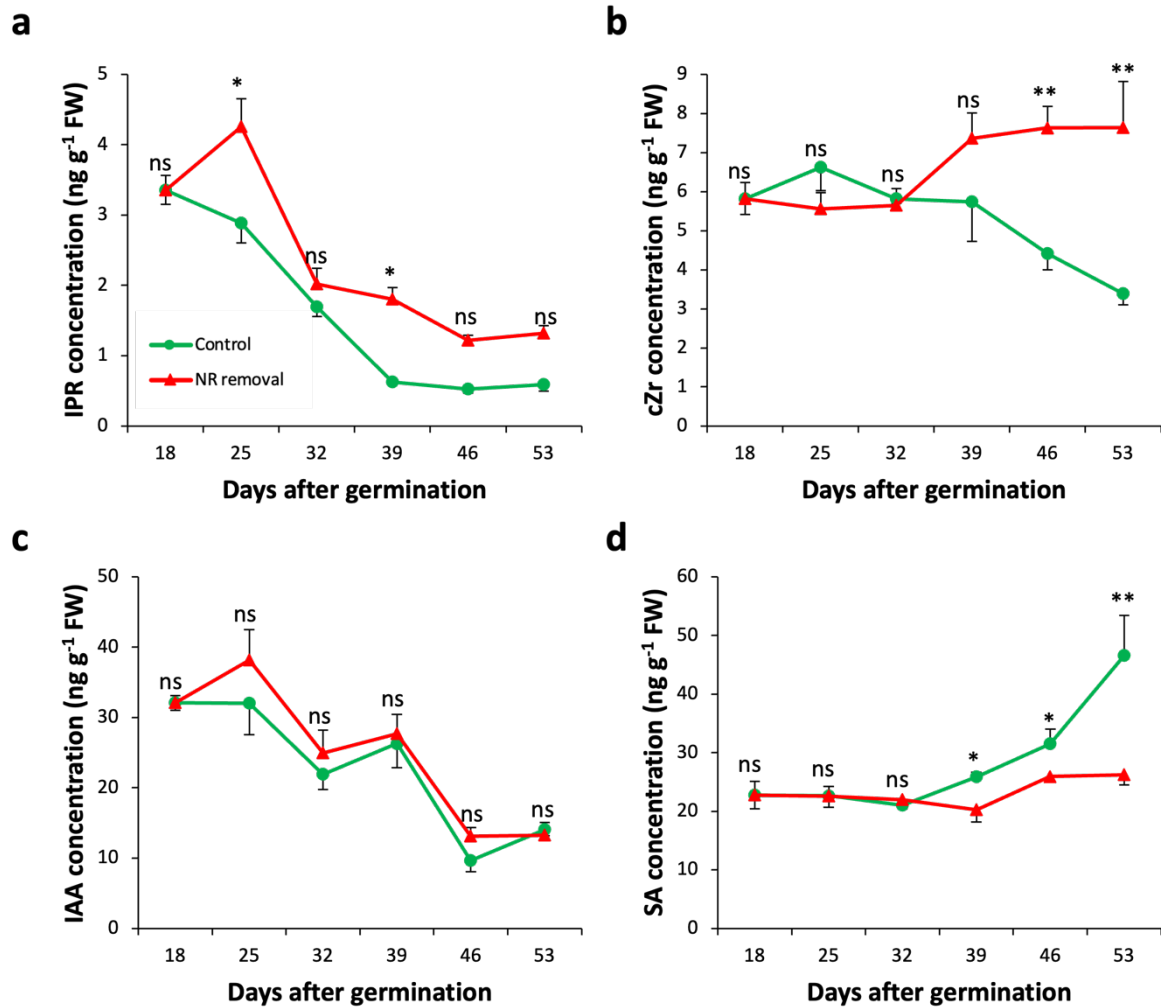
**Figure 9. Phytohormone concentrations in seminal roots as affected by the removal of nodal roots. (a-d)** Concentrations of isopentenyladenine-riboside (iPR) **(a)**, cis-zeatin riboside (cZR) **(b)**, indole-3-acetic acid (IAA) **(c)** and salicylic acid (SA) **(d)** in the seminal roots of control (green) and treatment (red) groups. Here, treatment refers to the continuous removal of nodal roots from their emergence onwards (i.e. 21 days after germination). Symbols show means ± SE (n=5). Asterisks denote significant differences between control and treatment at * P < 0.05 or ** P < 0.01 by two-tailed Student's *t* test. ns, not significant.

**Figure 10. Transcript abundance of genes involved in ABA biosynthesis and ABA degradation.** **(a-d)** Transcript abundance of barley *9-CIS-EPOXYCAROTENOID DIOXYGENASE-1* (*HvNCED1*) **(a)** and -2 (*HvNCED2*) **(b)**, *ABSCISIC ACID 8'-HYDROXYLASE* -1 (*HvABA8'OH-1*) **(c)** and -3 (*HvABA8'OH-3*) **(d)** in seminal roots 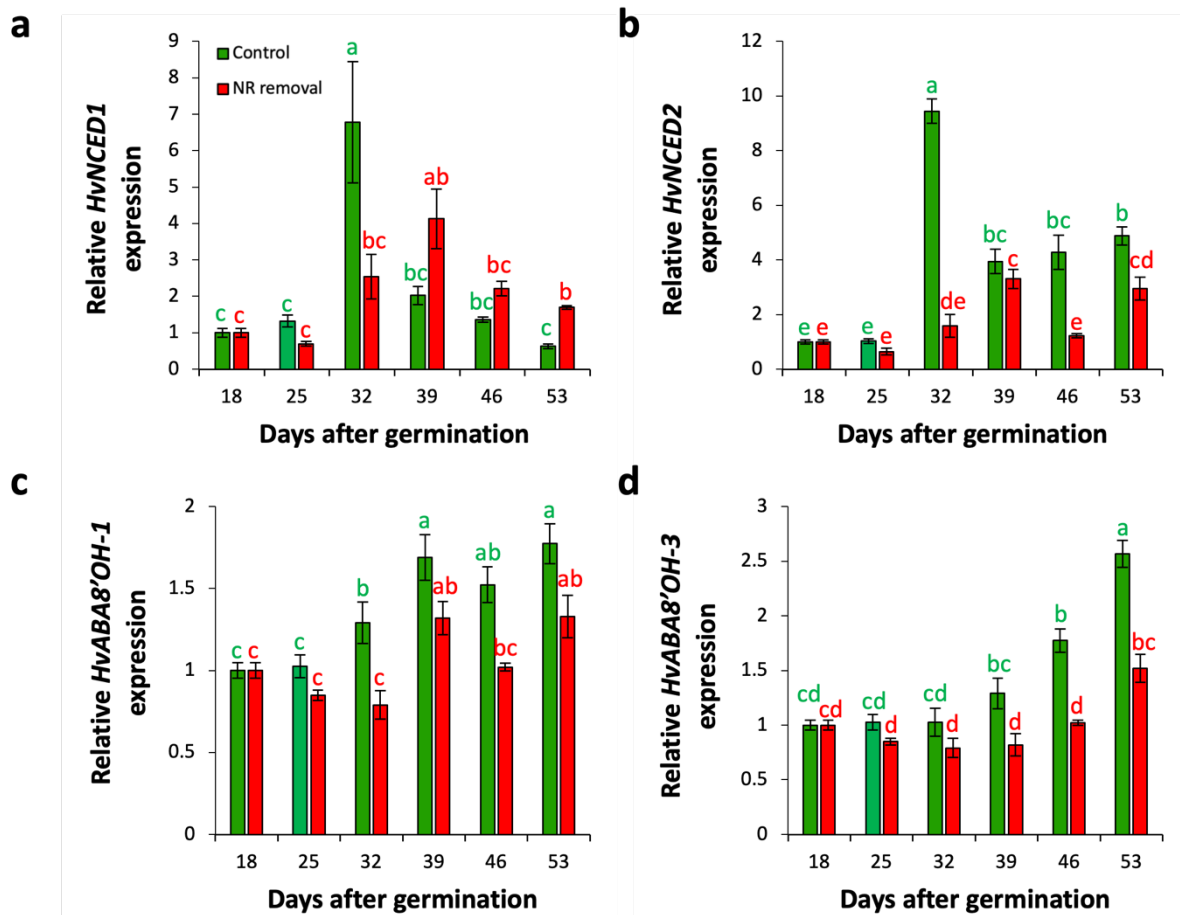of control (green) and treatment (red) groups with progressing tissue age. Here, treatment refers to the continuous removal of nodal roots from their emergence onwards (i.e. 21 days after germination). Gene expression was determined by quantitative reverse transcription PCR (qRT-PCR) and was normalized to *ADP-ribosylation factor 1* (*ADP*) and *UBIQUITIN* (*UBI*). Values of control plants at 18 DAG were set to 1. Bars show means ± SE **(**n=6). Different letters indicate significant differences between means according to two-way ANOVA followed by Tukey's post-hoc test at p<0.05.

To elucidate the impact of removing nodal roots on senescence-associated transcription factors, transcript levels of *HvNAC003* and *HvNAC005* were determined. *HvNAC003* expression in control plants showed early upregulation by 2-fold at 25 DAG, peaking up to 6-fold at 32 DAG and were then maintained at high levels, whereas removal of nodal roots delayed the upregulation of *HvNAC003* by one week (Figure 11.a). Likewise, the gradual accumulation of *HvNAC005* transcripts with progressing tissue age was suppressed by approx. 2-fold through the removal of nodal roots (Figure 11.b).
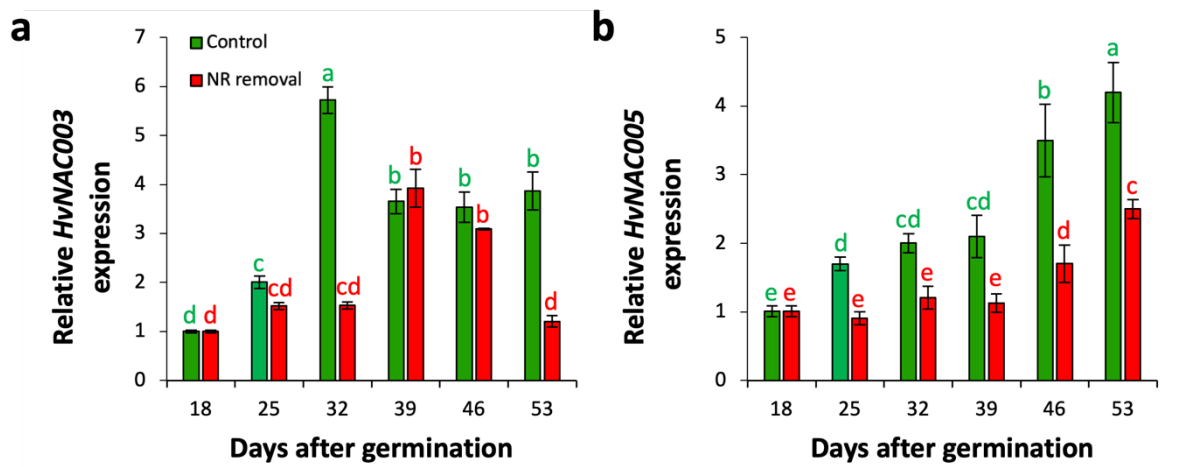
**Figure 11. Transcript abundance of senescence-associated NAC transcription factors. (a-b)** Relative transcript abundance of *HvNAC003* **(a)** and *HvNAC005* **(b)** in seminal roots of control (green) and treatment (red) groups with progressing tissue age. Here, treatment refers to the continuous removal of nodal roots from their emergence onwards (i.e. 21 days after germination). Gene expression was determined by quantitative reverse transcription PCR (qRT-PCR) and was normalized to *ADP-ribosylation factor 1* (*ADP*) and *UBIQUITIN* (*UBI*). Values of control plants at 18 DAG were set to 1. Bars show means ± SE (n=6). Different letters indicate significant differences between means according to two-way ANOVA followed by Tukey's post-hoc test at p<0.05.

In the transcriptome of senescent barley roots, the MYB-type transcription factor *HvMYB15* and the WRKY-type transcription factor *HvWRKY53* were shown to be upregulated before the onset of root senescence (Liu et al., 2019). Under control conditions, the expression of both transcription factors peaked at 32 DAG, as characterized by a 5- to 6-fold increase in transcript abundance. Thereafter, transcript levels decreased slowly back almost to initial levels (Figure 12). In contrast, removal of nodal roots delayed the upregulation of *HvWRKY53* transcript levels by three weeks (Figure 12.a) and that of *HvMYB15* by one week (Figure 12.b), and in both cases the expression peak tended to be toned down. Collectively, the present results confirmed the aging-dependent transcriptional regulation of the examined NAC-, WRKY- and MYB-type TFs, and that removing nodal roots delayed their upregulation, which supports a possible involvement in the onset of seminal root senescence.

Like in leaves, senescence processes in roots are associated with protein degradation, as evidenced by the upregulation of the cysteine protease genes *HvPAP15* and

*HvPAP17* in the previous study by Liu et al. (2019). To assess the onset of protein degradation processes during seminal root aging in the presence and absence of nodal roots, transcript levels of *HvPAP15* and *HvPAP17* were determined. In control roots, *HvPAP15* transcript abundance increased sharply at 39 DAG and then stayed at elevated levels (Figure 13.a) while that of *HvPAP17* gradually accumulated from 32 DAG on with progressing tissue age (Figure 13.b). In the absence of nodal roots, the sharp increase in *HvPAP15* expression was absent and transcript accumulation remained suppressed, and the first transcripts were detectable only at 46 DAG (Figure 13.a). Likewise, removal of nodal roots deregulated also *HvPAP17* expression, and caused a delay by one week in the accumulation of *PAP17* transcripts compared to control plants (Figure 13.b). Taken together, these observations indicated that protein degradation in seminal roots was delayed and partly suppressed by the removal of nodal roots.
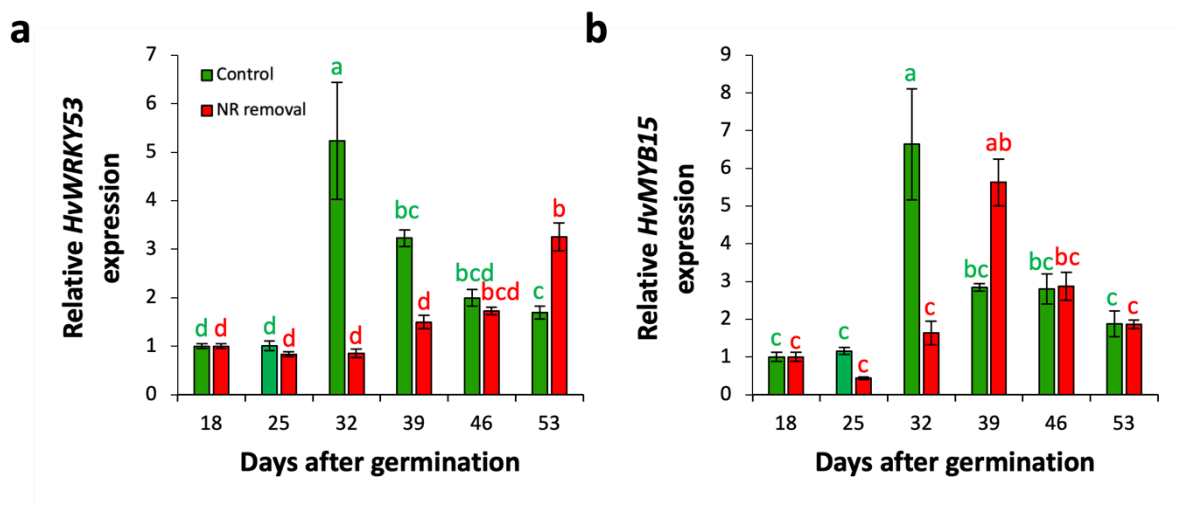


**Figure 12. Transcript abundance of two putatively senescence-associated transcription factors. (a-b)** Relative transcript abundance of *HvWRKY53* **(a)** and *HvMYB15* **(b)** in seminal roots of control (green) and treatment (red) groups with progressing tissue age. Here, treatment refers to the continuous removal of nodal roots from their emergence onwards (i.e. 21 days after germination). Gene expression was determined by quantitative reverse transcription PCR (qRT-PCR) and was normalized to *ADP-ribosylation factor 1* (*ADP*) and *UBIQUITIN* (*UBI*). Values of control plants at 18 DAG were set to 1. Bars show means ± SE (n=6). Different letters indicate significant differences between means according to two-way ANOVA followed by Tukey's post-hoc test at p<0.05.
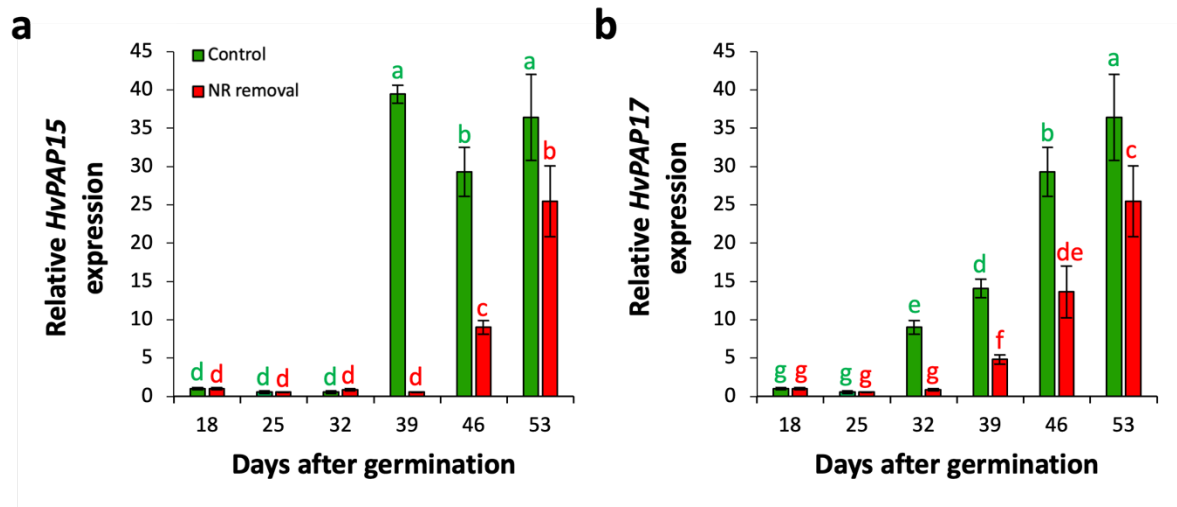
**Figure 13. Transcript abundance of two putatively senescence-associated cysteine proteases.**
**(a-b)** Relative transcript abundance of *HvPAP15* **(a)** and *HvPAP17* **(b)** in seminal roots of control (green) and treatment (red) groups with progressing tissue age. Here, treatment refers to the continuous removal of nodal roots from their emergence onwards (i.e. 21 days after germination). Gene expression was determined by quantitative reverse transcription PCR (qRT-PCR) and was normalized to *ADP-ribosylation factor 1* (*ADP*) and *UBIQUITIN* (*UBI*). Values of control plants at 18 DAG were set to 1. Bars show means ± SE **(**n=6). Different letters indicate significant differences between means according to two-way ANOVA followed by Tukey's post-hoc test at p<0.05.

### 3.1.2. Impact of modulated root CK levels on seminal root senescence

At the onset of root senescence, a sharp peak of ABA accumulation coincided with a steady decline in CK levels in (Liu et al., 2019). To investigate the role of CKs at the onset of root senescence, transgenic lines with root-specific overexpression of *Arabidopsis Cytokinin Oxidase/Dehydrogenase 2* (*EPP:AtCKX2*-72 and *EPP:AtCKX2*-16, abbreviated as CKX-72 and CKX-16, respectively) were grown hydroponically along with WT plants over 53 days and were monitored for physiological and molecular markers of root senescence. As reduced cytokinin (CK) levels in roots were expected to allow for an earlier accumulation of ABA through the antagonistic action of CKs, it was tested, whether ectopic expression of *AtCKX2* causes an earlier onset of senescence-associated events in roots.
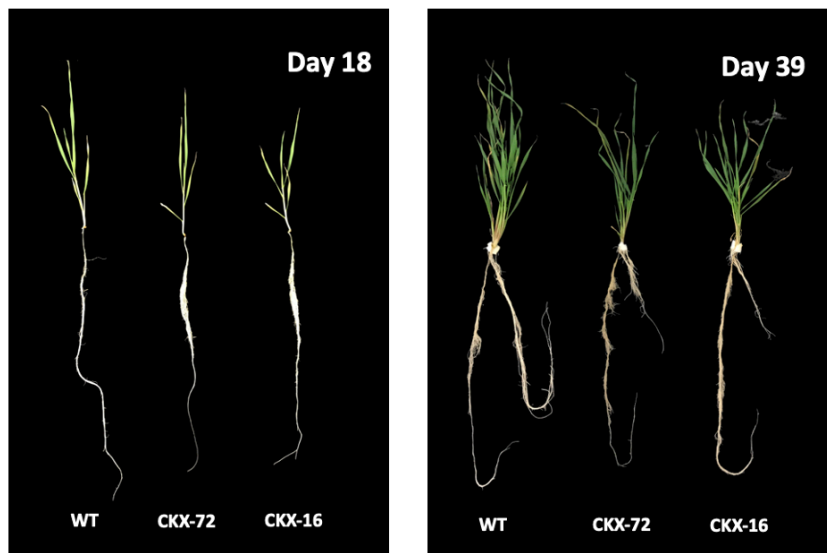


**Figure 14. Early stages of growth and development in barley plants with ectopic expression of *AtCKX2* in roots.** Visual appearance of wild-type (WT) and transgenic lines with root-specific overexpression of Arabidopsis *CYTOKININ OXIDASE/DEHYDROGENASE 2* (*AtCKX2*), namely CKX-72 and CKX-16, at early stages of growth and development. Transgenic lines were grown hydroponically along with WT plants over 53 days. Images were taken after 18 and 39 days.

Throughout the experimental period, transgenic lines with root-specific overexpression of *AtCKX2* (CKX-72 and CKX-116) exhibited different shoot and root phenotypes as compared to WT. Both lines, CKX-72 and CKX-116, produced shorter shoots and had thinner leaves in comparison to WT (Figure 14). Moreover, based on the visual inspections, the developmental progression of nodal roots was found to be delayed and slowed down in transgenic lines. In both CKX lines the shoot biomass was

significantly lower than in the WT during all developmental stages (Figure 15.a). ~~The~~ reduction in shoot biomass was even greater for CKX-72 than for CKX-16, which became most prominent at 53 DAG, when the shoot dry weight was 57% lower in line CKX-72 and 33% lower in CKX-16 compared to the WT (Figure 15.a). In line with the lower shoot biomass, both CKX lines produced significantly less tillers than the WT (Figure 15.b). Total root biomass of transgenic lines was similar to that of WT during early stages of growth (i.e. 18-32 DAG), whereas it became significantly lower in CKX-72 and CKX-16 starting from 39 and 46 DAG, respectively (Figure 15.c). Furthermore, root-to-shoot ratio was up to 2-fold higher in transgenic lines compared to WT during the most developmental stages, with the exception of 39 and 46 DAG (Figure 15.d)

Root development was also qualitatively altered in transgenic lines ectopically expressing *AtCKX2* in roots. Although seminal root biomass of both CKX lines was similar to WT at 18 DAG, that of CKX-16 was significantly higher than of the WT during later developmental stages (Figure 16.a). Seminal root biomass of CKX-72 became also higher than in the WT starting from 46 DAG and the differential increase in seminal root biomass became more pronounced at later time points. At 53 DAG, seminal root biomass in CKX-72 and CKX-16 was approx. 32% higher than in the WT. To investigate the impact of ectopic root-specific expression of *AtCKX2* on the onset of seminal root senescence, dynamics of seminal root growth was evaluated. Seminal root biomass of all lines examined increased over time until it became stagnant starting from 46 DAG (Figure 16.a). Seminal root length in transgenic lines was similar to that of WT at 18 DAG, but that of CKX-16 was higher at 25 DAG compared to WT (Figure 16.b). Interestingly, starting from 32 DAG, in both CKX lines, seminal root length was significantly lower compared to WT. Moreover, an arrest in the seminal root elongation was observed much earlier in transgenic lines than in the WT. WT plants stopped elongating after 46 DAG, whereas both CKX-72 and CKX-16 plants stopped elongating after 32 DAG (Figure 16.b). Taken together, ectopic expression of *AtCKX2* in roots increased seminal root biomass but did not prolong the time frame of the biomass accumulation, whereas it decreased the duration of root elongation leading to lower total seminal root length at later developmental stages compared to the WT.

The emergence and development of nodal roots was also altered in transgenic lines. The first nodal root of WT emerged at 20 DAG, whereas nodal roots of CKX-72 and

CKX-16 started to form inconsistently among biological replicates at 28 and 25 DAG, respectively (Figure 16.c). Moreover, nodal root biomass of CKX-72 and CKX-16 was significantly lower than of WT during all developmental stages examined. The differential growth of seminal (Figure 16.a) and nodal roots (Figure 16.c) led to dramatic changes in the seminal root-to-nodal root (SR-to-NR) biomass ratio (Figure 16.d). In WT plants, the proportion of seminal to nodal root biomass significantly declined starting from 25 DAG. Strikingly, the SR-to-NR biomass ratio of transgenic lines was up to 25-fold higher at 32 DAG compared to WT. Over time, proliferation of nodal roots decreased the SR-to-NR biomass ratio also in transgenic lines. Furthermore, a closer look at the root system architecture showed that the ectopic root-specific expression of *AtCKX2* increased lateral root branching at seminals during early stages of growth (i.e. 18 DAG) (Figure 17).

To investigate time-dependent changes of root activity and to what extent it is influenced by the ectopic expression of *AtCKX2*, the N uptake capacity of seminal roots was monitored weekly by a short-term $^{15}$N-labelled $NO_3^-$ influx experiment. N uptake capacity of CKX-72 was higher at 18 and 53 DAG, whereas that of CKX-16 was higher at 32, 46 and 53 DAG compared to WT (Figure 18). Most importantly, while N uptake rates of WT plants remained at similar levels from 18 until 46 DAG and then started to decline, that of both CKX lines remained at relatively higher levels during later developmental stages. At 53 DAG, N uptake capacity of transgenic lines was up to 78% higher compared to WT (Figure 18), suggesting prolonged physiological activity of the seminal roots.

To verify *AtCKX2* expression in transgenic lines, mRNA levels of *AtCKX2* were determined by qRT-PCR. In both CKX lines, the transcript levels of the transgene were very high, which are expressed as ($40-\Delta C_t$), where $\Delta C_t$ is the difference between the $C_t$ values of the gene of interest and the reference gene (Figure 19). Expectedly, *AtCKX2* transcripts were not detected in WT plants.
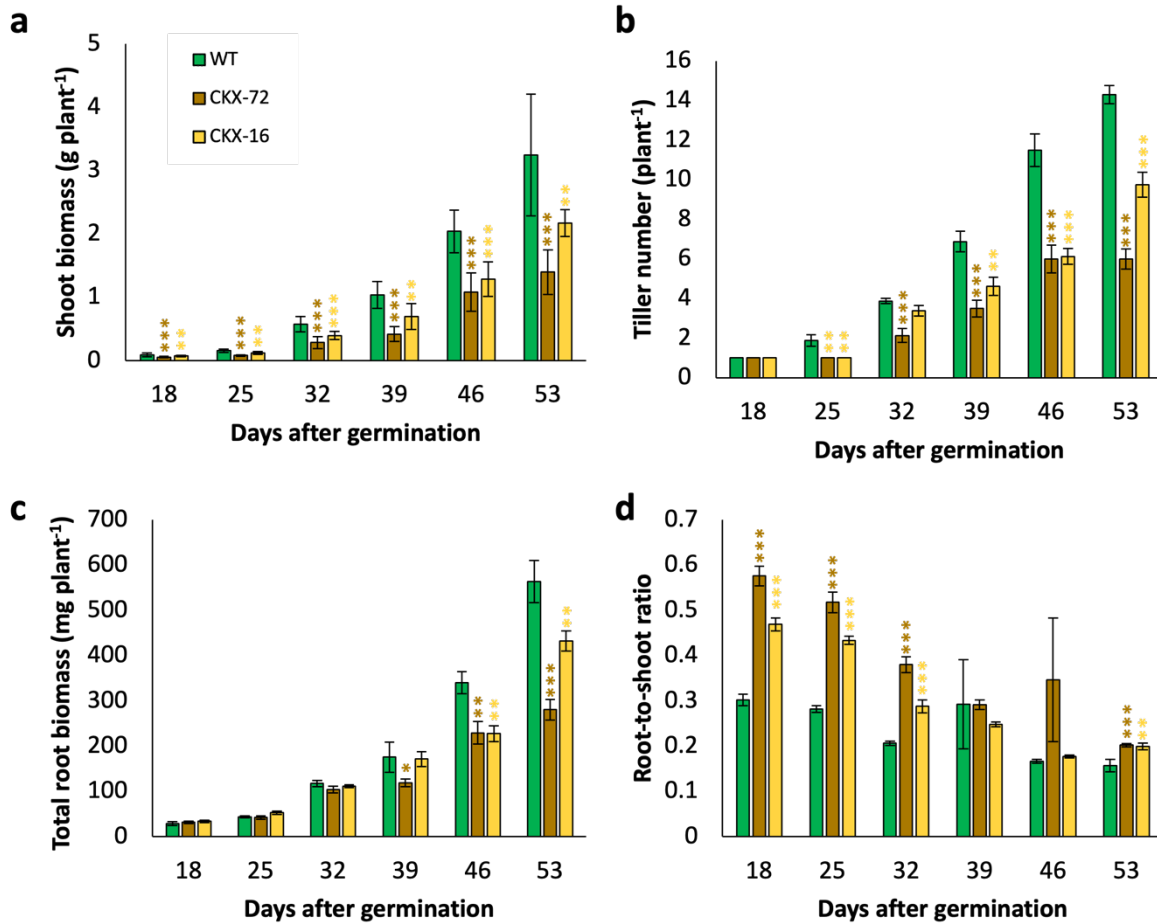
**Figure 15. Above- and belowground growth traits in transgenic lines ectopically expressing *AtCKX2* in roots. (a-d)** Shoot biomass **(a)**, number of tillers **(b)**, total root biomass **(c)** and root-to-shoot biomass ratio **(d)** of wild-type (WT), *EPP:AtCKX2*-72 and *EPP:AtCKX2*-16 over time. Transgenic barley lines with root-specific overexpression of Arabidopsis *CYTOKININ OXIDASE/DEHYDROGENASE 2* (*AtCKX2*) were grown hydroponically along with the WT plants over 53 days and harvested weekly to monitor root senescence-related processes. Bars show means $\pm$ SE (n=8). Asterisks denote significant differences between WT and transgenic lines at $*$ P < 0.05, $**$ P < 0.01 or $***$ P <0.001 by two-tailed Student's *t* test.
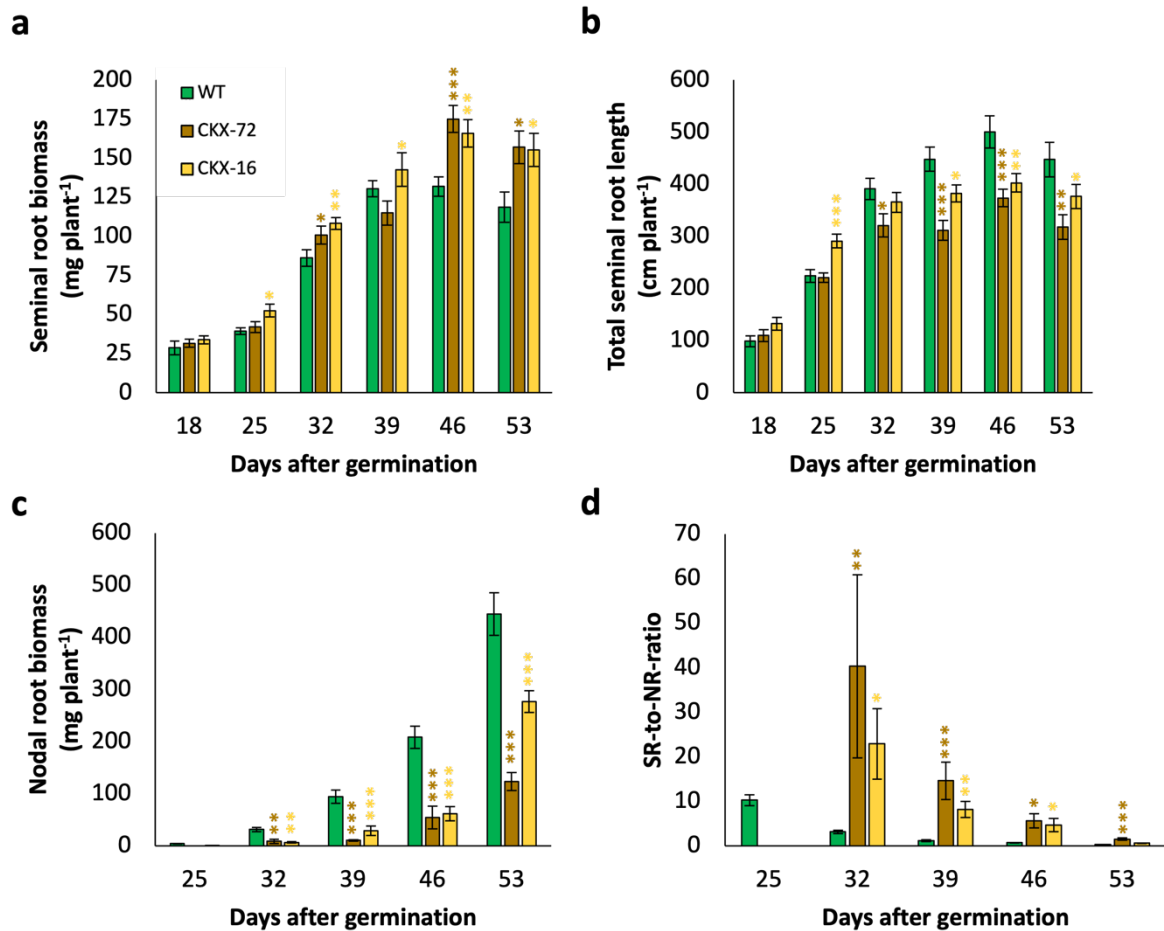
**Figure 16. Seminal and nodal growth and development in transgenic lines ectopically expressing *AtCKX2* in roots. (a-d)** Seminal root biomass **(a)**, total seminal root length **(b)**, nodal root biomass **(c)** and seminal root-to-nodal root (SR-to-NR) biomass ratio **(d)** of wild-type (WT), *EPP:AtCKX2*-72 and *EPP:AtCKX2*-16 over time. Transgenic barley lines with root-specific overexpression of Arabidopsis *CYTOKININ OXIDASE/DEHYDROGENASE 2* (*AtCKX2*) were grown hydroponically along with the WT plants over 53 days and harvested weekly to monitor root senescence-related processes. Bars show means ± SE (n=8). Asterisks denote significant differences between WT and transgenic lines at ∗ P < 0.05, ∗∗ P < 0.01 or ∗∗∗ P <0.001 by two-tailed Student's *t* test.
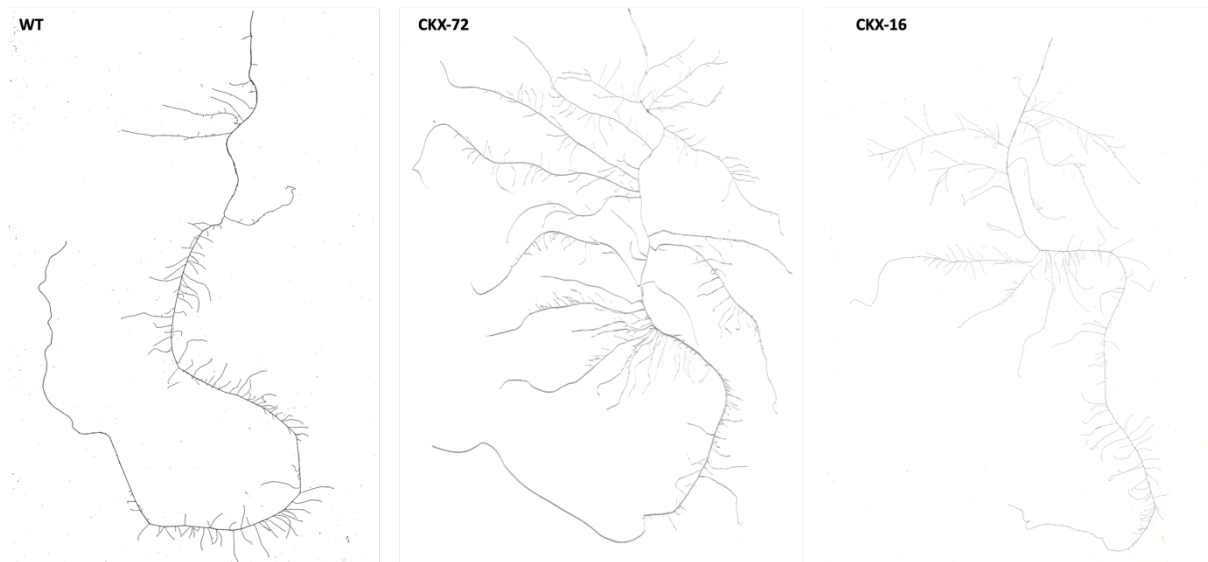
**Figure 17. Modulated root architecture in transgenic lines ectopically expressing *AtCKX2* in roots.** Representative root scans of individual seminal roots of wild-type (WT) and two independent transgenic lines with root-specific overexpression of Arabidopsis *CYTOKININ OXIDASE/DEHYDROGENASE 2* (*AtCKX2*), namely CKX-72 and CKX-16. Transgenic lines along with the WT plants were grown hydroponically for 53 days. Seminal roots were combed and scanned individually at 18 days after germination (DAG) to visualize lateral root branching.
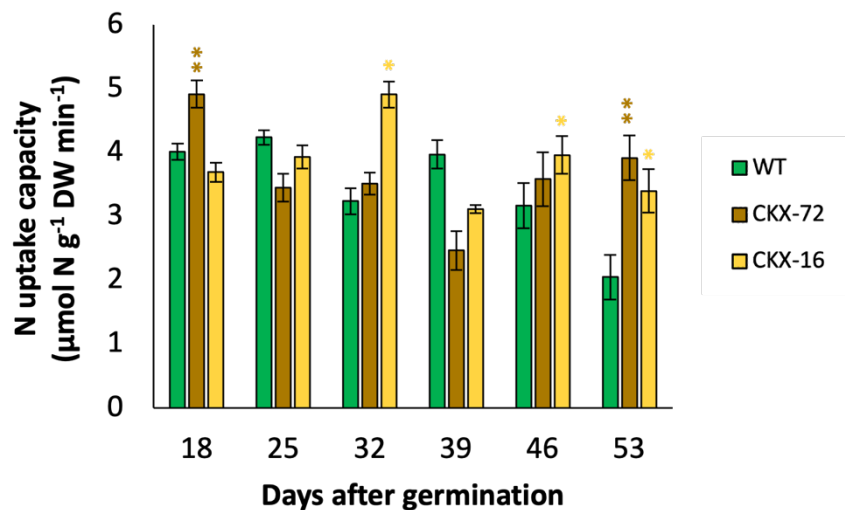


**Figure 18. Nitrate uptake capacity with progressing plant age as affected by ectopic expression of *AtCKX2* in transgenic barley roots.** Short-term nitrate influx of seminal roots in wild-type (WT), *EPP:AtCKX2*-72 and *EPP:AtCKX2*-16 over time. Transgenic barley lines with ectopic root-specific expression of Arabidopsis *CYTOKININ OXIDASE/DEHYDROGENASE 2* (*AtCKX2*) were grown hydroponically along with the WT plants over 53 days and subjected to an $^{15}N$-labelled nitrate-influx assay once a week to monitor the changes in the root physiological activity over time. Roots were exposed to 1 mM $^{15}N$-labeled $NO_3^-$ for 10 min. Bars show means $\pm$ SE (n=4). Asterisks denote significant differences between WT and transgenic lines at $*$ $P < 0.05$ or $**$ $P < 0.01$ by two-tailed Student's *t* test.

To elucidate the impact of root-specific overexpression of *AtCKX2* on the root CK concentrations, seminal roots were subjected to the analysis of phytohormones by UPLC-MS/MS. In higher plants, CKs can be found in numerous forms (Kieber and Schaller, 2014). In this study, only a limited subset of CK derivatives could be quantified. Among the quantifiable CK forms, isopentenyl-adenine riboside (IPR) concentrations of CKX-72 were higher by up to 70% compared to WT during most of the experimental period, with the exception of 18 and 46 DAG (Figure 20.a). In CKX-16, IPR levels were only higher at 32 DAG and 46 DAG. CKX-72 showed also higher *cis*-zeatin riboside (cZr) levels at 32, 39 and 53 DAG compared to WT (Figure 20.b). At 32 DAG, a 2-fold increase was observed in the cZr concentrations of transgenic lines. *trans*-zeatin (tZ) concentrations, on the other hand, were mostly unaffected by the ectopic overexpression of AtCKX2 in roots, with the exception of CKX-72, for which tZ levels were lower at 32 DAG and higher at 53 DAG (Figure 20.c). However, since the absolute values are very low here, the present data should be evaluated carefully. tZ-riboside (tZr) concentrations in CKX lines were highly similar to that of WT at during early developmental stages (i.e. 18-32 DAG), whereas they became higher in CKX-72 starting from 39 DAG (Figure 20.d). tZR levels of CKX-16 were found to be higher only at 46 DAG. Taken together, the root-specific overexpression of *AtCKX2* did not result in decreased concentrations of CK-ribosides and tZ.
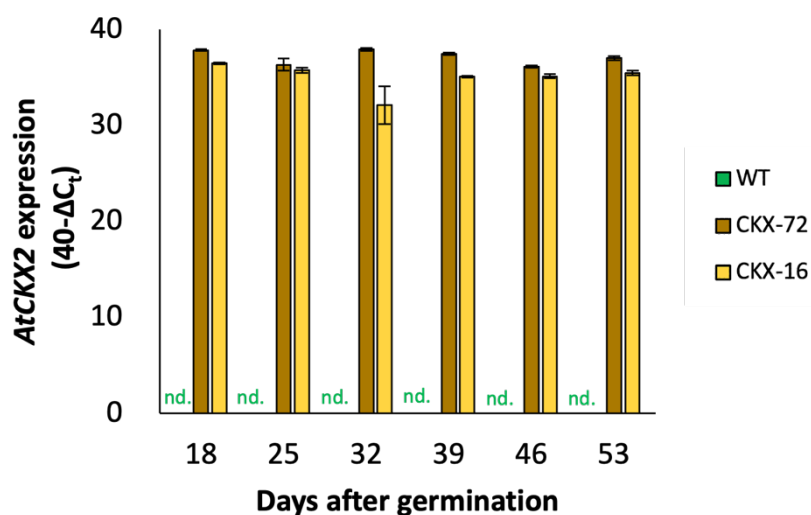


**Figure 19. Transcript abundance of *AtCKX2* in transgenic lines.** Relative expression of *AtCKX2* under the control of the *EPP* promoter was determined in seminal roots of WT and transgenic lines at different developmental stages. Transcript levels were determined by qRT-PCR using *ADP-ribosylation factor 1* (*ADP*) and *UBIQUITIN* (*UBI*) as reference genes. Expression is represented as 40-$\Delta C_t$ value, with 26 being the threshold value for expressed genes. Bars show means ± SE (n=6). nd., not determined

To validate the accumulation of ABA during onset of root senescence and to elucidate how it is affected in the transgenic lines ectopically expressing *AtCKX2* in roots, ABA concentrations were quantified. In the WT, ABA concentrations were low from 18 to 39 DAG (Figure 20.e). At 46 DAG, ABA concentrations increased by 2.5-fold in WT and sharply dropped thereafter, thereby reflecting the same peak as reported previously (Liu et al., 2019). By contrast, in transgenic lines ABA concentrations remained constantly at a rather low level except at 53 DAG, when ABA increased in line CKX-72 (Figure 20.e).

Next, transcript abundance of genes involved in ABA biosynthesis and degradation was determined. In WT plants, mRNA levels of the ABA biosynthesis genes *HvNCED1* and *HvNCED2* peaked at 46 DAG after an 11- and 4.5-fold increase, respectively, and thereafter remained relatively high (Figure 21.a, b). In contrast, *HvNCED1* and *HvNCED2* mRNA levels in CKX-72 and CKX-16 did not change over time, except for *HvNCED1* in CKX-72 at 53 DAG (Figure 21.a, b). *HvABA-8'OH-2* and *-3* are involved in the rate-limiting step of ABA degradation. In WT plants, *HvABA-8'OH-2* was upregulated at 46 DAG by almost 3-fold relative to 18 DAG (Figure 21.c). Similarly, *HvABA-8'OH-3* transcript levels increased by 2.5-fold starting from 39 DAG and maintained at relatively high levels until the end of the experiment (Figure 21.d). Apparently, ectopic root-specific expression of *AtCKX2* led to downregulation of *HvABA-8'OH-2* and *-3* in both transgenic lines.

To investigate how modulated CK levels affect the expression of transcription factors that were supposed to be involved in the onset of seminal root senescence, mRNA levels of three NAC-type TFs were determined. *HvNAC003* mRNA abundance strongly increased at 46 and 53 DAG in WT plants, while this upregulation was absent in the transgenic lines (Figure 22.a). Likewise, transcripts of *HvNAC005* gradually accumulated from 46 DAG onwards in WT roots, whereas in transgenic lines they did not show any peak or significant increase (Figure 22.b), suggesting a link between *AtCKX2* expression and *HvNAC003* and *HvNAC003*. Another NAC-type TF, *HvNAM1*, has been shown to be upregulated in senescing leaves (Christiansen et al., 2011) and roots (Liu et al., 2019) of barley. mRNA levels of *HvNAM1* in WT roots increased by 6-fold and peaked at 39 DAG and thereafter remained relatively high (Figure 22.c). Interestingly, this temporal expression pattern of *HvNAM1* was exactly the same in

transgenic lines as they showed a strong and continued upregulation starting from 39 DAG. Furthermore, the transcript abundance of *HvMYB15* and *HvWRKY53* was determined, since they were also shown to be upregulated with the onset of root senescence (Liu et al., 2019). In WT plants, the expression of both transcription factors peaked at 32 DAG, as characterized by a 4.5 to 5-fold increase in transcript abundance (Figure 23). Thereafter, transcript levels slightly decreased but stayed higher compared to initial levels. The expression pattern of *HVMYB15* and *HvWRKY53* was highly similar in both transgenic lines, as their transcript levels also peaked at 32 DAG and showed the same decline as in WT plants (Figure 23).   This observation suggests that *HvNAM1, HvMYB15 and HvWRKY53* were not affected by the ectopic expression of *AtCKX2*.
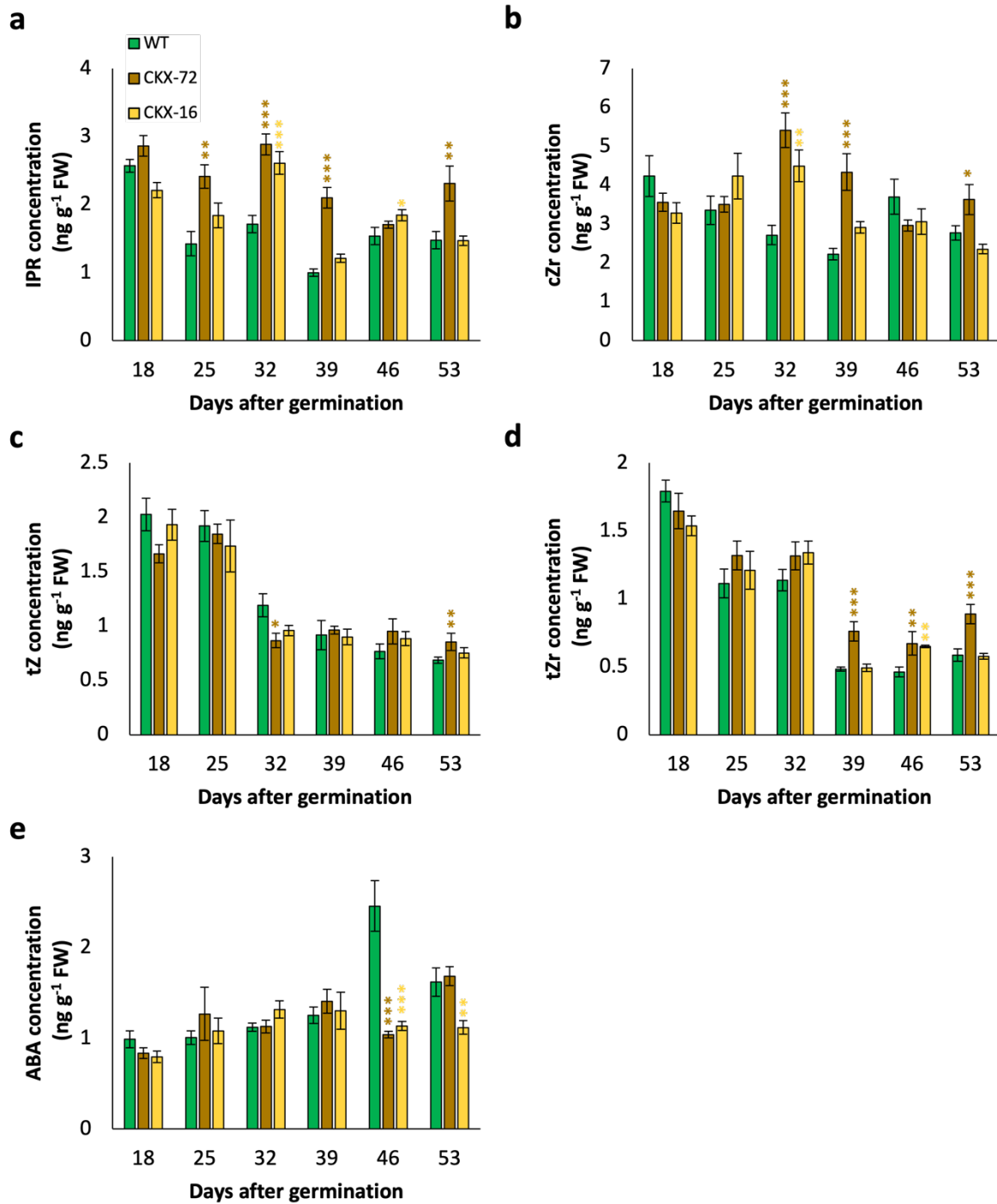
**Figure 20. Root cytokinin and ABA concentrations as affected by ectopic expression of *AtCKX*2 during progression of root aging. (a-d)** Concentrations of isopentenyladenine-riboside (IPR) **(a)**, *cis*-zeatin riboside (cZr) **(b)**, *trans*-zeatin (tZ) **(c)** and trans-zeatin riboside (tZr) **(d)** and abscisic acid (ABA) **(e)** in seminal roots of WT and transgenic lines with ectopic root-specific overexpression of Arabidopsis *CYTOKININ OXIDASE/DEHYDROGENASE 2* (*AtCKX2*), namely CKX-72 and CKX-16. Transgenic lines were grown hydroponically along with the WT plants over 53 days and harvested weekly to monitor root senescence-related processes. Bars show means ± SE (n=6). Asterisks denote significant differences between WT and transgenic lines at ∗ P < 0.05, ∗∗ P < 0.01 or ∗∗∗ P <0.001 by two-tailed Student's *t* test. ns, not significant.

**Figure 21. Transcript abundance of genes involved in ABA biosynthesis and degradation as affected by ectopic expression of *AtCKX2* during progression of root aging. (a-b)** Expression of ABA-biosynthesis genes. Relative transcript abundance of *HvNCED1* **(a)** and *HvNCED2* **(b)** in seminal roots. **(c-d)** Expression of ABA-degradation genes. Relative transcript abundance of *HvABA'8-OH-2* **(c)** and *HvABA'8-OH-3* **(d)** in seminal roots of WT and transgenic lines with root-specific overexpression of Arabidopsis *CYTOKININ OXIDASE/DEHYDROGENASE 2* (*AtCKX2*). Transgenic lines were grown hydroponically along with the WT plants.  Transcript levels were determined by qRT-PCR and normalized to barley reference genes *ADP-ribosylation factor 1* (*ADP*) and *UBIQUITIN* (*UBI*)**.** Transcript abundance of WT at 18 days after germination (DAG) was set to 1. Bars show means ± SE (n=6). Asterisks denote significant differences between WT and transgenic lines at ∗ P < 0.05, ∗∗ P < 0.01 or ∗∗∗ P <0.001 by two-tailed Student's *t* test. ns, not significant.

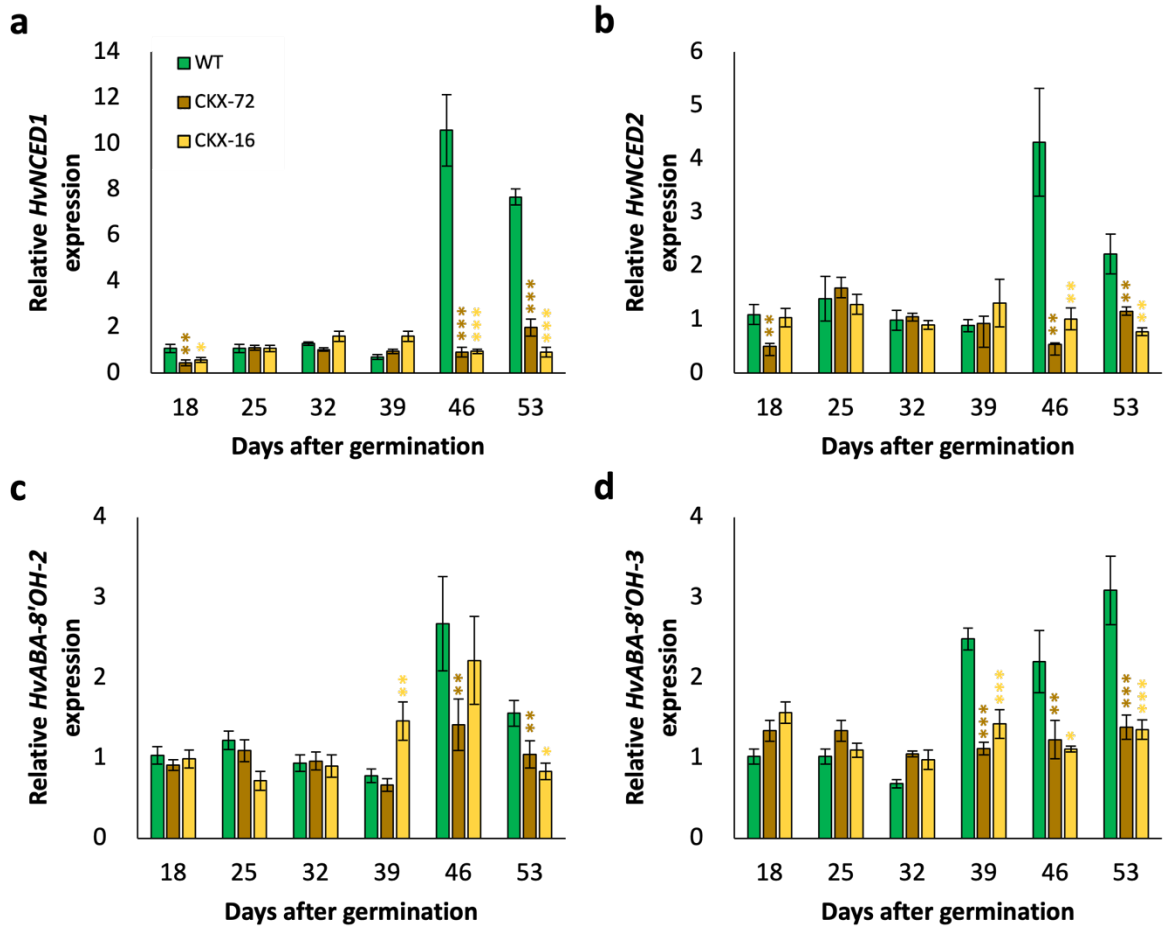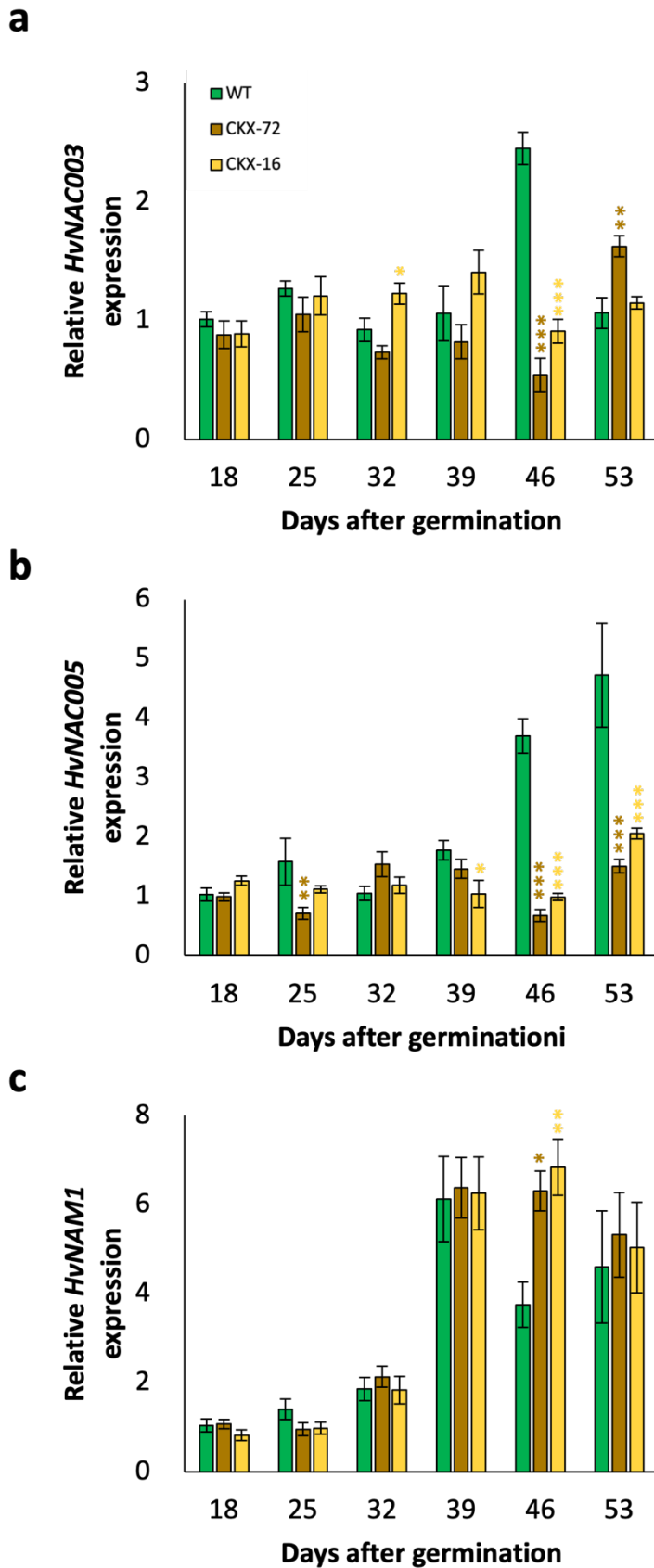**Figure 22. Transcript abundance of senescence-NAC transcription factors as affected by ectopic expression of *AtCKX2* during progression of root aging. (a-c)** Relative transcript abundance of *HvNAC003* **(a)**, *HvNAC005* **(b)** and *HvNAM1* **(c)** in seminal roots of wild-type (WT) and transgenic lines with root-specific overexpression of *Arabidopsis CYTOKININ OXIDASE/DEHYDROGENASE 2 (AtCKX2)*, namely CKX-72 and CKX-16. Transgenic lines were grown hydroponically for 53 days along with the WT plants and monitored for senescence-related processes. Transcript levels were determined by qRT-PCR and normalized to barley reference genes *ADP-ribosylation factor 1* (*ADP*) and *UBIQUITIN* (*UBI*)**.** Transcript abundance of WT at 18 days after germination (DAG) was set to 1. Bars show means $\pm$ SE (n=6). Asterisks denote significant differences between WT and transgenic lines at * P < 0.05, ** P < 0.01 or *** P <0.001 by two-tailed Student's *t* test.
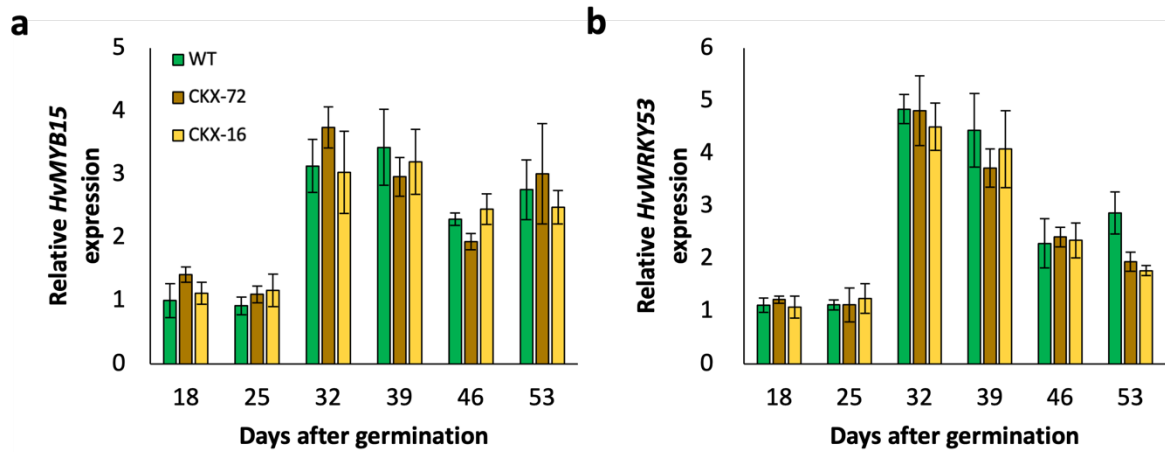
**Figure 23. Transcript abundance of *HvMYB15* and *HvWRKY53* as affected by ectopic expression of *AtCKX2* during progression of root aging. (a-b)** Relative transcript abundance of *HvMYB15* **(a)** and *HvWRKY53* **(b)** in seminal roots of wild-type (WT) and transgenic lines with ectopic root-specific expression of *Arabidopsis CYTOKININ OXIDASE/DEHYDROGENASE 2 (AtCKX2)* (EPP:*AtCKX2*-72 and EPP:*AtCKX2*-16). Transgenic lines were grown hydroponically for 53 days along with the WT plants. Transcript levels were determined by qRT-PCR and normalized to barley reference genes *ADP-ribosylation factor 1* (*ADP*) and *UBIQUITIN* (*UBI*). Transcript abundance of WT at 18 days after germination (DAG) was set to 1. Bars show means $\pm$ SE (n=6). Significance of differences between WT and transgenic lines were evaluated by two-tailed Student's *t* test.

**3.2. *in silico* analysis of the candidate genes regulating root senescence**

To characterize novel transcription factors, namely *HvWRKY53* and *HvMYB15*, which were proposed to be involved in the regulation of root senescence (Liu et al., 2019), *in silico* approaches were used, especially for the revision of the barley WRKY and MYB family members as well as the analysis of the *cis*-acting elements in the promoter regions.

**3.2.1. *in silico* analysis of the transcription factor *WRKY53* in barley**

*HvWRKY53* (HORVU3Hr1G080860/HORVU.MOREX.r3.3HG0297450) is located on Chr 3 and consist of 3 exons and 2 introns. The coding sequence is 771 bp long and translates into a 256 amino acid (aa) long protein.

So far, the existing literature on the WRKY transcription factors in barley is contradicting, regarding the number of WRKY members and their nomenclature. To revisit the WRKY-type TFs in barley, members of WRKY family, which were identified based on protein BLAST and genome mining by annotation, were used to conduct a phylogenetic analysis. In line with the most recent publication on the barley WRKY members, 93 unique sequences were identified as putative WRKY proteins (Figure 24). A closer look at the chromosomal locations revealed that Chromosome 3 and 5 contained the largest numbers of *HvWRKY*s.

To gain further insights about the candidate gene *HvWRKY53*, WRKY proteins from barley, Arabidopsis and rice were used to construct a phylogenetic tree, with the aim of identifying closest orthologues genes in different species (Figure 25). *OsWRKY22* (Os01t0820400) and *AtWRKY38* (AT5G22570) were found to be closest relatives of *HvWRKY53*, when all WRKY proteins of Arabidopsis, barley and rice were compared. The two genes from Arabidopsis and rice have been shown to be involved in disease resistance (Kim et al., 2008; Abbruscato et al., 2012). *Cis*-regulatory elements are composed of linear nucleotide sequences of non-coding DNA that can directly influence gene regulation.
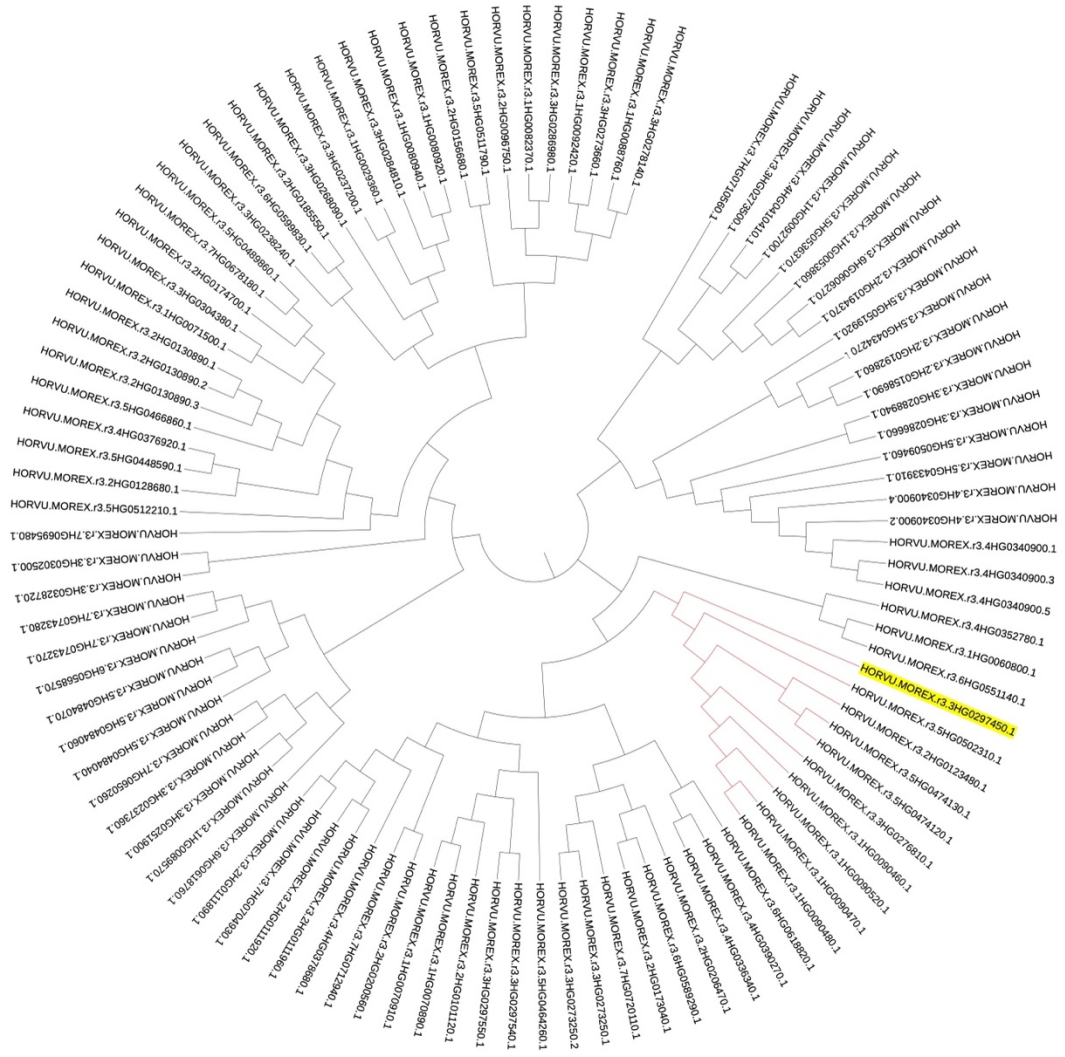
**Figure 24. Phylogenetic tree of the WRKY TF family in barley.** Based on protein BLAST and genome mining by annotation 93 unique sequences were identified as putative WRKY proteins in barley. Neighbor-joining method was used to construct the phylogenetic tree using the online tool CLUSTAL Omega (https://www.ebi.ac.uk/Tools/msa/clustalo/). *HvWRKY53* (*HORVU3Hr1G080860*/*HORVU.MOREX.r3.3HG0297450*) is highlighted in yellow.

To gain further information on the spatio-temporal expression of *HvWRKY53*, the promoter region (2 kb-upstream of the coding sequence) was analyzed for the cis-acting elements using the online tools PLACE (Higo et al., 2008) and PlantCARE (Lescot et al., 2002). The promoter region of *HvWRKY53* contains numerous different motifs. Several motifs, including CANNTG (N=A/T/G/C) (MYCCONSENSUSAT),

ATATT (ROOTMOTIFTAPOX1), YACT (Y=T/C) (CACTFTPPCA1), and AAAG (DOFCOREZM) were found to be overrepresented in the promoter. MYCCONSENSUSAT is a MYC recognition sequence, and genes binding to this site have been shown to be involved in drought and cold tolerance (Chinnusamy et al., 2003). CACTFTPPCA1 and ROOTMOTIFTAPOX1 are organ-specific elements, which are responsible for the mesophyll- and root-specific gene expression, respectively (Elmayan and Tepfer, 1995; Gowik et al., 2004). DOFCOREZM, on the hand, is the core site required for binding of *ZmDof* TFs, which participates in carbon metabolism (Yanagisawa, 2000). W-boxes (TTGAC, TGACT, TGACY and TGAC; Y=C/T), also known as the DNA-binding sites of WRKY proteins, were found to be distributed across the 2 kb-long promoter sequence, being dominantly present between 1 and 2 kb (3'-5'). Moreover, the promoter region is also rich in different motifs of MYB-binding and recognition. Other motifs identified in the promoter region are associated with phytohormone signaling/response/inducibility with an emphasis on ABA, auxin and methyl-jasmonate. Drought- (DRE), cold- (CRE) and light-responsive elements (LRE) are among the detected motifs, which are involved in stress responses. Taken together, promoter analysis of *HvWRKY53* provides suggests that *HvWRKY53* can be regulated by other TFs and is putatively involved in phytohormone signaling and plant responses to environmental stress factors. Organ-specific elements further imply tissue-specific expression of *HvWRKY53*.

**a**

**b**

AT5G22570.1
Os08t0276200-01
HORVU.MOREX.r3.3HG0297450.1
Os01t0820400-01
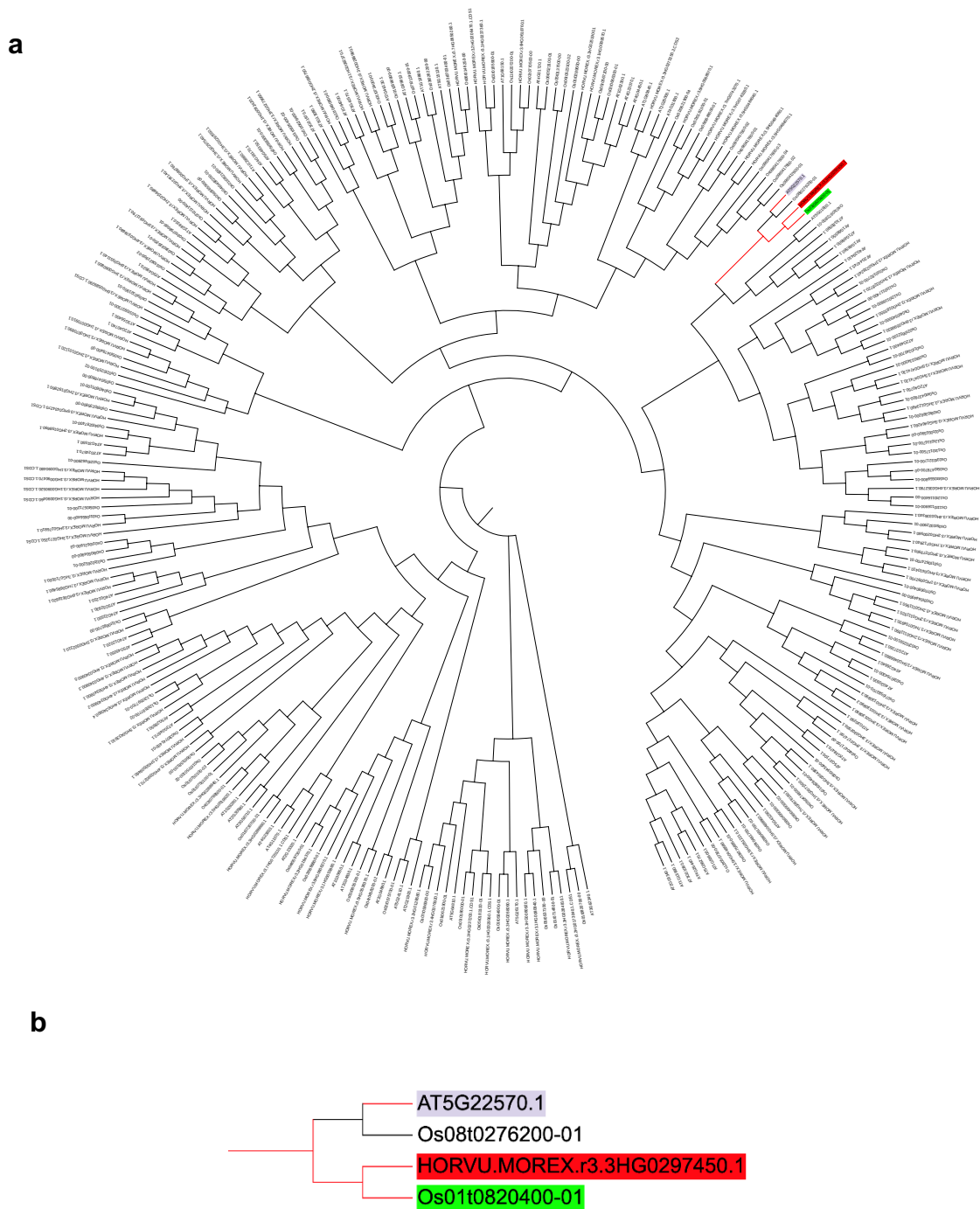
**Figure 25. Phylogenetic analysis of WRKY TFs in barley, rice, and Arabidopsis. (a)** Identified members of barley, rice and Arabidopsis WRKY TFs were used to build a phylogenetic tree to reveal closest orthologous genes of different WRKY members. Neighbor-joining method was used to construct the phylogenetic tree using the online tool CLUSTAL Omega (https://www.ebi.ac.uk/Tools/msa/clustalo/). **(b)** Close-up view of the gene *HvWRKY53* (red) and its closest orthologues in rice (green) and Arabidopsis (lilac).

**3.2.2. *In silico* analysis of the transcription factor *MYB15* in barley**

Members of the MYB-type TFs constitute one of the largest TF families in plants with 198 and 183 members in Arabidopsis and rice, respectively (Yanhui et al, 2006). In barley, up to 276 proteins have been identified as MYB-type proteins (Tombuloglu et al., 2013). However, using the latest genome assembly, only 155 unique sequences could be identified as MYB proteins in this study (Figure 26). *HvMYB15* (*HORVU6Hr1G058580*/*HORVU.MOREX.r3.6HG0596330*) is a gene that is located on Chr 6, consists of a 732 bp long single exon and encodes a 243 aa-long plant-specific R2R3-type MYB TF containing two repeats of the MYB-domain with triplet tryptophan residues on each repeat.

Comparative phylogenetic analysis of barley, rice and Arabidopsis MYB-type TFs revealed orthologues genes of *HvMYB15* (Figure 27). *AtMYB15* and *OsMYB30* have been identified as closest relatives in Arabidopsis and rice, respectively. Interestingly, according to the literature, both genes are involved in similar pathways, indicating a conserved function. *AtMYB15* and *OsMYB30* have been both shown to be negative regulators of cold tolerance (Kim et al., 2017; Lv et al., 2017). Similarly, both TFs are involved in defense-induced lignification in Arabidopsis and rice (Chezem et al., 2017; Li et al., 2020).

To gain further knowledge about the regulation of *HvMYB15*, the 2 kb-long promoter region upstream of the coding sequence was analyzed as described in 3.3.1. The promoter region contained numerous motifs that might be important for *HvMYB15* expression. Mostly overrepresented motifs include ACGT (ACGTATERD1), NGATT (N=A/T/G/C) (ARR1AT), CATT (CAATBOX1), YACT (Y=T/C) (CACTFTPPCA1), and AAAG (DOFCOREZM). ARR1AT in Arabidopsis is a binding element of the cytokinin response regulator (ARR1), which acts as transcriptional activator (Sakai et al., 2000). DOFCOREZM is a DNA-binding site and represents the most abundant motif found on the promoter. Likewise, many other motifs for MYB-, MYC- and WRKY-binding (W-box) were scattered on the promoter. CAATBOX1 and CACTFTPPCA are organ-specific elements that are required for seed- and mesophyll-specific gene expression
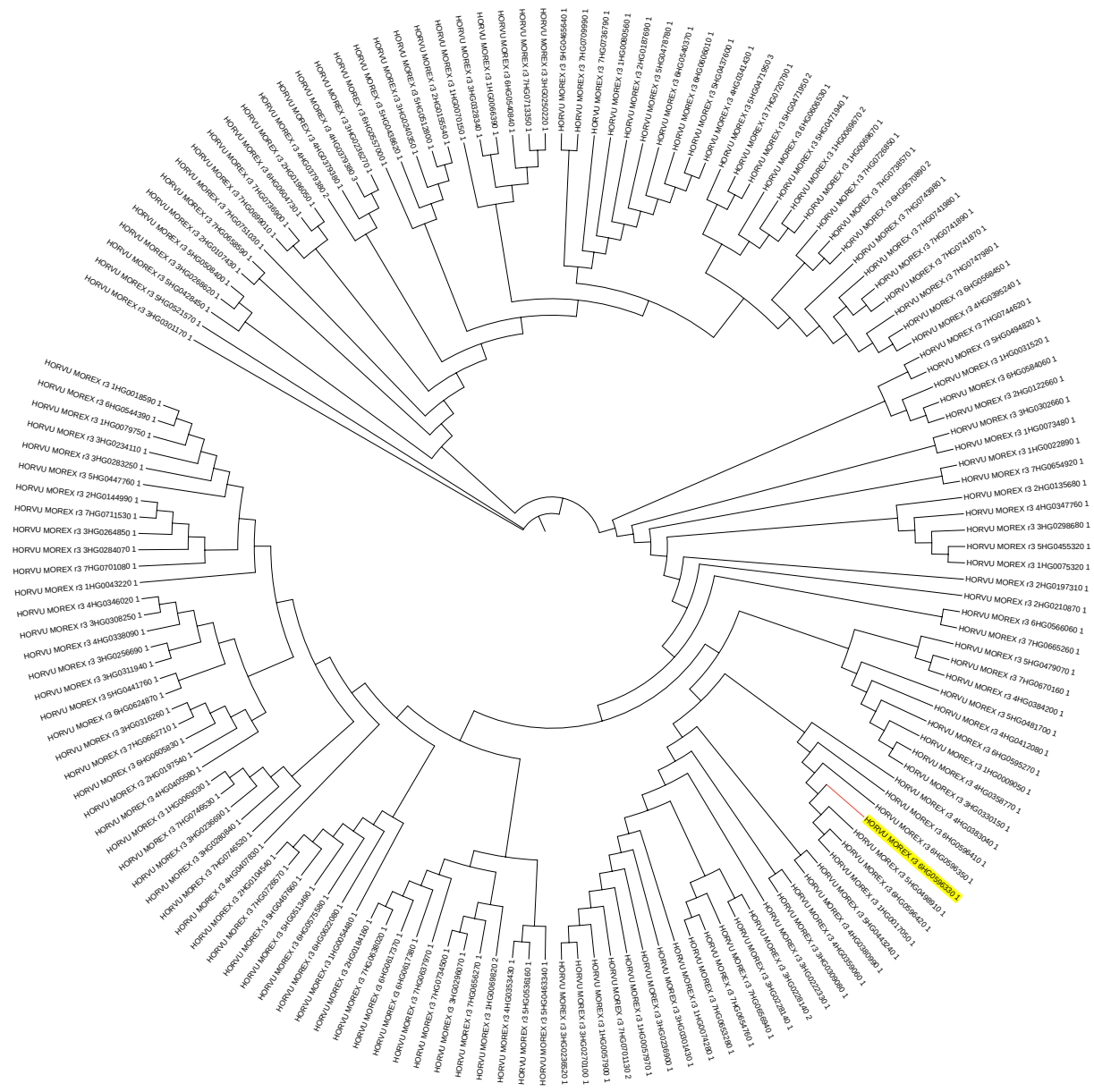
**Figure 26. Phylogenetic tree of the MYB TF family in barley.** Based on protein BLAST and genome mining by annotation 155 unique sequences have been identified as putative MYB proteins in barley. *HvMYB15* (*HORVU6Hr1G058580/HORVU.MOREX.r3.6HG0596330*) is highlighted in yellow. Neighbor-joining method was used to construct the phylogenetic tree using the online tool CLUSTAL Omega (https://www.ebi.ac.uk/Tools/msa/clustalo/).

(Shirsat et al., 1989; Gowik et al., 2004). Another element, associated with tissue-specific regulation was ATATT (ROOTMOTIFTAPOX1), which is required for the root-specific expression. Interestingly, many motifs including ACTTTG (TBOXATGAPB), GATAAG (IBOX), GATAA (IBOXCORE), GRWAAW (GT1CONCENSUS), GATA (GATABOX) and SCGAYNRNNNNNNNNNNNNNNNNHD (PRECONSCRHSP70A) were found to be involved in light responsiveness (Terzaghi and Cashmore, 1995; Gilmartin et al., 1990; Zhou, 1999). Other detected motifs were mostly associated with

cold, drought, ABA, auxin, gibberellin (GA) and jasmonic acid (JA). Collectively, identified *cis*-acting regulatory elements indicate that *HvMYB15* can be regulated by other TFs and may participate in abiotic stress responses. Moreover, existence of phytohormone-responsive elements suggest that *HvMYB15* expression can be regulated by phytohormones.

**a**



**b**

AT3G23250.1
LOC Os04g43680.1
HORVU.MOREX.r3.6HG0596350.1
LOC Os02g41510.1
HORVU.MOREX.r3.6HG0596330.1
HORVU.MOREX.r3.6HG0596420.1
HORVU.MOREX.r3.6HG0596410.1
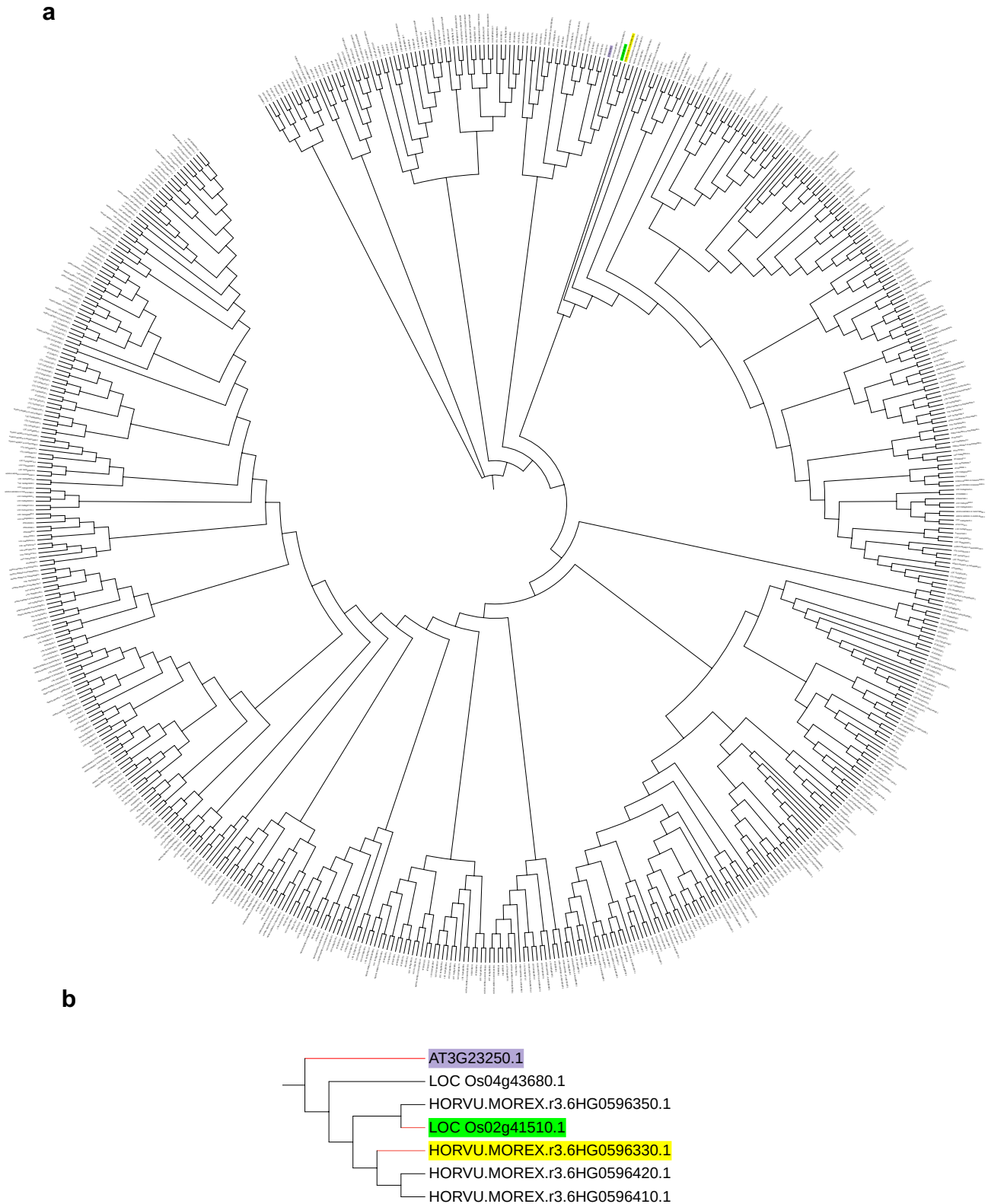
**Figure 27. Phylogenetic analysis of MYB TF in barley, rice and Arabidopsis. (a)** Identified members of barley, rice and Arabidopsis MYB TFs were used to build a phylogenetic tree to reveal closest orthologous genes of different MYB members. Neighbor-joining method was used to construct the phylogenetic tree using the online tool CLUSTAL Omega (https://www.ebi.ac.uk/Tools/msa/clustalo/). **(b)** Close-up view of the gene *HvMYB15* (yellow) and its closest orthologues in rice (green) and Arabidopsis (lilac).

63

### 3.3. Generation of transgenic barley lines

### 3.3.1. Generation of root-specific overexpression lines of *HvWRKY53* and *HvMYB15*

In order to investigate the regulatory function of the transcription factors in root senescence, a transgenic approach was employed, in which root-specific overexpression lines of *HvWRKY53* or *HvMYB15* were generated. The overexpression cassette of the binary vector (pIPKb001, Supplementary Figure 5) comprises of the coding sequence of *HvWRKY53* or *HvMYB15* under control of a root-specific promoter from rice (expressed protein promoter; EPP; *LOC_Os04g11040;* Ramireddy et al., 2018) (Figure 28.a, b). Approximately 210 immature embryos were used for the *Agrobacterium*-mediated transformation with the generated constructs (Table 4).

**Table 4. Summary of the transgenic approach used to generate homozygous overexpression lines of *HvWRKY53* and *HvMYB15*.** Selection of homozygous lines was based on the integration of the transgene *Hygromycin phosphotransferase* (*Hpt)* on genomic DNA, validated by PCR. IE, immature embryos used for transformation; HMZ, homozygous.

| Construct ID | Description | IEs | Regenerants ($T_0$) | Positive $T_0$ plants | Analyzed $T_1$ plants | Analyzed $T_2$ plants | Analyzed $T_3$ plants | Selected HMZ lines |
|---|---|---|---|---|---|---|---|---|
| BG804 | Root-specific overexpression of *HvMYB15* | 210 | 17 | 16 | 5*16=80 | 6*15=90 | 5*30=180 | 3 |
| BG805 | Root-specific overexpression of *HvWRKY53* | 210 | 6 | 5 | 5*5=25 | 6*15=90 | 4*30=180 | 3 |

Agrobacterium-mediated transformation of immature embryos with the MYB15-(BG804) and WRKY53-overexpression-vector (BG805) resulted in the regeneration of 17 and 6 primary transformants ($T_0$), respectively. Leaf samples from the primary transformants were collected at the three-to-four leaf stage to extract genomic DNA and subject it to molecular analysis. Among 17 putative *EPP:HvMYB15* (BG804) and 6 putative *EPP*:*HvWRKY53* (BG805) $T_0$-plants, in 16 (Figure 28c) and 5 (Figure 28d) of them, respectively, the sequence of hygromycin phosphotransferase (*Hpt*) was found to be integrated in the genomic material as validated by polymerase chain reaction (PCR). Upon genetic analysis, positive $T_0$ plants were accepted as transgenic and were brought to the next generation by selfing in the greenhouse.
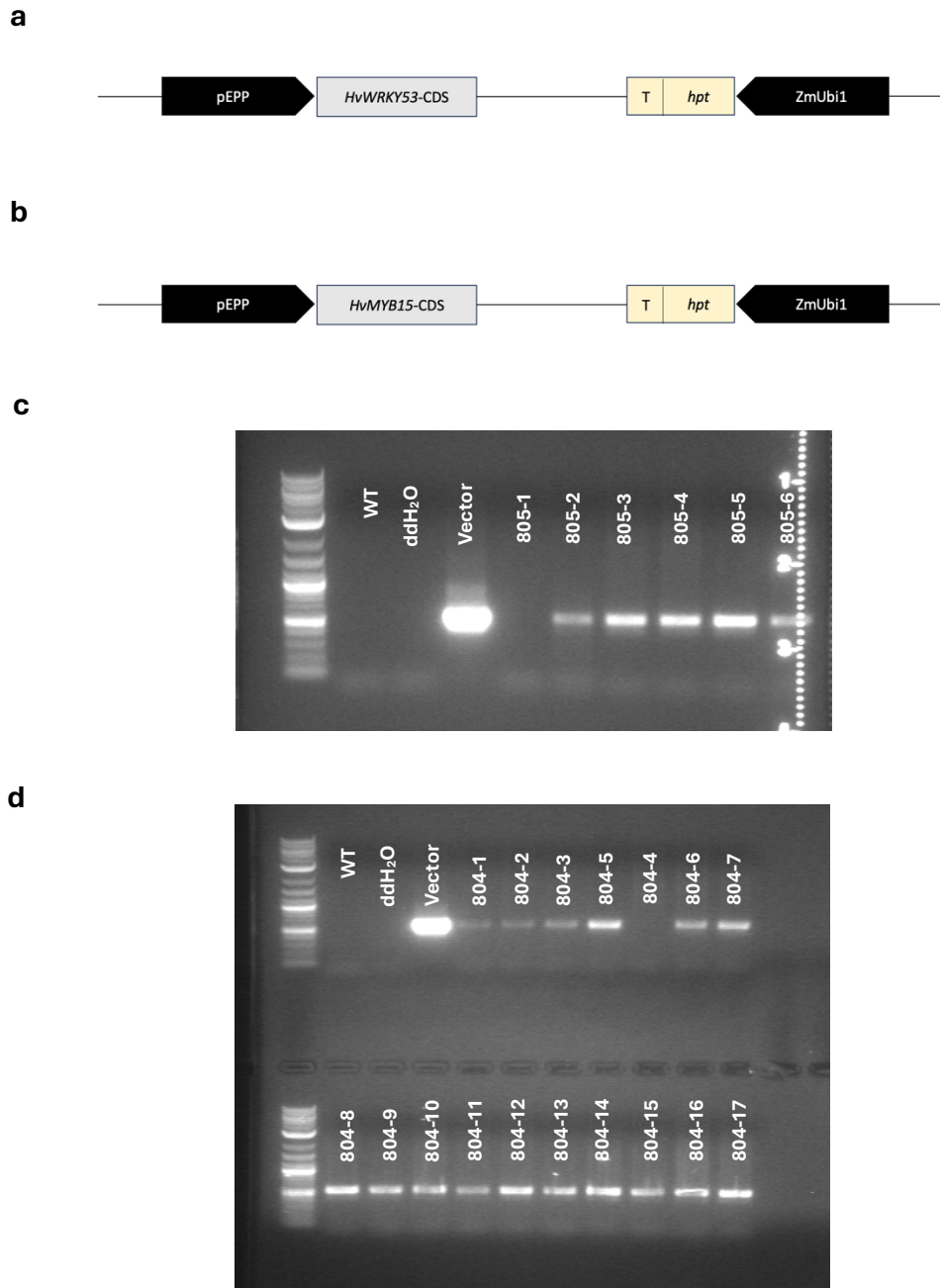
**Figure 28. Generation of root-specific overexpression lines of *HvWRKY53* and *HvMYB15*.**
**(a-b)** Schematic representation of the binary overexpression cassettes generated in this study. Coding sequences of *HvWRKY53* **(a)** and *HvMYB15* **(b)** were cloned into a binary vector pIPKb001 carrying a root-specific promoter sequence (*pEPP*) from *Oryza sativa* to drive the expression of the gene of interest, and the plant selection marker *Hygromycin phosphotransferase* (*Hpt*) gene driven by *ZmUbi1*-promoter. **(c-d)** Identification of putative overexpression lines of *HvWRKY53* and *HvMYB15*. Validation of transgene integration in six **(c)** and seventeen **(d)** primary transformants (T$_0$) of *HvWRKY53* and *HvMYB15*, respectively. Genomic DNA of each T$_0$ plant was tested for the integration of the transgenic marker, *Hpt* (~1kb), by polymerase chain reaction (PCR). Vector, vector used for the transformation of *Agrobacterium* (BG804 or BG805), CDS, coding sequence; T, terminator.

Five seeds of each independent putative transgenic line were then grown in the greenhouse and brought to the next generation by selfing. At three-to-four leaf stage, leaf samples were collected for the extraction of genomic DNA, which was then used for the validation of the transgene, *Hpt*, by PCR (Figure 29). All $T_1$ plants analyzed were found to be positive for the transgene, since these lines were expected to be in a heterozygotic state in this generation. All $T_1$ plants were grown until maturity in the greenhouse to obtain the $T_2$-seeds.



**Figure 29. Genetic analysis of the $T_1$ generation of overexpression lines of *HvWRKY53* and *HvMYB15*.** Validation of the presence of the transgene, *hpt* (~1kb), by polymerase chain reaction (PCR) in the $T_1$ generation of the selected putative overexpression lines of *HvWRKY53* and *HvMYB15*. Gel image is representative. 5 progenies of each line that was selected in the previous generation were grown in the greenhouse, validated for the presence of the transgene, *Hpt*, and were brought to the next generation ($T_2$) by selfing.

Based on the Mendelian laws of genetics, the $T_2$ generation is expected to be a segregating population. However, integration of the transfer DNA (T-DNA) during *Agrobacterium*-mediated transformation of barley comprises of a complex mechanism and may result in transgenic loci consisting of several copies of the transgene (De Neve et al., 1997). In this case, transgene segregation may become distorted, and inheritance may follow a non-Mendelian segregation pattern. Thus, in order to obtain homozygous lines in the $T_3$ generation, it is essential to analyze the segregation pattern of the $T_2$ generation and select only for lines segregating in a 3:1 ratio. For this purpose, at least 15 progenies of each of the six putative independent transgenic lines

of BG804 and BG805 were screened for the presence of the transgene, *Hpt*, by PCR (Figure 30, Table 4). Five of the analyzed BG804-lines and four of the analyzed BG805-lines followed a Mendelian segregation ratio of 3:1. Selected progenies were continued to grow in the greenhouse until maturity and brought to the next generation by selfing.
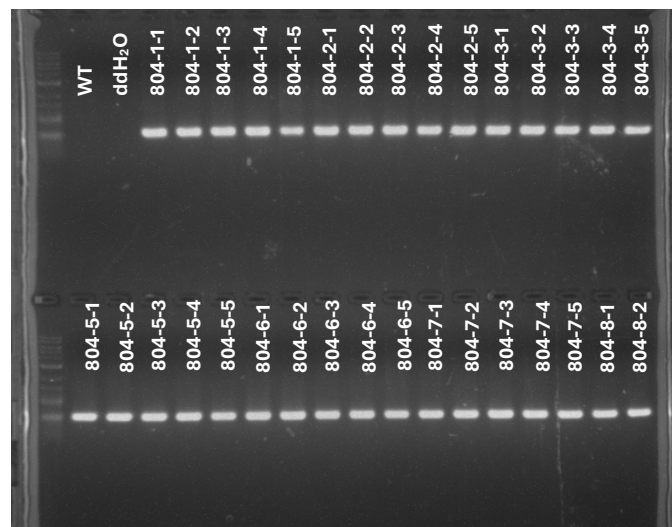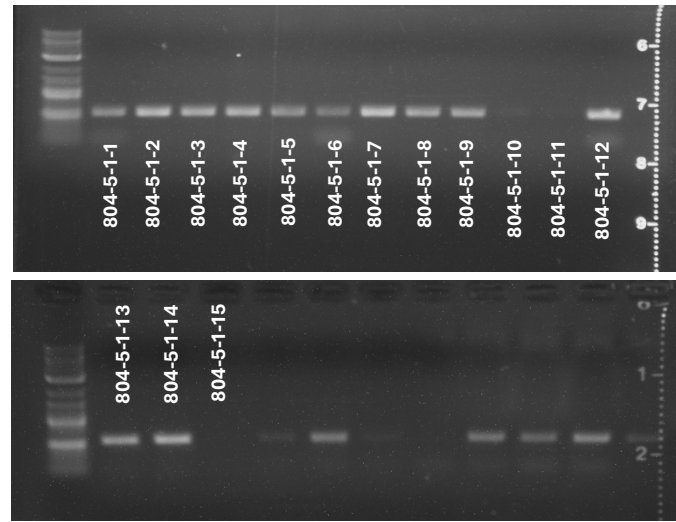


**Figure 30. Genetic analysis of the T$_2$ generation of overexpression lines of *HvWRKY53* and *HvMYB15*.** Validation of the presence of the transgene, *Hpt* (~1kb), by polymerase chain reaction (PCR) in the T$_2$ generation of the selected putative overexpression lines of *HvWRKY53* and *HvMYB15*. Gel images are representative. T$_2$ plants were screened for the presence of the transgene, *Hpt*, and only plants following a 3:1 segregation pattern were continued to grow for the generation of T$_3$ seeds.

In order to identify homozygous lines, 30 progenies of each selected individual line during T$_2$ generation were screened for the presence of the transgene, *Hpt* (Figure 31). Among them, all progenies of four individual lines of BG804 and BG805 were positive for the transgene. Finally, three individual lines of BG804, namely BG804-5-1-8, BG804-7-4-6 and BG804-10-2-15, and three individual lines of BG805, namely BG805-4-10, BG805-5-4-9 and BG805-6-3-10, were selected to be used for physiological analyses throughout the present study. For confirmation, during each experiment performed, all transgenic plants were subjected to genetic analysis for the presence of the transgene, *Hpt*. Moreover, gene expression levels were determined by quantitative reverse transcription PCR (qRT-PCR).
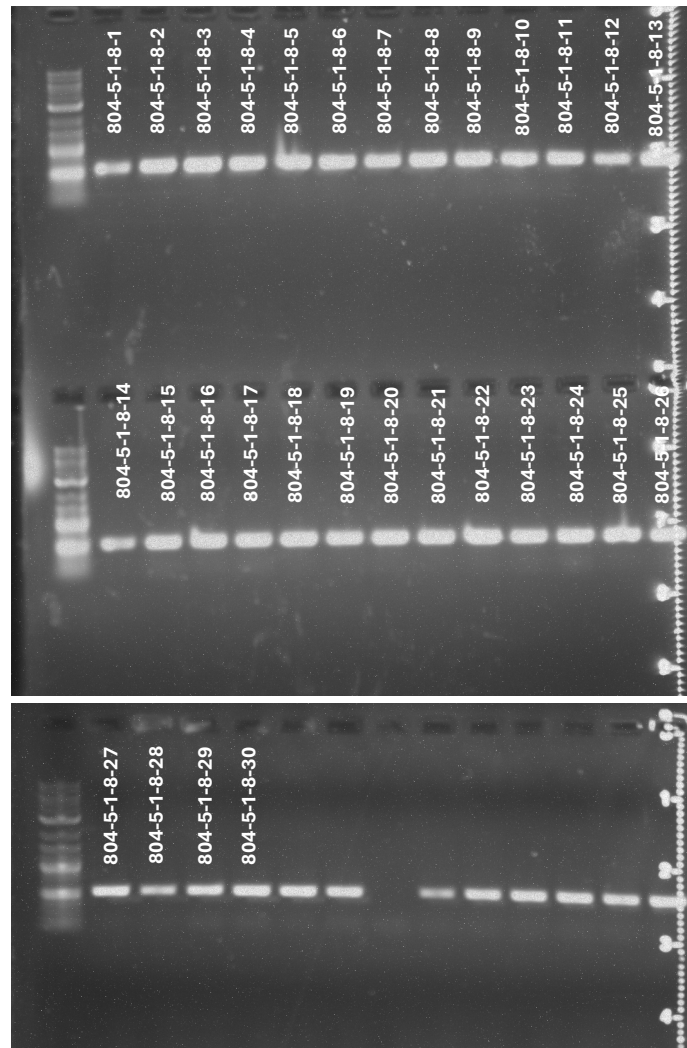
**Figure 31. Identification of homoyzgous transgenic lines with root-specific overexpression of *HvWRKY53* and *HvMYB15*.** Validation of homozygousity in the selected overexpression lines of *HvWRKY53* and *HvMYB15*. 30 progenies from each line selected during the previous generation, $T_2$, were grown in the greenhouse and subjected to genetic analysis. The presence of the transgene, *Hpt* (~1kb), was tested by polymerase chain reaction (PCR). Only those lines with 100 % transgenic progenies were accepted as homozygous and selected for physiological analysis. Gel images are representative.

### 3.3.2. Generation of knock-out mutants of *HvWRKY53* by CRISPR/Cas9-mediated genome editing

In order to investigate the regulatory function of the transcription factor *HvWRKY53* in root senescence, a CRISPR/Cas9-mediated genome editing approach was employed to generate loss-of-function mutations in the coding sequence of *HvWRKY53*. The target motifs as well as the on- and off-target activity scores were determined by using the online platform DESKGEN (Table 5; Hough et al., 2016, Doench et al., 2016). Target motifs that were present in the first exon and close to the ATG site were favored during the selection and analyses. The secondary structure of the putative gRNA sequences was evaluated by using the RNAfold Server (Figure 32; Gruber et al., 2008). Based on the activity score and the RNA secondary structure analysis, gRNA 1 and gRNA 4 were selected to target the *HvWRKY53* gene by Cas9 endonuclease (Figure 33.a).

**Table 5. Structural properties of analyzed gRNA sequences of *HvWRKY53*.** Target motifs and structural features were determined using the online platform DESKGEN (Hough et al., 2016; https://www.deskgen.com/). PAM, protospacer adjacent motif.

| Guide | Target Gene | Sequence | PAM | DNA-Strand | Exon | DESKGEN On-target Activity | DESKGEN Off-target score |
|---|---|---|---|---|---|---|---|
| gRNA 1 | WRKY53 | GCAGCATGCTCAGCTCCATT | GGG | + | 1 | 42 | 98 |
| gRNA 2 | WRKY53 | ATGCTGCAGCAGGACTGCAG | TGG | + | 1 | 62 | 81 |
| gRNA 3 | WRKY53 | GCTCCATTGGGAGCAACAAA | AGG | + | 1 | 47 | 94 |
| gRNA 4 | WRKY53 | CTGCAGCAGGACTGCAGTGG | CGG | + | 1 | 63 | 89 |



**Figure 32. *In silico* prediction of the secondary structure of selected gRNAs for *HvWRKY53*.** Two-dimensional representation of the structures of candidate gRNAs as well as the ta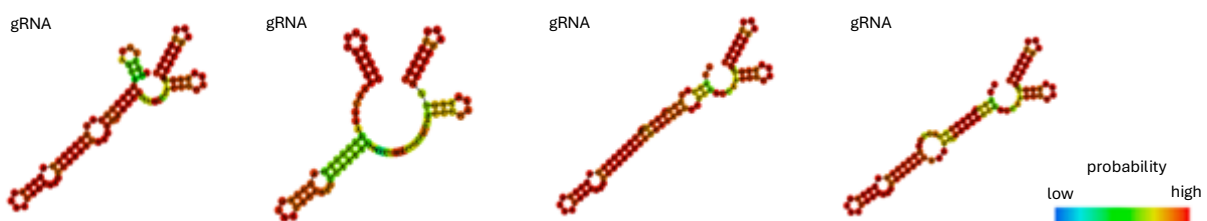rget-unspecific 3'-region of gRNAs (gRNA scaffold) were predicted using the RNAfold webserver (http://rna.tbi.univie.ac.at//cgi-bin/RNAWebSuite/RNAfold.cgi). Different colours indicate base-pairing probabilities (blue: low; red: high).

The transcription factor *HvWRKY53* was targeted to induce loss-of-function mutations by two means: In the first approach, selected gRNAs were used individually in two different constructs to target *HvWRKY53* and drive the Cas9-endonuclease. In an alternative approach, the two gRNAs were used in a single binary construct to target *HvWRKY53* simultaneously. For this purpose, three different binary constructs, namely BE201, BE202 and BE301, were generated to be used for the *Agrobacterium*-mediated transformation of immature embryos (Table 6).

Different number of immature embryos were used to transform barley with the generated constructs (Table 6). Due to very low efficiency in the callus formation, 450 immature embryos were used for each of the transformation event with the constructs BE201 and BE202, whereas the transformation with the construct BE301 took place only using 210 immature embryos. The highest regeneration rate (5.7 %) was achieved with the construct BE301, whereas for BE201 and BE202 it was only 1.1 % and 1.3 %, respectively. Very low regeneration rates might have been caused by the poor quality of the donor plant or immature embryos.

**Table 6. Summary of the targeted mutagenesis approach of *HvWRKY53* in barley.** Number of regenerants represent primary transformants ($T_0$). Putative mutants were identified by confirming transgene integration in the genome and subsequent sequencing of the Cas9-target region. Sequencing chromatograms with double peak positions in the target region were accepted as mutations in a heterozygous or chimeric state. IEs, immature embryos used for transformation.

| Construct | Description | IEs | Regenerants ($T_0$) | Regeneration rate (%) | Putative mutants | Mutation efficiency (%) |
|---|---|---|---|---|---|---|
| BE 201 | gRNA 1 | 450 | 5 | 1.1 | 3 | 60 |
| BE 202 | gRNA 4 | 450 | 6 | 1.3 | 2 | 33.3 |
| BE 301 | gRNA 1 + gRNA 4 | 210 | 12 | 5.7 | 9 | 81.8 |

All regenerants or primary transformants ($T_0$) were subjected to genetic analysis to identify putative mutants. The genomic material of all regenerants was firstly screened for the integration of the *Cas9* gene by PCR (Fig 33.b). Among 5 (BE201), 6 (BE202) and 11 (BE301) regenerants, *Cas9* was present in the genome of 3, 2 and 9 of the regenerants, respectively. The amplification of the Cas9-target region by PCR (Figure 33.c) and subsequent Sanger-sequencing in the plants that carried *Cas9*, resulted in

the detection of the putative mutants. Sequencing chromatograms (Figure 33.d, e) showing double peaks in the target region were indicative of heterozygous or chimeric mutations, which were found in all of the sequenced regenerants, yielding a mutation efficiency ranging from 33.3 to 81.3 % (Table 6).
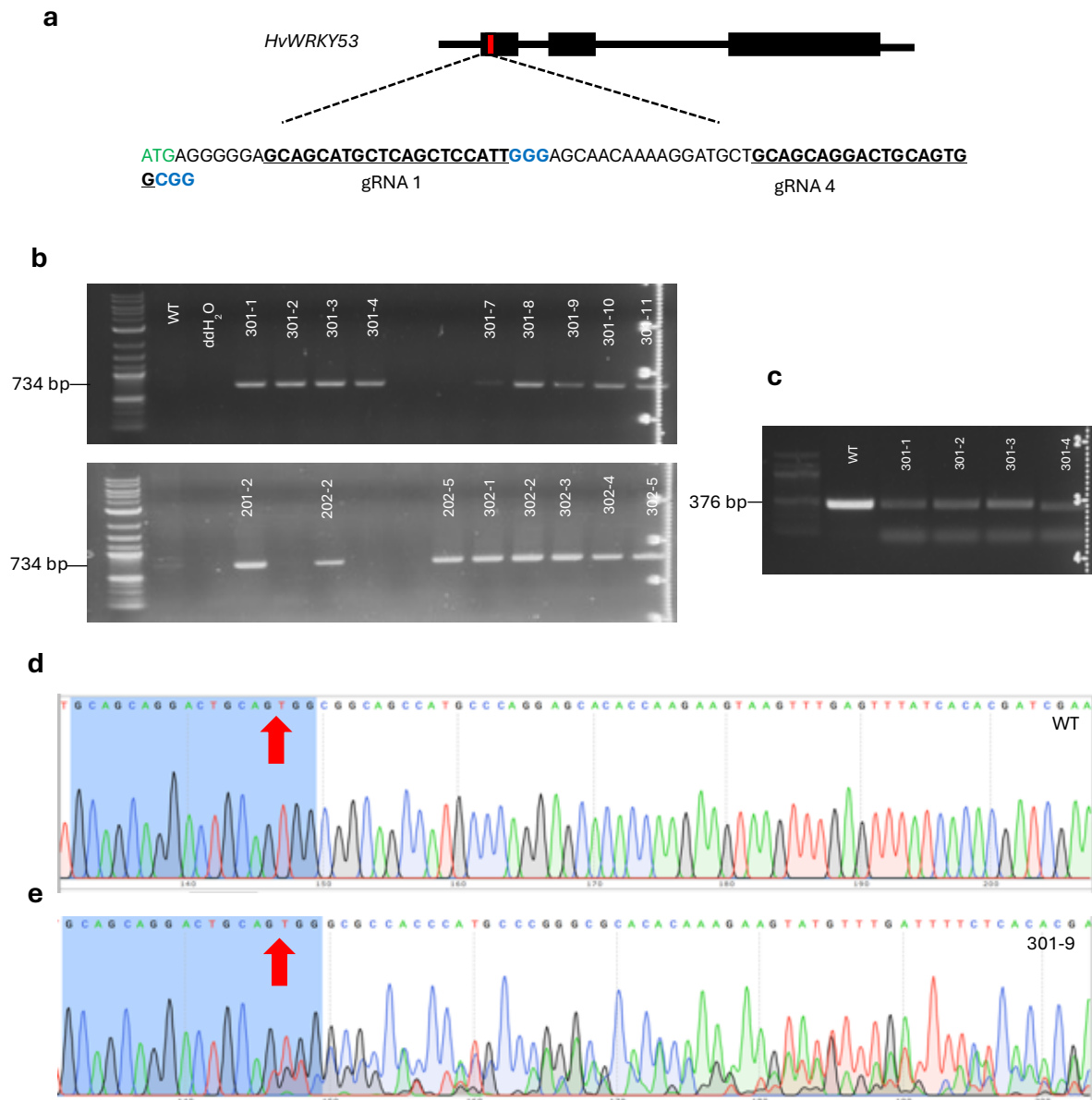


**Figure 33. Genetic analysis of primary transformants (T₀) and identification of putative CRISPR/Cas9-lines of *HvWRKY53*. (a)** Schematic representation of the *HvWRKY53* gene structure consisting of 3 exons and 2 introns with location of the target motifs (red) selected for Cas9. gRNA sequences are underlined, promoter adjacent motif (PAM) is indicated in blue. **(b)** Verification of transgene integration (*Cas9*; amplicon size 734 bp) by polymerase chain reaction (PCR). **(c)** Amplification of the target region (amplicon size 376 bp) in those plants that were positive for the transgene *Cas9*. **(d-e)** Chromatograms of wild-type (WT) **(d)** and a putative mutant (line 301-9) **(e)** *HvWRKY53* sequence obtained by Sanger sequencing. Target sequence is highlighted in blue, and the red arrow designates the Cas9-cutting site (3-4 bp upstream of PAM). Noisy background in the chromatogram starting from the Cas9-cutting site indicates heterozygous or chimeric mutations in that region.

To obtain homozygous mutations in the target region of *HvWRKY53*, all regenerants ($T_0$) were grown until maturity and brought to the next generation by selfing. 20-30 progenies ($T_1$) of each individual putative mutant line ($T_0$) were screened for the presence of *Cas9* in the genome (Figure 34.b). Since *Cas9* should be segregating along with the induced mutations in the $T_1$ generation (Zhang et al., 2014), only those progenies that lost the transgene, *Cas9*, were selected for further analyses. The proportion of *Cas9*-negative to *Cas9*-positive progenies varied significantly among the individual primary mutants ($T_0$) and ranged from 4/26 up to 15/15 (results not shown). The Cas9-target region was amplified, and the modified sequences were obtained by Sanger-sequencing, which were then aligned against Golden Promise *HvWRKY53* sequence to identify CRISPR/Cas9-induced mutations (Figure 34.c).

All the detected mutations were homozygous in the analysed lines during $T_1$ generation. Mutations included insertions and deletions at one or both target sites, however, no base substitutions were observed (Table 7). In case of the use of a single gRNA to target *HvWRKY53* (i.e., BE201 or BE202), observed mutations included +1 bp insertion, -1 or -2 bp deletions. Simultaneous use of both gRNAs (i.e., BE301) resulted in different mutation patterns. in this case mutations were found either at one of the two target sites, at both of the target sites, or in-between the two target sites. For instance, line 301-3-24 harboured at the first target site a -1bp deletion and at the second target site a -4 bp deletion. On the contrary, in line 301-9-10, mutations were observed only at the second target site (-12 bp deletion). Likewise, line 301-11-21 had mutations only at the first target site (-6 bp deletion). Modifications taking place at only one of the two target sites might be a result of the competition between the two gRNAs for Cas9 (Xie et al., 2014). Interestingly, 38 bp in-between the two target sites were found to be completely deleted from the genome of line 301-4-11 (Figure 34.c, Table 7). This mutation was the largest deletion among all identified mutations. Moreover, only this line, 301-4-11, had modifications in-between the two target sites.
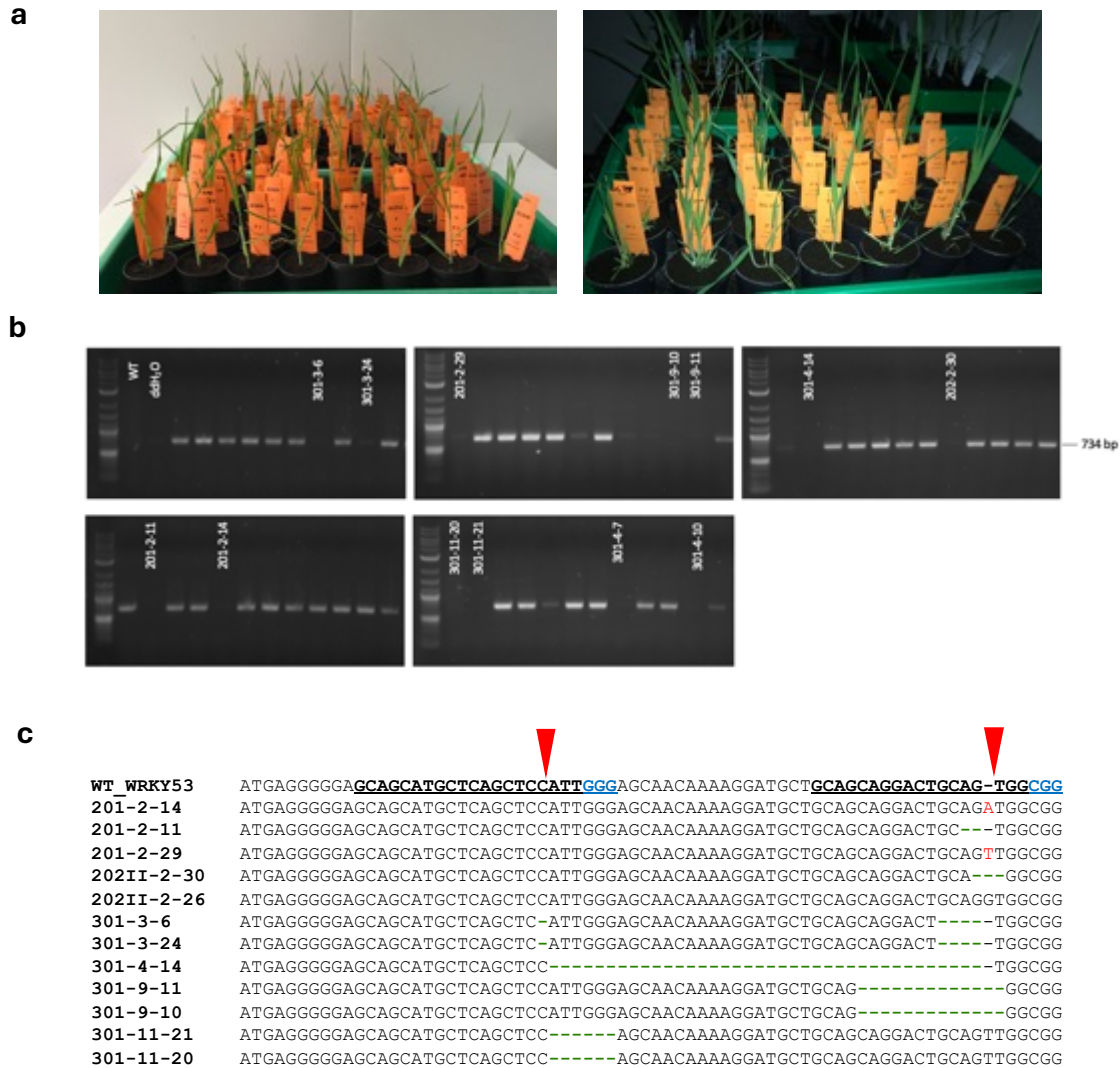
**Figure 34. Genetic analysis and identification of transgene-free $T_1$ mutants of *HvWRKY53* generated by CRISPR/Cas9-mediated genome editing. (a)** Three-to-four leaf stage progenies of $T_1$ plants, grown in the greenhouse for genetic analysis. **(b)** Genotypic identification of putative $T_1$ mutants using a segregating molecular marker (*Cas9*; amplicon size 734 bp). Those plants, that were negative for the transgene, were further used to amplify the target region. **(c)** CRISPR/Cas9-induced mutations detected by Sanger sequencing in the target region. Two different target sites are underlined, protospacer adjacent motif (PAM), insertions and deletions are indicated in blue, red, or as green dashes, respectively. Red arrows 3-bp upstream of PAM indicate DNA-cutting site.

**Table 7. Characterization of the CRISPR/Cas9-induced mutations in the coding region of _HvWRKY53_.** Modifications in the genomic sequence were obtained by Sanger sequencing. Site 1 and site 2 designate the DNA-binding site (target region) for gRNA 1 and gRNA 4, respectively. bp, base pair.

| Construct ID | Plant ID | Mutation | Location | Type |
|---|---|---|---|---|
| BE 201 | 201-2-11 | Δ2 bp | site 1 | deletion |
| | 201-2-14 | Δ1 bp | site 1 | insertion |
| | 201-2-29 | Δ1 bp | site 1 | insertion |
| BE 202 | 202-2-26 | Δ1 bp | site 2 | insertion |
| | 202-2-30 | Δ2 bp | site 2 | deletion |
| BE 301 | 301-3-6 | Δ1 bp; Δ4 bp | site 1 and 2 | deletion |
| | 301-3-24 | Δ1 bp; Δ4 bp | site 1 and 2 | deletion |
| | 301-4-14 | Δ38 bp | between site 1 and 2 | deletion |
| | 301-9-10 | Δ12 bp | site 2 | deletion |
| | 301-9-11 | Δ12 bp | site 2 | deletion |
| | 301-11-20 | Δ6 bp | site 1 | deletion |
| | 301-11-21 | Δ6 bp | site 1 | deletion |

To determine the impact of the modifications in the nucleotide sequence at the translational level, modified nucleotide sequences of _HvWRKY53_ in the selected lines (301-3-24, 301-4-14, 301-9-10) were translated into amino acid sequences using the online translation tool Expasy (https://web.expasy.org/translate/). Obtained amino acid sequences were then aligned against the wild-type HvWRKY53 protein sequence from Golden Promise (Figure 35). The Golden Promise HvWRKY53 protein is 256 amino acid long, whereby lines 301-3-24, 301-4-14, and 301-9-10 were predicted to produce only 55, 44 and 29 amino acid-long proteins, respectively, resulting from the introduction of a premature stop codon. Moreover, in all lines, biosynthesis of the truncated protein is predicted to lead to the loss of the conserved WRKY-DNA binding domain. Based on these predictions, these lines were selected as independent homozygous knock-out lines of _HvWRKY53_ and used for further physiological analyses throughout this study.

```
301-3-24     MRGSSMLSSLGATKGCCSRTWRQPCPGAHQEVSLSLSHDRNCYCFHAWTFMPKLS-----     55
301-4-14     MRGSSML-------------SSWRQPCPGAHQEVSLSLSHDRNCYCFHAWTFMPKLS-----     44
301-9-10     MRGSSMLSSIGSNKRM-----LQ-----GGSHAQEHTKK----------------------     29
GP_WRKY53    MRGSSMLSSIGSNKRM-----LQQDCSGGSHAQEHTKKKARV-GMRTDYTYAPYHDGFQWR     55
             *******                   :    *. :   . : .

301-3-24     ------------------------------------------------------------     55
301-4-14     ------------------------------------------------------------     44
301-9-10     ------------------------------------------------------------     29
GP_WRKY53    KYGQKVIRGNAFPRCYYRCTYHQDHGCSASKHVEQHNSADPPLFRVVYTNDHTCSGAAAA     115

301-3-24     ------------------------------------------------------------     55
301-4-14     ------------------------------------------------------------     44
301-9-10     ------------------------------------------------------------     29
GP_WRKY53    ASDYMASSMHIQQIADASLRKADTEPERPPRPQQPRSGGGGAAAIKEEKDVIVSSLLAVI     175

301-3-24     ------------------------------------------------------------     55
301-4-14     ------------------------------------------------------------     44
301-9-10     ------------------------------------------------------------     29
GP_WRKY53    RGSCDVAKSDAAHQGYSSASSLASANCYAMSPSVAGGSREGSSSSSVSPAVLPAPDDMGL     235

301-3-24     -----------------------     55
301-4-14     -----------------------     44
301-9-10     -----------------------     29
GP_WRKY53    GLDFMVESHWFEPLDLGWFVE        256
```

**Figure 35. CRISPR/Cas9-induced modifications in transgenic lines result in truncated and non-functional HvWRKY53 protein sequences.** Multiple sequence alignment of wild-type (GP_WRKY53) and CRISPR/Cas9-modified (301-3-24, 301-4-14, 301-9-10) HvWRKY53 protein. Nucleotide sequences were firstly translated into protein sequences, which were then aligned using an online multiple protein sequence alignment tool CLUSTAL OMEGA (EMBL-EBI; https://www.ebi.ac.uk/Tools/msa/clustalo/).

### 3.3.3. Generation of knock-out mutants of *HvMYB15* by CRISPR/Cas9-mediated genome editing

With the aim to characterize *HvMYB15* in transgenic barley, similar approaches as described in 3.3.1. were followed to generate knock-out mutants of *HvMYB15* employing CRISPR/Cas9-mediated genome editing. The target sequences as well as the on- and off-target scores were obtained using the online gRNA prediction platform DESKGEN (Table 8). Based on the on- and off-target activity scores obtained using DESKGEN and the RNA secondary structures predicted using RNAfold Server (Figure 36), gRNA 6 and gRNA 7 were selected to target the *HvMYB15* gene by Cas9 endonuclease (Figure 37.a).

**Table 8. Structural properties of analyzed gRNA sequences of *HvMYB15*.** Target motifs and structural features were determined using the online platform DESKGEN (Hough et al., 2016; https://www.deskgen.com/). PAM, protospacer adjacent motif.

| Guide | Target Gene | Sequence | PAM | DNA-Strand | Exon | DESKGEN On-target Activity | DESKGEN Off-target score |
|-------|-------------|----------|-----|------------|------|-----------------------------|---------------------------|
| gRNA 5 | MYB15 | CTCCTTGCTGCGAGAAGATG | GGG | + | 1 | 48 | 24 |
| gRNA 6 | MYB15 | GAGAAGATGGGGCTCAAGAG | GGG | + | 1 | 45 | 34 |
| gRNA 7 | MYB15 | GGAGGAGGACATGACCCTGG | TGG | + | 1 | 69 | 43 |



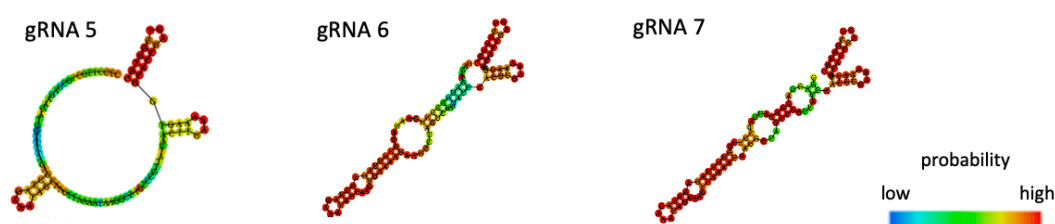**Figure 36. *In silico* prediction of the secondary structure of selected gRNAs for *HvMYB15*.** Two-dimensional representation of the structures of candidate gRNAs as well as the target-unspecific 3'-region of gRNAs (gRNA scaffold) were predicted using the RNAfold webserver (http://rna.tbi.univie.ac.at//cgi-bin/RNAWebSuite/RNAfold.cgi). Different colours indicate base-pairing probabilities (blue: low; red: high).

The transcription factor gene *HvMYB15* was targeted to induce loss-of-function mutations by different means: Three different constructs were generated to target either one of the two sites or both sites simultaneously (Table 9). Eventually, binary constructs, namely BE 203, 204 and 302 were used for the *Agrobacterium*-mediated transformation of barley. Approximately 210 immature embryos were used for each transformation event (Table 9). Transformation events with three different constructs yielded different numbers of regenerants ($T_0$). Highest number of regenerants was obtained from the transformation with the construct BE203, yielding the highest regeneration rate (6.6 %), while it was 3.3 and 2.3 % for BE204 and BE302, respectively (Table 9).

**Table 9. Summary of the targeted mutagenesis approach of *HvMYB15* in barley.** Number of regenerants represent primary transformants ($T_0$). Putative mutants were identified by confirming transgene integration in the genome and subsequent sequencing of the Cas9-target region. Sequencing chromatograms with double peaks in the target region were accepted as mutations in a heterozygous or chimeric state. IEs, immature embryos used for transformation.

| Construct | Description | IEs | Regenerants ($T_0$) | Regeneration rate (%) | Putative mutants | Mutation efficiency (%) |
|---|---|---|---|---|---|---|
| BE 203 | gRNA 6 | 210 | 14 | 6.6 | 12 | 85.7 |
| BE 204 | gRNA 7 | 210 | 7 | 3.3 | 7 | 100 |
| BE 302 | gRNA 6 + gRNA 7 | 210 | 5 | 2.3 | 4 | 80 |

To identify putative mutants, all regenerants ($T_0$) were screened for the integration of the Cas9-endonuclease. Among 14 (BE203), 7 (BE204) and 5 (BE302) regenerants, *Cas9* was present in the genome of 12, 7 and 4 of the regenerants, respectively (Table 9). Subsequently, the target region of all *Cas9*-positive plants was sequenced to identify putative mutants. Chromatograms (not shown) showing double peaks in the target region were accepted as heterozygous or chimeric mutations. Homozygous mutations did not occur in the $T_0$-generation. Transformation events with the constructs BE203, 204 and 302 resulted in very high mutation efficiencies reaching up to 100 % (Table 9). All putative mutants were grown further until maturity and brought to the next generation by selfing. In the $T_1$ generation, the plants, i.e. approx. 10-20 progenies of each putative $T_0$-mutant, were screened again for the presence of *Cas9*. Most of the analysed plants were still *Cas9*-positive, indicating heterozygosity. The proportion of *Cas9*-negative to *Cas9*-positive progenies varied significantly among each individual primary mutant ($T_0$) and ranged from 0/19 up to 9/11 (results not

shown). In total, 21 plants (T$_1$) were *Cas9*-negative. Only two of the three constructs used to target *HvMYB15* (i.e. BE204 and BE302) resulted in *Cas9*-negative plants during T$_1$ generation. In all progenies of the T$_0$ plants, which were generated through transformation using the construct BE203, *Cas9* was still detectable. Usually, presence of *Cas9* in the genome is indicative of mutations that are still heterozygous. Thus, the target region of only *Cas9*-negative plants was amplified by PCR. Subsequently, sequences of the *Cas9*-target region obtained by Sanger sequencing were aligned against the Golden Promise *HvMYB15* sequence to identify CRISPR/Cas9-induced mutations (Figure 37.b).
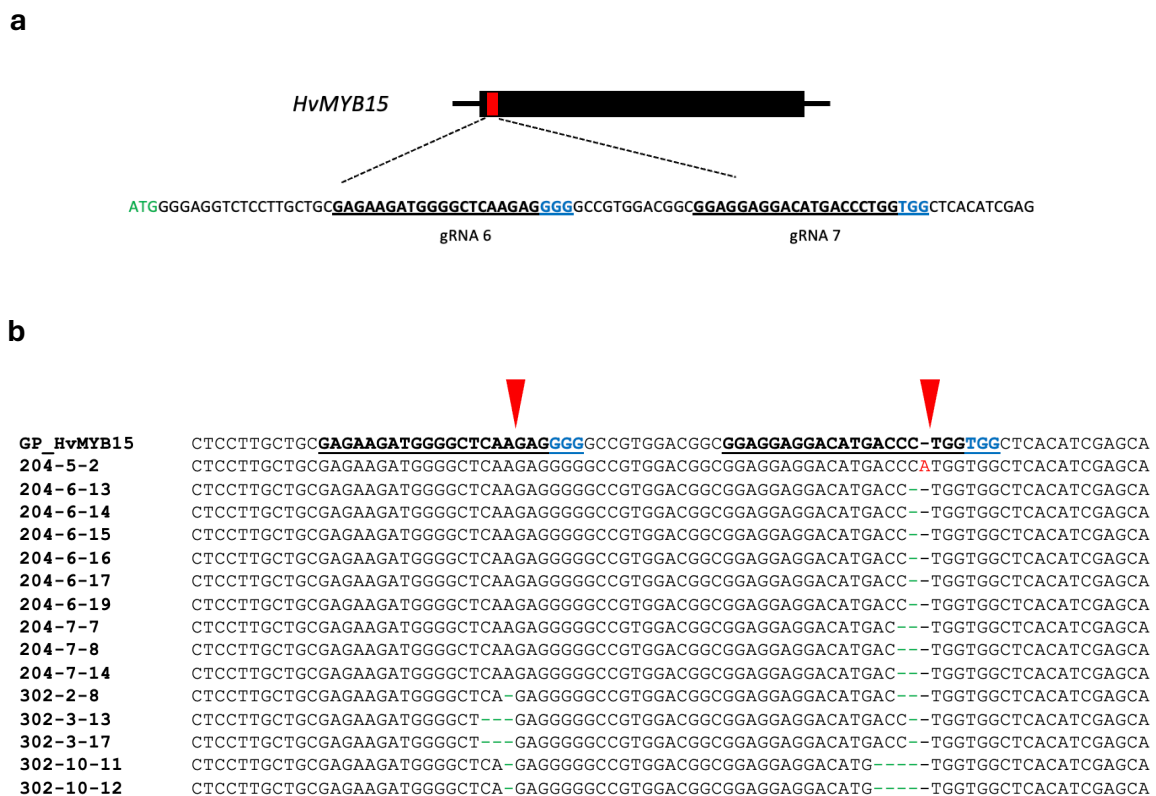


**a**

HvMYB15

ATGGGGAGGTCTCCTTGCTGC**GAGAAGATGGGGCTCAAGAGGGG**GCCGTGGACGGC**GGAGGAGGACATGACCCTGGTGG**CTCACATCGAG

gRNA 6          gRNA 7

**b**

```
GP_HvMYB15    CTCCTTGCTGCGAGAAGATGGGGCTCAAGAGGGGGCCGTGGACGGCGGAGGAGGACATGACCC-TGGTGGCTCACATCGAGCA
204-5-2       CTCCTTGCTGCGAGAAGATGGGGCTCAAGAGGGGGCCGTGGACGGCGGAGGAGGACATGACCCATGGTGGCTCACATCGAGCA
204-6-13      CTCCTTGCTGCGAGAAGATGGGGCTCAAGAGGGGGCCGTGGACGGCGGAGGAGGACATGACC--TGGTGGCTCACATCGAGCA
204-6-14      CTCCTTGCTGCGAGAAGATGGGGCTCAAGAGGGGGCCGTGGACGGCGGAGGAGGACATGACC--TGGTGGCTCACATCGAGCA
204-6-15      CTCCTTGCTGCGAGAAGATGGGGCTCAAGAGGGGGCCGTGGACGGCGGAGGAGGACATGACC--TGGTGGCTCACATCGAGCA
204-6-16      CTCCTTGCTGCGAGAAGATGGGGCTCAAGAGGGGGCCGTGGACGGCGGAGGAGGACATGACC--TGGTGGCTCACATCGAGCA
204-6-17      CTCCTTGCTGCGAGAAGATGGGGCTCAAGAGGGGGCCGTGGACGGCGGAGGAGGACATGACC--TGGTGGCTCACATCGAGCA
204-6-19      CTCCTTGCTGCGAGAAGATGGGGCTCAAGAGGGGGCCGTGGACGGCGGAGGAGGACATGACC--TGGTGGCTCACATCGAGCA
204-7-7       CTCCTTGCTGCGAGAAGATGGGGCTCAAGAGGGGGCCGTGGACGGCGGAGGAGGACATGAC---TGGTGGCTCACATCGAGCA
204-7-8       CTCCTTGCTGCGAGAAGATGGGGCTCAAGAGGGGGCCGTGGACGGCGGAGGAGGACATGAC---TGGTGGCTCACATCGAGCA
204-7-14      CTCCTTGCTGCGAGAAGATGGGGCTCAAGAGGGGGCCGTGGACGGCGGAGGAGGACATGAC---TGGTGGCTCACATCGAGCA
302-2-8       CTCCTTGCTGCGAGAAGATGGGGCTCA-GAGGGGGCCGTGGACGGCGGAGGAGGACATGAC---TGGTGGCTCACATCGAGCA
302-3-13      CTCCTTGCTGCGAGAAGATGGGGCT---GAGGGGGCCGTGGACGGCGGAGGAGGACATGACC--TGGTGGCTCACATCGAGCA
302-3-17      CTCCTTGCTGCGAGAAGATGGGGCT---GAGGGGGCCGTGGACGGCGGAGGAGGACATGACC--TGGTGGCTCACATCGAGCA
302-10-11     CTCCTTGCTGCGAGAAGATGGGGCTCA-GAGGGGGCCGTGGACGGCGGAGGAGGACATG-----TGGTGGCTCACATCGAGCA
302-10-12     CTCCTTGCTGCGAGAAGATGGGGCTCA-GAGGGGGCCGTGGACGGCGGAGGAGGACATG-----TGGTGGCTCACATCGAGCA
```

**Figure 37. *HvMYB15* gene structure and CRISPR/Cas9-induced mutations in transgenic lines.** **(a)** Gene structure of *HvMYB15* (exons indicated by black boxes) and location of the target motifs of gRNA 6 and gRNA 7. **(b)** Modified *HvMYB15* sequences of transgenic lines that have lost the transgene *Cas9* in the T$_1$-generation, aligned against the *HvMYB15* nucleotide sequence of Golden Promise. CRISPR/Cas9-induced mutations were identified by Sanger sequencing. The two target sites are underlined, protospacer adjacent motif (PAM), insertions and deletions are indicated in blue, red, and as green dashes, respectively. Red arrows 3-bp upstream of PAM indicate DNA-cutting site.

Mutations induced comprised of insertions and deletions at either one or both target sites (Table 10). An insertion of 1 bp was only observed in line 204-5-2, whereas deletions of different sizes were found in the rest of the transgenic lines that were analysed. All progenies of line 204-6 and 204-7 exhibited 1 and 2 bp deletions in the second target site, respectively. Targeting both sites simultaneously resulted in deletions at both target sites. Line 302-2-8 had 1 and 2 bp deletions at the first and second target site, respectively. Line 302-3-13 and 302-3-17 harboured a 3 bp deletion at the first, and a 1 bp deletion at the second target site, whereas for line 302-10-11 and 302-10-12, a 1 bp deletion at the first and 4 bp deletion at the second target site were found to be induced by CRISPR/Cas9-mediated genome editing.

**Table 10. Characterization of the CRISPR/Cas9-induced mutations in the coding region of *HvMYB15*.** Modifications in the genomic sequence were obtained by Sanger sequencing. Site 1 and site 2 designate the DNA-binding sites (target region) for gRNA 6 and gRNA 7, respectively. bp, base pair.

| Construct ID | Plant ID | Mutation | Location | Type |
|---|---|---|---|---|
| | 204-5-2 | Δ1 bp | site 1 | insertion |
| | 204-6-13 | Δ1 bp | site 1 | deletion |
| | 204-6-14 | Δ1 bp | site 1 | deletion |
| | 204-6-15 | Δ1 bp | site 1 | deletion |
| | 204-6-16 | Δ1 bp | site 1 | deletion |
| BE 204 | 204-6-19 | Δ1 bp | site 1 | deletion |
| | 204-7-7 | Δ2 bp | site 1 | deletion |
| | 204-7-8 | Δ2 bp | site 1 | deletion |
| | 204-7-14 | Δ2 bp | site 1 | deletion |
| | 204-7-17 | Δ2 bp | site 1 | deletion |
| | 302-2-8 | Δ1 bp; Δ2 bp | site 1 and 2 | deletion |
| | 302-3-13 | Δ3 bp; Δ1 bp | site 1 and 2 | deletion |
| BE 302 | 302-3-17 | Δ3 bp; Δ1 bp | site 1 and 2 | deletion |
| | 302-10-11 | Δ1 bp; Δ4 bp | site 1 and 2 | deletion |
| | 302-10-12 | Δ1 bp; Δ4 bp | site 1 and 2 | deletion |

To determine the impact of the modifications in the nucleotide sequence at the translational level, modified nucleotide sequences of *HvMYB15* in the selected lines (204-5-2, 204-6-14 and 204-7-17) were translated into amino acid sequences using the online translation tool Expasy (https://web.expasy.org/translate/). Obtained amino acid sequences were then aligned against the Golden Promise HvMYB15 protein sequence (Figure 38). The Golden Promise HvMYB15 protein is 243 amino acid long, whereas lines 204-5-2, 204-6-14 and 204-7-17 were predicted to produce only 128, 193 and 120 amino acid-long proteins, respectively, as a consequence of the premature introduction of a stop codon. Moreover, in all lines, biosynthesis of the truncated protein is predicted to lead to the disruption of the highly conserved MYB-DNA binding domain. Based on these predictions, these lines were selected as independent homozygous knock-out lines of *HvMYB15* and used for further physiological analyses throughout this study.
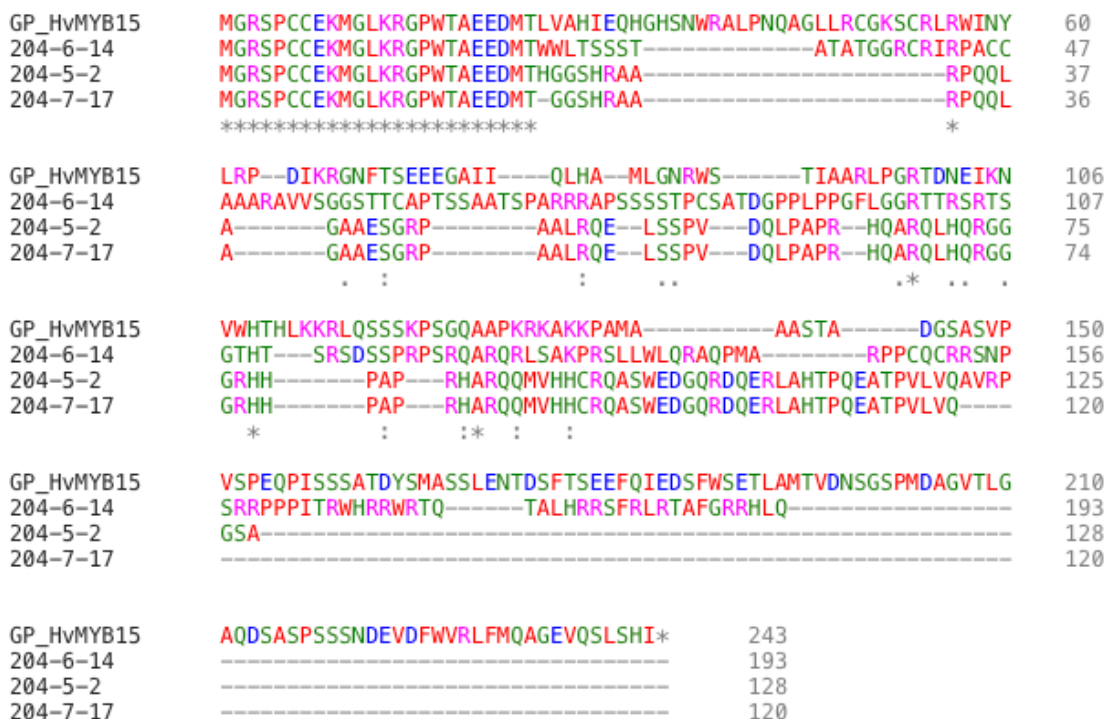


```
GP_HvMYB15    MGRSPCCEKMGLKRGPWTAEEDMTLVAHIEQHGHSNWRALPNQAGLLRCGKSCRLRWINY    60
204-6-14      MGRSPCCEKMGLKRGPWTAEEDMTWWLTSSST--------------ATATGGRCRIRPACC  47
204-5-2       MGRSPCCEKMGLKRGPWTAEEDMTHGGSHRAA----------------------RPQQL   37
204-7-17      MGRSPCCEKMGLKRGPWTAEEDMT-GGSHRAA----------------------RPQQL   36
              ***********************                               *

GP_HvMYB15    LRP--DIKRGNFTSEEEGAII----QLHA--MLGNRWS-------TIAARLPGRTDNEIKN  106
204-6-14      AAARAVVSGGSTTCAPTSSAATSPARRRAPSSSSTPCSATDGPPLPPGFLGGRTTRSRTS  107
204-5-2       A-------GAAESGRP--------AALRQE--LSSPV---DQLPAPR--HQARQLHQRGG   75
204-7-17      A-------GAAESGRP--------AALRQE--LSSPV---DQLPAPR--HQARQLHQRGG   74
                         . :              :    ..          .*  .. .

GP_HvMYB15    VWHTHLKKRLQSSSKPSGQAAPKRKAKKPAMA-----------AASTA------DGSASVP  150
204-6-14      GTHT---SRSDSSPRPSRQARQRLSAKPRSLLWLQRAQPMA--------RPPCQCRRSNP  156
204-5-2       GRHH--------PAP---RHARQQMVHHCRQASWEDGQRDQERLAHTPQEATPVLVQAVRP  125
204-7-17      GRHH--------PAP---RHARQQMVHHCRQASWEDGQRDQERLAHTPQEATPVLVQ----  120
                *             :    :*  :   :

GP_HvMYB15    VSPEQPISSSATDYSMASSLENTDSFTSEEFQIEDSFWSETLAMTVDNSGSPMDAGVTLG  210
204-6-14      SRRPPPITRWHRRWRTQ------TALHRRSFRLRTAFGRRHLQ---------------- 193
204-5-2       GSA--------------------------------------------------------- 128
204-7-17      ------------------------------------------------------------ 120

GP_HvMYB15    AQDSASPSSSNDEVDFWVRLFMQAGEVQSLSHI*              243
204-6-14      --------------------------------------          193
204-5-2       --------------------------------------          128
204-7-17      --------------------------------------          120
```

**Figure 38. CRISPR/Cas9-induced modifications in transgenic lines is predicted to result in truncated HvMYB15 protein sequences.** Multiple sequence alignment of wild-type (GP_HvMYB15) and CRISPR/Cas9-modified (204-5-2, 204-6-14, 204-7-17) HvMYB15 protein. Nucleotide sequences were firstly translated into protein sequences, which were then aligned using an online multiple protein sequence alignment tool CLUSTAL OMEGA (EMBL-EBI; https://www.ebi.ac.uk/Tools/msa/clustalo/).

### 3.4.1. Expression of *HvWRKY53* in different tissues and in response to different stimuli

Based on database mining and the publicly available expression atlas of barley (IPK Barley Blast Server, https://apex.ipk-gatersleben.de/apex/f?p=284:57::::::), *HvWRKY53* was found to be highly expressed in old roots and slightly in embryos. In order to validate the tissue-specific expression of *HvWRKY53*, WT barley plants were grown in the greenhouse. During late flowering stage (BBCH 65-69) different tissues were collected and subjected to gene expression analysis. Root samples were prepared after removing soil from washed-out root tips.

In line with the database information, transcripts of *HvWRKY53* were most abundant in the root tissue (Figure 39). In contrast, old leaf sheaths, flag leaf sheaths, flag leaf blades, 1st node, 3rd node, 5th node, rachis, caryopsis and grains had relatively lower transcript levels, but especially in old leaf blades, old leaf sheaths and flag leaf blades transcript levels were still quite high. These results suggest that *HvWRKY53* is expressed preferentially in vegetative and maybe more aged shoot tissues, however it mostly accumulates in the roots.

Next, to gain further insights about the transcriptional regulation of *HvWRKY53* and whether it is expressed in response to different abiotic stress factors, salt stress, drought and N or P deficiency were induced in hydroponically-grown WT barley plants. In parallel, plants were subjected to ABA treatment. Among those treatments, ABA and P starvation did not affect *HvWRKY53* expression in the young seminal roots (Figure 40). In contrast, PEG-6000, NaCl and N starvation significantly induced *HvWRKY53* expression (Figure 40). The strongest induction was observed for PEG-6000 treatment after 3 hours, whereas *HvWRKY53* expression dropped back to normal levels 24 hours after treatment. Likewise, NaCl treatment only induced *HvWRKY53* expression 3 hours after the treatment and thereafter *HvWRKY53* expression dropped to basal levels. Strikingly, N starvation led to approx. 7, 12.5 and 4.7-fold increase in *HvWRKY53* transcript abundance 3, 24 and 48 hours after treatment, respectively (Figure 40). Taken together, these results suggests that *HvWRKY53* is induced in young seminal roots in response to different stimuli.
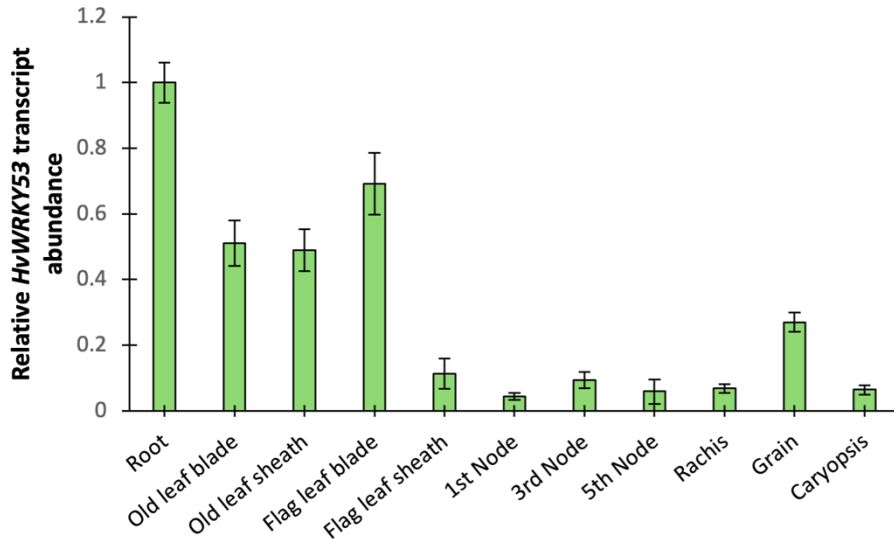
**Figure 39. Relative transcript abundance of *HvWRKY53* in different barley tissues.** Barley plants were grown in the greenhouse until late flowering stage (BBCH 65-69) and different tissues were subjected to gene expression analysis. Gene expression was determined by qPCR. *HvWRKY53* expression in roots was set to 1. Bars show means ± SD (n=3-5).
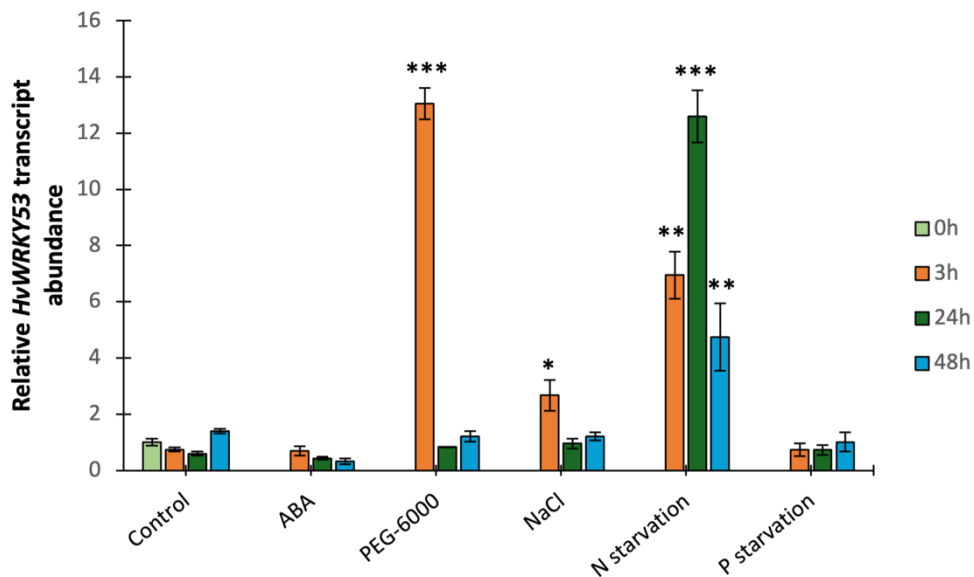


**Figure 40. Relative transcript abundance of *HvWRKY53* in response to different stimuli.** Relative transcript abundance of *HvWRKY53* in response to ABA, NaCl, PEG-6000, N starvation and P starvation treatments after 3, 24 or 48 hours. WT barley plants were grown in hydroponic culture for 21 days. After 21 days, roots were exposed to the nutrient solution containing 70 μM ABA, 150 mM NaCl or 5% PEG-6000. For N or P starvation, N or P sources were completely withdrawn from the nutrient solution. Gene expression was determined by qPCR. Transcript abundance of control plants at 0 h after treatment was set to 1. Bars show means ± SD (n=4). Asterisks denote significant differences between control and treatment at ∗ P < 0.05, ∗∗ P < 0.01, ∗∗∗ P < 0.001 by two-tailed Student's *t* test.

### 3.4.2. The role of *HvWKY53* in early plant growth and development

To characterize the role of *HvWRKY53* in early plant growth and development, three independent lines overexpressing *HvWRKY53* and three independent CRISPR/Cas9 lines of *HvWRKY53* were grown in soil-filled rhizoboxes under greenhouse conditions (Figure 41). The transparent front glass of the rhizoboxes allows the monitoring of root growth non-destructively in real-time. 23 days after sowing (DAS) rhizoboxes were scanned prior to the harvesting of seminal root tips, whole roots, and shoots.

Throughout the whole experimental period WT plants exhibited green and healthy shoots. On 23 DAS, WT plants had in average 650 mg plant$^{-1}$ and approx. 5 tillers (Figure 42.a, b). In contrast, shoot biomass in transgenic lines overexpressing *HvWRKY53* (805-6-3-10, 805-4-3-10, 805-5-4-9) was lower up to 30 %, although the number of tillers was similar to that of the WT. The reduction in shoot biomass was stronger in the CRISPR/Cas9-lines of *HvWRKY53* (301-4-14, 301-3-24, 301-9-10) reaching up to 50% (Figure 42.a). The number of tillers was 20% lower in these lines (Figure 42.b). Seminal and nodal roots were harvested collectively, washed off from soil and oven dried. Root dry matter was found to be significantly lower in both overexpression and CRISPR/Cas9 lines of *HvWRKY53* (Figure 42.c). Overall, CRISPR/Cas9-lines showed a more dramatic reduction in root biomass.
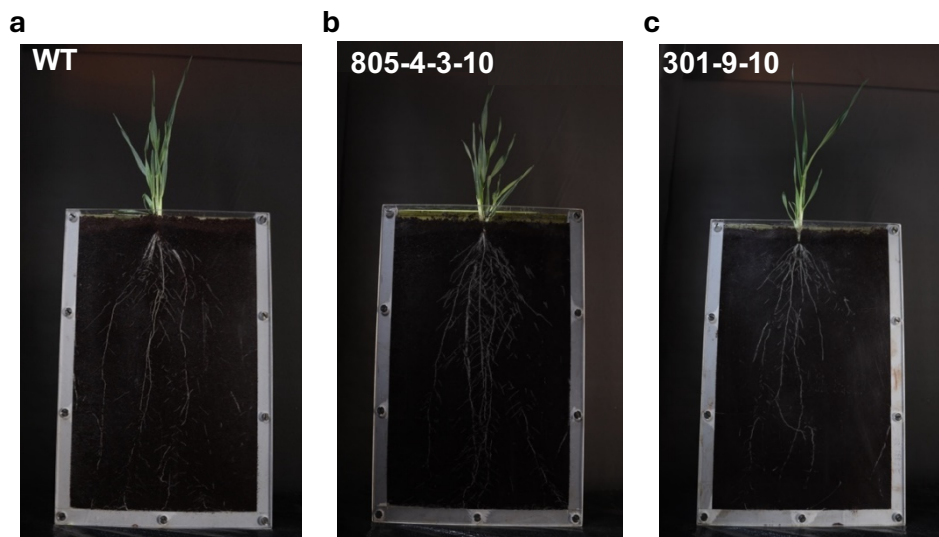


**Figure 41. Root phenotypes of transgenic lines with modified expression of *HvWRKY53*.** Representative images of shoots and roots of wild-type (WT) **(a)**, the *HvWRKY53* overexpression line 805-4-3-10 **(b)** and the corresponding knock-out line 301-9-10 **(c)**. Plants were grown in soil-filled rhizoboxes to monitor root growth and architecture. Images were taken after 23 days.

To determine whether the seminal root growth rate was influenced by the modulated *WRKY53* expression in transgenic lines, every visible root was traced daily from 10 DAS to 20 DAS to quantify the length of the newly formed root tip segment. Manual measurements revealed that the seminal root growth rate was 11% lower in the lines 805-4-3-10 and 805-5-4-9 overexpressing *HvWRKY53* (Figure 42.d). In contrast, the seminal root growth rate in line 805-6-3-10 was similar to the WT. A slightly stronger reduction in the seminal root growth rate was observed in the CRISPR/Cas9-lines of *HvWRKY53* (301-4-14, 301-3-24, 301-9-10). Taken altogether, transgenic lines with altered expression of *HvWRKY53* exhibited stunted shoot and root growth under greenhouse conditions.
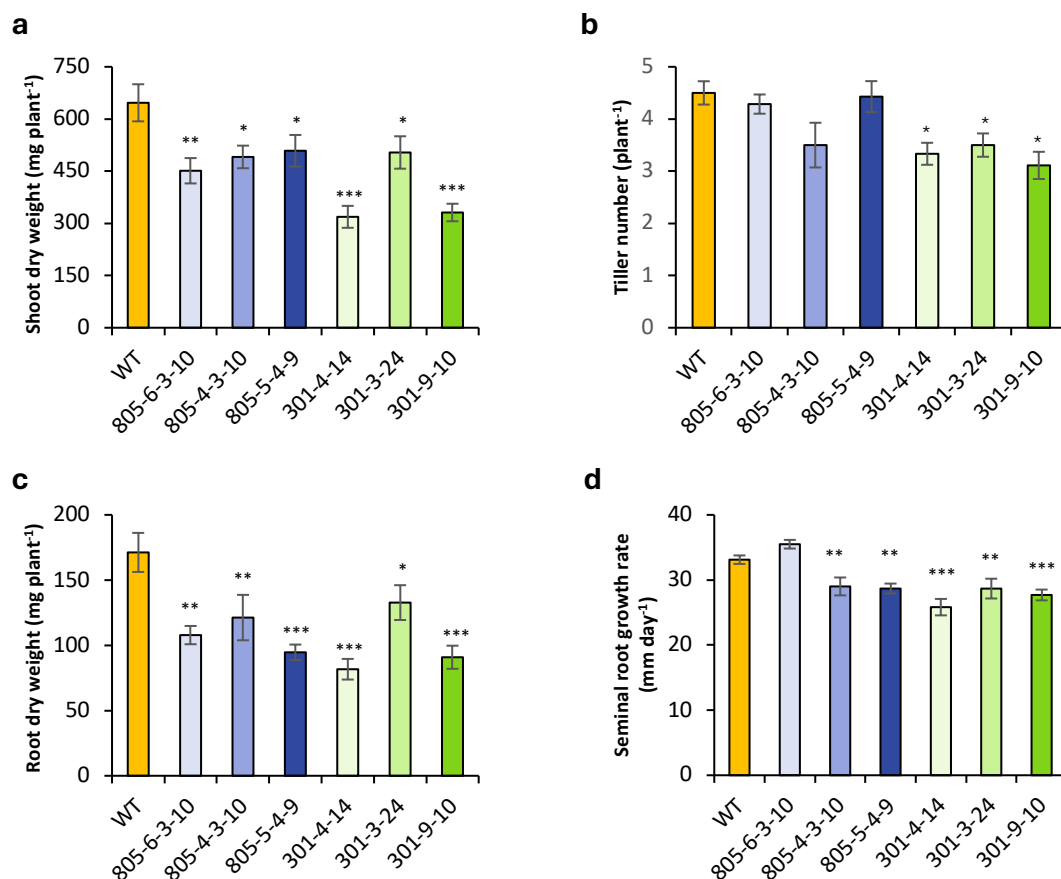


**Figure 42. Shoot and root growth in overexpression and knock-out lines of *HvWRKY53*.** Shoot dry weight **(a)**, tiller number **(b)**, root dry weight **(c)** of wild-type (WT), overexpression (805-6-3-10, 805-4-3-10, 805-5-4-9) and CRISPR/Cas9 lines (301-4-14, 301-3-24, 301-9-10) 23 days after sowing (DAS). Bars show means ± SD (n=6-10 biological replicates). **(d)** Seminal root growth rate of WT and transgenic lines. Each visible seminal root of the plants was traced and measured manually on a daily basis for 10 consecutive days starting from 10 DAS. Bars show means ± SD (n=36-75). Asterisks denote significant differences between means at ∗ P < 0.05, ∗∗ P < 0.01, ∗∗∗ P < 0.001 by two-tailed Student's *t* test. In **(d)**, statistical significance was evaluated by nonparametric comparisons using Wilcoxon method.

To validate modulated *HvWRKY53* expression levels in the overexpression lines, seminal root tips of each plant were collected and used for gene expression analysis by qPCR. In all independent overexpression line (805-6-3-10, 805-4-3-10 and 805-5-4-9), *HvWRKY53* was strongly upregulated (Figure 43). *HvWRKY53* transcript levels in 805-4-3-10 and 805-5-4-9 were highly similar reaching up to 75-fold stronger expression compared to WT. Line 805-6-3-10 exhibited slightly lower transcript levels, but still approx. 30-fold higher than in WT.
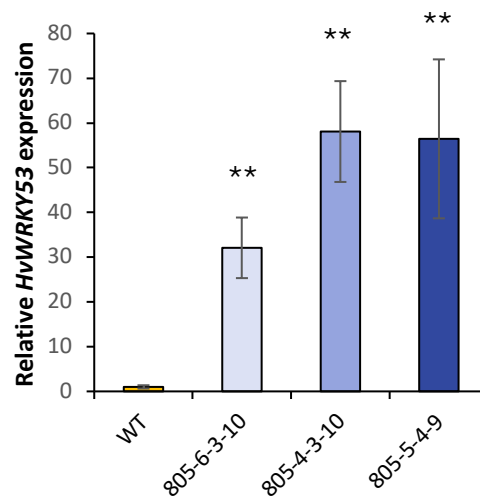


**Figure 43. Transcript abundance of *HvWRKY53* in overexpression lines.** Transcript abundance of *HvWRKY53* in wild-type (WT) and overexpression (805-6-3-10, 805-4-3-10, 805-5-4-9) lines as determined by quantitative real-time polymerase chain reaction (qPCR). Barley plants were grown in soil-filled rhizoboxes to monitor root growth and development. 23 days after sowing (DAS), rhizoboxes were opened and seminal root tips were collected for gene expression analysis. Gene expression levels were normalized to *ADP* and WT-*HvWRKY53* expression was set to 1. Bars show means ± SE (n=6-8 biological replicates). Asterisks (**) denote significant differences between WT and transgenic lines at p<0.01 as assessed by nonparametric comparison by Wilcoxon method.

To investigate whether overexpression or knock-out of *HvWRKY53* modulated root architecture, rhizoboxes were scanned at 23 DAS prior to harvesting of different tissues. Due to the low contrast of the root scans (Figure 44.a), some of the root fractions could not be detected and analysed by the root image analysis software 'saRIA' (Narisetti et al., 2019). Thus, based on the original root scans enhanced segmentation images (Figure 44.b) were created, enabling recognition and analysis of all root traits to be detected by saRIA.

In line with the lower root biomass, root architectural traits were significantly affected in the CRISPR/Cas9-lines of *HvWRKY53* (301-4-14, 301-3-24, 301-9-10). Total root length in lines 301-4-14, 301-3-24 and 301-9-10 was 31, 24.7 and 34 %, respectively, lower than in the corresponding WT (Figure 44.c). Similarly, total root area in all knock-out lines decreased by 27.4 % in average (Figure 44.d). Total root area describes the total number of root pixels in the image, whereas total root surface area describes the surface at each root object of skeleton approximated by tubular shape (Narisetti et al., 2019). Root surface area was found to be affected similarly as the total root area, and was lower in lines 301-4-14, 301-3-24 and 301-9-10 by 28.6, 28.8 and 32 %, respectively (Figure 44.e). Across different genotypes, there was no significant difference in specific root length, which is calculated as the ratio of total length to total volume (Figure 44.f). In contrast to the knock-out lines, root morphological traits in overexpression lines were found to be similar to the WT with the exception of total root length that which was significantly lower in lines 805-5-4-9 and 805-4-3-10 (Figure 44.c).

To evaluate the effect of the weaker root growth on the shoot nutritional status, concentrations of macro- and micronutrients in shoots were determined by inductively coupled plasma optical emission spectroscopy (ICP-OES). With the exception of Zn, concentrations of macro- (i.e. K, Mg, S, Ca and P) and micronutrients (i.e. Fe and Mn) in both overexpression (805-6-3-10, 805-4-3-10, 805-5-4-9) and CRISPR/Cas9-lines of *HvWRKY53* (301-4-14, 301-3-24, 301-9-10) were similar to WT (Supplementary Figure 6). Although Zn concentrations were found to be approx. 20% higher in the shoots of lines 805-6-3-10, 805-4-3-10, 301-4-14 and 301-9-10, this increase was not considered to be meaningful, since absolute values of Zn concentrations were in the luxury range indicating adequate Zn nutrition (Supplementary Figure 6).
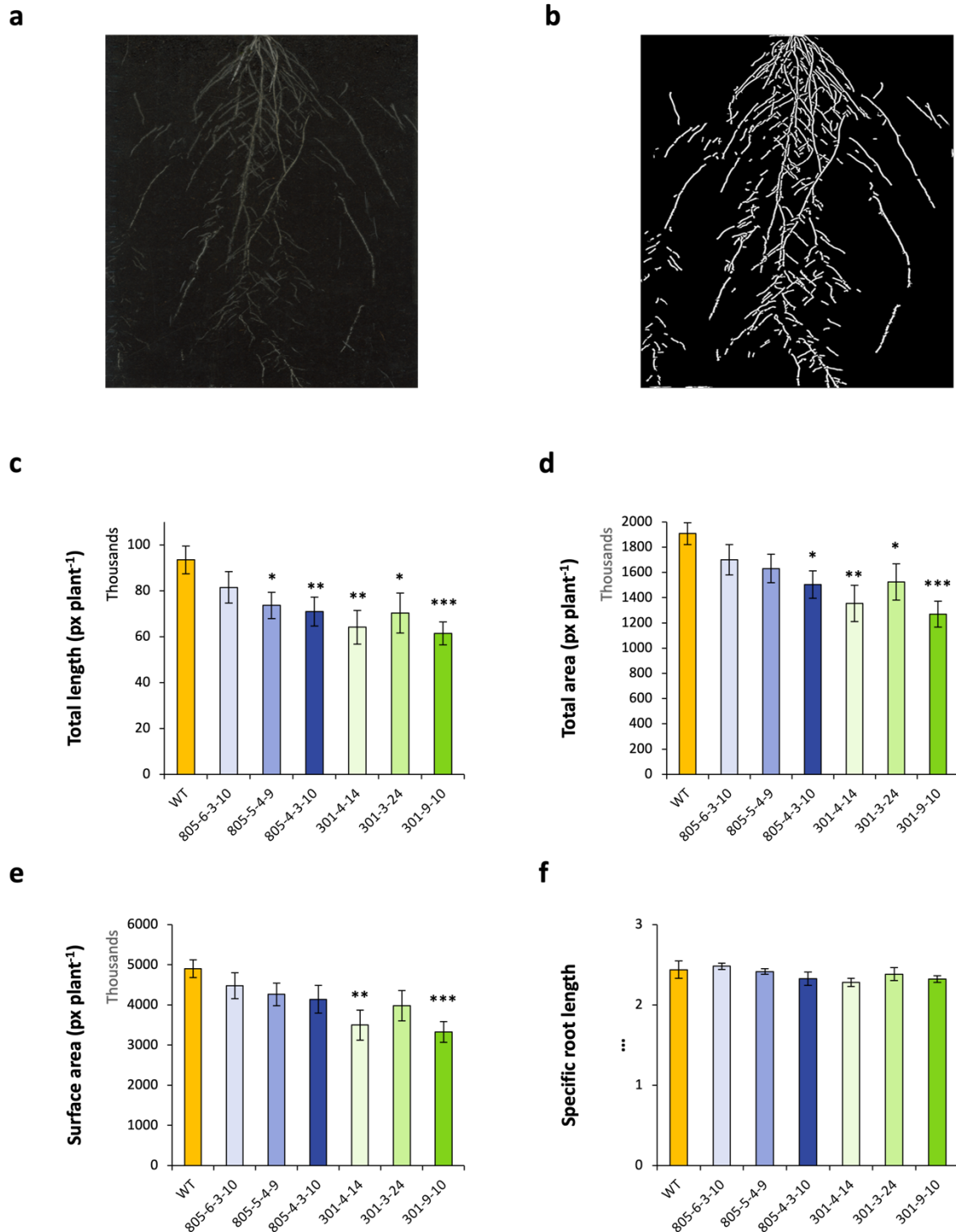
**Figure 44. Root architectural traits as affected by modified *HvWRKY53* expression. (a)** Representative scan of a rhizobox 23 days after sowing (DAS). **(b)** A representative enhanced segmentation image, which was eventually used for the image analysis. **(c-g)** Root morphological traits of wild-type (WT), overexpression (805-6-3-10, 805-4-3-10, 805-5-4-9) and CRISPR/Cas9 lines (301-4-14, 301-3-24, 301-9-10) obtained by the image analysis software saRIA (Narisetti et al., 2019). Total length **(c)**, total area **(d)**, surface area **(e)** and specific root length **(f)**. Transgenic lines of *HvWRKY53* along with the WT were grown in soil-filled rhizoboxes. At 23 DAS, rhizoboxes were scanned individually and analyzed for root morphological traits. Bars show means ± SE (n=5-11 biological replicates). Asterisks denote significant differences among means at ∗ P < 0.05, ∗∗ P < 0.01, or ∗∗∗ P < 0.001 by two-tailed Student's *t* test.

### 3.4.3. Characterization of *HvWRKY53* in soil-filled rhizotrons

With the aim to cover a broader developmental period than the previous small-scale rhizobox experiment as described in 3.4.2, as well as to be able to evaluate the dynamics of seminal and nodal root growth, overexpression and knock-out lines of *HvWRKY53* were grown in soil-filled rhizotrons along with the WT plants for 55 days in a fully climate-controlled plant cultivation facility (PhenoSphere, IPK Gatersleben). Images of roots and shoots were captured daily by two identical imaging towers and the plants were irrigated adequately in a fully automated manner.

Among the three independent overexpression lines, one of the lines, line 805-6-3-10, showed poor germination rates and severely retarded shoot and root development, which was not related to the modulated *HvWRKY53* expression. Thus, only two overexpression lines of *HvWRKY53*, namely 805-4-3-10 and 805-5-4-9, could be examined in this experiment. Throughout the experiment, WT plants visually appeared healthy with completely green shoots. At the end of the experiment, i.e. at 55 DAG, WT plants reached approx. 70 cm in height, had 26 tillers and the shoot dry weight accounted for 13 g plant$^{-1}$ (Figure 45.a, b, c). The overexpression lines of *HvWRKY53* appeared visually similar to the WT plants. Plant height, tiller number and shoot biomass were unaffected by the ectopic overexpression of *HvWRKY53* in roots (Figure 45.a, b, c). In contrast, aboveground development was suppressed in knock-out lines and this was more prominent in line 301-4-14.  Plant height in the transgenic line 301-4-14 was 26.5% lower than in the WT (Figure 45.a). It also had 28.5% less tillers (Figure 45.b) and its shoot biomass was 42% lower than the WT (Figure 45.c). A trend for lower shoot DW and tiller number was also observed for the other knock-out line. Transgenic lines ectopically overexpressing *HvWRKY53* in roots had slightly lower root biomass, however this was statistically not significant (Figure 46.d). Root biomass of the knockout line 304-4-14 was dramatically reduced by 56% compared to WT, whereas that of line 304-9-10 was only slightly lower than the WT.

To evaluate the impact of root-specific overexpression and knock-out of *HvWRKY53* on root architectural traits, daily taken root images (Figure 46) were subjected to fully-automated image analysis (faRIA, Narisetti et al., 2020). Visual appearance of overall root architecture appeared similar, and also seminal root number of transgenic lines was unaffected by modulated *HvWRKY53* expression. Total root length, total root

area, root surface area and specific root length of individual lines were determined. Overall, quantitative root traits of transgenic lines were very similar to the WT (Figure 47). Only the knock-out line 304-4-14 showed lower total root length at 14, 24 and 34 DAG compared to WT, but this was diminished at later developmental stages. Taken together, these results suggest that *HvWRKY53* does not affect root architecture.

To assess whether modulated *HvWRKY53* expression affects the nutritional status of the plants, whole shoots were analyzed for mineral elements. Overall, concentrations macro- and microelements in WT shoots indicated an adequate nutritional status (Supplementary Figure 7). Concentrations of mineral elements in transgenic lines were highly similar to WT plants, with the exception of line 805-5-4-9, which showed slightly higher Ca, Na and S concentrations. However, this increase was not considered to be biologically meaningful after the evaluation of the absolute values. These results suggest that *HvWRKY53* does not affect shoot nutritional status during vegetative phase under control conditions.
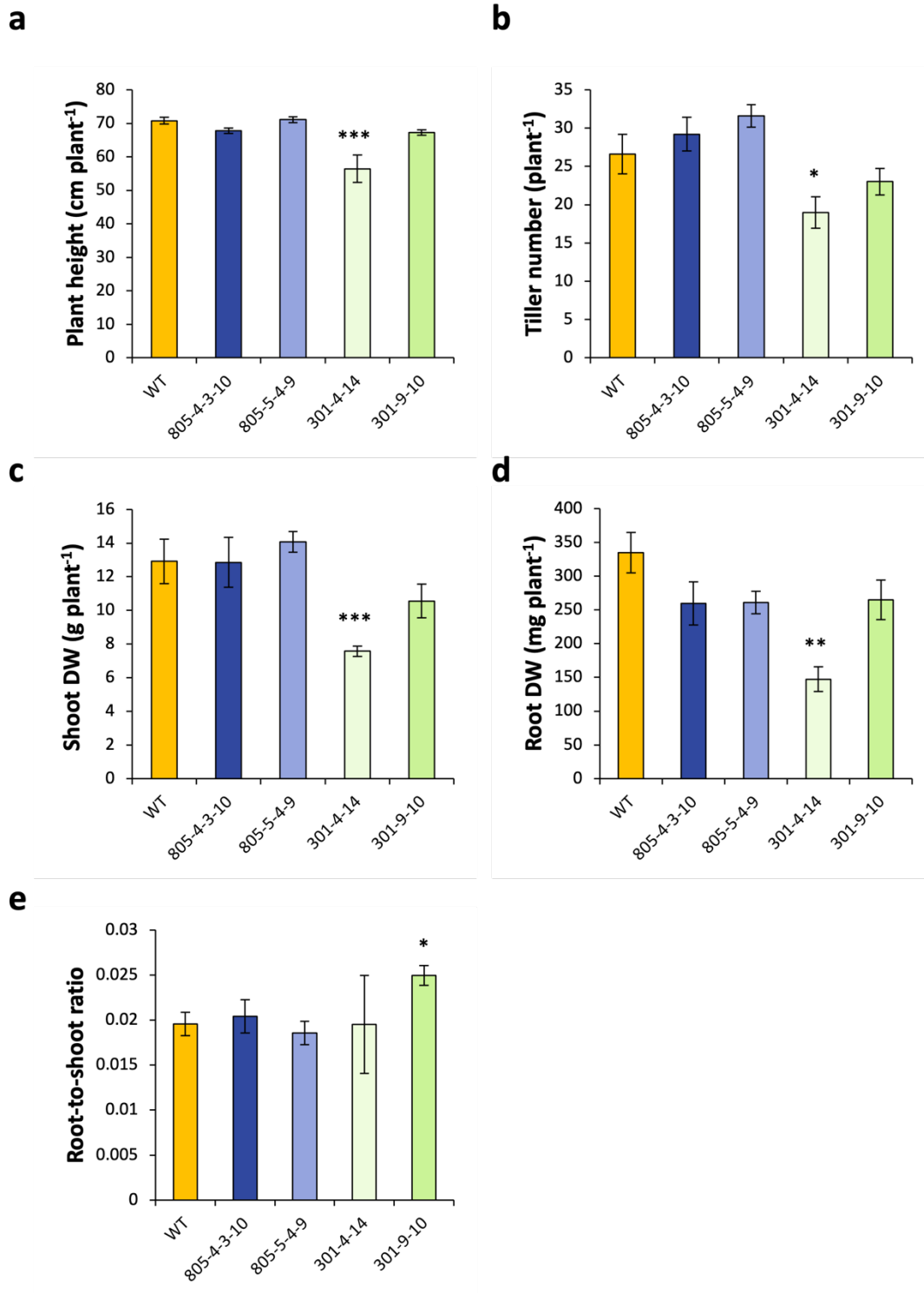
**Figure 45. Above- and belowground plant growth of barley as affected by modulated *HvWRKY53* expression.** Plant height **(a)**, number of tillers **(b),** shoot dry weight (DW) **(c)**, root DW **(d)** and root-to-shoot ratio **(e)** of WT, overexpression (805-4-3-10 and 805-5-4-9) and knock-out lines (301-4-14 and 301-9-10) of *HvWRKY53*. Transgenic lines were grown in soil-filled rhizotrons along with the WT for 55 days. Bars show means ± SD (n=5). Asterisks denote significant differences between individual lines and the WT at ∗ P < 0.05, ∗∗ P < 0.01, ∗∗∗ P < 0.001 by two-tailed Student's *t* test.
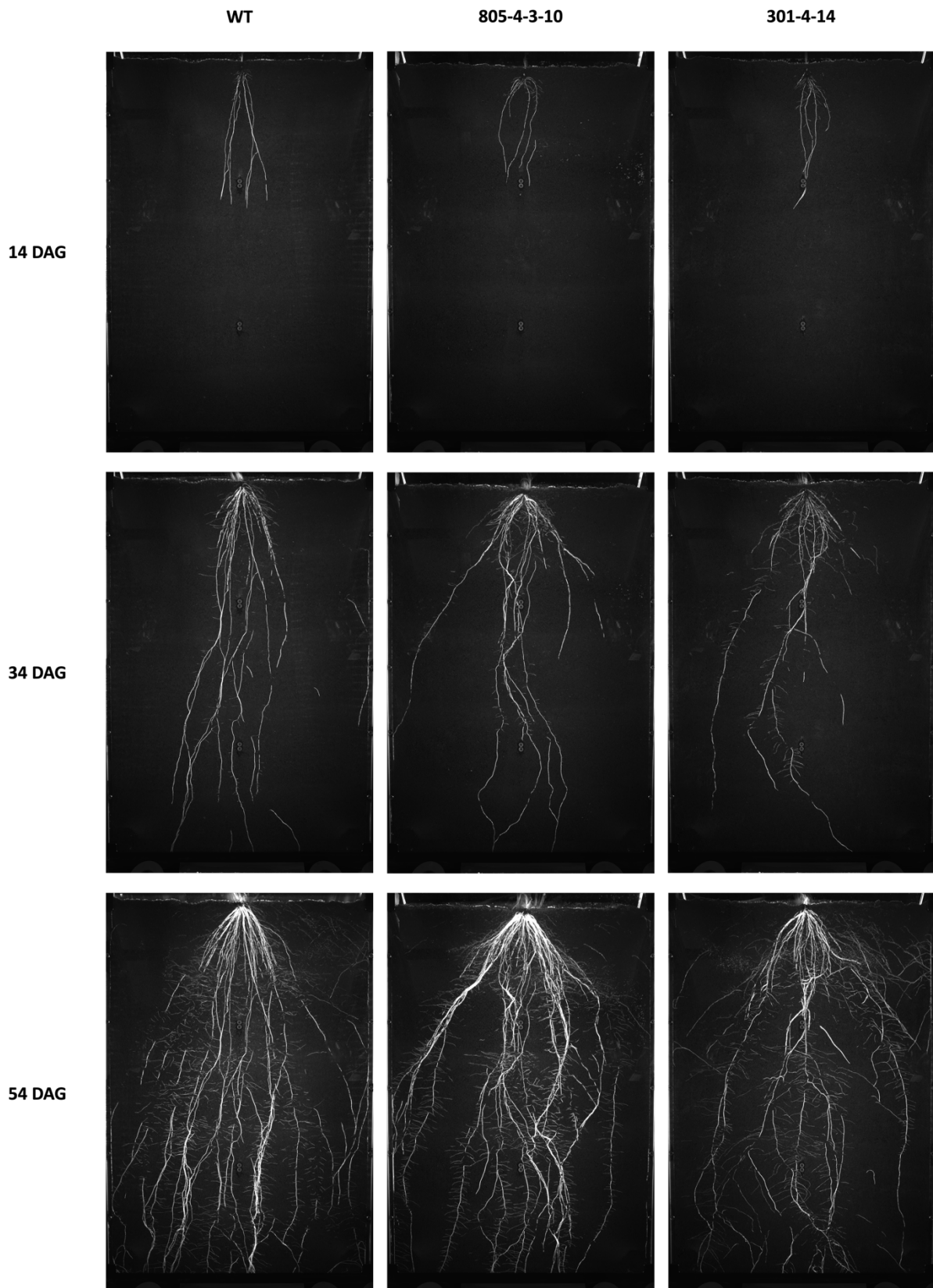
**Figure 46. Comparison of root architecture between wild type and lines with modulated** *HvWRKY53* **expression.** Representative root images of WT, the overexpression line 805-4-3-10 and the knock-out line 301-4-14 of *HvWRKY53* were taken on 14, 34 and 54 days after germination (DAG). Transgenic lines were grown in soil-filled rhizotrons along with the WT for 55 days. Roots and shoots were imaged non-destructively on a daily basis.
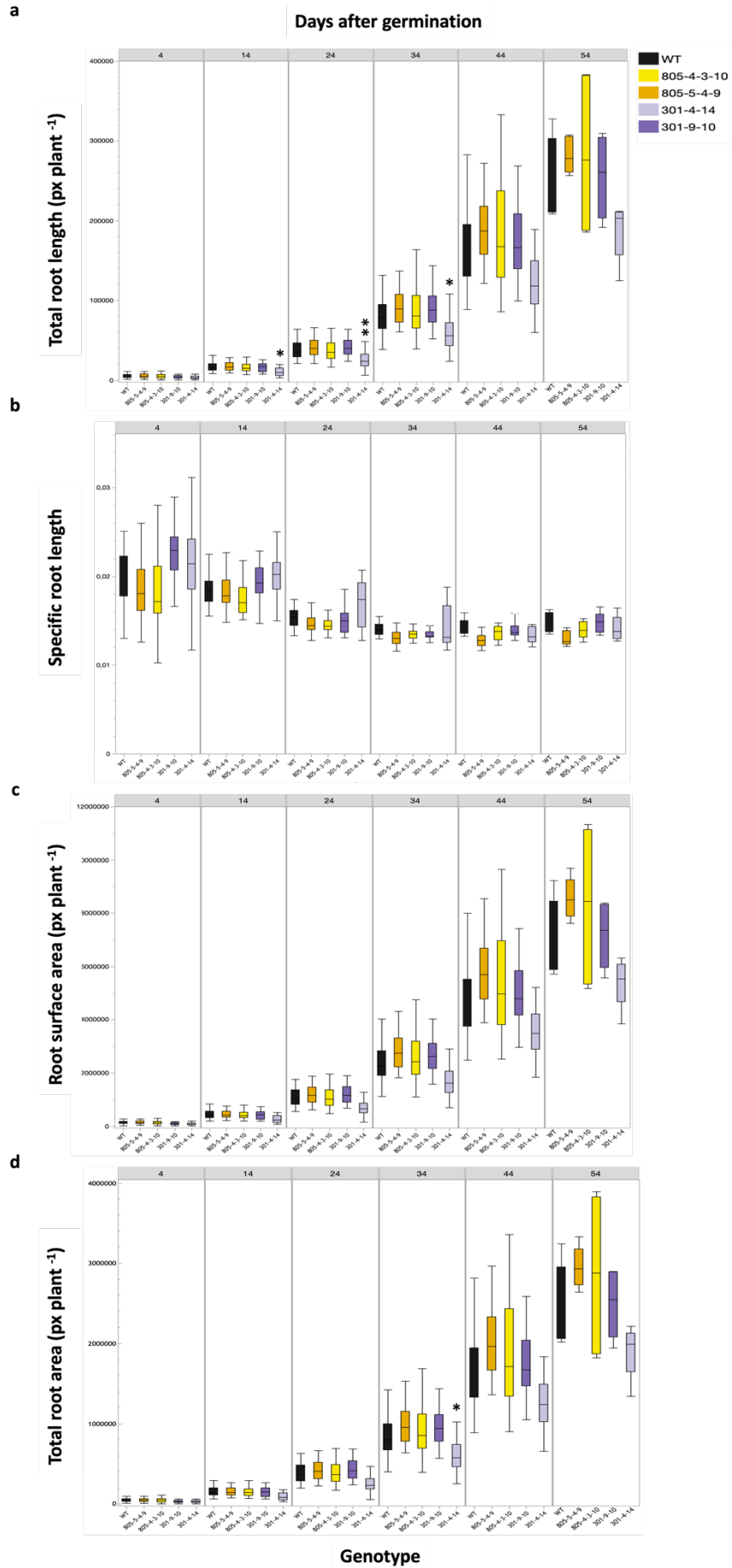
**Figure 47. Root architectural traits in transgenic barley lines as affected by modulated *HvWRKY53* expression.** Total root length **(a)**, specific root length **(b)**, root surface area **(c)** and total root area **(d)** of wild-type (WT, black), overexpression (805-4-3-10, dark yellow and 805-5-4-9, yellow) and knock-out lines (301-4-14, lilac and 301-9-10, purple) of *HvWRKY53*. Transgenic lines were grown in soil-filled rhizotrons along with the WT for 55 days. Dynamics of root and shoot growth were monitored non-destructively by daily imaging. Images were analyzed by the fully-automated root image analysis software faRIA (Narisetti et al., 2020). Bars show means $\pm$ SD (n=5). Asterisks denote significant differences between individual lines and the WT at $*$ P < 0.05 or $**$ P < 0.01 by two-tailed Student's *t* test. px, pixels.

### 3.4.4. The role of *HvWRKY53* in growth and maturation

To understand whether and to what extent manipulation of the senescence-associated TF *HvWRKY53* affects vegetative and reproductive growth, the nutritional status and grain yield-related parameters were determined. For this purpose, overexpression and CRISPR/Cas9-lines of *HvWRKY53* were grown together with WT plants in soil-filled pots under adequate fertilization and irrigation until maturity.

Throughout different stages of tillering (BBCH 20-29), stem elongation (BBCH 30-34), heading (BBCH 51-53) and maturity, plant height was significantly suppressed in overexpression lines of *HvWRKY53* (805-4-3-10, 805-5-4-9, 805-6-3-10) (Figure 48.a, 49.a, 51, 53.a). The number of tillers was not affected by overexpression of *HvWRKY53* during the vegetative phase, except for line 805-4-3-10, which showed slightly stronger tillering (Figure 48.a, b). Similar phenotypes were observed for the knock-out lines of *HvWRKY53*, as they also exhibited smaller shoots (301-4-14, 301-3-24, 301-9-10) (Figure 48.a). Tillering was found to be significantly enhanced only in line 301-9-10 (Figure 49.b).
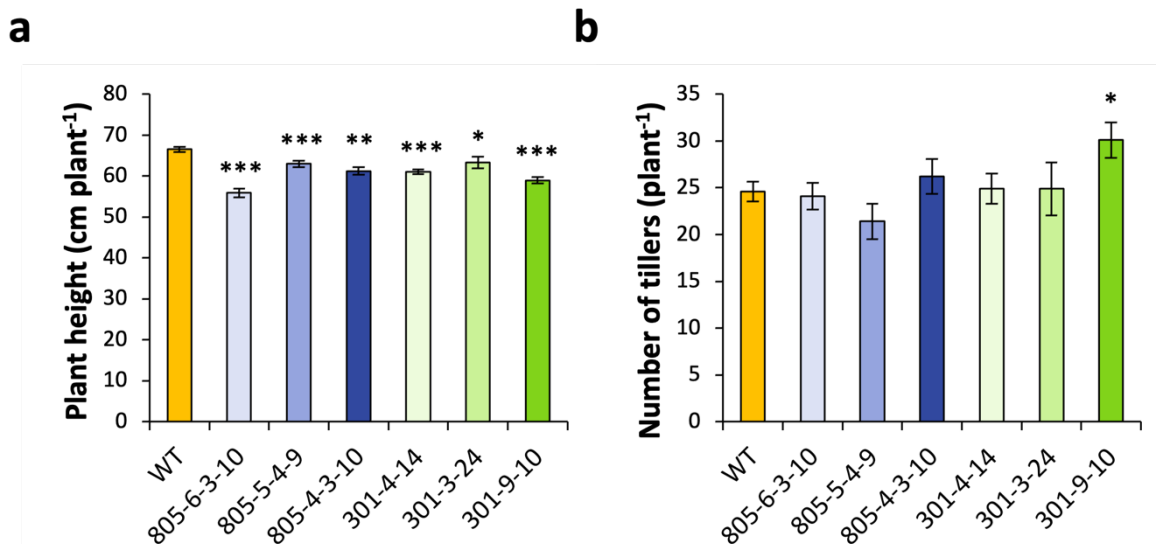


**Figure 48. Above-ground developmental traits in wild-type (WT) and transgenic lines of *HvWRKY53* at early vegetative growth. (a)** Plant height and **(b)** tiller number of WT, overexpression (805-4-3-10, 805-5-4-9, 805-6-3-10) and knock-out lines (301-4-14, 3-24, 9-10) of *HvWRKY53* at BBCH 31-34. Plants lines were grown in soil-filled pots in the greenhouse to be assessed for plant development and performance under adequate growth conditions. Bars show means ± SD (n=10 biological replicates). Asterisks denote significant differences between WT and individual lines at ∗ P < 0.05, ∗∗ P < 0.01, ∗∗∗ P < 0.001 by two-tailed Student's *t* test.

To assess whether modulated *HvWRKY53* transcripts in roots cause changes in the transition from vegetative to reproductive phase, plants were scored for inflorescence emergence (heading). All transgenic lines progressed in development in a similar way as the WT and did not show any significant difference in spike emergence.
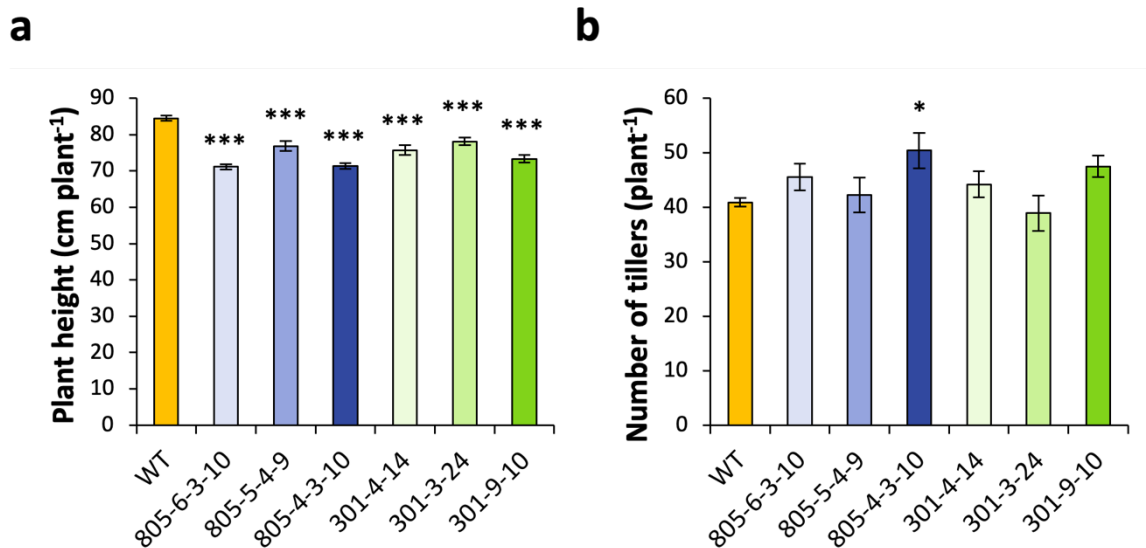


**Figure 49. Above-ground developmental traits in wild-type (WT) and transgenic lines of *HvWRKY53* at early inflorescence emergence. (a-b)** Plant height **(a)** and tiller number **(b)** of WT, overexpression (805-4-3-10, 805-5-4-9, 805-6-3-10) and knock-out lines (301-4-14, 3-24, 9-10) of *HvWRKY53* at BBCH 51-53. Plants lines were grown in soil-filled pots in the greenhouse to be assessed for plant development and performance under adequate growth conditions. Bars show means ± SE **(a-b)** or SD **(c)** (n=10 biological replicates). Asterisks denote significant differences between WT and individual lines at ∗ P < 0.05, ∗∗ P < 0.01, ∗∗∗ P < 0.001 by two-tailed Student's *t* test **(a-b)**.

To evaluate the impact of altered *HvWRKY53* expression in roots on the nutritional status of the plants, each 4th leaf (from the top) of the main tiller was sampled and analyzed for mineral elements by ICP-OES. Interestingly, most of the macro- and micronutrients showed remarkable changes in the overexpression lines (805-4-3-10, 805-5-4-9, 805-6-3-10). Among the macronutrients, leaf concentrations of Ca, P and Na were in average 36, 40 and 52 % higher than in WT plants, respectively (Figure 50.b, e, f). Similarly, Mg and K concentrations significantly increased in overexpression lines, with the exception of line 805-5-4-9, which showed slightly lower levels of K (Figure 50.a, c). A decline in leaf concentrations was only observed for S, on average by 33% (Figure 50.d). Except for Fe (Figure 51.c), changes in micronutrient concentrations were more prominent. On average, B and Zn concentrations increased by 30 and 37 %, respectively (Figure 51.a, d), whereas Mn concentrations decreased

by 52% in overexpression lines. Despite of showing statistically significant differences, absolute values of the increased or decreased macro- and micronutrient concentrations did not indicate any deficiency or toxicity. The decline in Mn concentrations was considered as the only critical change as it resulted in concentrations very close to the critical deficiency threshold.

In contrast to the overexpression lines, knock-out lines of *HvWRKY53* showed mostly similar nutrient concentrations to the WT, apart from K and Mn. While Mn concentrations were found to decrease by 27% (Figure 51.b), K concentrations were significantly higher (Figure 50.a) in the leaves of the knock-out lines, i.e. by 27% in average. Since K concentrations were the only being adversely influenced by the overexpression or knock-out of *HvWRKY53*, K homeostasis may have been directly or indirectly affected by *HvWRKY53* expression.

During the reproductive stages of growth and maturation, overexpression and knock-out lines of *HvWRKY53* were developmentally similar and completed their lifecycle simultaneously. To investigate whether and how modulated *HvWRKY53* expression in roots affected yield performance, individual yield components were examined. Overexpression lines produced similar number of spikes as the WT (Figure 53.c), while the number of grains significantly decreased in the lines 805-6-3-10, 805-5-4-9 and 805-4-3-10 overexpressing *HvWRKY53* in roots by 44, 36 and 30 %, respectively (Figure 53.e). Expectedly, similar trends were also observed for total spike and total grain weight, which were significantly lower in the overexpression lines of *HvWRKY53*. (Figure 53.d, f). Harvest index (HI) is a measure of crop yield and calculated as the ratio of grain to total shoot dry matter. HI in overexpression lines 805-6-3-10, 805-5-4-9 and 805-4-3-10 was dramatically lower, i.e. by 19, 13 and 15%, respectively (Figure 53.h).

To assess whether overexpression of *HvWRKY53* resulted in the changes in the grain morphology, grain morphological traits were analyzed using the seed analysis software MARVIN (Marvitech GmbH, Germany). Grain width and grain surface in the overexpression lines were completely unaffected and similar to WT (Figure 54.a, c), whereas only line 805-6-3-10 exhibited slightly elongated grains (Figure 54.b). However, this change in the grain length was not found to be biologically important.

Grain yield-related parameters also showed remarkable changes in the knock-out lines of *HvWRKY53*. At maturity, plant height was significantly lower in the lines 301-4-14, 301-3-24, 301-9-10 (Figure 53.a). Number of spikes produced by the lines 301-3-24 and 301-9-10 were similar as in the WT, whereas line 301-4-14 produced 25% less spikes than the WT (Figure 53.c). Grain yield drastically decreased in lines 301-4-14, 301-3-24, 301-9-10 by 54, 32 and 27 %, respectively (Figure 53.e). In accordance with the reduced grain yield, total spike (Figure 53.d) and total grain weight (Figure 53.f) were significantly lower in the knock-out lines. Interestingly, only line 301-9-10 exhibited significant changes in the grain morphological traits. Grain width (Figure 54.a) and surface area (Figure 54.c) were significantly reduced, whereas grain length was slightly increased (Figure 54.b). The changes observed in the grain width and surface area were positively correlated with thousand kernel weight (TKW), which was also 25% less than in the WT (Figure 53.g). Collectively, these data show that modulated levels of *HvWRKY53* transcripts resulted in a grain yield penalty in the transgenic lines.

During the grain-filling stage, nutrients are remobilized to the grains from the senescing tissues. Here, flag leaves play an important role as the remobilization of valuable resources from flag leaves to grains represents one of the major sources of grain nutrients. At maturity, flag leaf nutrient concentrations in the overexpression lines were comparable to those of the WT, with some exceptions (Figure 55, 56). Among the macronutrients, Mg accumulated in the flag leaves of line 805-4-3-10, 805-5-4-9 and 805-6-3-10 at 2.5-, 2.4- and 2.7-fold higher level, respectively (Figure 55.c). Similarly, Na levels were doubled in comparison to the WT (Figure 55.e). Among the micronutrients, dramatic changes were observed only for Mn concentrations, which were drastically reduced by 57% in average (Figure 56.b).  In comparison to the overexpression lines, the nutritional status of the flag leaves was found to be less affected in the knock-out lines of *HvWRKY53*. Strikingly, only P and Mg concentrations increased in the flag leaves of line 304-14 and 301-9-10 compared to the WT, by 47 and 155 % in average, respectively (Figure 55.b, c). Concentrations of B, Mn, Fe and Zn were at comparable levels as in the WT (Figure 56).

To evaluate whether the changes in the shoot nutritional status induced by the modulated *HvWRKY53* expression were reflected in the final product i.e. the seeds, grain nutrient concentrations of the overexpression and knock-out lines were determined. Grain nutrient profiles of the macronutrients in the overexpression lines were pretty much similar as in the WT except for Na, which tended to accumulate at up to 190% higher levels in the grains compared to the WT (Figure 57.e). Among the micronutrients, Zn significantly accumulated in the grains of line 805-6-3-10 and 805-4-3-10 (Figure 58.a), whereas Mn levels significantly dropped in the grains of the overexpression lines 805-5-4-9 and 805-4-3-10 (Figure 58.b). In knock-out lines, only S (Figure 57.d) and Zn (Figure 58.a) showed increased concentrations while the rest of the measured macro- and micronutrient levels were quite similar to the WT.
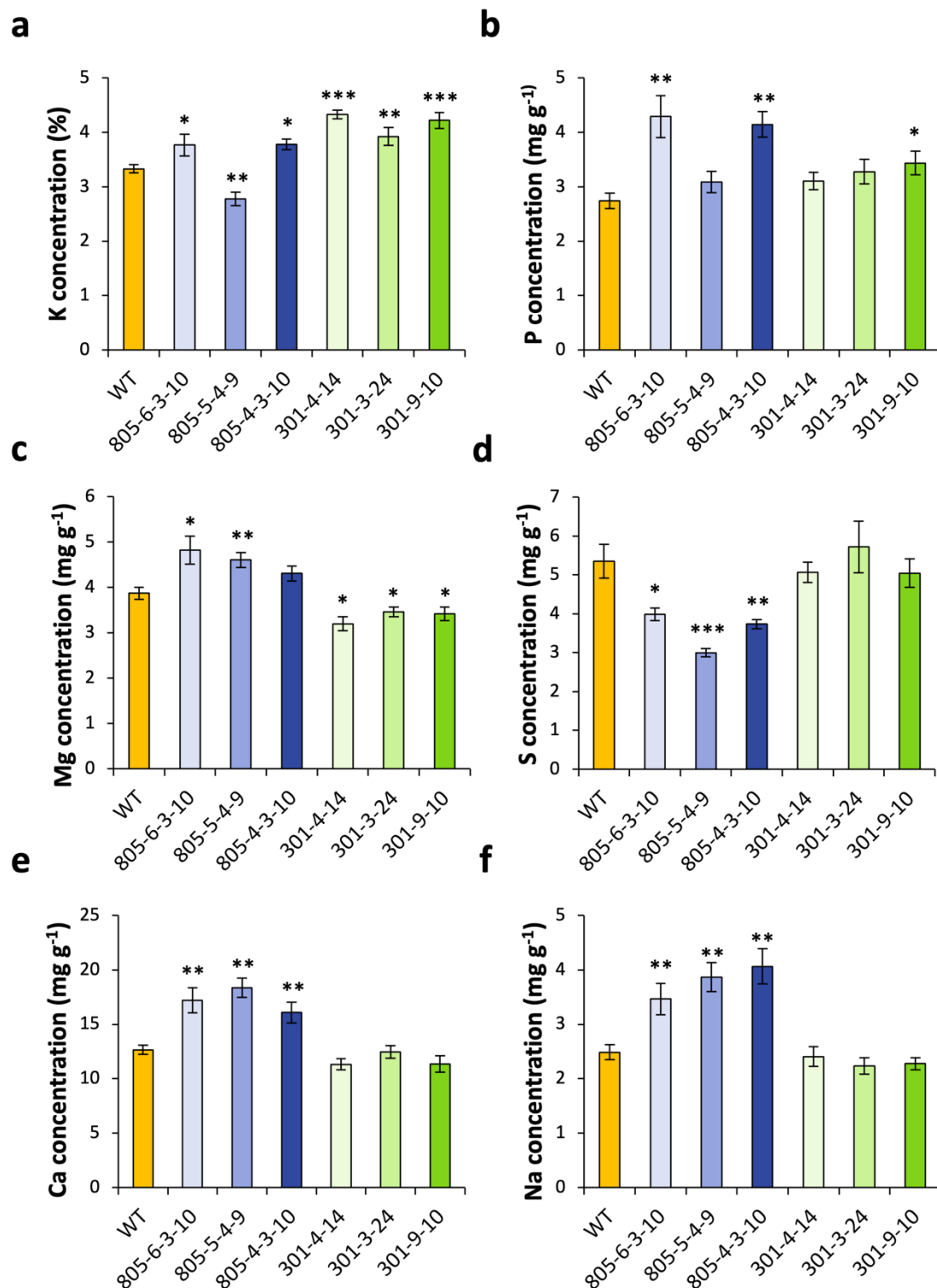
**Figure 50. Leaf macronutrient concentrations in wild-type (WT) and transgenic lines of *HvWRKY53* at early inflorescence emergence. (a-f)** Leaf concentrations of K **(a)**, P **(b)**, Mg **(c)**, S **(d)**, Ca **(e)** and Na **(f)** in WT, overexpression (805-4-3-10, 805-5-4-9, 805-6-3-10) and knock-out lines (301-4-14, 3-24, 9-10) of *HvWRKY53* at BBCH 51-53. Plants lines were grown in soil-filled pots in the greenhouse to be assessed for plant development and performance under adequate growth conditions. At BBCH 51-53, the $4^{th}$ leaf (from top) of each main tiller was collected and analyzed for mineral elements. Bars show means $\pm$ SE (n=7-10 biological replicates). Asterisks denote significant differences between WT and individual lines at $*$ P < 0.05, $**$ P < 0.01, $***$ P < 0.001 by two-tailed Student's *t* test **(a, d)** or by nonparametric comparisons using Wilcoxon method **(b-c, e-f)**.
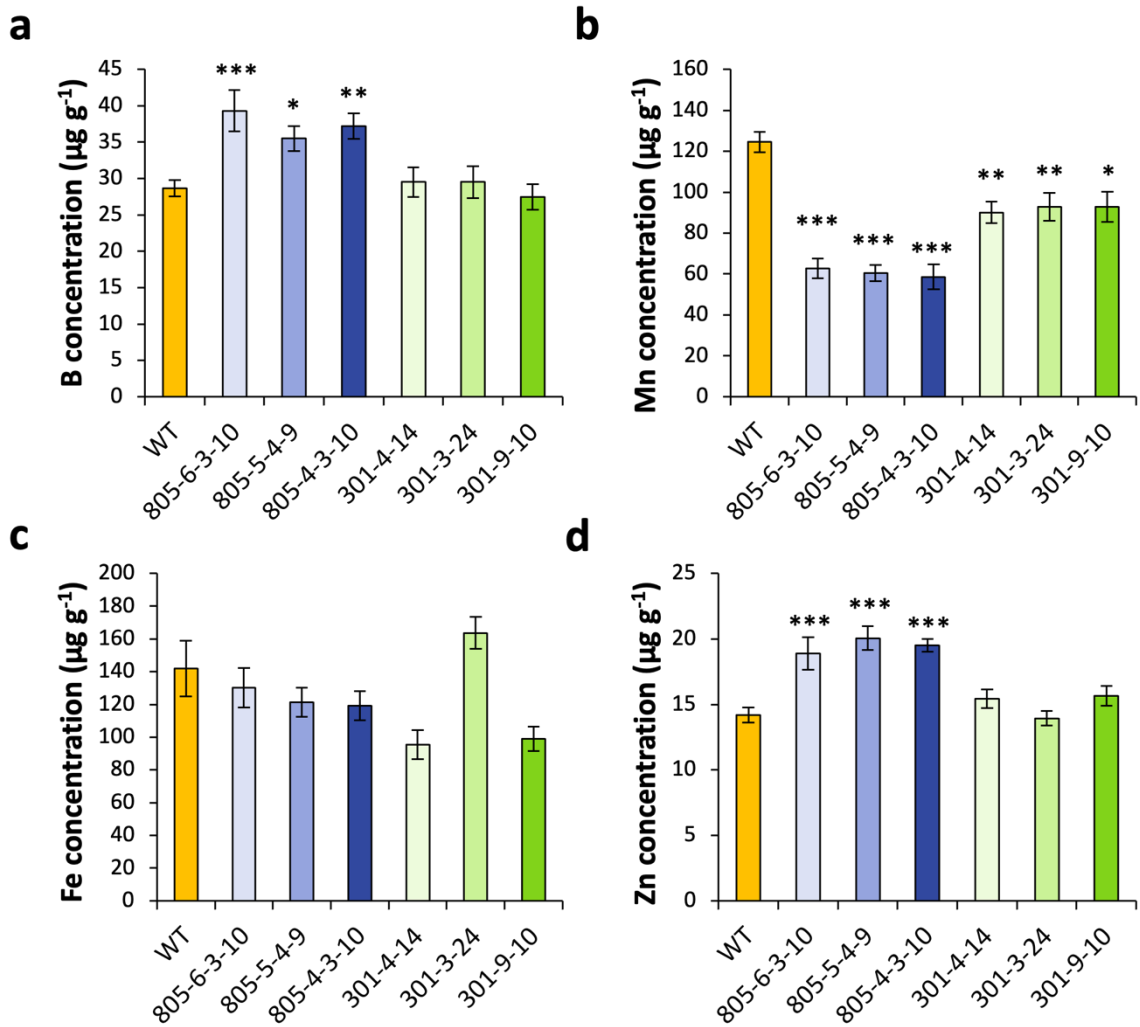
**Figure 51. Leaf micronutrient concentrations in wild-type (WT) and transgenic lines of *HvWRKY53*. (a-d)** Leaf concentrations of B **(a)**, Mn **(b)**, Fe **(c)** and Zn **(d)** in the leaves of WT, overexpression (805-4-3-10, 805-5-4-9, 805-6-3-10) and knock-out lines (301-4-14, 3-24, 9-10) of *HvWRKY53* at ~BBCH 51-53. Plants lines were grown in soil-filled pots in the greenhouse to be assessed for plant development and performance under adequate growth conditions. At BBCH 51-53, the 4th leaf (from top) of each main tiller was collected and analyzed for mineral elements. Bars show means ± SE (n=7-10 biological replicates). Asterisks denote significant differences between WT and individual lines at ∗ P < 0.05, ∗∗ P < 0.01, ∗∗∗ P < 0.001 by two-tailed Student's *t* test **(a, d)** or by nonparametric comparisons using Wilcoxon method **(b-c)**.

**Figure 52. Visual appearance of wild-type (WT), overexpression and knock-out lines of *HvWRKY53*.** Transgenic lines were grown along with the WT in the greenhouse until maturity under adequate growth conditions. From left to right: WT, three independent root-specific overexpression lines (805-4-3-10, 805-5-4-9, 805-6-3-10) and three independent knock-out lines (301-4-14, 3-24, 9-10) of *HvWRKY53*. Image was taken 203 days after sowing.

**Figure 53. Grain yield-related parameters in wild-type (WT) and transgenic lines.** Plant height of WT, overexpression (805-4-3-10, 805-5-4-9, 805-6-3-10) and knock-out lines (301-4-14, 3-24, 9-10) of *HvWRKY53*. **(b)** Shoot dry weight (DW), i.e. above-ground biomass excluding spikes. **(c)** Number of spikes, **(d)** total spike weight per plant, **(e)** number of grains and **(f)** total grain weight produced by a single plant. **(g)** Thousand kernel weight (TKW). **(h)** Harvest index (HI) (%). HI was calculated as the ratio of total grain weight to total above-ground biomass. Plants lines were grown in soil-filled pots in the greenhouse to be assessed for plant development and performance under adequate growth conditions. Bars show means $\pm$ SD (n=10 biological replicates). Asterisks denote significant differences between WT and individual lines at $*$ $P < 0.05$, $**$ $P < 0.01$, $***$ $P < 0.001$ by two-tailed Student's *t* test for **(a)** and **(c-e)** or nonparametric comparison by Wilcoxon method for **(b)** and **(f-h)**.
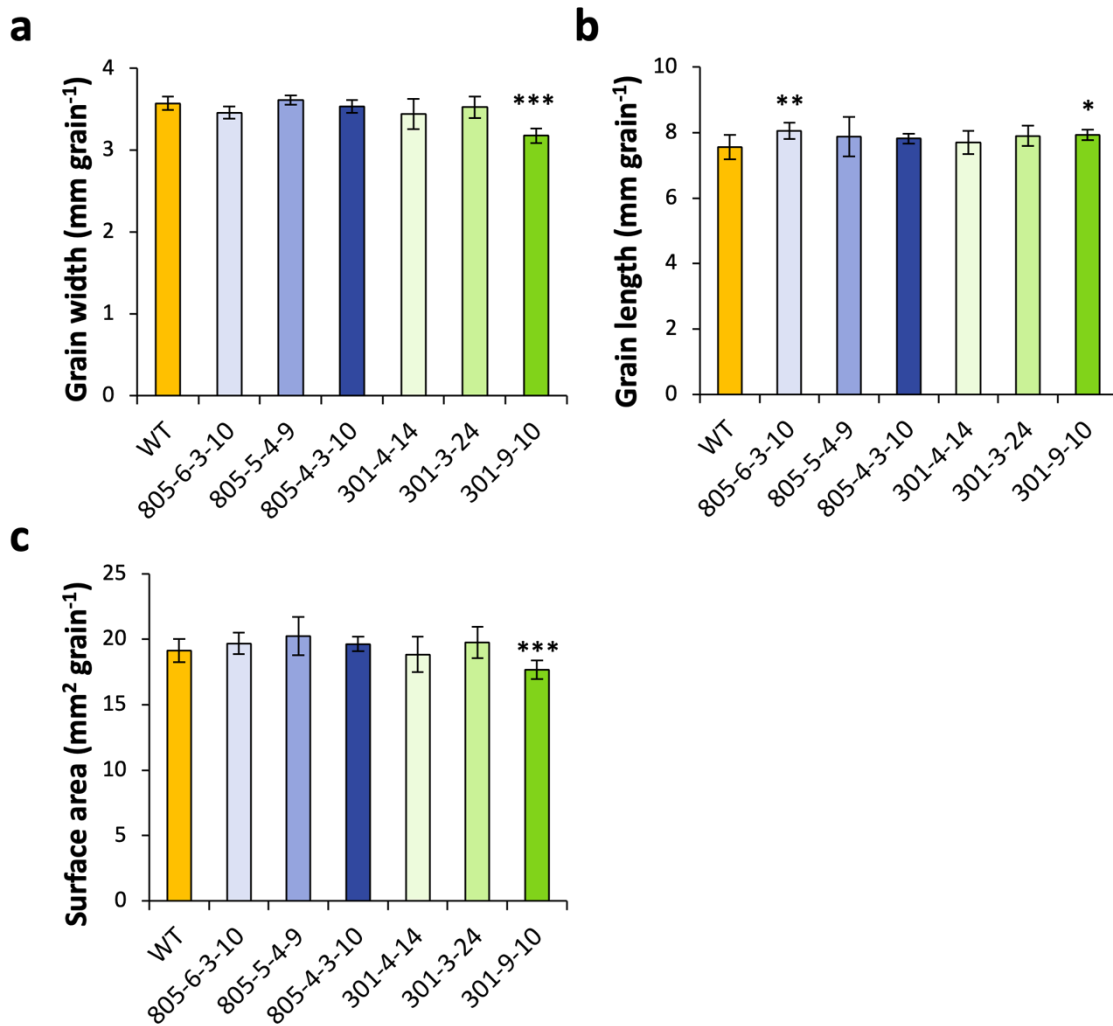
Figure is shown on the next page.
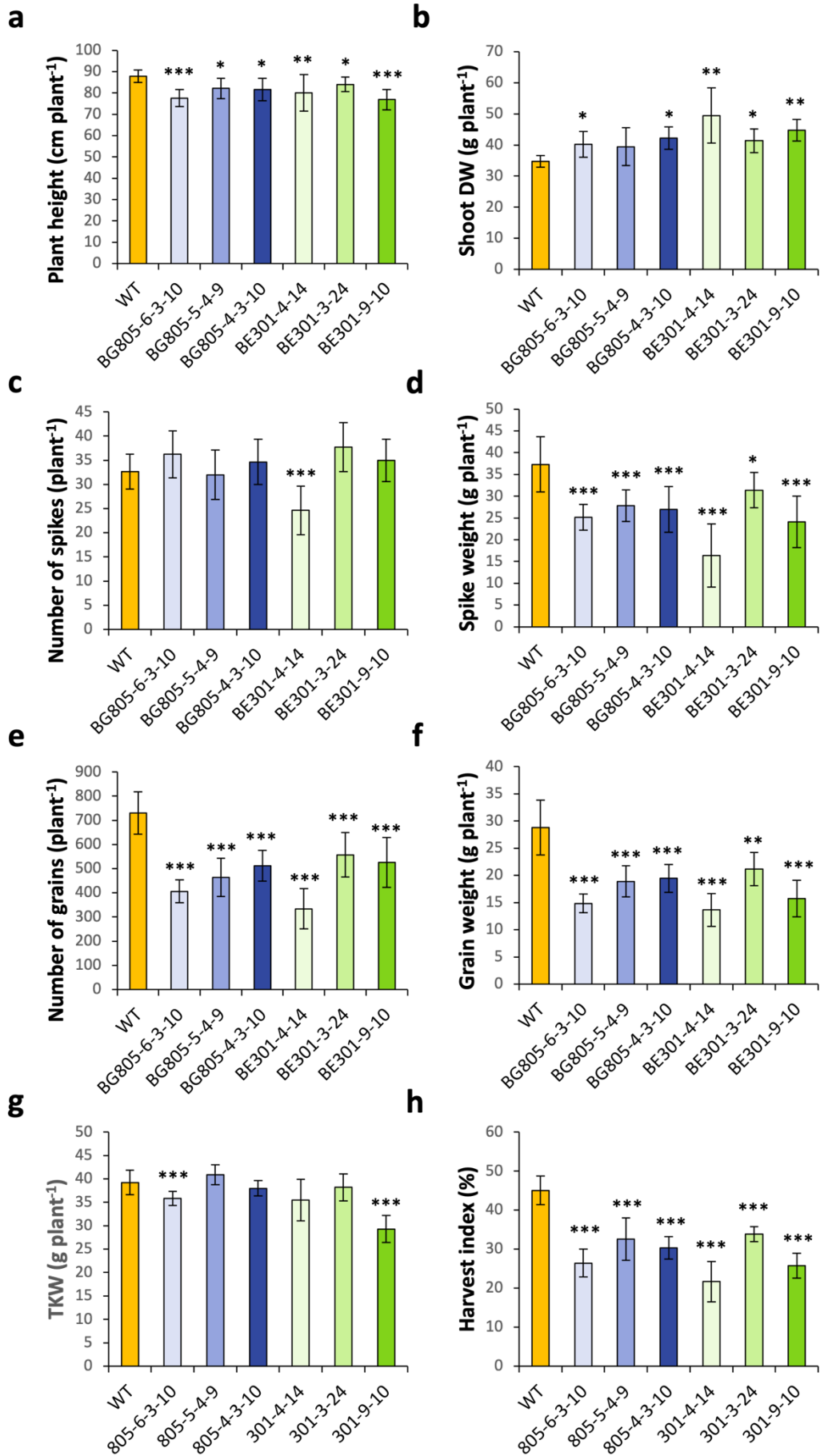
**Figure 54. Seed morphological traits in WT and transgenic lines. of *HvWRKY53*. (a-c)** Grain width **(a)**, grain length **(b)** and grain surface area **(c)** of WT, overexpression (805-4-3-10, 805-5-4-9, 805-6-3-10) and knock-out lines (301-4-14, 3-24, 9-10) of *HvWRKY53*. Plants lines were grown in soil-filled pots in the greenhouse to be assessed for plant development and performance under adequate growth conditions. Seed morphological traits were determined using MARVIN ProLine I Seed Analyzer (Marvitech GmbH, Germany). Bars show means ± SD (n=10 biological replicates). Asterisks denote significant differences between WT and individual lines at ∗ P < 0.05, ∗∗ P < 0.01, ∗∗∗ P < 0.001 by two-tailed Student's *t* test **(c)** or nonparametric comparison using Wilcoxon method for **(a-b)**.
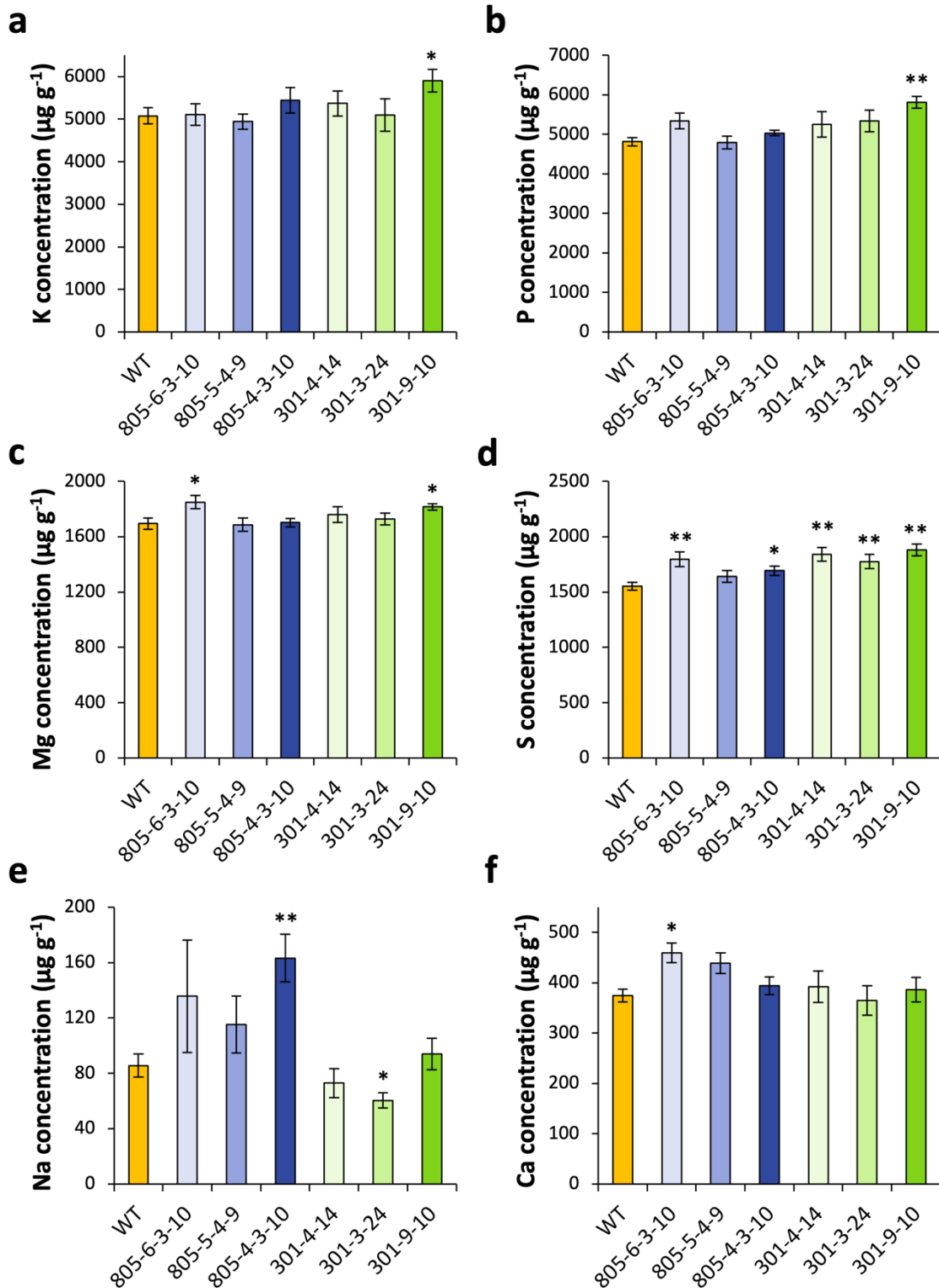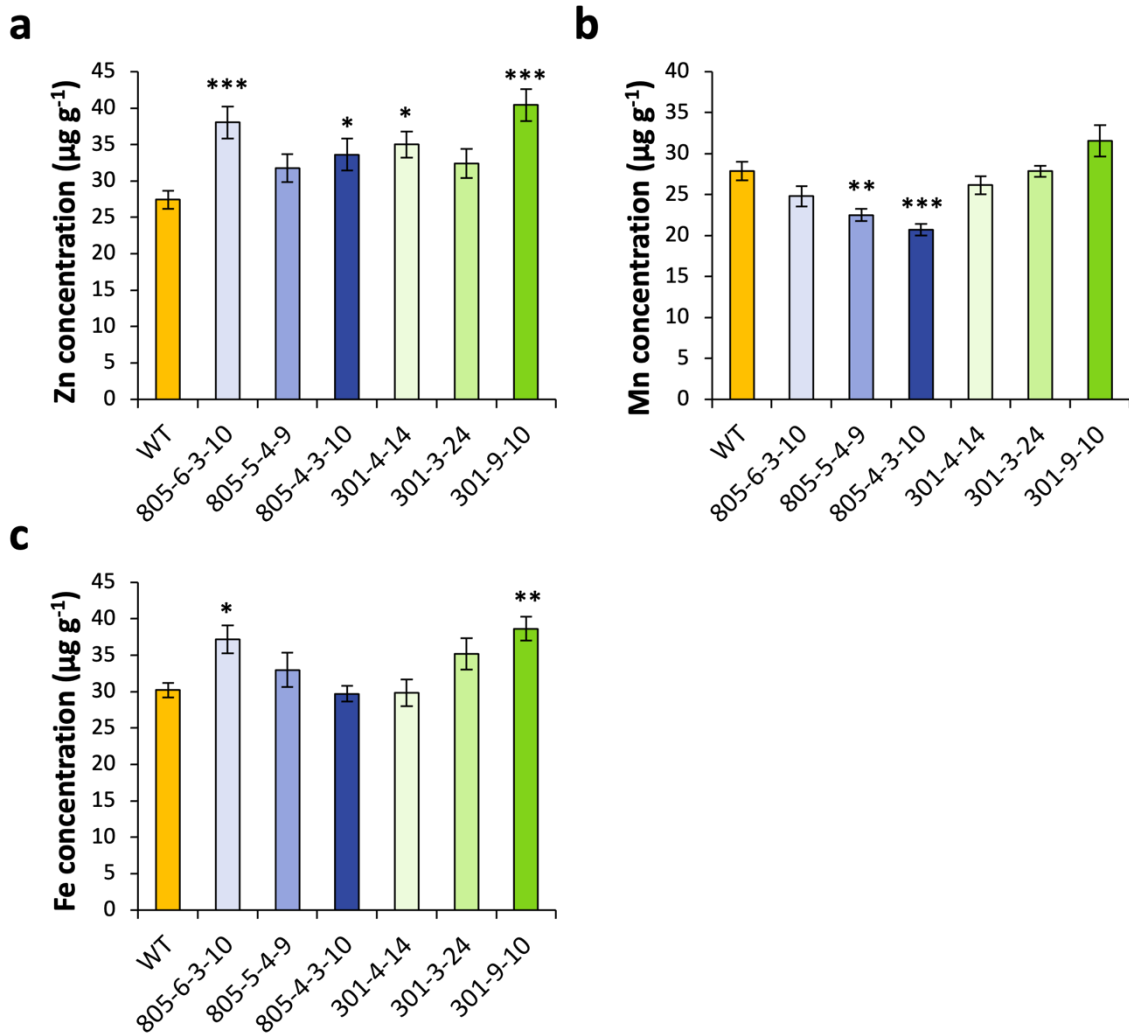
**Figure 55. Grain macronutrient concentrations of wild-type (WT) and transgenic lines of *HvWRKY53* at maturity (a-f)** Concentration of K **(a)**, P **(b)**, Mg **(c)**, S **(d)**, Na **(e)** and Ca **(f)** in the grains of WT, overexpression (805-4-3-10, 805-5-4-9, 805-6-3-10) and CRISPR/Cas9 lines (301-4-14, 3-24, 9-10) of *HvWRKY53*. Plants lines were grown in soil-filled pots in the greenhouse to be assessed for plant development and performance under adequate growth conditions. At maturity, different tissues were harvested separately and analyzed for mineral elements. Bars show means ± SE (n=8-10 biological replicates). Asterisks denote significant differences between WT and individual lines at ∗ P < 0.05, ∗∗ P < 0.01, ∗∗∗ P < 0.001 by two-tailed Student's *t* test **(c, f)** or by nonparametric comparisons using Wilcoxon method **(a-b, d-e)**.
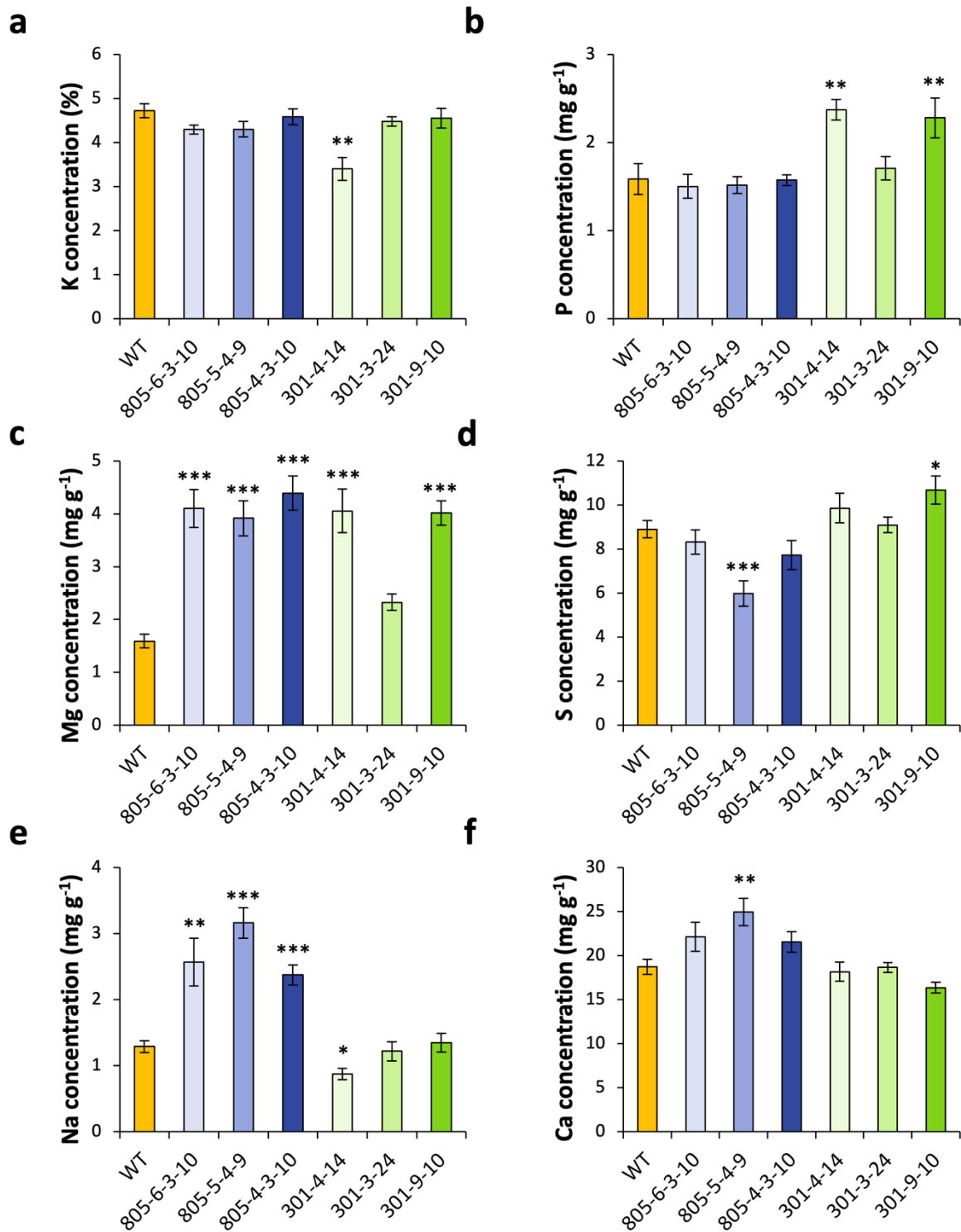
**Figure 56. Grain micronutrient concentrations of wild-type (WT) and transgenic lines of** *HvWRKY53* **at maturity. (a-c)** Concentration of Zn **(a)**, Mn **(b)** and Fe **(c)** in the grains of WT, overexpression (805-4-3-10, 805-5-4-9, 805-6-3-10) and knock-out lines (301-4-14, 3-24, 9-10) of *HvWRKY53*. Plants lines were grown in soil-filled pots in the greenhouse to be assessed for plant development and performance under adequate growth conditions. At maturity, different tissues were harvested separately and analyzed for mineral elements. Bars show means $\pm$ SE (n=8-10 biological replicates). Asterisks denote significant differences between WT and individual lines at $*$ P < 0.05, $**$ P < 0.01, $***$ P < 0.001 by two-tailed Student's *t* test **(a)** or by nonparametric comparisons using Wilcoxon method **(b-c)**.
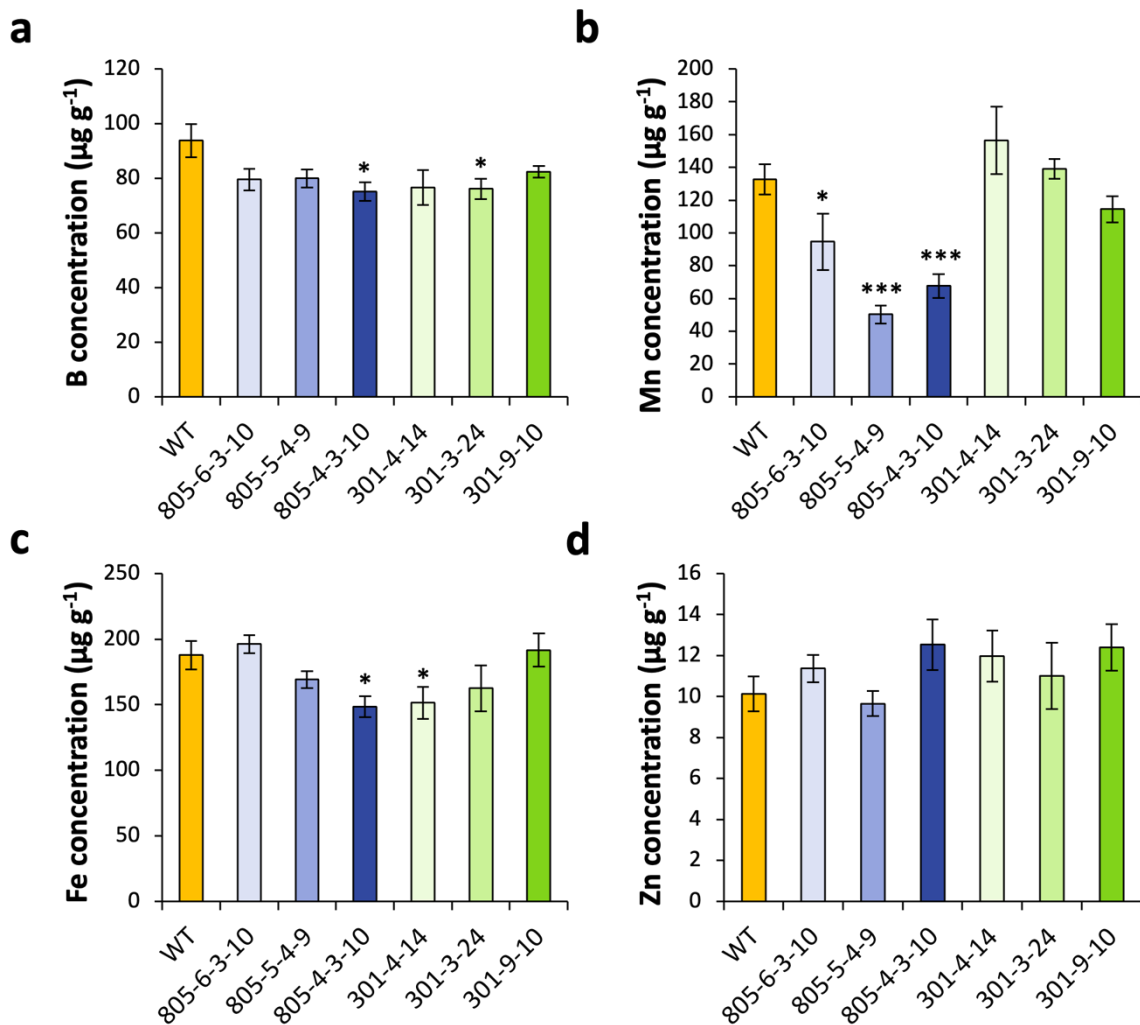
**Figure 57. Macronutrient concentrations in the flag leaves of wild-type (WT) and transgenic lines of *HvWRKY53* at maturity. (a-f)** Concentration of K **(a)**, P **(b)**, Mg **(c)**, S **(d)**, Na **(e)** and Ca **(f)** in the flag leaves of WT, overexpression (805-4-3-10, 805-5-4-9, 805-6-3-10) and knock-out lines (301-4-14, 3-24, 9-10) of *HvWRKY53*. Plants lines were grown in soil-filled pots in the greenhouse to be assessed for plant development and performance under adequate growth conditions. At maturity, flag leaves were collected and analyzed for mineral elements. Bars show means ± SE (n=8-10 biological replicates). Asterisks denote significant differences between WT and individual lines at ∗ P < 0.05, ∗∗ P < 0.01, ∗∗∗ P < 0.001 by two-tailed Student's *t* test **(b-d)** or by nonparametric comparisons using Wilcoxon method **(a, e-f)**.

**Figure 58. Micronutrient concentrations in the flag leaves of wild-type (WT) and transgenic lines of *HvWRKY53* at maturity. (a-c)** Concentration of B **(a)**, Mn **(b)**, Fe **(c)** and Zn **(d)** in the flag leaves of WT, overexpression (805-4-3-10, 805-5-4-9, 805-6-3-10) and knock-out lines (301-4-14, 3-24, 9-10) of *HvWRKY53*. Plants lines were grown in soil-filled pots in the greenhouse to be assessed for plant development and performance under adequate growth conditions. At maturity, flag leaves were collected and analyzed for mineral elements. Bars show means ± SE (n=8-10 biological replicates). Asterisks denote significant differences between WT and individual lines at ∗ P < 0.05, ∗∗ P < 0.01, ∗∗∗ P < 0.001 by two-tailed Student's *t* test **(b-c)** or by nonparametric comparisons using Wilcoxon method **(a,d)**.

### 3.5.1 Expression of *HvMYB15* in different tissues and in response to different stimuli

Liu et al. (2019) have shown that *HvMYB15* is expressed in senescing roots, but not in young or senescing leaves. Moreover, the publicly available expression atlas of barley shows *HvMYB15* expression mostly in old root tissues and relatively minor expression in nodes and inflorescences (IPK Barley Blast Server, https://apex.ipk-gatersleben.de/apex/f?p=284:57::::::). In order to investigate the tissue-specific expression of *HvMYB15*, WT barley plants were grown in the greenhouse until late flowering (BBCH 65-69) and different root and shoot tissues were subjected to gene expression analysis. Unexpectedly, *HvMYB15* was found to expressed in old leaf sheaths, old leaf blades and flag leaf sheaths, and there transcript abundance was even higher than in roots (Figure 59). Moreover, grains had similar transcript levels as roots (Figure 59). On the other hand, *HvMYB15* expression in flag leaf sheaths, 1$^{st}$, 3$^{rd}$ and 5$^{th}$ nodes, rachis and caryopsis was lower compared to the roots. These results suggest that *HvMYB15* is not exclusively expressed in the root tissue.
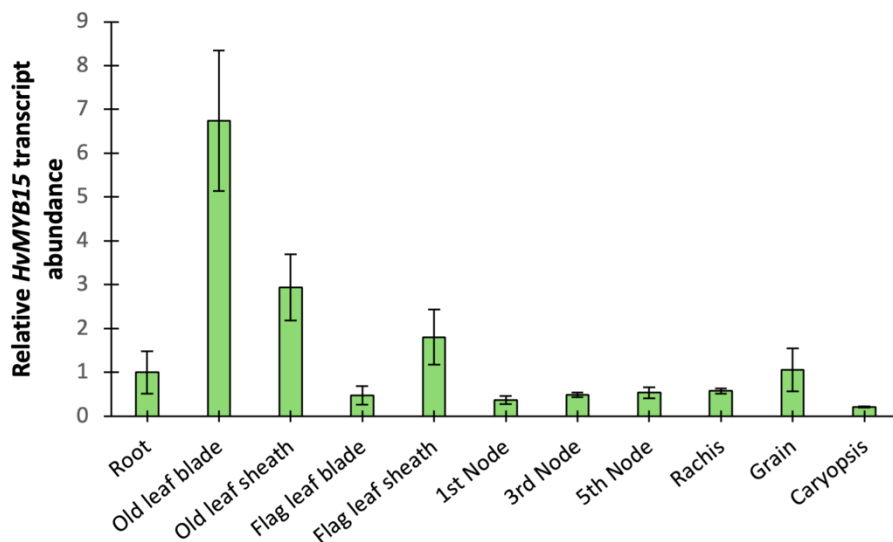


**Figure 59. Relative *HvMYB15* transcript abundance in different tissues.** Barley plants were grown in the greenhouse until late flowering stage (BBCH 65-69) and different tissues were subjected to gene expression analysis. Gene expression was determined by qPCR. *HvMYB15* expression in roots was set to 1. Bars show means ± SD (n=3-5).

To investigate the transcriptional regulation of *HvMYB15* in response to different stimuli, hydroponically-grown barley plants were subjected to salt or drought stress, N or P starvation or ABA treatment. Interestingly, ABA treatment led to the

downregulation of *HvMYB15* 3, 24 and 48 hours after treatment (Figure 60). PEG-6000 did not affect *HvMYB15* expression 3 hours after treatment, whereas it downregulated *HvMYB15* 24 and 48 hours after treatment. In contrast, NaCl treatment slightly upregulated *HvMYB15* 3 hours after treatment, however transcripts dropped back to basal levels 24 hours after treatment (Figure 60). *HvMYB15* was strongly upregulated in response to N starvation 3, 24 and 48 hours after treatment. On the other hand, withdrawal of the P source from the nutrient solution did not affect *HvMYB15* expression. These observations show that *HvMYB15* is also expressed in response to different stimuli with a particularly strong response to N starvation.
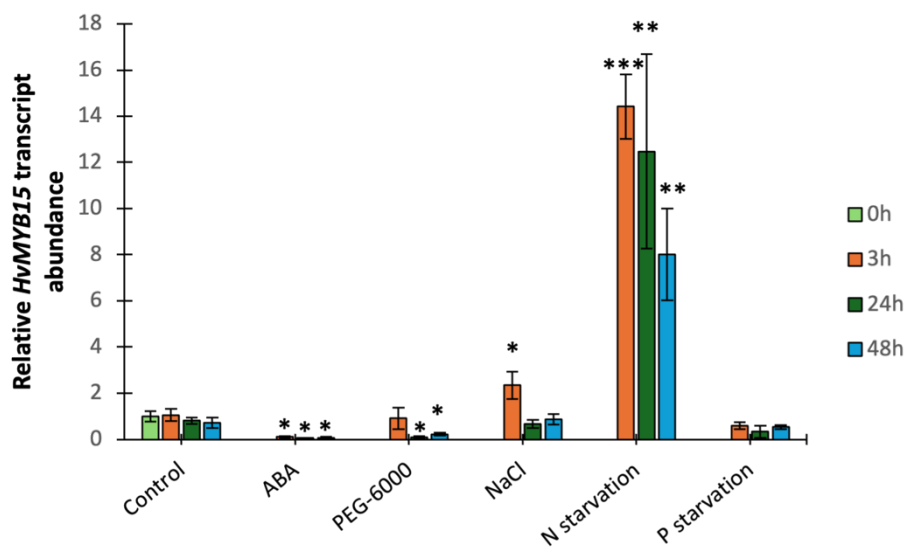


**Figure 60. Relative transcript abundance of *HvMYB15* in response to different stimuli.** Relative transcript abundance of *HvMYB15* in response to ABA, NaCl, or PEG-6000 treatments, or N starvation or P starvation after 3, 24 and 48 hours. WT barley plants were grown in hydroponic culture for 21 days. After 21 days, roots were exposed to 70 $\mu$M ABA, 150 mM NaCl or 5% PEG-6000 treatment in nutrient solution. For N or P starvation, N or P sources were completely withdrawn from the nutrient solution. Gene expression was determined by qPCR. Transcript abundance of control plants at 0 h after treatment was set to 1. Bars show means $\pm$ SD (n=4). Asterisks denote significant differences between control and treatment at $*$ P < 0.05, $**$ P < 0.01, $***$ P < 0.001 by two-tailed Student's *t* test.

### 3.5.2. Characterization of *HvMYB15* in soil-filled rhizotrons

To monitor and assess the impact of modulated *HvMYB15* expression on the dynamics of seminal and nodal root growth in real-time, overexpression and knock-out lines of *HvMYB15* were grown in soil-filled rhizotrons for 55 days in a fully climate-controlled plant cultivation facility (PhenoSphere, IPK Gatersleben). Roots and shoots were imaged daily by two identical imaging towers, by which the plants were also irrigated adequately in a fully automated manner. 55 days after germination (DAG), rhizotrons were demounted, fresh seminal and nodal root tips were collected for the validation of altered *HvMYB15* gene expression, and the rest of the whole root system was washed off from soil and oven dried along with the shoots.

The experimental period covered most of the vegetative growth. At the end of the experiment, plants were at mid-stem extension phase (BBCH 32-33). Transgenic lines ectopically expressing *HvMYB15* in roots were similar to WT in height, with the exception of line 804-10-2-15, which was slightly shorter (Figure 61.a). In contrast, both knock-out lines of *HvMYB15* were shorter than the WT plants. Among the overexpression lines, lines 804-5-1-8 and 804-7-4-6 tended to have higher number of tillers, whereas tiller production was unaffected in knock-out lines (Figure 61.b). Shoot biomass of overexpression lines was comparable to the WT, whereas it was 27% lower in the knock-out line 204-7-17 than the WT (Figure 61.c). Moreover, root-to-shoot ratio of the overexpression line 804-10-2-15 was significantly higher than the WT, whereas it was not affected in other transgenic lines (Figure 61.d).

At the end of the experiment, total root biomass of WT plants was approx. 260 mg plant$^{-1}$ (Figure 62.a). Strikingly, transgenic lines with root-specific overexpression of *HvMYB15* had up to 83% higher root biomass compared to WT plants. In contrast, root biomass of line 204-7-17 was 20% lower than the WT. Modulated *HvMYB15* expression did not affect the number of seminal roots (Figure 62.b). Line 804-7-4-6 had a slight reduction in the seminal root number, however this was considered as biologically not meaningful. Furthermore, continuous monitoring of the root system allowed the monitoring of root growth rates. Overall, root growth of WT plants and transgenic lines increased exponentially over time (Figure 62.c). During the very early stages of growth, i.e. 4-21 DAG, root growth rate of WT plants and the overexpression lines was highly similar. After 21 DAG, overexpression lines tended to have slightly

higher root growth rates. In contrast, knock-out lines had continuously lower root growth rates compared to WT plants and this became more prominent at later developmental stages (Figure 62.c). The reduction in root growth rate was even stronger for line 204-7-17, which had up to 39% lower root growth rates throughout the experiment.
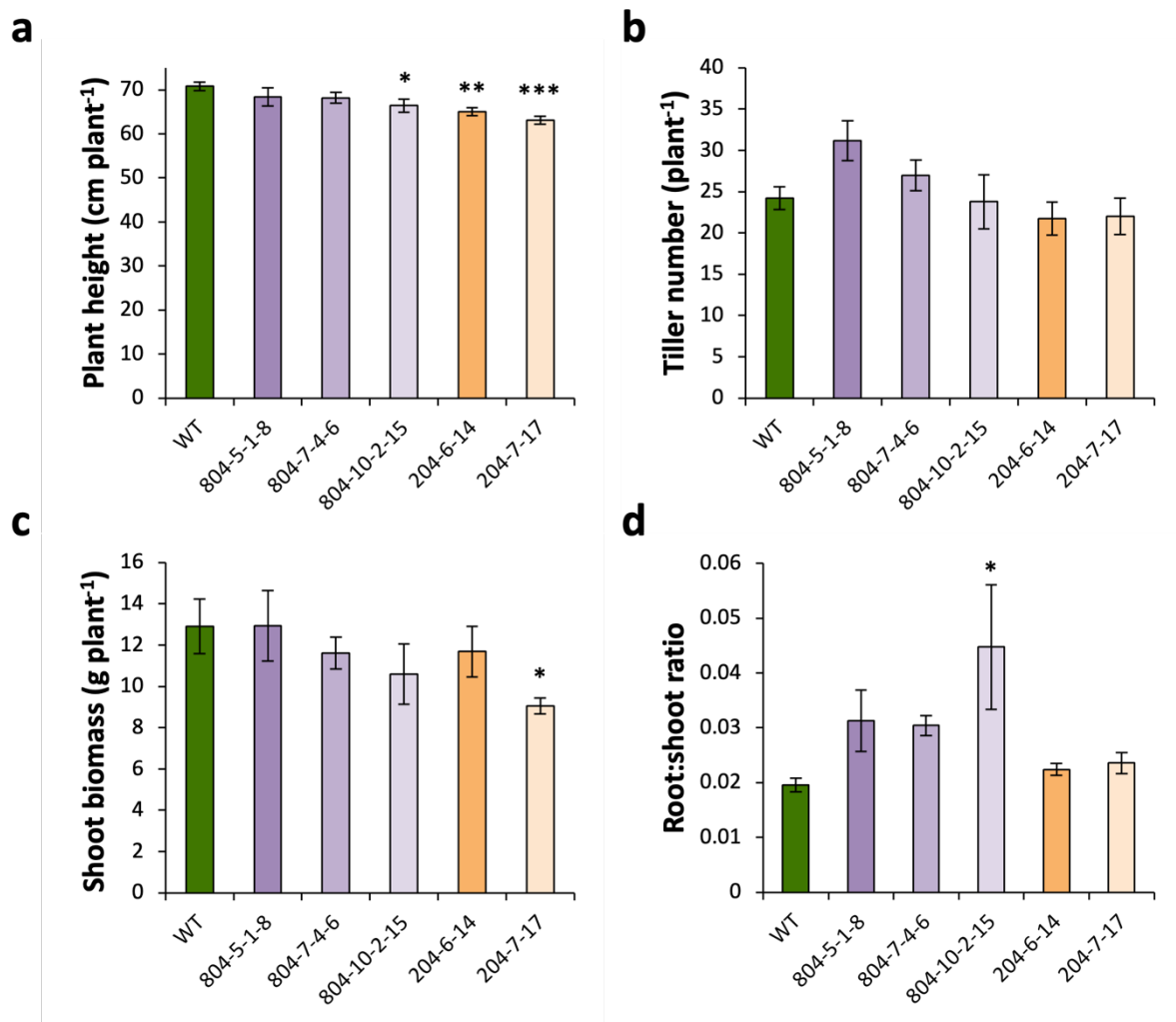


**Figure 61. Aboveground growth and development of barley as affected by modulated *HvMYB15* expression.** Plant height **(a)**, number of tillers **(b),** shoot biomass **(c)** and root-to-shoot biomass ratio **(d)** of overexpression (804-5-1-8, 804-7-4-6, 804-10-2-15) and knock-out lines (204-6-14, 204-7-17) of *HvMYB15*. Transgenic lines were grown in soil-filled rhizotrons for 55 days. Dynamics of root and shoot growth were monitored non-destructively by daily imaging. Bars show means ± SE (n=5). Asterisks denote significant differences between individual lines and the WT at $*$ $P < 0.05$, $**$ $P < 0.01$ or $***$ $P < 0.001$ by two-tailed Student's *t* test.

Next, to confirm increased *HvMYB15* transcript levels in overexpression lines under rhizotron growth conditions, fresh seminal root tips were subjected to RNA extraction and subsequent gene expression analysis. *HvMYB15* transcripts in the transgenic lines 804-5-1-8 and 804-10-2-15 were 9- and 11-fold higher than in WT (Figure 63). Among the overexpression lines, *HvMYB15* transcripts in line 804-7-4-6 were lowest, i.e. only 4 times higher than in the WT.
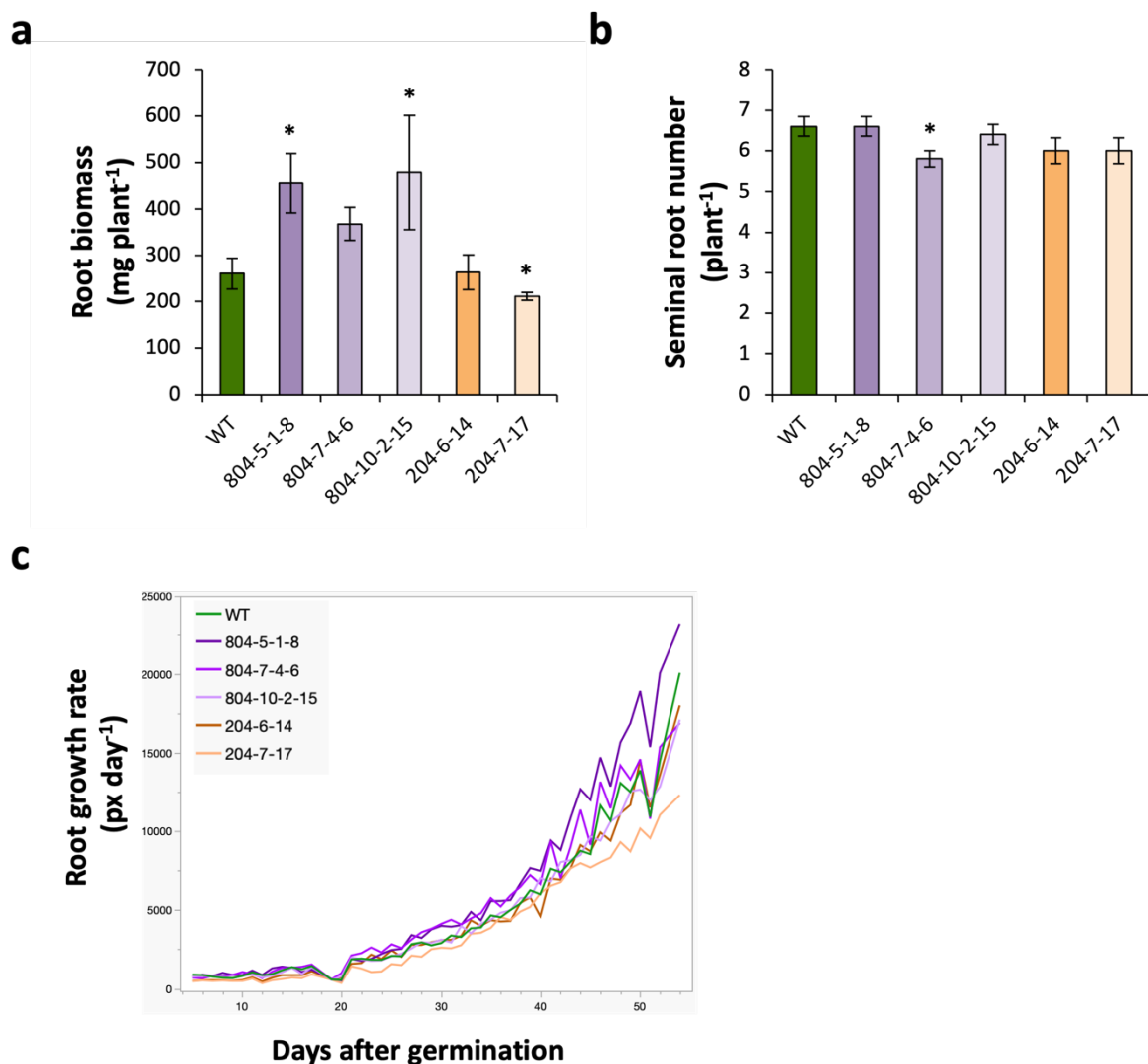


**Figure 62. Belowground root growth of barley as affected by modulated *HvMYB15* expression.** Root biomass **(a)**, number of seminal roots **(b)** and root growth rate **(c)** of overexpression (804-5-1-8, 804-7-4-6, 804-10-2-15) and knock-out lines (204-6-14, 204-7-17) of *HvMYB15*. Transgenic lines were grown in soil-filled rhizotrons for 55 days. Dynamics of root and shoot growth were monitored non-destructively by daily imaging. Bars show means ± SE (n=5). Asterisks denote significant differences between individual lines and the WT at ∗ P < 0.05 by two-tailed Student's *t* test.

Before quantitative evaluation of root traits, visual appearance of the root system was compared at subsequent three time points. From day 34, clear phenotypic differences appeared in the knock-out line 204-6-14, which showed poorer growth especially of lateral roots (Figure 64). By contrast, the root system of the overexpression line 804-5-1-8 appeared to be more dense than that of the WT. To evaluate the impact of modulated *HvMYB15* on root architectural traits, daily taken root images were analyzed using the software faRIA (Narisetti et al., 2020). Among the investigated traits, total root length, total root area and root surface area of WT plants showed an exponential increase over time (Figure 65.a, b, c). During the early developmental stages, i.e. 4-14 DAG, total root length of overexpression lines was very similar to the WT, whereas it became significantly higher in lines 804-5-1-8 and 804-7-4-6 compared to the WT starting from 44 DAG (Figure 65.a). In contrast, total root length of knock-out lines was lower than the WT and this reduction was stronger for line 204-7-17. Total root area and root surface area of overexpression lines and the WT did not differ until 44 DAG, but thereafter they became higher in lines 805-5-1-8 and 804-7-4-6 than the WT (Figure 65.b, c). The differences among the individual lines and the WT became more pronounced with the progression of time. Knock-out line 204-7-17, on the other hand, had lower total root area and root surface area than the WT, whereas these traits of line 204-4-14 were lower only during early stages of growth, i.e. 4-14 DAG compared to WT (Figure 65.b, c). Specific root length was unaffected in overexpression lines of *HvMYB15*, whereas that of knock-out line 204-7-17 was lower than the WT (Figure 65.d).
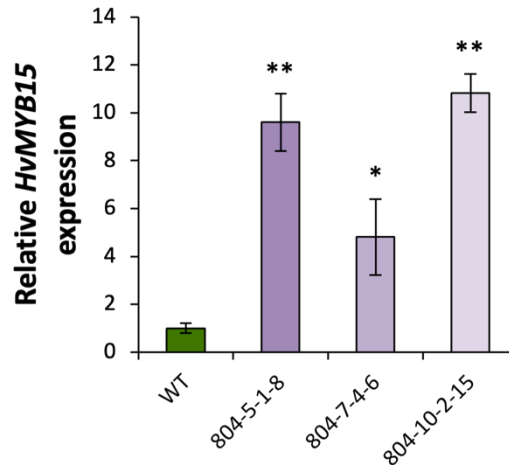
**Figure 63. Transcript abundance of *HvMYB15* in overexpression lines.** Transcript abundance of *HvMYB15* in wild-type (WT) and overexpression (804-5-1-8, 804-7-4-6, 804-10-2-15) lines as determined by quantitative real-time polymerase chain reaction (qPCR). Transgenic lines were grown in soil-filled rhizotrons along with the WT for 55 days. Transcript levels were determined by qRT-PCR and normalized to barley reference genes *ADP-ribosylation factor 1* (*ADP*) and *UBIQUITIN* (*UBI*)**.** Transcript abundance of WT was set to 1. Gene expression levels were normalized to *ADP* and WT-*HvMYB15* expression was set to 1. Bars show means ± SE (n=5). Asterisks denote significant differences between individual lines and the WT at ∗ $P < 0.05$ or ∗∗ $P < 0.01$ by two-tailed Student's *t* test.

To assess the shoot nutritional status of the plants with modulated *HvMYB15* expression, shoots were analyzed for mineral elements. Evaluation of the mineral element concentrations indicated an adequate shoot nutritional status for all examined elements of the WT plants (Supplementary Figure 8). Concentrations of macronutrients, including K, Mg, S, Na and P, were very similar in transgenic lines and the WT. Only the knock-out line 204-7-17 had higher Ca concentration than the WT but this was considered not to be biologically relevant. Among the micronutrients, Zn and Fe concentrations were up to 27% higher in lines 804-7-4-6 and 204-7-17 compared to WT, however this increase did not lead to critical toxicity levels (Supplementary Figure 9). Mn and B concentrations in all transgenic lines were comparable to the WT, except for line 804-10-2-15, which had slightly increased shoot Mn concentrations (Supplementary Figure 9). Taken together, significant differences in nutrient uptake or status were not found as result of modulated *HvMYB15* expression.
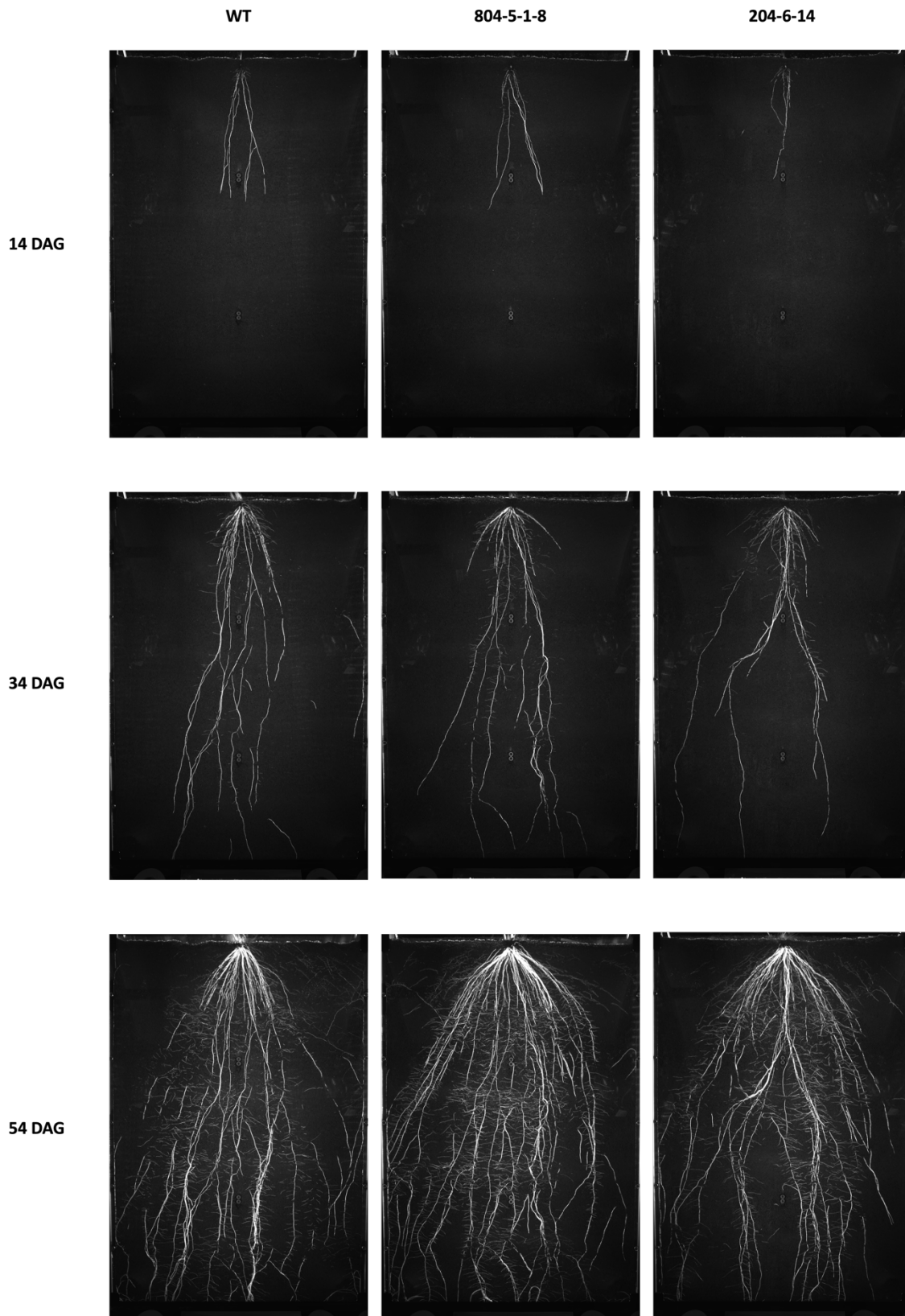
**Figure 64. Comparison of root architecture between wild type and lines with modulated** *HvMYB15* **expression.** Representative root images of WT, the overexpression line 805-4-3-10 and the knock-out line 301-4-14 of *HvMYB15* taken on 14, 34 and 54 days after germination (DAG). All lines were grown in soil-filled rhizotrons along with the WT for 55 days. Roots and shoots were imaged non-destructively on a daily basis.
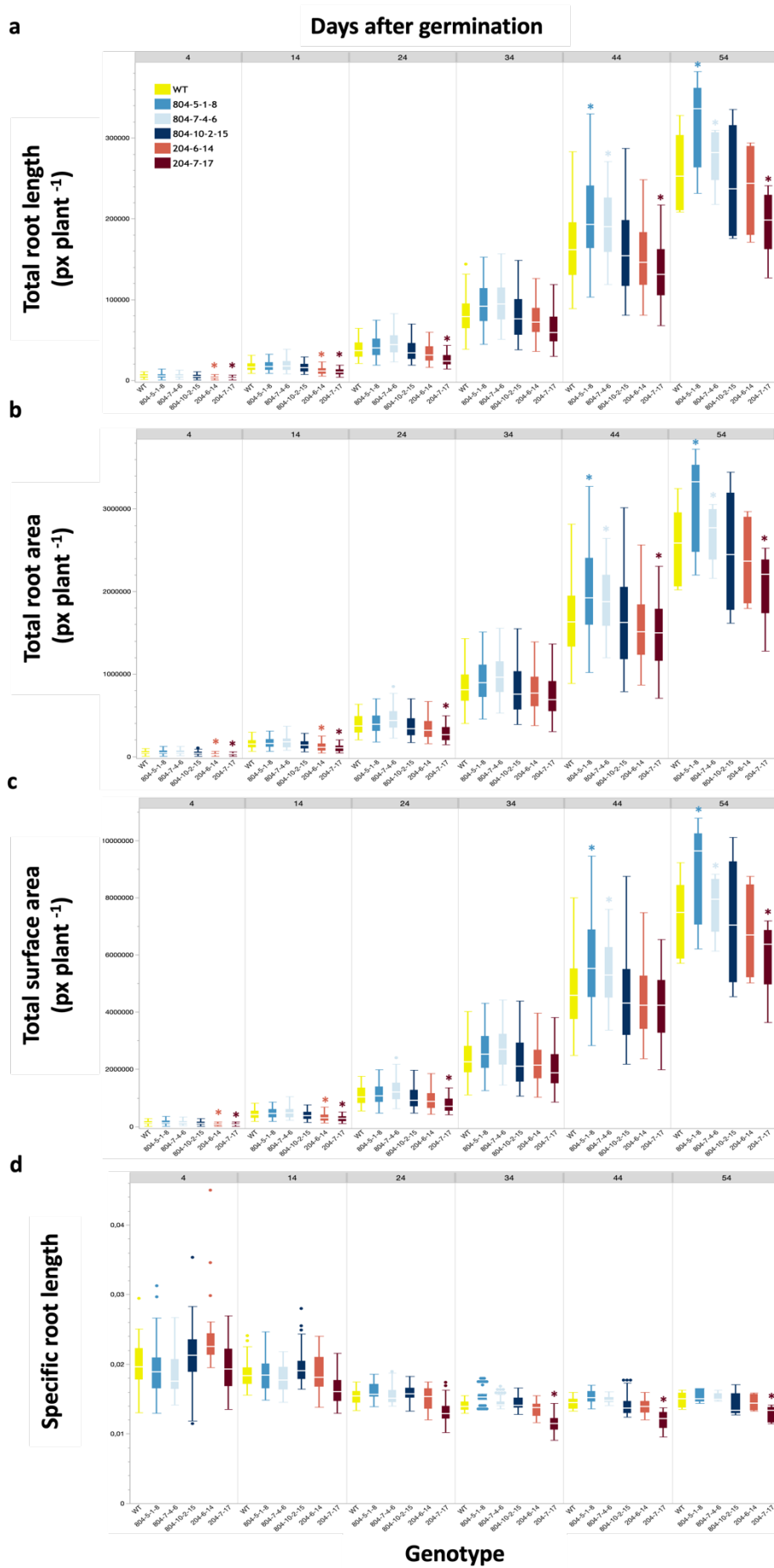
**Figure 65. Root architectural traits in transgenic barley lines as affected by modulated *HvMYB15* expression.** Total root length **(a)**, total root area **(b)**, root surface area **(c)** and specific root length **(d)** of wild-type (WT, black), overexpression (804-5-1-8, 804-7-4-6, 804-10-2-15) and knock-out lines 204-6-14, 204-7-17) of *HvMYB15* at 4, 14, 24, 34, 44 and 54 days after germination (DAG). Transgenic lines were grown in soil-filled rhizotrons along with the WT for 55 days. Dynamics of root and shoot growth were monitored non-destructively by daily imaging. Images were analyzed by the fully-automated root image analysis software faRIA (Narisetti et al., 2020). The boxes represent the first quartile, median and third quartile, whereas the whiskers indicate the minimum and maximum values (n=5). Asterisks denote significant differences between individual lines and the WT at $*$ P < 0.05 by two-tailed Student's *t* test. px, pixels.

## 4. Discussion

### 4.1. Modulation of seminal root senescence by nodal root development

In barley, embryonic seminal roots emerge from the embryo, whereas post-embryonic roots originate from either existing roots as lateral roots or from non-root tissues as nodal roots. Nodal roots are superior to embryonic seminal roots in terms of water and nutrient uptake, and their significant proliferation coincides with the decline in physiological activity and the arrest in elongation of seminal roots (Liu et al., 2019; 2020). On the other hand, the maize *rcts* mutant that is defective in the formation of post-embryonic roots, including crown roots and seminal laterals, can reach maturity and set seeds (Hetz et al., 1996). Likewise, the *mortal* mutant of white clover can reproduce, although it cannot form any adventitious nodal roots throughout its development (White et al., 1998). These observations indicate that in the absence of nodal or adventitious roots, embryonic roots should stay functional until the end of the plant's life cycle to allow for reproduction. Thus, it was hypothesized that the signal initiating the onset of seminal root senescence comes from the nodal roots. To test this hypothesis, nodal roots were cut off daily and the plants were allowed to grow only in the presence of seminal roots.

When nodal roots were removed daily, seminal roots continued to elongate and increase their biomass over a period of more than three weeks (Figure 5.a, b). Moreover, removal of nodal roots increased lateral root branching at seminals (Figure 6). These results were in consistence with a recent study in maize, in which the partial excision of nodal roots resulted in increased embryonic root biomass and a greater lateral to axial root ratio (Guo and York, 2019). Enhanced lateral root branching of seminal roots was expected to be associated with increased assimilate allocation into seminals due to the lack of nodal roots that are competing for carbohydrates. Surprisingly, in the absence of nodal roots, concentrations of soluble carbohydrates in seminal roots were highly similar to those with permitted nodal root growth (Figure 8). In rice, cytokinin accumulation in roots has an inhibitory effect on lateral root initiation but it stimulates lateral root elongation (Debi et al., 2005). A negative relationship between the growth of seminal and nodal roots was also observed in transgenic barley lines overexpressing *AtCKX2* in roots. These plants exhibited increased seminal root biomass (Figure 16.b) and enhanced lateral root branching at seminals (Figure 17). Thus, continuous degradation of CKs in roots promotes lateral root branching.

Interestingly, in contrast to the stimulated seminal root growth, the emergence and development of nodal roots was delayed in transgenic lines compared to WT (Figure 16.c). All these observations suggest that there might be a hormonal signaling effect on the growth and development of different root systems rather than a simple competition between them for the carbon resources delivered from the shoot.

As for the dynamics of seminal root growth, the present data show that although seminal root biomass kept increasing in the absence of nodal roots, the rate of biomass accumulation clearly declined at later developmental stages (Figure 5.a). In addition, when nodal roots were removed some of the seminal root tips were still degrading - albeit to a lower extent (Figure 5.c). Taken together, these results suggest that removing nodal roots suppressed and delayed but did not inhibit the onset or the progression of seminal root senescence. Thus, seminal root senescence is not exclusively dependent on a nodal root signal or any other physiological interaction.

Seminal root activity, measured as N uptake rate, remained constant in the absence of nodal roots and did not drop as in case of permitted nodal root development (Figure 7), suggesting expanded physiological activity of seminal roots. Despite the loss of nodal roots, enhanced growth and prolonged activity of seminal roots did not cause significant changes in aboveground plant biomass (Figure 4.c, d) implying that the seminal root system was sufficient to feed the shoot and a sufficiently strong sink to cope with the shoot for the excess available carbon that was not allocated to nodal roots. On the other hand, considering that removing nodal roots did not change the concentrations of carbohydrates in seminals (Figure 8), it is likely that there is another driving force for the extended seminal root activity besides energy. Nevertheless, it should be beard in mind that here the experimental period covered only vegetative growth stages, meaning that sink-creating reproductive organs were still absent and aboveground nutrient demands remained low. A very early study has shown that the absence of nodal roots leads to significant reductions in the formation of spikes as well as in straw yield of the tillers (Krassovsky, 1926). Considering that the nodal root biomass started to dominate over that of seminal roots from day 46 onwards (Figure 4.b, 5.a) and accounted for 83% of the total root biomass at 53 DAG under control conditions (data not shown), it is likely that the prolonged seminal root activity alone

may not suffice to sustain proper aboveground growth at later developmental stages and the plant's maximum yield potential.

Senescence of different tissues are under control of transcriptional regulation. Some of the well-described TFs involved in leaf senescence in barley (i.e. *HvNAC003* and *HvNAC005*, Podzimska-Sroka et al., 2015), have been shown to be expressed also during the senescence of roots (Liu et al., 2019). Moreover, *HvWRKY53* and *HvMYB15* have been proposed to regulate aging-related processes exclusively in roots (Liu et al., 2019). In the present study, these TFs were also upregulated in seminal roots starting from 32 DAG under control conditions (Figure 11) confirming their involvement in the regulation of root senescence. Furthermore, the accumulation of the transcripts was detectable even before any of the aging symptoms could be observed. This suggests that these TFs are involved in the early regulation of senescence-related processes. Taken further, the delay in the upregulation of these putative early regulators by the removal of nodal roots (Figure 11, 12) suggests that the onset of seminal root senescence had been postponed.

A hallmark of leaf senescence is protein degradation as evidenced in Arabidopsis by the increased transcript and protein abundance of the cysteine protease AtSAG12, which is also a widely used marker (Guo et al., 2004). Transcripts of the *AtSAG12* ortholog *HvPap17* in barley as well as its close homolog *HvPap15* also accumulated in senescing barley roots (Liu et al., 2019), whereas their expression was suppressed in the absence of nodal roots (Figure 13), indicating suppressed protein degradation and thereby delayed progression of senescence-typical processes in seminal roots.

Senescence of roots is associated with temporal changes in phytohormone homeostasis (Liu et al., 2019; Ryser et al., 2020). SA has been shown to accumulate in senescing leaves and induce the expression of senescence-associated genes (Morris et al., 2000; Lim et al., 2007). Similarly, senescing roots also showed increased SA concentrations (Liu et al., 2019) and upregulation of genes involved in the SA metabolism and signaling (Wojciechowska et al., 2020) in barley and poplar, respectively. In consistence with these reports, SA in seminal roots gradually accumulated with the progression of age under control conditions, whereas it remained constantly at a lower level in the absence of nodal roots (Figure 9.d). The

role of SA in root senescence is not known. However, as it was proposed for the senescence of leaves that SA may act as a signaling molecule aiding the transition from senescence to PCD (Morris et al., 2000). In fact, SA signaling promotes ROS production and homeostasis (Wang et al., 2015). In senescing barley roots, upregulation of ROS-scavenging enzymes, as e.g. the catalases *HvCAT2* and *HvCAT3* (Liu et al., 2019) also pointed to an increased accumulation of ROS. Therefore, increasing SA accumulation in senescing roots can be directly linked with ROS-mediated PCD. Removal of nodal roots clearly lowered SA levels (Figure 9), which is indicative for delayed seminal root senescence.

ABA is another molecular marker of root senescence as increased concentrations of ABA have been proposed to act as a physiological trigger for initiating senescence-related events in roots (Liu et al., 2019). As ABA could not be quantified in this study, transcript abundance of genes involved in ABA biosynthesis, namely *HvNCED1* and *HvNCED2* (Seiler et al., 2011), and degradation, *HvABA'8-OH-1* and *3* (Cutler and Kruchko, 1999), were determined. Upregulation of the examined genes in control roots (Figure 10) confirms that ABA is part of the age-dependent changes in the seminal roots. Removal of nodal roots, on the other hand, suppressed the biosynthesis and the degradation of ABA (Figure 10), again suggesting that the onset of seminal root senescence in the absence of nodal roots is delayed.

Collectively, investigation of the physiological and molecular markers of seminal root senescence showed that continuous removal of nodal roots can expand seminal root physiological activity and developmental lifespan, albeit only to a certain extent. Upregulation of the senescence-related TFs in a delayed manner suggests that aging-related processes were postponed, but not completely inhibited in seminal roots, even though they were the only source for the plant for water and nutrient acquisition from the soil. Liu et al. (2019) have proposed that the onset of seminal root senescence in barley is not under direct control of the shoot. In Arabidopsis, roots can maintain their respiratory activity for a certain time even after the complete maturation of aboveground parts (Fanello et al., 2017). Moreover, there is evidence that the root system of the annual species soybean can survive independently following leaf senescence (Fanello et al., 2020). Thus, the major determinant for developmental root senescence appears to be the tissue age.

As a component of tissue age, stem cell aging of the root apical meristem may be a direct cause for seminal roots to senesce. In soil-grown maize, the apical meristems of the first-order branches of the primary root are lost as the roots age (Fusseder, 1987). Decaying root tips observed under control conditions as well as in the absence of nodal roots (Figure 5.c) are also indicative of apical meristem degradation. In Arabidopsis, root tip abnormalities are associated with the damage or activation of the quiescent center (QC) (Jiang et al., 2003). Maintenance of the stem cell niche and the QC is essential for root survival. The TF *WUSCHEL-RELATED HOMEOBOX 5* (*WOX5*) functions as a suppressor of *CYCLIN-D3.3* (*CYCD3.3)* expression, which is required to restrict cell division in the QC (Forzani et al., 2014). Recently, *WOX5* expression was shown to gradually decrease with progressing tissue age in *Arabidopsis* (Wein et al., 2020). Moreover, high levels of endogenous SA as well as its exogenous application significantly reduced *WOX5* expression in root tips and promoted cell division in the QC through a ROS-dependent pathway (Wang et al., 2020). Moreover, Kong et al. (2018) have shown that exogenous $H_2O_2$ application also leads to QC activation. Notably, QC cell divisions occur more frequently in aging plants compared to younger plants (Timilsina et al., 2019). Therefore, it is likely that seminal root senescence is also under control of QC quiescence in the root apical meristems. Taken together, it can be concluded that seminal root senescence is a complex developmental program that is determined by endogenous signals like tissue age of the seminals, however, it can be delayed by signals from other organs, in particular nodal roots), In this regard, senescence of seminal roots shows an analogy to that of leaves, considering that leaf senescence can be delayed but not completely inhibited by the removal of sink organs like spikes or fruits (Thomas and Stoddart, 1980; Noodén and Guiamét, 1989).

## 4.2. Genetic modulation of seminal root senescence by the ectopic expression of *AtCKX2* in roots

ABA and CKs antagonistically regulate many developmental processes and stress responses; this also holds true for leaf senescence (Pospisilova, 2003; Kundu and Gantait, 2017; Huang et al., 2018). Increased levels of ABA at the onset of root senescence went along with a sharp drop in CKs (Liu et al., 2019). Thus, it was hypothesized here that lower CK levels in roots can promote or accelerate root senescence, since they are expected to allow for an earlier accumulation of ABA. To

test this hypothesis a transgenic approach was employed. Transgenic lines with root-specific overexpression of *AtCKX2* (*EPP:AtCKX2*; Ramireddy et al., 2018) were grown along with WT plants in hydroponic culture and assessed for physiological and molecular markers of root senescence.

To determine when senescence-related processes set in, the dynamics of seminal root growth was evaluated. Under control conditions, the arrest in seminal root biomass increase and termination of elongation coincided (Figure 5.a, b, 16.a, b) and this coincidence has been characterized as a trait of seminal root senescence (Liu et al., 2019). Both *AtCKX2*-expressing lines had higher seminal root biomass compared to WT starting from 32 DAG, but stopped increasing it at 46 DAG similar to WT plants (Figure 16.a). Seminal root elongation, in contrast, was arrested in transgenic lines 2 weeks earlier than in WT (Figure 16.b). Consequently, total seminal root length of both CKX lines was lower than that of WT starting from 32 DAG. These results indicate that the increased seminal root biomass was not a consequence of increased axial root elongation. Indeed, both *AtCKX2*-expressing lines exhibited increased lateral root branching starting from early stages of growth (Figure 17). These results were consistent with previous reports, that have shown that root-specific or constitutive overexpression of CKX-genes resulted in increased primary root or total root length as well as enhanced lateral root branching in both mono- and dicotyledonous plants (Werner et al., 2010; Ramireddy et al., 2018; Nehnevajova et al., 2019; Ramireddy et al., 2021). However, these studies investigated the effect of CKX-overexpression on root elongation only at very early stages growth (i.e. 6-to-15 DAG). Here, earlier arrest of seminal root elongation in transgenic lines might have resulted from the over-elongation-favored enhanced lateral root branching. Previously, it has been shown that recombinant inbred lines of maize with few and long lateral roots had increased seminal root length compared to lines bearing more and shorter laterals (Zhan et al., 2015). Zhan and Lynch (2015) have reported a negative relationship between lateral root branching and rooting depth, suggesting that there might be a trade-off between primary or seminal root length and lateral root density. Thus, it is likely that increased lateral root branching in transgenic lines created a stronger sink that diverted carbon and other resources away from axial root meristems (Borch et al., 1999; Miller et al., 2003; Lynch, 2007), consequently leading to lower total seminal root length and earlier termination of root elongation in comparison to WT plants (Figure 16.b).

To elucidate to what extent the CK levels were modulated in response to increased *AtCKX2* transcripts, seminal roots of WT and transgenic lines were subjected to phytohormone analysis. In higher plants, iP, cZ, and tZ as well as their ribosylated and glucosylated forms constitute the major CK pool. In this study, only a limited number of CK derivatives could be determined in the seminal roots of WT and *AtCKX2*-expressing lines. Among the quantified CKs, iPR, tZ, tZR and cZR concentrations in transgenic lines were found to be either similar or even higher than the WT (Figure 20.a, b, c, d). In fact, Ramireddy et al. (2018) also reported similar results for above-mentioned CK derivates in transgenic barley lines ectopically expressing *AtCKX2* in roots and have shown that the reduced CK forms comprised of iP-, cZ-, and tZ-*N*- and *O*-glucosides, which could not be quantified in this study. This may be due to differences in the phytohormone extraction methods and measurement protocols or the different growth conditions.

To further investigate whether ectopic expression of *AtCKX2* affects ABA homeostasis, ABA concentrations in seminal roots were quantified. ABA levels in WT seminal roots showed a temporal peak at 46 DAG, characterized by a 2.5-fold increase, which was absent in both transgenic lines (Figure 20.e). Moreover, the two ABA biosynthesis genes *HvNCED1* and *HvNCED2* also peaked at 46 DAG in WT plants (Figure 21.a, b), probably related to the accumulation of ABA (Figure 20.e). In contrast, ectopic expression of *AtCKX2* suppressed the upregulation of both endogenous *HvNCED* genes (Figure 21.a, b). Likewise, the expression of the ABA-degrading gene *HvABA'8-OH-3* was also suppressed in *AtCKX2*-expressing lines compared to WT (Figure 21.d). ABA is one of the phytohormones that can accelerate the senescence of leaves. In rice, increased ABA levels can antagonize with CKs by inducing the expression of *OsCKX11* leading to reduced CK concentrations in senescing leaves (Zhang et al., 2021). Here, continuous degradation of the CKs in roots was initially hypothesized to allow ABA to accumulate earlier and thereby promoting the onset of root senescence. However, the present data here indicate that ABA was not antagonistically affected by the root-specific overexpression of *AtCKX2*. Moreover, absence of the ABA peak in *AtCKX2* lines further implies that senescence-related events had been postponed.

As the termination of root growth and elongation went along with a decline in the N uptake capacity (Chapter 3.1.1; Liu et al., 2019), $NO_3^-$ uptake rates with progressing plant age were examined. WT plants showed a steady decline in their $NO_3^-$ uptake capacity starting from 46 DAG, coinciding with the termination of root growth and elongation (Figure 16.a, b, 18). In contrast, the $NO_3^-$ uptake capacity of the *AtCKX2*-expressing lines did not drop and remained constant over time, implying an extended physiological activity of the seminal roots. CKs are involved in the regulation of N acquisition, and they can repress the expression of *NRT* genes in roots resulting in the reduction of $NO_3^-$ uptake (Kiba et al., 2011). Therefore, sustained $NO_3^-$ uptake rates with the progression of root age in *AtCKX2*-expressing lines might be a direct consequence of the lower CK levels in roots.

To gain further insights into the onset and progression of root senescence, gene expression levels of the TFs that are differentially expressed during aging-related processes were examined. The two senescence-associated NACs *HvNAC003* and *HvNAC005* were upregulated at 46 DAG in WT plants, whereas their expression was suppressed by the overexpression of *AtCKX2* in transgenic lines (Figure 22.a, b). The exact function of *HvNAC005* and *HvNAC003* in root senescence is not known. *HvNAC005* is involved in the early regulation of leaf senescence, and it regulates the expression of several genes related to secondary metabolism and hormone homeostasis that are related to development, stress and transport (Christiansen et al., 2016). Overexpression of *HvNAC003* delays dark-induced leaf senescence (McGrann et al., 2015). Moreover, the expression of both NAC-TFs is deregulated by ABA. *HvNAC005* is upregulated, whereas *HvNAC003* is downregulated by exogenous ABA supply (Christiansen et al., 2011). Furthermore, *HvNAC005* has been shown to regulate the expression of *HvNCED1* and the two *PP2C* (*PP2C-1* and *PP2C-2*) genes that are involved in ABA biosynthesis and ABA signaling, respectively (Christiansen et al., 2011). Therefore, it has been hypothesized that *HvNAC003* and *HvNAC005* also function in ABA homeostasis during root senescence and their expression may be directly linked to the ABA levels in the roots. In consistence with this, upregulation of *HvNCED1* went along with the upregulation of *HvNAC005* in WT roots (Figure 21.a, 22.b) suggesting a NAC-NCED-ABA regulatory module during root senescence. Most importantly, Christiansen et al. (2011) have reported the induction of a putative *CK-glucosyltransferase*, *ZOG*, in *HvNAC005* overexpressing barley lines. Song et al.

(2019) showed that upregulation of *ZOG* genes is part of flag leaf senescence in wheat. Thus, it is likely that *HvNAC005* is involved in a complex crosstalk between CK and ABA signaling during the senescence of roots.

*HvNAM1* is another NAC-type TF that is upregulated during leaf and root senescence (Podzimska-Sroka et al., 2015; Liu et al., 2019). *HvNAM1* as well as its wheat orthologue *TaNAM-B1* are involved in nutrient remobilization during flag leaf senescence and grain protein content (Uauy et al., 2006a, b). However, its function during root senescence has not been investigated. In the present study, *HvNAM1* was upregulated both in WT and *AtCKX2*-expressing lines concomitantly (Figure 22.c). Likewise, *HvMYB15* and *HvWRKY53*, which have been shown to be upregulated during root senescence (Liu et al., 2019), were upregulated starting from 32 DAG both in WT and in *AtCKX2*-expressing lines (Figure 23). Thus, expression of these genes was not informative with regard to the impact of decreased CK levels on the progression of root senescence.

Taken together, several important markers of seminal root senescence were altered by the ectopic overexpression of *AtCKX2* in roots. Among those, seminal root $NO_3^-$ uptake capacity was sustained for a longer period of time, ABA peak as well as increased transcript abundance of ABA biosynthesis and degradation genes were absent, and the two senescence-associated NAC TFs were not upregulated in transgenic lines in comparison to WT. These results suggest that these markers are directly or indirectly regulated by *AtCKX2*-mediated CK degradation during root senescence. Notably, changes in these physiological and molecular markers indicate a delay in seminal root senescence. In contrast, the senescence-related TFs *HvNAM1*, *HvMYB15* and *HvWRKY53* were unaffected by the root-specific overexpression of *AtCKX2*, suggesting that they may be either not senescence-associated in roots or in a regulatory loop that is unrelated to CK levels or the NAC-NCED-ABA-module.

From an agricultural perspective, modification of leaf senescence can be of advantage in terms of crop production. Genetic manipulation of leaf senescence through phytohormone-based molecular techniques has been proven successful for agricultural improvements. Delayed plant or organ senescence can be achieved by either suppressing senescence-promoting hormones or overproducing senescence-

inhibiting hormones (Gan, 2003). For instance, transgenic tobacco expressing CK biosynthesis gene *IPT* under control of a senescence-specific promoter *SAG12* displayed delayed leaf senescence associated with a longer period of high photosynthetic activities as well as a marked increase in grain yield and biomass (Gan and Amasino, 1995). Similarly, extended physiological activity of roots can be highly beneficial especially under water- or nutrient-limiting conditions. Ramireddy et al. (2018) have already reported that *AtCKX2*-overexpressing lines perform better under drought conditions. Although drought tolerance of transgenic lines was mainly attributed to the enhanced root system and the action of CKs in leaves, the present results indicate that this might have also resulted from prolonged root activity. Collectively, the present data suggest that senescence-related processes in roots can be also modified through hormone-based biotechnological approaches and this provides a basis to achieve agricultural improvements.

## 4.3. Characterization of a putative role of the transcription factor *HvWRKY53* in root development

The transcriptome of senescing barley roots revealed that the so-far uncharacterized WRKY-type TF *HvWRKY53* is upregulated before the onset of root senescence and that its expression is maintained at relatively high levels during the progression of root senescence (Liu et al., 2019). Based on database mining, *HvWRKY53* was found to be expressed exclusively in roots. Thus, it has been proposed that *HvWRKY53* is a positive regulator of the senescence-related events in roots. Under control conditions expression of *HvWRKY53* in roots was similar to the previous report by Liu et al. (2019), characterized by a peak in transcript abundance before any other physiological or morphological symptom of root senescence was observed, and a continuous high expression level thereafter (Figure 12.a, 23.b). Furthermore, removal of nodal roots went along with suppression of *HvWRKY53* and a delay in its upregulation (Figure 12.b). These results confirm the involvement of *HvWRKY53* in root-aging related developmental processes. While the main role of HvWRKY53 in root senescence still remains to be elucidated, gene expression analysis indicated that *HvWRKY53* is also expressed in old leaf sheaths, blades and flag leaf blade (Figure 39). In this case, expression in leaf blades and sheaths may suggest a gene function in leaf development (Li et al., 2010). Thus, although not found earlier in fully expanded young or senescent leaves (Liu et al., 2019), the present analysis shows *HvWRKY53*

expression in leaf tissues. It should therefore be considered that HvWRKY53 might have a shared function in leaf and root development.

With the aim to investigate a functional role of *HvWRKY53* in root senescence, overexpression lines and knock-out mutants had been generated. While root-senescence processes were expected to be accelerated by root-specific overexpression of *HvWRKY53*, corresponding knock-out lines were expected to show a delayed root senescence phenotype. Unfortunately, despite a large number of trials, establishment of a hydroponic culture could not be achieved with these lines. Microscopic observations revealed that the seed material was heavily contaminated with fungi probably inherited from the mother plants. Alternatively, transgenic lines were characterized in soil-filled pots, rhizoboxes or rhizotrons with the disadvantage that eventual root senescence-related phenotypes could only be estimated based on visual inspection of roots from the soil culture. However, visual observations did not indicate any acceleration or slowing down of root senescence-related traits.

Monitoring in real-time of root architectural trait changes in knock-out lines of *HvWRKY53* showed a slight suppression of root growth and development during early stages (Figure 41, 47). However, this effect was no longer detectable in rhizotrons later on, indicating that HvWRKY53 did not consistently modulate root architectural traits. In contrast, although root architecture of both, overexpression and knock-out lines were similar to WT plants at the late vegetative stage, all transgenic lines exhibited suppressed plant height and yield penalty compared to WT (Figure 53). These morphological changes in the above-ground plant traits induced by the root-specific overexpression and knock-out of *HvWRKY53* underscore the importance of maintaining the proper balance and dosage of *HvWRKY53* expression for proper plant development.

Evaluation of the shoot nutritional status of the transgenic lines at different developmental stages showed that modulated *HvWRKY53* expression does not cause any critical changes in shoot nutrient levels during vegetative growth (Supplementary Figure 6, 7). In contrast, during the reproductive growth phase, overexpression lines were characterized by lower Mn and higher Na concentrations (Figure 57, 58). However, Mn concentrations did not drop below critical deficiency levels (Marschner,

2012) and the increase in Na did not lead to toxicity. Interestingly, *HvWRKY53* was upregulated within 3 hours in response to NaCl treatment, while its expression dropped to basal levels 24 hours after treatment (Figure 40). These observations suggest that *HvWRKY53* might have a role in the early salt stress response.

Furthermore, investigation of *cis*-acting elements in the *HvWRKY53*-promoter region (Chapter 3.2.1) as well as the expression analysis in response to different stimuli (Figure 40) clearly show that drought stress can induce *HvWRKY53* expression. Since both drought and salt stress increase the osmotic potential of the nutrient or soil solution and lead to physiological water deficit, early responses to drought and salt stress are considered to be highly similar (Cao et al., 2023). Thus, HvWRKY53 may take over a function in response to drought and salt stress.

In conclusion, root-specific overexpression and knock-out lines of *HvWRKY53* did not show a strongly accelerated or delayed root senescence phenotype. However, it should be kept in mind that in soil culture, one of the most important root traits, physiological root activity, could not be assessed. Considering that *HvWRKY53* is expressed under N starvation (Figure 40), it is strongly recommended to investigate the nutrient uptake capacity of overexpressors and knock-out lines of *HvWRKY53* with progressing root age. Moreover, while these lines did not show a strong phenotype under control conditions, it would be interesting to evaluate their performance under nutrient-limiting conditions.

## 4.4. Characterization of a role of the transcription factor *HvMYB15* in root development

*HvMYB15* is an R2R3-type MYB TF and was shown to be upregulated just before the onset of root senescence in barley, while its transcripts were not detectable in young or senescent leaves (Liu et al., 2019). Based on these results, *HvMYB15* was proposed to positively regulate root senescence. To test this hypothesis, root-specific overexpression lines and corresponding knock-out lines were generated and characterized in soil-filled rhizotrons. Unfortunately, due to a severe contamination of the seed material as described above, evaluation of the senescence-related traits in hydroponics was not possible.

Evaluation of the impact of modulated *HvMYB15* expression on root architecture showed that increased transcript levels of *HvMYB15* in roots resulted in higher root biomass (Figure 62) and higher total root length and area (Figure 65.a,b,c). In contrast, the knock-out line 204-7-17 of *HvMYB15* had lower root biomass, total root length and total root area (Figure 62, 65.a,b,c). These results were in consistence with changes in the root growth rate, which was higher for overexpression lines and lower for knock-out lines of *HvMYB15* compared to WT (Figure 62.c). These observations indicate that *HvMYB15* is involved in the regulation of root growth and root architectural traits in barley. However, enhanced or suppressed root growth of transgenic lines did not affect the shoot nutritional status (except for N, which was not determined) during the vegetative growth phase– at least under adequate growth conditions (Supplementary Figure 8,9). Nutrient and water acquisition from the rhizosphere greatly depend on root morphological and architectural traits. Roots permitting enhanced soil exploitation and nutrient foraging can be of advantage especially under water- or nutrient-limiting conditions. Ramireddy et al. (2018) have reported that CKX-mediated enhanced root growth in barley translates into greater drought tolerance as well as higher mineral element concentrations. Similar results were observed for Arabidopsis and tobacco (Werner et al., 2010). Therefore, it is assumed that growth conditions here were not sufficiently limiting to reveal a possible impact of HvMYB15. Accordingly, it will be interesting in future experiments to evaluate the performance of the transgenic lines with modulated *HvMYB15* expression under water- or nutrient-limiting conditions.

Orthologous genes of *HvMYB15* in both rice (*OsMYB30*) and Arabidopsis (*AtMYB15*) have been shown to positively regulate basal resistance to biotic stress through enhanced lignification in leaves (Chezem et al., 2017; Li et al., 2020). Interestingly, in one of the soil culture attempts in the greenhouse, which was severely affected by aphid invasion, knock-out lines of *HvMYB15* did not set seeds, whereas the corresponding lines with root-specific overexpression behaved similar to the WT plants. Although these results were not included in this thesis because of the lack of a healthy control group, these observations may support a role of HvMYB15 in biotic stress resistance. Furthermore, analysis of the *cis*-regulatory elements in the *HvMYB15* promoter region (Chapter 3.2.2) as well as the gene expression analysis in response to different abiotic stress factors (Figure 60) showed that *HvMYB15* is responds to stress. While drought treatment downregulated *HvMYB15* expression,

NaCl exposure of roots induced *HvMYB15* 3 hours after treatment (Figure 60), suggesting that *HvMYB15* might participate in the early salt stress response. Moreover, both *AtMYB15* and *OsMYB30* are negative regulators of cold tolerance (Kim et al., 2017; Lv et al., 2017).

Most strikingly, *HvMYB15* was strongly upregulated by the withdrawal of the N sources from the growth medium (Figure 60). In this regard, *HvMYB15* responded to N starvation in a similar way as *HvWRKY53* (Figure 40). Considering that both of these TFs were upregulated concomitantly during developmental root senescence (Figure 12, 13; Liu et al., 2019), it is likely that these TFs are co-expressed. In line with this hypothesis, *HvMYB15* was more strongly expressed in the overexpression lines of *HvWRKY53* compared to WT plants (Supplementary Figure 10). Likewise, *HvWRKY53* transcripts were more abundant in the overexpression lines of *HvMYB15* than in WT plants (Supplementary Figure 11). These results suggest that *HvMYB15* and *HvWRKY53* might take part in the same regulatory loop.

Taken together, although the main role of HvMYB15 in root senescence could not be elucidated, the present study characterized HvMYB15 as regulator of root growth and development. However, such a role is likely not root-specific, because expression analysis showed that *HvMYB15* is also expressed in shoots (Figure 59), suggesting its role also in leaf development.

## 5. Summary

Senescence is a genetically-determined developmental program during which valuable resources from senescing old tissues are remobilized into the newly developing sink organs. To date, the most extensively studied organ-level senescence is the senescence of leaves. However, aging- and senescence-related processes in roots are poorly understood. Recently, morphological and physiological processes and putative molecular regulators and markers related to root senescence have been identified (Liu et al., 2019). However, it remains unclear whether and to what extent the senescence of roots is regulated independently from the other organs. To investigate whether the onset of seminal root senescence simply depends on the nodal root growth and development, barley plants were grown in a hydroponic culture and the nodal roots were removed daily, allowing the plants to grow only in the presence of seminal roots. Excision of nodal roots delayed the onset of seminal root senescence - albeit to a certain extent, suggesting that other endogenous signals act on top in determining the senescence of seminal roots. In parallel, to exploit the role of phytohormones during the progression of root senescence, we grew transgenic barley lines with enhanced cytokinin (CK) degradation in roots and monitored physiological and molecular senescence-related processes. Present results indicate that lower CK levels in roots can prolong the physiological activity and longevity of seminal roots. Taken together, both approaches provide evidence that root senescence in barley is a plastic trait that is subject to hormonal regulation.

In the third part, one- MYB and one WRKY-type TF were identified as candidate genes that putatively regulate senescence-related events exclusively in roots. To characterize these genes and validate their function in root senescence, root-specific overexpression and knock-out lines were generated. Under control conditions, transgenic lines of *HvWRKY53* did not show a relevant phenotype. On the other hand, while aboveground plant growth remained unaffected by the manipulation of *HvMYB15* transcript levels, evaluation of root growth dynamics in transgenic lines revealed a putative role of *HvMYB15* in the regulation of root growth and architectural traits in barley.

## 6. References

Abbruscato, P., Nepusz, T., Mizzi, L., Del Corvo, M., Morandini, P., Fumasoni, I., and FAIVRE-RAMPANT, O. D. I. L. E. (2012). OsWRKY22, a monocot WRKY gene, plays a role in the resistance response to blast. Molecular plant pathology, 13(8), 828-841.

Adu, M. O., Chatot, A., Wiesel, L., Bennett, M. J., Broadley, M. R., White, P. J. and Dupuy, L. X. (2014). A scanner system for high-resolution quantification of variation in root growth dynamics of Brassica rapa genotypes. Journal of Experimental Botany, 65(8), 2039-2048.

Ahkami, A.H., Lischewski, S., Haensch, K.-T., Porfirova, S., Hofmann, J., Rolletschek, H., Melzer, M., Franken, P., Hause, B., Druege, U. and Hajirezaei, M.R. (2009), Molecular physiology of adventitious root formation in Petunia hybrida cuttings: involvement of wound response and primary metabolism. New Phytologist, 181: 613-625.

Ahmed, M. A., Zarebanadkouki, M., Meunier, F., Javaux, M., Kaestner, A. and Carminati, A. (2018). Root type matters: measurement of water uptake by seminal, crown, and lateral roots in maize. Journal of Experimental Botany, 69(5), 1199-1206.

Arora, A. (2008) Biochemistry of flower senescence. Postharvest Biology and Technology of Fruits, Vegetables, and Flowers, 51.

Atkinson, J. A., and Wells, D. M. (2017). An updated protocol for high throughput plant tissue sectioning. Frontiers in Plant SScience, 8, 1721.

Atkinson, J. A., Rasmussen, A., Traini, R., Voß, U., Sturrock, C., Mooney, S. J., Wells, D.M. and Bennett, M. J. (2014). Branching out in roots: uncovering form, function, and regulation. Plant Physiology, 166(2), 538-550.

Bagniewska-Zadworna, A., Stelmasik, A. and Minicka, J. (2014). From birth to death – Populus trichocarpa fibrous roots functional anatomy. Biologia Plantarum, 58(3), 551-560.

Balazadeh, S., Kwasniewski, M., Caldana, C., Mehrnia, M., Zanor, M.I., Xue, G.-P. and Mueller-Roeber, B. (2011). ORS1, an H2O2-Responsive NAC Transcription Factor, Controls Senescence in Arabidopsis thaliana. Molecular Plant, 4(2), 346-360.

Baldi, E., Wells, C. E., and Marangoni, B. (2010). Nitrogen absorption and respiration in white and brown peach roots. Journal of Plant Nutrition, 33(3), 461-469.

Bodner, G., Nakhforoosh, A., Arnold, T. and Leitner, D. (2018). Hyperspectral imaging: a novel approach for plant root phenotyping. Plant Methods, 14, 84.

Borch, K., Bouma, T. J., Lynch, J. P., and Brown, K. M. (1999). Ethylene: a regulator of root architectural responses to soil phosphorus availability. Plant, Cell and Environment, 22(4), 425-431.

Bouma, T. J., Yanai, R. D., Elkin, A. D., Hartmond, U., Flores-Alva, D. E., and Eissenstat, D. M. (2001). Estimating age-dependent costs and benefits of roots with contrasting life span: comparing apples and oranges. New Phytologist, 150, 685-695.

Bresson, J., Bieker, S., Riester, L., Doll, J. and Zentgraf, U. (2018). A guideline for leaf senescence analyses: from quantification to physiological and molecular investigations, Journal of Experimental Botany, 69 (4), 769–786.

Brunner, I., and Godbold, D. L. (2007). Tree roots in a changing world. Journal of Forest Research, 12(2), 78-82.

Buchanan-Wollaston, V., Page, T., Harrison, E., Breeze, E., Lim, P. O., Nam, H. G., Lin, J-F., Wu, S-H., Swidzinski, J., Ishizaki, K. and Leaver, C. J. (2005).

Comparative transcriptome analysis reveals significant differences in gene expression and signalling pathways between developmental and dark/starvation-induced senescence in Arabidopsis. The Plant Journal, 42(4), 567-585.

Cao, H., Ding, R., Kang, S., Du, T., Tong, L., Zhang, Y., and Shukla, M. K. (2023). Drought, salt, and combined stresses in plants: Effects, tolerance mechanisms, and strategies. Advances in Agronomy, 178, 107-163.

Ceccon, C., Tagliavini, M., Schmitt, A.O. and Eissenstat, D.M. (2016). Untangling the effects of root age and tissue nitrogen on root respiration in Populus tremuloides at different nitrogen supply. Tree Physiology, 36(5), 618–627.

Chen, D., Chai, S., McIntyre, C.L. and Xue, G.-P. (2018). Overexpression of a predominantly root-expressed NAC transcription factor in wheat roots enhances root length, biomass and drought tolerance. Plant Cell Reports, 37, 225–237.

Chen, H.Y.H., and Brassard, B.W. (2013). Intrinsic and Extrinsic Controls of Fine Root Life Span, Critical Reviews in Plant Sciences, 32:3, 151-161.

Chen, X., Yao, Q., Gao, X., Jiang, C., Harberd, N.P. and Fu, X. (2016). Shoot-to-root mobile transcription factor HY5 coordinates plant carbon and nitrogen acquisition. Current Biology, 26(5), 640-646.

Chen, Y., Zhang, J., Li, Q., He, X., Su, X., Chen, F., Yuan, L. and Mi, G. (2015) Effects of nitrogen application on post-silking root senescence and yield of maize. Agronomy Journal, 107(3), 835-842.

Chezem, W. R., Memon, A., Li, F. S., Weng, J. K., and Clay, N. K. (2017). SG2-type R2R3-MYB transcription factor MYB15 controls defense-induced lignification and basal immunity in Arabidopsis. The Plant Cell, 29(8), 1907-1926.

Chinnusamy, V., Ohta, M., Kanrar, S., Lee, B. H., Hong, X., Agarwal, M., and Zhu, J. K. (2003). ICE1: a regulator of cold-induced transcriptome and freezing tolerance in Arabidopsis. Genes and development, 17(8), 1043-1054.

Christiansen, M. W., Holm, P. B., and Gregersen, P. L. (2011). Characterization of barley (Hordeum vulgare L.) NAC transcription factors suggests conserved functions compared to both monocots and dicots. BMC research notes, 4, 1-13.

Christiansen, M. W., Matthewman, C., Podzimska-Sroka, D., O'Shea, C., Lindemose, S., Møllegaard, N. E., and Gregersen, P. L. (2016). Barley plants over-expressing the NAC transcription factor gene HvNAC005 show stunting and delay in development combined with early senescence. Journal of experimental botany, 67(17), 5259-5273.

Comas, L. H., Eissenstat, D. M., and Lakso, A. N. (2000). Assessing root death and root system dynamics in a study of grape canopy pruning. The New Phytologist, 147(1), 171-178.

Commisso, M., Negri, S., Bianconi, M., Gambini, S., Avesani, S., Ceoldo, S., Avesani, L. and Guzzo, F. (2019). Untargeted and targeted metabolomics and tryptophan decarboxylase in vivo characterization provide novel insight on the development of kiwifruits (Actinidia deliciosa). International Journal of Molecular Sciences, 20(4), 897.

Cutler, A.J. and Krochko, J.E. (1999). Formation and breakdown of ABA. Trends in Plant Science. 4(12). 472-478.

Danjon, F., Stokes, A., and Bakker, M. R. (2013). Root systems of woody plants in Plant Roots: The Hidden Half, 4th Edn, eds A. Eshel and T. Beeckman (Boca Raton, FL: CRC Press), 29.1–29.21.

De Neve, M., De Buck, S., Jacobs, A., Van Montagu, M., and Depicker, A. (1997). T-DNA integration patterns in co-transformed plant cells suggest that T-DNA repeats originate from co-integration of separate T-DNAs. The Plant Journal, 11(1), 15-29.

Debi, B. R., Taketa, S., and Ichii, M. (2005). Cytokinin inhibits lateral root initiation but stimulates lateral root elongation in rice (Oryza sativa). Journal of plant physiology, 162(5), 507-515.

Distelfeld, A., Avni, R. and Fischer, A.M. (2014). Senescence, nutrient remobilization, and yield in wheat and barley. Journal of Experimental Botany, 65(14), 3783-98.

Doench, J. G., Fusi, N., Sullender, M., Hegde, M., Vaimberg, E. W., Donovan, K. F., and Root, D. E. (2016). Optimized sgRNA design to maximize activity and minimize off-target effects of CRISPR-Cas9. Nature biotechnology, 34(2), 184-191.

Doench, J. G., Fusi, N., Sullender, M., Hegde, M., Vaimberg, E. W., Donovan, K. F., and Root, D. E. (2016). Optimized sgRNA design to maximize activity and minimize off-target effects of CRISPR-Cas9. Nature biotechnology, 34(2), 184-191.

Doench, J. G., Hartenian, E., Graham, D. B., Tothova, Z., Hegde, M., Smith, I., and Root, D. E. (2014). Rational design of highly active sgRNAs for CRISPR-Cas9–mediated gene inactivation. Nature biotechnology, 32(12), 1262-1267.

Eggert, K., and von Wirén, N. (2017). Response of the plant hormone network to boron deficiency. New Phytologist, 216(3), 868-881.

Elmayan, T., and Tepfer, M. (1995). Evaluation in tobacco of the organ specificity and strength of the rolD promoter, domain A of the 35S promoter and the 35S2 promoter. Transgenic Research, 4(6), 388-396.

Fanello, D. D., Bartoli, C. G., and Guiamet, J. J. (2017). Qualitative and quantitative modifications of root mitochondria during senescence of above-ground parts of Arabidopis thaliana. Plant Science, 258, 112-121.

Fanello, D. D., Kelly, S. J., Bartoli, C. G., Cano, M. G., Alonso, S. M., and Guiamet, J. J. (2020). Plasticity of root growth and respiratory activity: Root responses to above-ground senescence, fruit removal or partial root pruning in soybean. Plant science, 290, 110296.

Fendrych, M., van Hautegem, T., van Durme, M., Olvera-Carrillo, Y., Huysmans, M., Karimi, M., Lippens, S., Guérin, C.J., Krebs, M., Schumacher, K. and Nowack, M.K. (2014). Programmed Cell Death Controlled by ANAC033/SOMBRERO Determines Root Cap Organ Size in Arabidopsis. Current Biology, 24(9), 931-940.

Feng, Q., de Rycke, R., Dagdas, Y. and Nowack M.K. (2022). Autophagy promotes programmed cell death and corpse clearance in specific cell types of the Arabidopsis root cap. Current Biology, 32(9), 2110-2119.

Fisher, M. C., Eissenstat, D. M., and Lynch, J. P. (2002) Lack of evidence for programmed root senescence in common bean (Phaseolus vulgaris) grown at different levels of phosphorus supply. New Phytologist, 153(1), 63-71.

Forzani, C., Aichinger, E., Sornay, E., Willemsen, V., Laux, T., Dewitte, W., and Murray, J. A. (2014). WOX5 suppresses CYCLIN D activity to establish quiescence at the center of the root stem cell niche. Current Biology, 24(16), 1939-1944.

Freschet, G.T., Cornwell, W.K., Wardle, D.A., Elumeeva, T.G., Liu, W., Jackson, B.G., Onipchenko, V.G., Soudzilovskaia, N.A., Tao, J. and Cornelissen, J.H.C. (2013). Linking litter decomposition of above- and below-ground organs to plant–soil feedbacks worldwide. Journal of Ecology 101: 943-952.

Freschet, G.T., Roumet, C., Comas, L.H., Weemstra, M., Bengough, A.G., Rewald, B., Bardgett, R.D., De Deyn, G.B., Johnson, D., Klimešová, J., Lukac, M., McCormack, M.L., Meier, I.C., Pagès, L., Poorter, H., Prieto, I., Wurzburger, N., Zadworny, M., Bagniewska-Zadworna, A., Blancaflor, E.B., Brunner, I., Gessler, A., Hobbie, S.E., Iversen, C.M., Mommer, L., Picon-Cochard, C., Postma, J.A., Rose, L., Ryser, P., Scherer-Lorenzen, M., Soudzilovskaia, N.A., Sun, T., Valverde-Barrantes, O.J., Weigelt, A., York, L.M. and Stokes, A. (2021). Root traits as drivers

of plant and ecosystem functioning: current understanding, pitfalls and future research needs. New Phytologist, 232, 1123-1158.

Fusseder, A. (1987). The longevity and activity of the primary root of maize. Plant and Soil, 101, 257-265.

Gan, S. (2003). Mitotic and postmitotic senescence in plants. Science of Aging Knowledge Environment, 2003(38), re7-re7.

Gan, S., and Amasino, R. M. (1995). Inhibition of leaf senescence by autoregulated production of cytokinin. science, 270(5244), 1986-1988.

Gilbert S.F. (2000). Developmental Biology. 6th edition. Sunderland (MA): Sinauer Associates.

Gill, R. A., and Jackson, R. B. (2000) Global patterns of root turnover for terrestrial ecosystems. The New Phytologist, 147(1), 13-31.

Gilmartin, P. M., Sarokin, L., Memelink, J., and Chua, N. H. (1990). Molecular light switches for plant genes. The Plant Cell, 2(5), 369.

Glanz-Idan, N., Lach, M., Tarkowski, P., Vrobel, O. and Wolf S. (2022). Delayed Leaf Senescence by Upregulation of Cytokinin Biosynthesis Specifically in Tomato Roots. Frontiers in Plant Science, 13, 922106.

Gniazdowska, A., Mikulska, M. and Rychter, A. (1998). Growth, nitrate uptake and respiration rate in bean roots under phosphate deficiency. Biologia Plantarum 41, 217–226

Gowik, U., Burscheidt, J., Akyildiz, M., Schlue, U., Koczor, M., Streubel, M., and Westhoff, P. (2004). cis-Regulatory elements for mesophyll-specific gene expression in the C4 plant Flaveria trinervia, the promoter of the C4 phosphoenolpyruvate carboxylase gene. The Plant Cell, 16(5), 1077-1090.

Gregersen, P.L., Holm, P.B. and Krupinska, K. (2008). Leaf senescence and nutrient remobilisation in barley and wheat. Plant Biology, 10: 37-49.

Gruber, A. R., Lorenz, R., Bernhart, S. H., Neuböck, R., and Hofacker, I. L. (2008). The vienna RNA websuite. Nucleic acids research, 36(suppl_2), W70-W74.

Gruber, A. R., Lorenz, R., Bernhart, S. H., Neuböck, R., and Hofacker, I. L. (2008). The vienna RNA websuite. Nucleic acids research, 36(suppl_2), W70-W74.

Guo, H., and York, L. M. (2019). Maize with fewer nodal roots allocates mass to more lateral and deep roots that improve nitrogen uptake and shoot growth. Journal of experimental botany, 70(19), 5299-5309.

Guo, Y., Cai, Z., and Gan, S. (2004). Transcriptome of Arabidopsis leaf senescence. Plant, cell and environment, 27(5), 521-549.

Guo, Y., Ren, G., Zhang, K., Li, Z., Miao, Y. and Guo, H. (2021). Leaf senescence: progression, regulation, and application. Molcular Horticulture. 1, 5.

Hano, S., Shibuya, T., Imoto, N., Ito, A., Imanishi, S., Aso, H., and Kanayama, Y. (2017). Serotonin content in fresh and processed tomatoes and its accumulation during fruit development. Scientia Horticulturae, 214, 107-113.

Hao, Y. J., Wei, W., Song, Q. X., Chen, H. W., Zhang, Y. Q., Wang, F., Zou, H. F., Lei, G., Tian, A. G., Zhang, W. K., Ma, B., Zhang, J. S. and Chen, S. Y. (2011). Soybean NAC transcription factors promote abiotic stress tolerance and lateral root formation in transgenic plants. The Plant Journal 68, 302-313.

Havé, M., Marmagne, A., Chardon, F. and Masclaux-Daubresse, C. (2017). Nitrogen remobilization during leaf senescence: lessons from Arabidopsis to crops, Journal of Experimental Botany, 68, 2513–2529.

Heilmeier H., Schultze E.D., Whale D.M. (1986). Carbon and nitrogen partitioning in the biennial monocarp Arctium tomentosum Mill. Oecologia. 70, 466–474.

Henry, C.M. and Deacon, J.W. (1981). Natural (non-pathogenic) death of the cortex of wheat and barley seminal roots, as evidenced by nuclear staining with acridine orange. Plant and Soil, 60, 255–274.

Hensel, G., Kastner, C., Oleszczuk, S., Riechen, J., and Kumlehn, J. (2009). Agrobacterium-mediated gene transfer to cereal crop plants: current protocols for barley, wheat, triticale, and maize. International Journal of Plant Genomics, 2009.

Hetz, W., Hochholdinger, F., Schwall, M., and Feix, G. (1996). Isolation and characterization of rtcs, a maize mutant deficient in the formation of nodal roots. The Plant Journal, 10(5), 845-857.

Heuermann D., Gentsch N., Guggenberger G., Reinhold-Hurek B., Schweneker D., Feuerstein U., Heuermann M.-C., Groß J., Kümmerer R., Bauer B., von Wirén N. (2022) Catch crop mixtures have higher potential for nutrient carry-over than pure stands under changing environments. Europ. J. Agron. 136, 126504.

Higo, K., Ugawa, Y., Iwamoto, M., and Korenaga, T. (1999). Plant cis-acting regulatory DNA elements (PLACE) database: 1999. Nucleic acids research, 27(1), 297–300.

Hochholdinger, F., Park, W. J., Sauer, M., and Woll, K. (2004). From weeds to crops: genetic analysis of root development in cereals. Trends in Plant Science 9, 42-48.

Hochholdinger, F., Yu, P., and Marcon, C. (2018). Genetic control of root system development in maize. Trends in Plant Science 23, 79-88.

Hoppe, D. C., McCully, M. E., and Wenzel, C. L. (1986). The nodal roots of Zea: their development in relation to structural features of the stem. Canadian Journal of Botany, 64(11), 2524-2537.

Hough, S. H., Ajetunmobi, A., Brody, L., Humphryes-Kirilov, N., and Perello, E. (2016). Desktop genetics. Personalized medicine, 13(6), 517-521.

Huang, Q., Wang, Y., Li, B., Chang, J., Chen, M., Li, K., Yang, G. and He, G. (2015). TaNAC29, a NAC transcription factor from wheat, enhances salt and drought tolerance in transgenic Arabidopsis. BMC Plant Biology, 15, 268.

Huang, X., Hou, L., Meng, J., You, H., Li, Z., Gong, Z., and Shi, Y. (2018). The antagonistic action of abscisic acid and cytokinin signaling mediates drought stress response in Arabidopsis. Molecular plant, 11(7), 970-982.

Jackson, R. B., Lajtha, K., Crow, S. E., Hugelius, G., Kramer, M. G., and Piñeiro, G. (2017) The ecology of soil carbon: pools, vulnerabilities, and biotic and abiotic controls. Annual Review of Ecology, Evolution, and Systematics, 48, 419-445.

Jiang, K., Meng, Y. L., and Feldman, L. J. (2003). Quiescent center formation in maize roots is associated with an auxin-regulated oxidizing environment.

Kang, K., Kim, Y. S., Park, S., and Back, K. (2009). Senescence-induced serotonin biosynthesis and its role in delaying senescence in rice leaves. Plant physiology, 150(3), 1380-1393.

Kiba, T., Kudo, T., Kojima, M., and Sakakibara, H. (2011). Hormonal control of nitrogen acquisition: roles of auxin, abscisic acid, and cytokinin. Journal of experimental botany, 62(4), 1399-1409.

Kim, H. K., Lee, S., Kim, Y., Park, J., Min, S., Choi, J. W., and Kim, H. H. (2020). High-throughput analysis of the activities of xCas9, SpCas9-NG and SpCas9 at matched and mismatched target sequences in human cells. Nature biomedical engineering, 4(1), 111-124.

Kim, K. C., Lai, Z., Fan, B., and Chen, Z. (2008). Arabidopsis WRKY38 and WRKY62 transcription factors interact with histone deacetylase 19 in basal defense. The Plant Cell, 20(9), 2357-2371.

Kim, S. H., Kim, H. S., Bahk, S., An, J., Yoo, Y., Kim, J. Y., and Chung, W. S. (2017). Phosphorylation of the transcriptional repressor MYB15 by mitogen-activated

protein kinase 6 is required for freezing tolerance in Arabidopsis. Nucleic Acids Research, 45(11), 6613-6627.

Kong, X., Tian, H., Yu, Q., Zhang, F., Wang, R., Gao, S., and Ding, Z. (2018). PHB3 maintains root stem cell niche identity through ROS-responsive AP2/ERF transcription factors in Arabidopsis. Cell Reports, 22(5), 1350-1363.

Kosslak, R.M., Chamberlin, M.A., Palmer, R.G. and Bowen, B.A. (1997), Programmed cell death in the root cortex of soybean root necrosis mutants. The Plant Journal, 11: 729-745.

Krassovsky, I. (1926). Physiological activity of the seminal and nodal roots of crop plants. Soil Science, 21(4), 307.

Krassovsky, I. (1926). Physiological activity of the seminal and nodal roots of crop plants. Soil Science, 21(4), 307.

Kuai, B., Chen, J., and Hörtensteiner, S. (2018). The biochemistry and molecular biology of chlorophyll breakdown. Journal of Experimental Botany, 69(4), 751-767.

Kundu, S., and Gantait, S. (2017). Abscisic acid signal crosstalk during abiotic stress response. Plant Gene, 11, 61-69.

Kushiro, T., Okamoto, M., Nakabayashi, K., Yamagishi, K., Kitamura, S., Asami, T., Hirai, N., Koshiba, T., Kamiya, Y. and Nambara, E. (2004). The Arabidopsis cytochrome P450 CYP707A encodes ABA 8'-hydroxylases: key enzymes in ABA catabolism. The EMBO Journal. 23(7).1647-56.

Last, F. T., Mason, P. A., Wilson, J., and Deacon, J. W. (1983). Fine roots and sheathing mycorrhizas: their formation, function and dynamics. In Tree Root Systems and Their Mycorrhizas (pp. 9-21). Springer, Dordrecht.

Lauenroth, W. K., and Gill, R. (2003) Turnover of root systems. In Root Ecology (pp. 61-89). Springer, Berlin, Heidelberg.

Lescot, M., Déhais, P., Thijs, G., Marchal, K., Moreau, Y., van de Peer, Y., Rouzé, P. and Rombauts, S. (2002). PlantCARE, a database of plant cis-acting regulatory elements and a portal to tools for in silico analysis of promoter sequences. Nucleic Acids Research. 30(1). 325–327.

Li, W., Wang, K., Chern, M., Liu, Y., Zhu, Z., Liu, J., and Chen, X. (2020). Sclerenchyma cell thickening through enhanced lignification induced by OsMYB30 prevents fungal penetration of rice leaves. new phytologist, 226(6), 1850-1863.

Li, Z., Peng, J., Wen, X. and Guo, H. (2012). Gene Network Analysis and Functional Studies of Senescence-associated Genes Reveal Novel Regulators of Arabidopsis Leaf Senescence. Journal of Integrative Plant Biology, 54, 526-539.

Liljeroth E. (1995). Comparisons of early root cortical senescence between barley cultivars, Triticum species and other cereals. New Phytologist, 130: 495–501.

Liljeroth, E. and Bryngelsson, T. (2001). DNA fragmentation in cereal roots indicative of programmed root cortical cell death. Physiologia Plantarum, 111: 365-372.

Lim, P. O., Kim, H. J., and Gil Nam, H. (2007) Leaf senescence. Annual Review of Plant Biology, 58, 115-136.

Lim, P. O., Kim, H. J., and Gil Nam, H. (2007). Leaf senescence. Annu. Rev. Plant Biol., 58, 115-136.

Liu, Z., Giehl, R. F. H., Hartmann, A., Hajirezaei, M. R., Carpentier, S., and von Wirén, N. (2020). Seminal and nodal roots of barley differ in anatomy, proteome and nitrate uptake capacity. Plant and Cell Physiology, 61(7), 1297-1308.

Liu, Z., Marella, C. B., Hartmann, A., Hajirezaei, M. R., and von Wirén, N. (2019) An age-dependent sequence of physiological processes defines developmental root senescence. Plant physiology, 181(3), 993-1007.

Lorenz, R., Bernhart, S. H., Höner zu Siederdissen, C., Tafer, H., Flamm, C., Stadler, P. F., and Hofacker, I. L. (2011). ViennaRNA Package 2.0. Algorithms for molecular biology, 6, 1-14.

Lv, Y., Yang, M., Hu, D., Yang, Z., Ma, S., Li, X., and Xiong, L. (2017). The OsMYB30 transcription factor suppresses cold tolerance by interacting with a JAZ protein and suppressing β-amylase expression. Plant physiology, 173(2), 1475-1491.

Lynch, J. P. (2007). Roots of the second green revolution. Australian journal of Botany, 55(5), 493-512.

Marschner, H. (Ed.). (2012). Marschner's mineral nutrition of higher plants. Academic press.

Matamala, R., Gonzalez-Meler, M. A., Jastrow, J. D., Norby, R. J., and Schlesinger, W. H. (2003) Impacts of fine root turnover on forest NPP and soil C sequestration potential. Science, 302(5649), 1385-1387.

Matsushima, R., Tang, L.Y., Zhang, L., Yamada, H., Twell, D., and Sakamoto, W. (2011). A Conserved, Mg2+-Dependent Exonuclease Degrades Organelle DNA during Arabidopsis Pollen Development. The Plant Cell, 23(4), 1608–1624.

McCormack, M. L., Dickie, I. A., Eissenstat, D. M., Fahey, T. J., Fernandez, C. W., Guo, D., Helmissari, H.-S., Hobbie, E.A., Iversen, C.M., Jackson, R.B., Leppälammi-Kujansuu, J., Norby, R.J., Philips, R.P., Pregitzer, K.S., Pritchard, S.G., Rewald, B. and Zadworny, M. (2015) Redefining fine roots improves understanding of below-ground contributions to terrestrial biosphere processes. New Phytologist, 207(3), 505-518.

McCormack, M. L., Eissenstat, D. M., Prasad, A. M., and Smithwick, E. A. (2013). Regional scale patterns of fine root lifespan and turnover under current and future climate. Global Change Biology, 19(6), 1697-1708.

McGrann, G. R., Steed, A., Burt, C., Goddard, R., Lachaux, C., Bansal, A., and Brown, J. K. (2015). Contribution of the drought tolerance-related Stress-responsive NAC 1 transcription factor to resistance of barley to R amularia leaf spot. Molecular plant pathology, 16(2), 201-209.

Miao, Y., Laun, T., Zimmermann, P. and Zentgraf, U. (2004). Targets of the WRKY53 transcription factor and its role during leaf senescence in Arabidopsis. Plant Molecular Biology. 55(6), 853-867.

Miller, C. R., Ochoa, I., Nielsen, K. L., Beck, D., and Lynch, J. P. (2003). Genetic variation for adventitious rooting in response to low phosphorus availability: potential utility for phosphorus acquisition from stratified soils. Functional Plant Biology, 30(9), 973-985.

Mommer, L., Padilla, F.M., van Ruijven, J., de Caluwe, H., Smit-Tiekstra, A., Berendse, F. and de Kroon, H. (2015). Diversity effects on root length production and loss in an experimental grassland community. Functional Ecology, 29, 1560-1568.

Morris, K., -Mackerness, S. A. H., Page, T., John, C. F., Murphy, A. M., Carr, J. P., and Buchanan-Wollaston, V. (2000). Salicylic acid has a role in regulating gene expression during leaf senescence. The Plant Journal, 23(5), 677-685.

Munné-Bosch S. (2008). Do perennials really senesce? Trends in Plant Science, 13(5):216-20.

Munné-Bosch, S. (2007). Aging in Perennials. Critical Reviews in Plant Sciences, 26(3), 123–138.

Narisetti, N., Henke, M., Seiler, C., Junker, A., Ostermann, J., Altmann, T., and Gladilin, E. (2021). Fully-automated root image analysis (faRIA). Scientific Reports, 11(1), 16047.

Narisetti, N., Henke, M., Seiler, C., Shi, R., Junker, A., Altmann, T., and Gladilin, E. (2019). Semi-automated root image analysis (saRIA). Scientific reports, 9(1), 19674.

Negri, S., Commisso, M., Avesani, L., and Guzzo, F. (2021). The case of tryptamine and serotonin in plants: a mysterious precursor for an illustrious metabolite. Journal of Experimental Botany, 72(15), 5336-5355.

Nehnevajova, E., Ramireddy, E., Stolz, A., Gerdemann-Knörck, M., Novák, O., Strnad, M., and Schmülling, T. (2019). Root enhancement in cytokinin-deficient oilseed rape causes leaf mineral enrichment, increases the chlorophyll concentration under nutrient limitation and enhances the phytoremediation capacity. BMC Plant Biology, 19, 1-15.

Noh, Y.S. and Amasino, R.M. (1999) Identification of a promoter region responsible for the senescence-specific expression of SAG12. Plant Molecular Biology. 41. 181–194 (1999).

Noodén, L. D., and Guiamét, J. J. (1989). Regulation of assimilation and senescence by the fruit in monocarpic plants. Physiologia Plantarum, 77(2), 267-274.

Olvera-Carrillo, Y., Van Bel, M., van Hautegem, T., Fendrych, M., Huysmans, M., Simaskova, M., van Durme, M., Buscaill, P., Rivas, S., Coll, N.S., Coppens, F., Maere, S. and Nowack, M.K. (2015). A Conserved Core of Programmed Cell Death Indicator Genes Discriminates Developmentally and Environmentally Induced Programmed Cell Death in Plants. Plant Physiology, 169(4), 2684–2699.

Osmont, K.S., Sibout, R. and Hardtke, C.S. (2007). Hidden Branches: Developments in Root System Architecture. Annual Reviews in Plant Biology, 58, 93-113.

Pfaffl, M. W. (2001). A new mathematical model for relative quantification in real-time RT–PCR. Nucleic acids research, 29(9), e45-e45.

Podzimska-Sroka, D., O'Shea, C., Gregersen, P. L., and Skriver, K. (2015). NAC transcription factors in senescence: from molecular structure to function in crops. Plants, 4(3), 412-448.

Podzimska-Sroka, D., O'Shea, C., Gregersen, P., and Skriver, K. (2015). NAC Transcription Factors in Senescence: From Molecular Structure to Function in Crops. Plants, 4(3), 412–448.

Pospíšilová, J. (2003). Interaction of cytokinins and abscisic acid during regulation of stomatal opening in bean leaves. Photosynthetica, 41, 49-56.

Pregitzer, K. S., Zak, D. R., Curtis, P. S., Kubiske, M. E., Teeri, J. A., and Vogel, C. S. (1995) Atmospheric CO2, soil nitrogen and turnover of fine roots. New Phytologist, 129(4), 579-585.

Qiu, K., Li, Z., Yang, Z., Chen, J., Wu, S., Zhu, X., Gao, S., Gao, J., Ren, G., Kuai, B. and Zhou, X. (2015). EIN3 and ORE1 accelerate degreening during ethylene-mediated leaf senescence by directly activating chlorophyll catabolic genes in Arabidopsis. PLoS Genetics, 11(7), e1005399.

Ramireddy, E., Nelissen, H., Leuendorf, J. E., Van Lijsebettens, M., Inzé, D., and Schmülling, T. (2021). Root engineering in maize by increasing cytokinin degradation causes enhanced root growth and leaf mineral enrichment. Plant Molecular Biology, 106, 555-567.

Ramireddy, E., Nelissen, H., Leuendorf, J. E., Van Lijsebettens, M., Inzé, D., and Schmülling, T. (2021). Root engineering in maize by increasing cytokinin degradation causes enhanced root growth and leaf mineral enrichment. Plant Molecular Biology, 106, 555-567.

Rankenberg T., Geldhof B., van Veen, H., Holsteens, K., Van de Poel, B. and Sasidharan, R. (2021). Age-dependent abiotic stress resilience in plants. Trends in Plant Science, 26(7), 692-705.

Reece-Hoyes, J. S., and Walhout, A. J. M. (2018). Gateway Recombinational Cloning. Cold Spring Harbor protocols, 2018(1), pdb.top094912.

Rich, S.M., Christopher, J., Richards, R. and Watt, M. (2020). Root phenotypes of young wheat plants grown in controlled environments show inconsistent correlation with mature root traits in the field. Journal of Experimental Botany, 71(16), 4751-4762.

Rongsawat, T., Peltier, J.-B., Boyer, J.-C., Véry, A.-A. and Sentenac, H. (2021). Looking for Root Hairs to Overcome Poor Soils. Trends in Plant Science, 26(1), 83-94.

Ryser, P., Puig, S., Müller, M., and Munné-Bosch, S. (2020). Abscisic acid responses match the different patterns of autumn senescence in roots and leaves of Iris versicolor and Sparganium emersum. Environmental and Experimental Botany, 176, 104097.

Ryser, P., Puig, S., Müller, M., and Munné-Bosch, S. (2020). Abscisic acid responses match the different patterns of autumn senescence in roots and leaves of Iris versicolor and Sparganium emersum. Environmental and experimental botany, 176, 104097.

Sakai, H., Aoyama, T., and Oka, A. (2000). Arabidopsis ARR1 and ARR2 response regulators operate as transcriptional activators. The Plant Journal, 24(6), 703-711.

Sakamoto, W. and Takami, T. (2014). Nucleases in higher plants and their possible involvement in DNA degradation during leaf senescence. Journal of Experimental Botany, 65(14), 3835–3843.

Schippers, J. H. M. (2015). Transcriptional networks in leaf senescence. Current Opinion in Plant Biology, 27, 77-83.

Schneider, H. M., Postma, J. A., Kochs, J., Pflugfelder, D., Lynch, J. P., and van Dusschoten, D. (2020). Spatio-temporal variation in water uptake in seminal and

nodal root systems of barley plants grown in soil. Frontiers in Plant Science, 11, 1247.

Schneider, H. M., Wojciechowski, T., Postma, J. A., Brown, K. M., Lücke, A., Zeisler, V., Schreiber, L. and Lynch, J. P. (2017) Root cortical senescence decreases root respiration, nutrient content and radial water and nutrient transport in barley. Plant, Cell and Environment, 40(8), 1392-1408.

Schneider, H. M., Wojciechowski, T., Postma, J. A., Brown, K. M., and Lynch, J. P. (2018). Ethylene modulates root cortical senescence in barley. Annals of botany, 122(1), 95-105.

Seiler, C., Harshavardhan, V. T., Rajesh, K., Reddy, P.S., Marc Strickert, M., Rolletschek, H., Scholz, U., Wobus, U. and Sreenivasulu, N. (2011). ABA biosynthesis and degradation contributing to ABA homeostasis during barley seed development under control and terminal drought-stress conditions, Journal of Experimental Botany. 62(8). 2615–2632.

Serra, O., Mähönen, A. P., Hetherington, A. J. and Ragni, L. (2022). The Making of Plant Armort: The Periderm. Annual Review of Plant Biology, 73:1, 405-432.

Shirsat, A., Wilford, N., Croy, R., and Boulter, D. (1989). Sequences responsible for the tissue specific promoter activity of a pea legumin gene in tobacco. Molecular and General Genetics MGG, 215, 326-331.

Shoji, K., Addicott, F.T. and Swets, W.A. (1951). Auxin in relation to leaf blade abscission. Plant Physiology. 126(1). 189-91.

Šimura, J., Antoniadi, I., Široká, J., Tarkowská, D. E., Strnad, M., Ljung, K., and Novák, O. (2018). Plant hormonomics: multiple phytohormone profiling by targeted metabolomics. Plant physiology, 177(2), 476-489.

Siqueira J.A., Otoni W.C., and Arauˊjo W.L. (2022). The hidden half comes into the spotlight: Peeking inside the black box of root developmental phases. Plant Communications. 3, 100246.

Soto-Burgos, J., Zhuang, X., Jiang, L. and Bassham, D.C. (2018). Dynamics of Autophagosome Formation. Plant Physiology, 176(1), 219-229.

Steele, S. J., Gower, S. T., Vogel, J. G., and Norman, J. M. (1997) Root mass, net primary production and turnover in aspen, jack pine and black spruce forests in Saskatchewan and Manitoba, Canada. Tree physiology, 17(8-9), 577-587.

Stein, N., Herren, G., and Keller, B. (2001). A new DNA extraction method for high-throughput marker analysis in a large-genome species such as Triticum aestivum. Plant breeding, 120(4), 354-356.

Strock, C. F., Burridge, J. D., Niemiec, M. D., Brown, K. M., and Lynch, J. P. (2021). Root metaxylem and architecture phenotypes integrate to regulate water use under drought stress. Plant, Cell and Environment, 44(1), 49-67.

Tang, G.-L.., Li, X.-Y.., Lin, L.-S., Gu, Z.-Y. and Zeng, F.-J. (2019). Leaf Senescence can be Induced by Inhibition of Root Respiration. Journal of Plant Growth and Regulation, 38, 980–991.

Tang, L.Y. and Sakamoto, W. (2011). Tissue-specific organelle DNA degradation mediated by DPD1 exonuclease. Plant Signaling and Behavior, 6(9), 1391-1393.

Teppabut, Y., Oyama, K. I., Kondo, T., and Yoshida, K. (2018). Change of Petals′ Color and Chemical Components in Oenothera Flowers during Senescence. Molecules, 23(7), 1698.

Terzaghi, W. B., and Cashmore, A. R. (1995). Light-regulated transcription. Annual review of plant biology, 46(1), 445-474.

Thomas, H., and Stoddart, J. L. (1980). Leaf senescence. Annual review of plant physiology, 31(1), 83-111.

Timilsina, R., Kim, J. H., Nam, H. G., and Woo, H. R. (2019). Temporal changes in cell division rate and genotoxic stress tolerance in quiescent center cells of Arabidopsis primary root apical meristem. Scientific reports, 9(1), 3599.

Timilsina, R., Kim, J.H., Nam, H.G. and Woo, H.R. (2019). Temporal changes in cell division rate and genotoxic stress tolerance in quiescent center cells of Arabidopsis primary root apical meristem. Scientific Reports 9, 3599.

Tombuloglu, H., Kekec, G., Sakcali, M. S., and Unver, T. (2013). Transcriptome-wide identification of R2R3-MYB transcription factors in barley with their boron responsive expression analysis. Molecular genetics and genomics, 288, 141-155.

Tracy, S.R., Nagel, K.A., Postma, J.A., Fassbender, H., Wasson, A. and Watt, M. (2020). Crop Improvement from Phenotyping Roots: Highlights Reveal Expanding Opportunities. Trends in Plant Science, 25(1), 105-118.

Uauy, C., Brevis, J. C., and Dubcovsky, J. (2006). The high grain protein content gene Gpc-B1 accelerates senescence and has pleiotropic effects on protein content in wheat. Journal of experimental botany, 57(11), 2785-2794.

Uauy, C., Distelfeld, A., Fahima, T., Blechl, A., and Dubcovsky, J. (2006). A NAC gene regulating senescence improves grain protein, zinc, and iron content in wheat. Science, 314(5803), 1298-1301.

Üstün, S., Hafrén, A. and Hofius, D. (2017). Autophagy as a mediator of life and death in plants. Current Opinion in Plant Biology, 40, 122-130.

van Hautegem, T., Waters, A.J., Goodrich, J. and Nowack, M.K. (2014). Only in dying, life: programmed cell death during plant development. Trends in Plant Science, 20(2), 102-113.

Vandesompele, J., De Preter, K., Pattyn, F., Poppe, B., Van Roy, N., De Paepe, A., and Speleman, F. (2002). Accurate normalization of real-time quantitative RT-PCR data by geometric averaging of multiple internal control genes. Genome biology, 3(7), 1-12.

Volder, A., Smart, D. R., Bloom, A. J., and Eissenstat, D. M. (2005). Rapid decline in nitrate uptake and respiration with age in fine lateral roots of grape: implications for root efficiency and competitive effectiveness. New Phytologist, 165(2), 493-502.

Wahbi, A., and Gregory, P. J. (1995). Growth and development of young roots of barley (Hordeum vulgare L.) genotypes. Annals of Botany, 75(5), 533-539.

Wang, H., and Schippers, J. H. (2019). The role and regulation of autophagy and the proteasome during aging and senescence in plants. Genes, 10(4), 267.

Wang, J., Defrenne, C., McCormack, M.L., Yang, L., Tian, D., Luo, Y., Hou, E., Yan, T., Li, Z., Bu, W., Chen, Y. and Niu, S. (2021). Fine-root functional trait responses to experimental warming: a global meta-analysis. New Phytologist, 230: 1856-1867.

Wang, X., Xu, C., Xiong, D., Yao, X., Chen, T., Jiang, Q., Jia, L., Fan, A. and Chen, G. (2022). Root age-related response of fine root respiration of Chinese fir seedlings to soil warming. Tree Physiology, 42(6), 1177–1187.

Wang, Z., Rong, D., Chen, D., Xiao, Y., Liu, R., Wu, S., and Yamamuro, C. (2021). Salicylic acid promotes quiescent center cell division through ROS accumulation and down-regulation of PLT1, PLT2, and WOX5. Journal of Integrative Plant Biology, 63(3), 583-596.

Wang, Z., Rong, D., Chen, D., Xiao, Y., Liu, R., Wu, S., and Yamamuro, C. (2021). Salicylic acid promotes quiescent center cell division through ROS accumulation and down-regulation of PLT1, PLT2, and WOX5. Journal of Integrative Plant Biology, 63(3), 583-596.

Wein, A., Le Gac, A. and Laux, T. (2020). Stem cell ageing of the root apical meristem of Arabidopsis thaliana. Mechanisms of Ageing and Development, 190, 111313.

Wein, A., Le Gac, A. L., and Laux, T. (2020). Stem cell ageing of the root apical meristem of Arabidopsis thaliana. Mechanisms of ageing and development, 190, 111313.

Werner, T., Nehnevajova, E., Köllmer, I., Novák, O., Strnad, M., Krämer, U., and Schmülling, T. (2010). Root-specific reduction of cytokinin causes enhanced root growth, drought tolerance, and leaf mineral enrichment in Arabidopsis and tobacco. The Plant Cell, 22(12), 3905-3920.

White, D. W., Woodfield, D. R., and Caradus, J. R. (1998). Mortal: a mutant of white clover defective in nodal root development. Plant physiology, 116(3), 913-921.

Wingler, A. and Henriques, R. (2022). Sugars and the speed of life—Metabolic signals that determine plant growth, development and death. Physiologia Plantarum, 174(2), e13656.

Withington, J. M., Reich, P. B., Oleksyn, J., and Eissenstat, D. M. (2006). Comparisons of structure and life span in roots and leaves among temperate trees. Ecological monographs, 76(3), 381-397.

Wojciechowska, N., Marzec-Schmidt, K., Kalemba, E. M., Ludwików, A., and Bagniewska-Zadworna, A. (2020b). Seasonal senescence of leaves and roots of Populus trichocarpa—is the scenario the same or different? Tree Physiology, 40(8), 987-1000.

Wojciechowska, N., Marzec-Schmidt, K., Kalemba, E. M., Zarzyńska-Nowak, A., Jagodziński, A. M., and Bagniewska-Zadworna, A. (2018) Autophagy counteracts instantaneous cell death during seasonal senescence of the fine roots and leaves in Populus trichocarpa. BMC Plant Biology, 18(1), 1-16.

Wojciechowska, N., Wilmowicz, E., Marzec-Schmidt, K., Ludwików, A., and Bagniewska-Zadworna, A. (2020a). Abscisic acid and jasmonate metabolisms are jointly regulated during senescence in roots and leaves of Populus trichocarpa. International Journal of Molecular Sciences, 21(6), 2042.

Woo, H. R., Kim, H. J., Lim, P. O., and Nam, H. G. (2019) Leaf senescence: systems and dynamics aspects. Annual Review of Plant Biology, 70, 347-376.

Woo, H. R., Kim, H. J., Nam, H. G., and Lim, P. O. (2013). Plant leaf senescence and death–regulation by multiple layers of control and implications for aging in general. Journal of Cell Science, 126(21), 4823-4833.

Xie, K., Minkenberg, B., and Yang, Y. (2015). Boosting CRISPR/Cas9 multiplex editing capability with the endogenous tRNA-processing system. Proceedings of the National Academy of Sciences, 112(11), 3570-3575.

Xie, K., Zhang, J., and Yang, Y. (2014). Genome-wide prediction of highly specific guide RNA spacers for CRISPR–Cas9-mediated genome editing in model plants and major crops. Molecular plant, 7(5), 923-926.

Xu, P., Chen, H and Cai, W. (2020). Transcription factor CDF4 promotes leaf senescence and floral organ abscission by regulating abscisic acid and reactive oxygen species pathways in Arabidopsis. EMBO Reports, 21, e48967.

Yamada, Y. and Umehara, M. (2015). Possible roles of strigolactones during leaf senescence. Plants, 4(3), 664-677.

Yanagisawa, S. (2000). Dof1 and Dof2 transcription factors are associated with expression of multiple genes involved in carbon metabolism in maize. The Plant Journal, 21(3), 281-288.

Yanhui, C., Xiaoyuan, Y., Kun, H., Meihua, L., Jigang, L., Zhaofeng, G., and Li-Jia, Q. (2006). The MYB transcription factor superfamily of Arabidopsis: expression

analysis and phylogenetic comparison with the rice MYB family. Plant molecular biology, 60, 107-124.

Yoshimoto, K., Hanaoka, H., Sato, S., Kato, T., Tabata, S., Noda, T. and Ohsumi, Y. (2004). Processing of ATG8s, Ubiquitin-Like Proteins, and Their Deconjugation by ATG4s Are Essential for Plant Autophagy, The Plant Cell. 16(11), 2967–2983.

Yu, P., Eggert, K., von Wirén, N., Li, C. and Hochholdinger, F. (2015). Cell-type specific gene expression analyses by RNA-Seq reveal local high nitrate triggered lateral root initiation in shoot-borne roots of maize by modulating auxin-related cell cycle-regulation. Plant Physiology 169: 690–704.

Zentgraf, U. and Doll, J. (2019). Arabidopsis WRKY53, a Node of Multi-Layer Regulation in the Network of Senescence. Plants, 8(12), 578.

Zentgraf, U., Andrade, A.G., Doll, J. (20121) Editorial for special issue "Leaf Senescence" in plants. Plants 10: 1490. doi.org/10.3390/plants10081490.

Zhan, A., and Lynch, J. P. (2015). Reduced frequency of lateral root branching improves N capture from low-N soils in maize. Journal of Experimental Botany, 66(7), 2055-2065.

Zhan, A., Schneider, H., and Lynch, J. P. (2015). Reduced lateral root branching density improves drought tolerance in maize. Plant physiology, 168(4), 1603-1615.

Zhang, F., Wen, Y., and Guo, X. (2014). CRISPR/Cas9 for genome editing: progress, implications and challenges. Human molecular genetics, 23(R1), R40-R46.

Zhang, H., Zhang, J., Wei, P., Zhang, B., Gou, F., Feng, Z., and Zhu, J. K. (2014). The CRISPR/C as9 system produces specific and homozygous targeted gene editing in rice in one generation. Plant biotechnology journal, 12(6), 797-807.

Zhang, W., Peng, K., Cui, F., Wang, D., Zhao, J., Zhang, Y., and Zhang, K. (2021). Cytokinin oxidase/dehydrogenase OsCKX11 coordinates source and sink relationship in rice by simultaneous regulation of leaf senescence and grain number. Plant biotechnology journal, 19(2), 335-350.

Zhao, L., Zhang, W., Song, Q., Xuan, Y., Li, K., Cheng, L., Qiao, H., Wang, G. and Zhou, C. (2020). A WRKY transcription factor, TaWRKY40-D, promotes leaf senescence associated with jasmonic acid and abscisic acid pathways in wheat. Plant Biology, 22(6), 1072-1085.

Zhou, D. X. (1999). Regulatory mechanism of plant gene transcription by GT-elements and GT-factors. Trends in plant science, 4(6), 210-214.

Zhu, L., Liu, L., Sun, H., Zhang, Y., Liu, X., Wang, N., Chen, J., Zhang, K., Bai, Z., Wang, G., Tian, L., and Li, C. (2022). The responses of lateral roots and root hairs to nitrogen stress in cotton based on daily root measurements. Journal of Agronomy and Crop Science, 208, 89–105.

# 7. Appendix
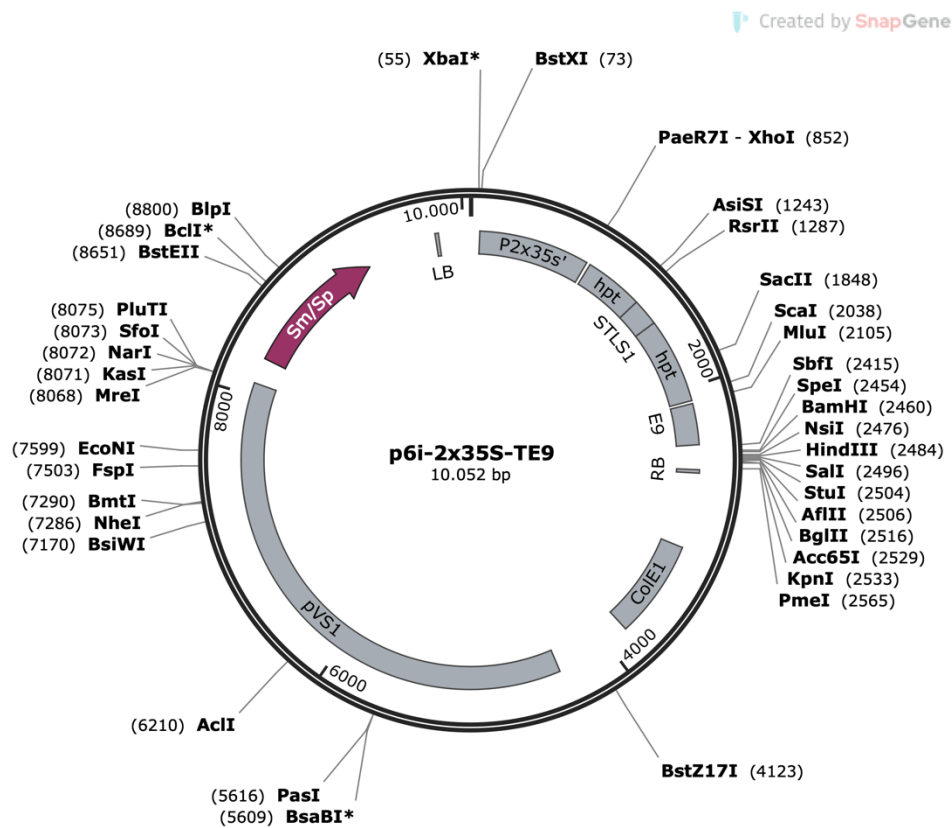


**Supplementary Figure 1. Vector map of the binary vector used for Agrobacterium-mediated transformation of barley in this study.** Structure of the binary backbone p6i_d35S_TE9, carrying the transgenic marker, *hpt*. All CRISPR/Cas9-vectors used for the transformation of barley were finally assembled with this binary vector backbone.
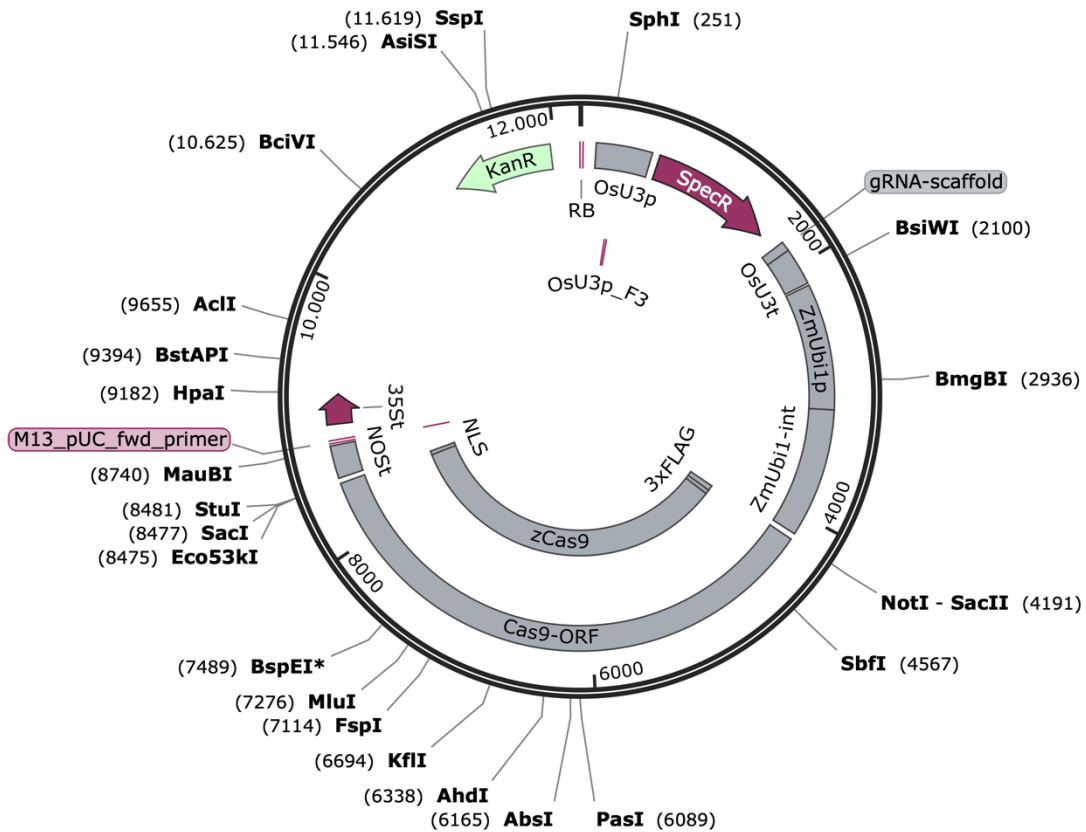
**pSH91 (OsU3-P_Spec_gRNA-Scaffolf_OsU3-T__Ubi-P_3xFLAG_NLS_zmCas9_NLS_NOS-T)**
12.198 bp

**Supplementary Figure 2. Intermediate CRISPR/Cas9 vector used to generate knock-out mutants.** pSH91 was used to target a single region. pSH91 carries the *OsU3*-promoter and *Zm-Ubi1*-promoter to drive the gRNA and *cas9* expression, respectively.
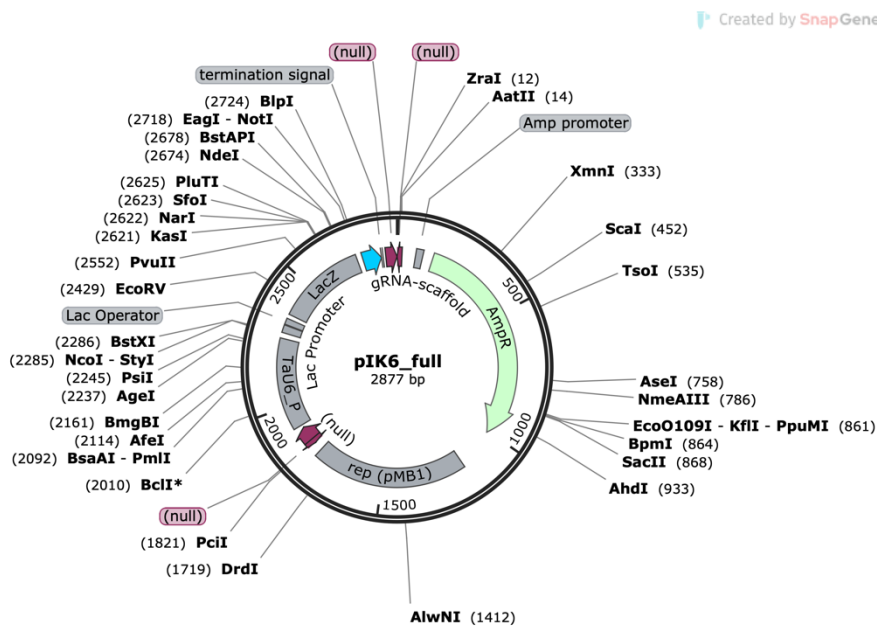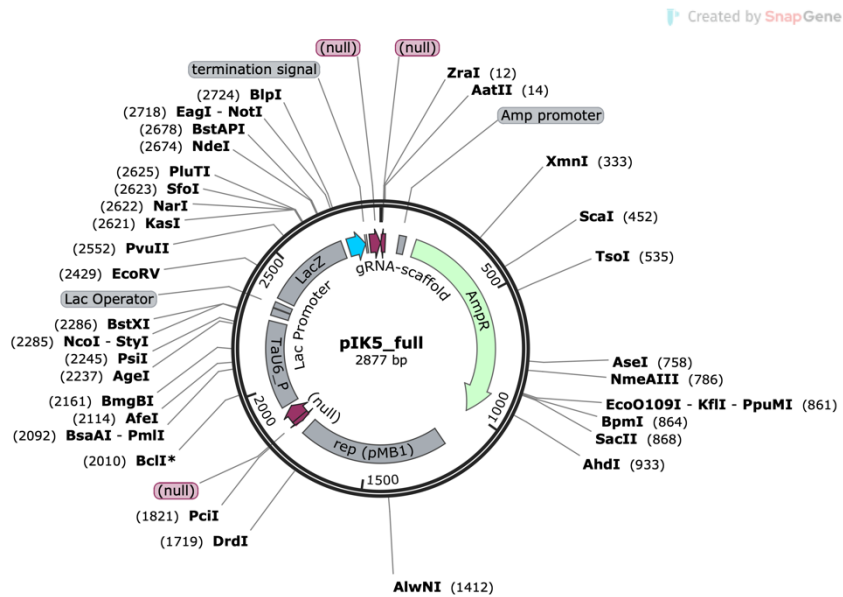
**Supplementary Figure 3. Intermediate vectors used for double-gRNA assembly.** Single gRNAs were firstly cloned into pIK5 and pIK6 separately. In the next step, both vectors carrying desired gRNAs driven by *TaU6*-promoter were assembled in another intermediate vector pIK60.
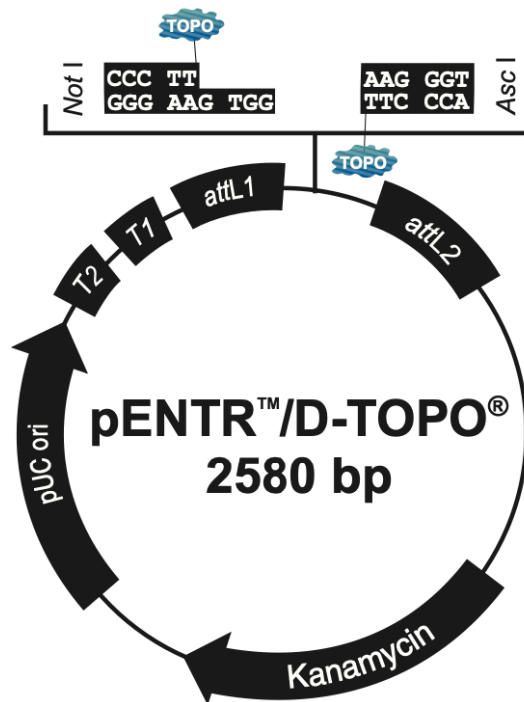
**Comments for pENTR™/D-TOPO®**
**2580 nucleotides**

*rrn*B T2 transcription termination sequence: bases 268-295
*rrn*B T1 transcription termination sequence: bases 427-470
M13 forward (-20) priming site: bases 537-552
*att*L1: bases 569-668 (c)
TOPO® recognition site 1: bases 680-684
Overhang: bases 685-688
TOPO® recognition site 2: bases 689-693
*att*L2: bases 705-804
T7 Promoter/priming site: bases 821-840 (c)
M13 reverse priming site: bases 845-861
Kanamycin resistance gene: bases 974-1783
pUC origin: bases 1904-2577

(c) = complementary sequence

**Supplementary Figure 4. Entry vector used in Gateway Cloning to generate overexpression constructs.** The pENTR/D-TOPO (Thermo Fisher Scientific. USA) vector was used as the entry vector to clone in the coding sequences of *HvWRKY53* and *HvMYB15*. Entry vectors carrying desired genes were ligated finally to the binary destination vector pIPKb001 (Supplementary Figure 5) through Gateway-LR reaction (https://assets.thermofisher.com/TFS-Assets%2FLSG%2Fmanuals%2Fpentr_dtopo_man.pdf).
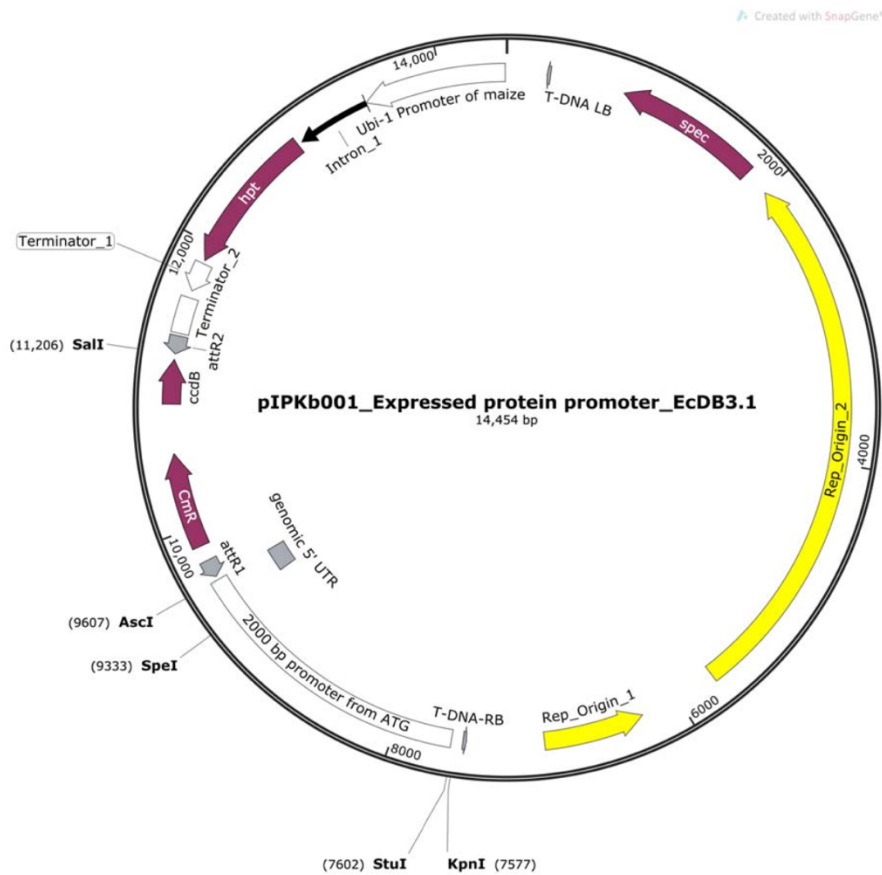
**Supplementary Figure 5. Destination vector used for the establishment of overexpression constructs.** The destination vector pIPKb001_Expressed protein promoter carries a root-specific promoter from rice (*Expressed protein; EPP; LOC_Os04g11040*) which will eventually drive the expression of the gene of interest, and the transgene marker, *hpt*.
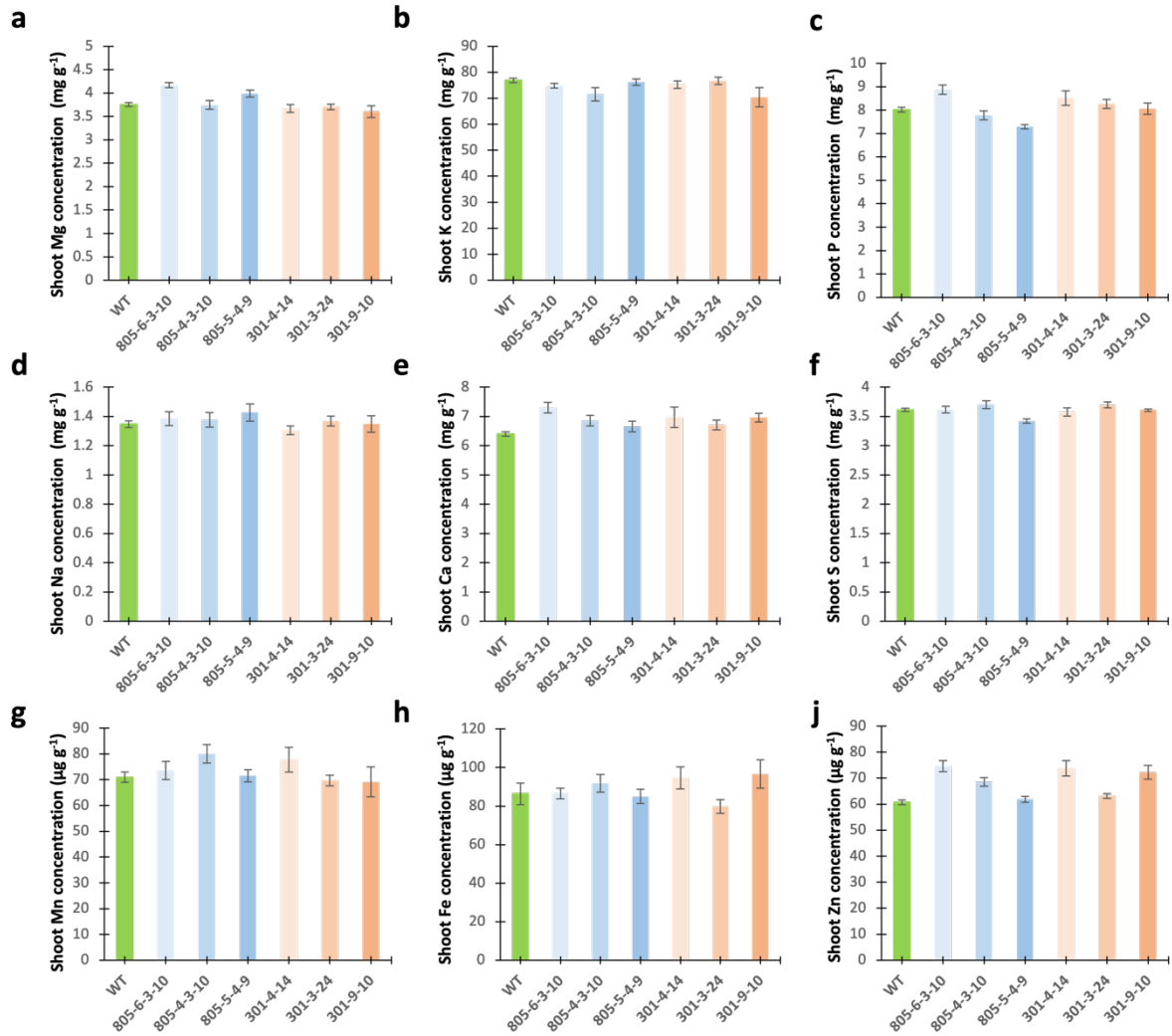
**Supplementary Figure 6. Shoot macro- and micronutrient concentrations in wild-type (WT) and transgenic lines of *HvWRKY53* during early vegetative growth. (a-i)** Shoot concentrations of Mg **(a)**, K **(b)**, p **(c)**, Na **(d)**, Ca **(e),** S **(f),** Mn **(g)**, Fe **(h)** and Zn **(i)** in WT, overexpression (805-4-3-10, 805-5-4-9, 805-6-3-10) and knock-out lines (301-4-14, 3-24, 9-10) of *HvWRKY53*. Transgenic lines of *HvWRKY53* along with the WT were grown in soil-filled rhizoboxes. At 23 DAS, whole shoots were collected and analyzed for mineral elements. Bars show means ± SD (n=5-7 biological replicates).
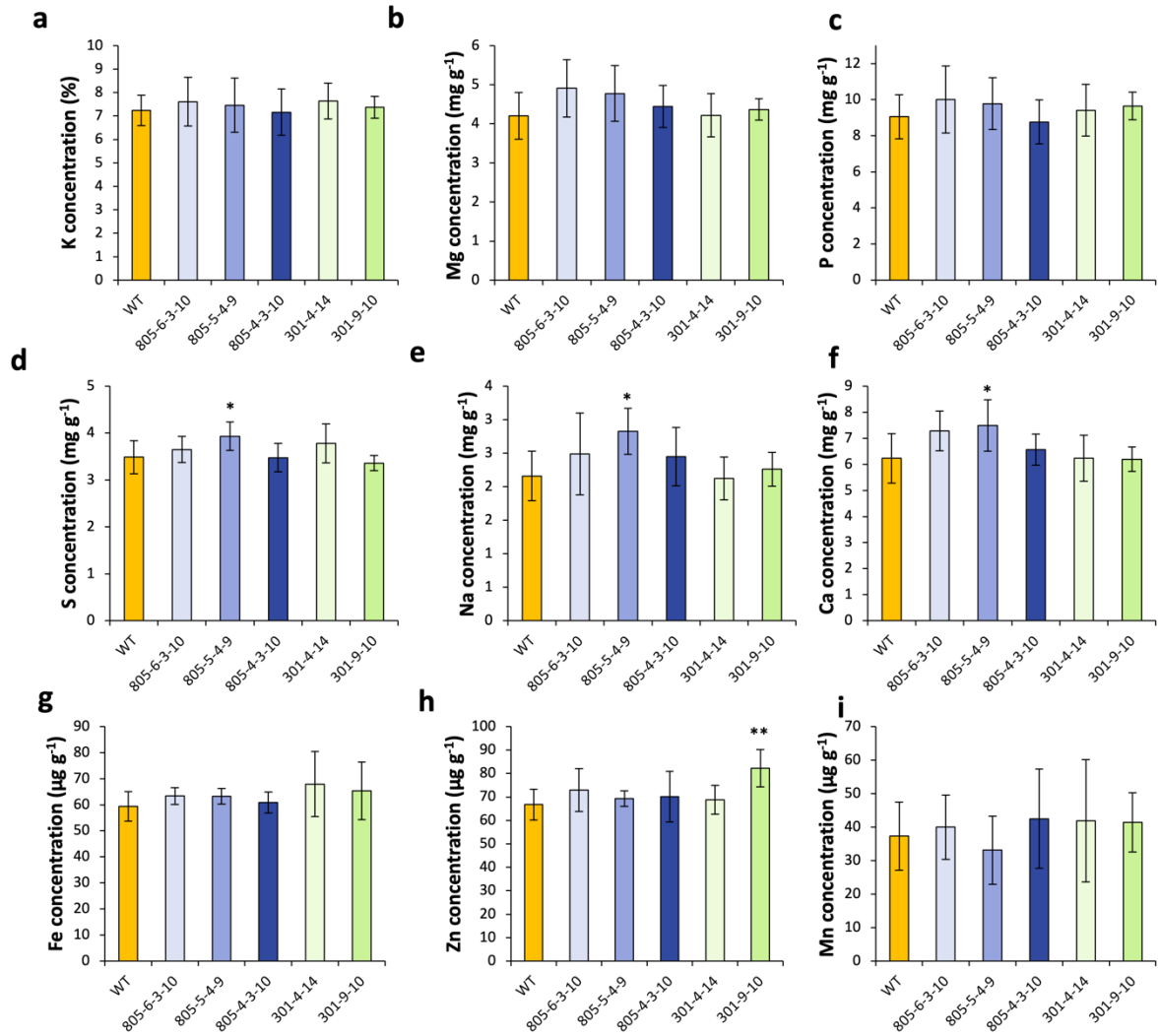
**Supplementary Figure 7. Shoot macro- and micronutrient concentrations in wild-type (WT) and transgenic lines of *HvWRKY53* at vegetative growth. (a-i)** Shoot concentrations of K **(a)**, Mg **(b)**, P **(c)**, Na **(d)**, Na **(e),** Ca **(f),** Fe **(g)**, Zn **(h)** and Mn **(i)** in WT, overexpression (805-4-3-10, 805-5-4-9, 805-6-3-10) and knock-out lines (301-4-14, 3-24, 9-10) of *HvWRKY53*. Transgenic lines were grown in soil-filled rhizotrons along with the WT for 55 days. Bars show means $\pm$ SD (n=5). Asterisks denote significant differences between individual lines and the WT at $*$ P < 0.05 or $**$ P < 0.01 by two-tailed Student's *t* test.
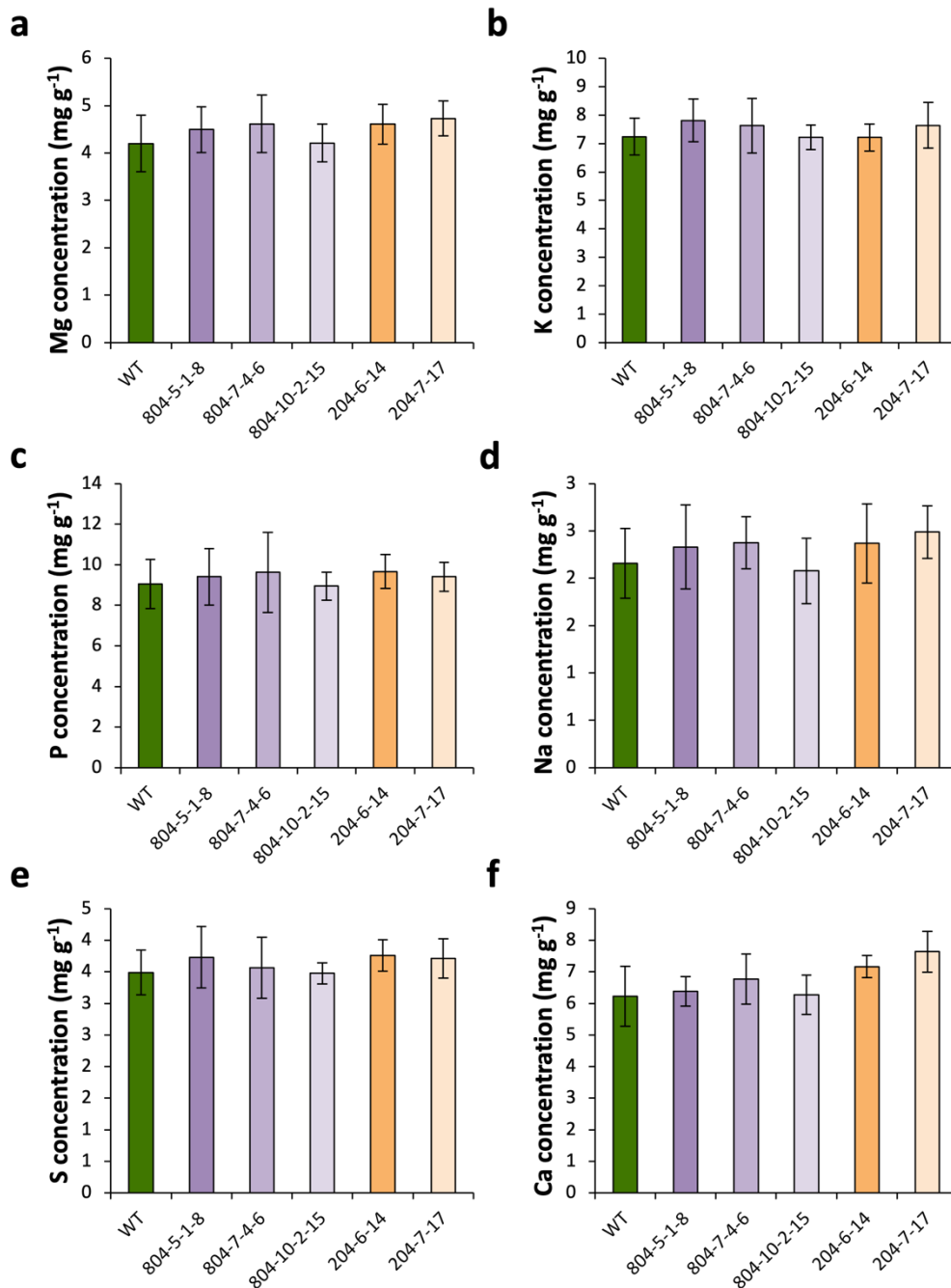
**Supplementary Figure 8. Shoot macronutrient concentrations in wild-type (WT) and transgenic lines of *HvMYB15* at vegetative growth. (a-f)** Shoot concentrations of Mg **(a)**, K **(b)**, P **(c)**, Na **(d)**, S **(e)** and Ca **(f)** in WT, overexpression (804-5-1-8, 804-7-4-6, 804-10-2-15) and knock-out lines (204-6-14, 204-7-17) of *HvMYB15*. Transgenic lines were grown in soil-filled rhizotrons along with the WT for 55 days. Bars show means ± SD (n=5).
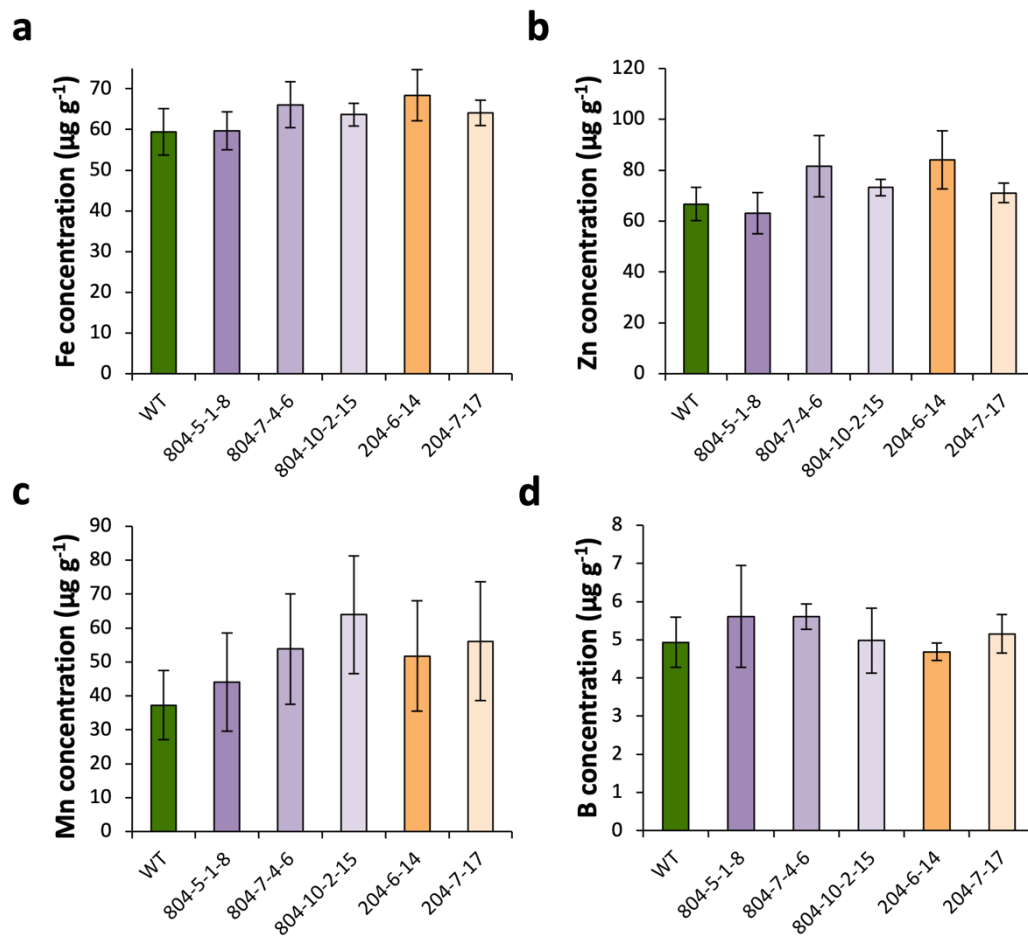
**Supplementary Figure 9. Shoot micronutrient concentrations in wild-type (WT) and transgenic lines of *HvMYB15* at vegetative growth. (a-d)** Shoot concentrations of Fe **(a)**, Zn **(b)**, Mn **(c)** and B **(d)** in WT, overexpression (804-5-1-8, 804-7-4-6, 804-10-2-15) and knock-out lines (204-6-14, 204-7-17) of *HvMYB15*. Transgenic lines were grown in soil-filled rhizotrons along with the WT for 55 days. Bars show means ± SD (n=5).
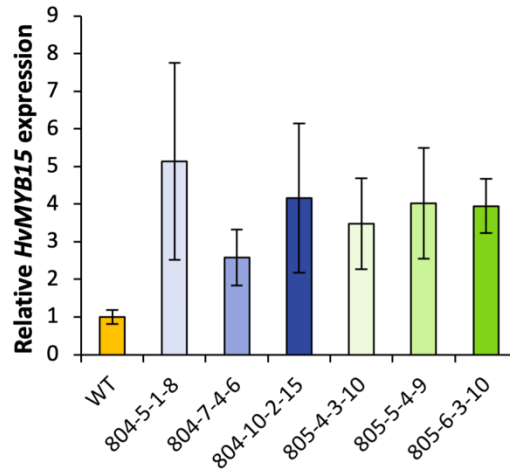
**Supplementary Figure 10. Transcript abundance of *HvMYB15* in wild-type (WT), overexpression lines of *HvMYB15* and overexpression lines of *HvWRKY53* at vegetative growth.** Relative transcript abundance of *HvMYB15* in WT, overexpression (804-5-1-8, 804-7-4-6, 804-10-2-15) of *HvMYB15* and overexpression (805-4-3-10, 805-5-4-9, 805-6-3-10) of *HvWRKY53*. Transgenic lines were grown in soil-filled rhizotrons along with the WT for 55 days. After 55 days, rhizotrons were opened up and fresh seminal root tips were collected for gene expression analysis. Gene expression of WT is set to 1. Bars show means ± SE (n=5).
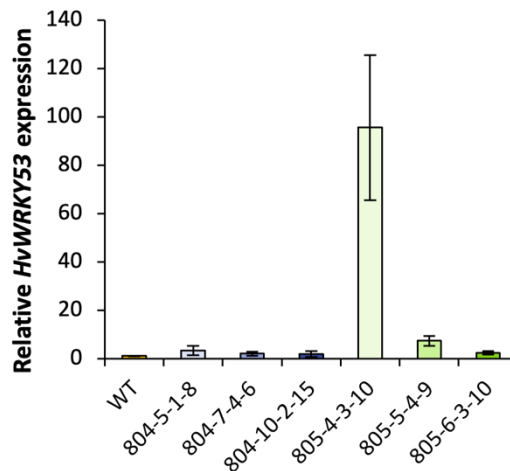


**Supplementary Figure 11. Transcript abundance of *HvWRKY53* in wild-type (WT), overexpression lines of *HvMYB15* and overexpression lines of *HvWRKY53* at vegetative growth.** Relative transcript abundance of *HvMYB15* in WT, overexpression (804-5-1-8, 804-7-4-6, 804-10-2-15) of *HvMYB15* and overexpression (805-4-3-10, 805-5-4-9, 805-6-3-10) of *HvWRKY53*. Transgenic lines were grown in soil-filled rhizotrons along with the WT for 55 days. After 55 days, rhizotrons were opened up and fresh seminal root tips were collected for gene expression analysis. Gene expression of WT is set to 1. Bars show means ± SE (n=5).

# 8. Curriculum Vitae

Name: Cevza Esin Tunc
OrcidID: 0000-0002-1431-2473

## Education

| | |
|---|---|
| **11/2017-present** | Ph.D in Biology, Leibniz-institute of Plant Genetics and Crop Plant Research (IPK), Gatersleben<br><br>Supervisor: Prof. Dr. Nicolaus von Wirén, Molecular Plant Nutrition<br>Dissertation tittle: "Physiological processes and molecular determinants of root senescence in barley" |
| **09/2015-08/2017** | M.Sc in Plant Nutrition, Sabanci University, Istanbul, Turkey<br><br>Supervisor: Dr. Levent Ozturk<br>Thesis title: "Changes in root morphology and nutrient uptake in wheat plants with varied potassium and magnesium supply" |
| **9/2011-6/2015** | B.Sc. in Biological Sciences and Bioengineering, Sabanci University, Istanbul, Turkey |

## Experience

| | |
|---|---|
| **07-09/2014** | Intern, Researcher<br>Max Delbrück Center for Molecular Medicine<br>Research Group Heinemann<br>Berlin, Germany |
| **03/2013-03/2015** | Undergraduate Researcher<br>Enzyme Engineering and Bioinformatics Group, Sezerman Lab.<br>Principal Investigator: Prof. O. Ugur Sezerman<br>Biological Sciences and Bioengineering, Sabanci University, Istanbul,, Turkey |

## Practical scientific training

| | |
|---|---|
| **25-29/03/2019** | AGRIPOLY-DPP Spring School. Mathin-Luther Universität Halle-Wittenberg. Halle, Germany. |

## Conferences

Cevza Esin Tunc, Thomas Schmülling and Nicolaus von Wirén. Modulation of the developmental seminal root lifespan in barley. Poster presentation. Botanik Tagung. Halle (Saale), Germany, 2024.

Cevza Esin Tunc and Nicolaus von Wirén. Root senescence processes as determinants of plant performance in barley. Poster presentation. Plant Science Student Conference, Gatersleben, Germany, 2018.

Cevza Esin Tunc and Nicolaus von Wirén. Root senescence processes as determinants of root performance in barley. Poster presentation. Plant Science Student Conference, Halle, Germany, 2017.

Cevza Esin Tunc, Muhammad Asif, Ismail Cakmak and Levent Ozturk. Changes in root morphological parameters in response to varied potassium supply. Poster presentation. Frontiers of Potassium, Rome, Italy, 2017.

Cevza Esin Tunc, Muhammad Asif and Levent Ozturk. Elevated $CO_2$ increases boron requirement of wheat plants. Poster presentation. AGROBOR 2016. Ankara, Turkey, 2016.

## Publications

Tunc, C. E. and von Wirén, N. Hidden aging: the secret role of root senescence. (*TiPS, submitted*)

Asif, M., Tunc, C. E., Yazici, M. A., Tutus, Y., Rehman, R., Rehman, A., and Ozturk, L. (2019). Effect of predicted climate change on growth and yield performance of wheat under varied nitrogen and zinc supply. Plant and Soil, 434, 231-244.

Asif, M., Tunc, C. E., & Ozturk, L. (2018). Changes in yield attributes and K allocation in wheat as affected by K deficiency and elevated $CO_2$. Plant and Soil, 426, 153-162.

## 9. Acknowledgements

her way of organizing so many different things for so many different people constantly. She has been a lifesaver during my stay in IPK.

Family means everything to me, and I owe everything to my family. I would like to thank my father and brother for being supportive and encouraging during my entire life. I would like to thank my mother, for being my best friend, supporting me in everything I do and being the best mom ever. *Annem*, I adore everything you do, I am your biggest fan. Without you and your support, I would not have made it here. Thank you for everything you have done for me. I love you.

Lastly, Yilmaz. My partner in life and my biggest supporter who has been there with me and for me since the moment he got into my life. Thank you for helping me with my experiments, for your scientific contributions, continuous emotional support and all the other things you have accompanied me during our time here. Thank you for your patience, calmness and being solution oriented. Thank you for taking this path with me. I was never alone.

## 10. Eidesstattliche Erklärung / *Declaration under Oath*

Ich erkläre an Eides statt, dass ich die Arbeit selbstständig und ohne fremde Hilfe verfasst, keine anderen als die von mir angegebenen Quellen und Hilfsmittel benutzt und die den benutzten Werken wörtlich oder inhaltlich entnommenen Stellen als solche kenntlich gemacht habe.

*I declare under penalty of perjury that this thesis is my own work entirely and has been written without any help from other people. I used only the sources mentioned and included all the citations correctly both in word or content.*

_____    _____
Datum / Date                                         Unterschrift des Antragstellers / *Signature of the applicant*

## 11. Erklärung über bestehende Vorstrafen und anhängige Ermittlungsverfahren / *Declaration concerning Criminal Record and Pending Investigations*

Hiermit erkläre ich, dass ich weder vorbestraft bin noch dass gegen mich Ermittlungsverfahren anhängig sind.

*I hereby declare that I have no criminal record and that no preliminary investigations are pending against me.*

_____    _____
Datum / Date                              Unterschrift des Antragstellers / *Signature of the applicant*